The repair of Topoisomerase 1 and 2 DNA-protein crosslinks in vivo

Antičević, Ivan

University of Zagreb

FACULTY OF SCIENCE
DEPARTMENT OF BIOLOGY

IVAN ANTIČEVIĆ

The repair of Topoisomerase 1 and 2 DNA-protein crosslinks *in vivo*

DOCTORAL THESIS

Zagreb, 2023

Sveučilište u Zagrebu

PRIRODOSLOVNO-MATEMATIČKI FAKULTET
BIOLOŠKI ODSJEK

IVAN ANTIČEVIĆ

Popravak križnih veza između DNA i topoizomeraza 1 i 2

DOKTORSKI RAD

Zagreb, 2023

This work was done in the Laboratory of Molecular ecotoxicology at Ruđer Bošković Institute, Zagreb, under supervision of Marta Popović, PhD, Research Group Leader. As a part of Postgraduate doctoral programme of Biology, this thesis is submitted for review to Department of Biology at Faculty of Science, University of Zagreb in order to achieve the academic degree Doctor of Biology.

Supervisor Biography

Dr. sc. Marta Popović was born in Zagreb, Croatia. She graduated magna cum laude in biology from the Faculty of Science at the University of Zagreb in 2005 and went on to study at the University of Oxford (UK), where she completed her Master's degree as a Chevening Scholar in 2007. In 2008, she started her PhD at the Ruder Boskovic Institute, under the supervision of Dr. Tvrtko Smital, where she worked on the biochemical characterisation of membrane transporters in zebrafish. During her PhD, she published 13 papers, including 6 first-author papers in Q1 scientific journals, and received a PhD in Molecular Biosciences at the Ruder Boskovic Institute in 2014. During her studies, she was awarded multiple scholarships and awards, including the OSI/FCO Chevening Scholarship (Open Society Institute/Foreign Commonwealth Office, UK), the "City of Zagreb" scholarship, the annual award for the best publication of young scientists in the field of molecular biology given by the Croatian Genetic Society, and numerous EMBO and FEBS student fellowships. After her PhD, Marta started postdoctoral studies at the University of Oxford (UK) in the group of Prof. Kristijan Ramadan at the CRUK/MRC Oxford Institute for Radiation Oncology where she investigated the mechanisms of DNA repair and published in high impact journals including Molecular Cell, Trends in Biochemical Sciences, Nature communications, Autophagy and Cell reports. After three years at Oxford, she returned to Zagreb in 2018 to establish her research group, where she received a five-year installation grant from the Croatian National Science Foundation for her work on DNA-protein crosslinks. Her research focuses on studying the mechanisms of DNA-protein crosslink repair in vitro, in cell culture and at the organism level using CRISPR/Cas gene editing in cell culture and zebrafish. She has also extended her focus to solving structures of DPC repair factors using Cryo-EM as a part of the collaborative Slovenian-Croatian Bilateral Project which she was awarded in 2020**.** She has authored 27 scientific publications, 10 of them as lead author and one as corresponding author. 26 of them were published in Q1 journals. The publications with the highest impact were published as first author, three of them in journals with very high impact (H index 15, number of citations 732). She co-edited the special issue "Genome Instability: old problem, new solutions" in Frontiers in Cell and Developmental Biology in 2022. Marta is a board member of the Croatian Society of Biochemistry and Molecular Biology (HDBMB), a member of the Federation of European Biochemical Societies (FEBS) and the International Union of Biochemistry and Molecular Biology (IUBMB), where she actively participates in the organisation of conferences, workshops and public outreach events. She supervised three

PhD students and more than 15 MSc and BSc students. She published in over 25 conference proceedings, gave two invited talks and chaired several sessions at international conferences, including a talk at the Gordon Research Conference and Seminar in 2017 (Ventura, USA). She is a lecturer for the elective course "Fish in biomedicine" in the PhD programme "Molecular Biosciences" and a member of several scientific societies, including the European Association for Cancer Research (EACR), the European zebrafish society (EZS), the European environmental mutagenesis & genomic society, the Croatian Association for Cancer Research (HDIR), the Croatian genetic society and the Croatian biophysical society. Details of her research can be found on the group's website: https://martafry.wixsite.com/popoviclab. Currently, Marta is a senior research associate and a group leader at the Ruđer Bošković Institute in Zagreb.

Acknowledgments

First and foremost, I wish to express my deep gratitude to my supervisor, Marta Popović. Your consistent support, guidance, and encouragement from the early stages of this research to the thesis writing and submission, had make this process much easier. Thanks for giving me the opportunity to work in your group and on this subject and I am looking forward to the challenges ahead along with the coffee breaks in front of the lab.

Special thanks go to my laboratory head, Tvrtko Smital, and my wonderful laboratory colleagues Cecile, Lana, Jelena, Jovica, Marin, Ivan M. and Christine, thanks for friendly and motivating working environment.

I would also like to thank my students Luka J., Luka V. and Matea, for their assistance with some experiments in this thesis.

I want to thank "my people," especially Miro and Tea, for putting up with me for these four years.

Big thanks to Vlade and Mirna, you are partially responsible for entering this PhD journey.

Finally, I want to express my gratitude to my parents and brothers for always being there for me and for their unwavering support. I promise you will see more of me in the future.

University of Zagreb
Faculty of Science
Department of Biology

Doctoral thesis

The repair of Topoisomerase 1 and 2 DNA-protein crosslinks *in vivo*

IVAN ANTIČEVIĆ

Ruđer Bošković Institute

DNA-protein crosslinks (DPCs) are frequent and damaging DNA lesions that affect all DNA transactions, which can lead to the formation of DSBs (double-strand DNA breaks), genomic instability and cell death. At the organismal level, impaired DPC repair (DPCR) is associated with cancer, aging, and neurodegeneration. Repair of the two most abundant enzymatic DPCs, involving topoisomerase 1 and 2 was studied in cell models, but data from organisms are still limited. Here, using a zebrafish model and human cells, we show that endogenous TOP1-DPCs are repaired by TDP1 and SPRTN through independent pathways. Notably, chemically induced TOP1-DPCs, using camptothecin or formaldehyde, require an epistatic action of both enzymes, and effectively prevent the accumulation of TOP1-DPC-related damage. Furthermore, we identified the zebrafish Tdp2 orthologue, Tdp2b, as the enzyme responsible for the removal of Top2-DPC residues. Reduced Tdp2 function, observed in both, living organisms and cellular models, causes significant phenotypic changes. This study provides the first insights into the repair of TOP1- and TOP2-DPCs *in vivo*.

(209 pages, 53 figures, 8 tables, 297 references, original in English)
Key words: TDP1, TDP2, Topoisomerase 1, Topoisomerase 2, DPC, zebrafish, SPRTN, DNA repair

Supervisor: Marta Popović, PhD, Senior Research Associate
Reviewers: Tvrtko Smital, PhD, Senior Scientist
Dragomira Majhen, PhD, Senior Scientist
Marko Močibob, PhD, Assistant Professor

Sveučilište u Zagrebu
Prirodoslovno-matematički fakultet
Biološki odsjek

Doktorski rad

Popravak križnih veza između DNA i topoizomeraza 1 i 2

IVAN ANTIČEVIĆ

Institut Ruđer Bošković

Križne veze proteina i DNA (eng. DPCs) su česte i štetne lezije DNA koje ometaju sve procese na DNA, što može dovesti do pojave dvostrukih lomova, genomske nestabilnosti i stanične smrti. Na razini organizma, neefikasan popravak križnih veza proteina i DNA povezan je s nastankom tumora, starenjem i neurodegeneracijom. Dok je popravak najčešćih enzimskih DPC-a, Topoizomeraze 1 i 2, pručavan u staničnim modelima, podaci o ovom popravku u organizmima još uvijek su nedostatni. U ovom istraživanju, koristeći model ribe zebrice i ljudske stanične kulture , pokazali smo *in vivo* da se endogeni popravak TOP1-DPC odvija putem enzima TDP1 i SPRTN, pri čemu ti enzimi djeluju neovisno jedan o drugome. Nadalje, DPC-evi s TOP1 inducirani kemijski, korištenjem kamptotecina ili formaldehida, zahtijevaju međusobno ovisno djelovanje oba enzima kako bi se učinkovito spriječilo nakupljanje oštećenja povezanih s TOP1-DPC-ovima. U ovom radu, pokazali smo kako je zebričin Tdp2 ortolog, Tdp2b, enzim odgovoran za uklanjanje ostataka Top2-DPC-a s DNA. Smanjenje aktivnosti Tdp2, kako u živim organizmima tako i u staničnim modelima, rezultira značajnim fenotipskim promjenama. Ovo istraživanje pruža prve uvide u mehanizme popravka TOP1- i TOP2-DPC-eva *in vivo*.

(209 stranica, 53 slike, 8 tablica, 297 literaturnih navoda, jezik izvornika engleski)
Ključne riječi: TDP1, TDP2, Topoizomeraza 1, Topoizomeraza 2, DPC, zebrica, SPRTN, DNA popravak
Mentor: Dr.sc. Marta Popović, Viši znanstveni suradnik
Ocjenjivači: Dr.sc. Tvrtko Smital, Znanstveni savjetnik
Dr.sc. Dragomira Majhen, Znanstveni savjetnik
Dr.sc. Marko Močibob, Docent

TABLE OF CONTENTS:

1. INTRODUCTION

DNA-protein crosslinks (DPCs) are diverse DNA lesions formed by various processes of DPC formation and interactions between proteins and DNA. Crosslinked range from small 15 kDa proteins such as histones to larger complexes of over 250 kDa (Kiianitsa & Maizels, 2020; Stingele et al., 2016; Vaz et al., 2017). DPCs are not restricted to intact DNA strands; they also occur in the vicinity of single-strand or double-strand DNA breaks (SSB or DSB) (Kühbacher & Duxin, 2020). DPCs can originate from endogenous sources, such as reactive oxygen species, helical DNA modifications and aldehydes formed during cellular metabolic activities such as histone demethylation, as well as from exposure to exogenous factors such as UV light, ionising radiation, and chemotherapeutic agents. DPCs can involve any protein located in close proximity to DNA that becomes trapped due to exposure to DPC-inducing agents (referred to as general DPCs), or DNA-processing enzymes that become trapped while preforming their functions(referred to as enzymatic DPCs) (Tretyakova et al., 2015).

Persistent DPCs can have significant consequences. They interfere with DNA processes including replication, transcription, chromatin remodelling, and DNA repair itself. This can result in genomic instability and apoptosis, and can trigger diseases including cancer, accelerated ageing, and neurodegeneration (Fielden et al., 2018; Ruggiano & Ramadan, 2021; Vaz et al., 2017). Importantly, human syndromes resulting from mutations in DPC repair genes, such as SPRTN (SprT-Like N-Terminal Domain), TDP1 (Tyrosyl DNA phosphodiesterase 1), and TDP2 (Tyrosyl DNA phosphodiesterase 2), exhibit severe phenotypic changes including severe ataxia, the development of cancer and intellectual disability (Errichiello et al., 2020; Hirano et al., 2007; Lessel et al., 2014; Maskey et al., 2017; van Waardenburg, 2016; Vaz et al., 2016; Zagnoli-Vieira et al., 2018). A deeper understanding of DPC repair mechanisms may reveal new avenues for drug development and new approaches to treat cancer and DPC-related diseases.

The most abundant enzymatic DPCs include DNA topoisomerases 1 and 2, DNA polymerases, and DNA methyltransferases (Kiianitsa & Maizels, 2020; Klages-Mundt & Li, 2017). In the process of DNA replication, the parental DNA strand is subjected to increased torsional stress, which can be relieved by generating an SSB. This is achieved by topoisomerase 1 (TOP1), which catalyses the cleavage of a DNA strand, resulting in relaxation by wrapping around an intact strand (Redinbo et al., 1998). In this process, TOP1 cleaves a DNA strand with its tyrosine residue within the active site, producing a temporary 3'-phosphotyrosine intermediate. Later, the detachment of TOP1 from DNA allows repair by

DNA ligases (Redinbo et al., 1998). However, under the influence of internal or external factors, TOP1 can irreversibly bind to the 3'-end of DNA and form covalent TOP1-DNA complexes (TOP1ccs or TOP1-DPCs) (Pommier et al., 2006). Specific chemotherapeutic agents such as camptothecin and its derivatives stabilise the attachment of TOP1 to DNA and cause TOP1-DPCs, which can trigger DSBs and eventually cause cancer cell death (Pommier, 2006). The key enzymes involved in TOP1-DPC repair include several mechanisms. TDP1 breaks the covalent bond between tyrosine in TOP1 and the 3' end of DNA (Pouliot et al., 1999). Importantly, mutations in the active site of TDP1such as H493R lead to the syndrome Spino Cerebellar Ataxia with axonal neuropathy (SCAN1) (El-Khamisy et al., 2005; Hirano et al., 2007). Second, the protease SPRTN, which cleaves DNA-crosslinked proteins, contributes to TOP1-DPC repair by partial proteolysis of TOP1 which leaves the crosslinked TOP1-peptide residue in the DNA backbone. Debulking of TOP1-DPCs allows TDP1 to resolve the bond between the tyrosine in TOP1 and the 3' end of DNA (Fielden et al., 2020; Stingele et al., 2016; Vaz et al., 2016). Apart from SPRTN-mediated TOP1-DPC debulking the ubiquitin-proteasome pathway can also mediate the degradation of TOP1-DPC, thus allowing TDP1 to access and cleave the phosphotyrosyl bond (C. P. Lin et al., 2008; Meroni et al., 2022; Sciascia et al., 2020). Furthermore, several proteases, including Ddi1/DDI1, FAM111A, and FAM111B, are implicated in the repair of TOP1-DPCs (Hoffmann et al., 2020; Kojima et al., 2020; Serbyn et al., 2020; Svoboda et al., 2019). Recent reports also show a TDP1-independent repair pathway involving the nucleases APEX1 and APEX2, which can remove TOP1-DPC residues by hydrolytic incision of the phosphodiester backbone at the damaged site (H. Zhang et al., 2022).

Enzymatic DPCs frequently involve topoisomerase 2 covalent complexes (TOP2cc or TOP2-DPCs). During DNA replication, TOP2 homodimers create DSBs to release torsional stress (Graille et al., 2008). After break formation, a transient intermediate is formed between TOP2 active site tyrosine and the 5' end of DNA, followed by the dissociation of TOP2 and DSB repair via the non-homologous end-joining (NHEJ) pathway (Dalvie & Osheroff, 2021; Graille et al., 2008). Drugs like etoposide stabilize TOP2-DNA binding, leading to the formation of TOP2-DPCs and eventually unrepaired DSBs (W. Zhang et al., 2021). Given the continuous need for DNA relaxation during the DNA transactions, the persistence of TOP2-DPCs poses a significant challenge to genome integrity (Gómez-Herreros et al., 2014). The repair of TOP2-DPCs is less well understood than the one of TOP1-DPCs and numerous factors have been implicated in TOP2-DPCs repair including (1) debulking by proteolysis followed by TDP2-mediated removal of the crosslinked TOP2 peptide, (2) removal of the

entire DPC by nuclease MRE11 (Hoa et al., 2016; Sun et al., 2022) during DNA resection, and (3) ZATT-induced conformational change of TOP2-DPC followed by TDP2-mediated removal of the entire DPC So far, it has been shown that SPRTN protease can cleave TOP2-DPCs *in vitro* and that cells lacking SPRTN accumulate TOP2-DPCs (Lessel et al., 2014; Vaz et al., 2016). The protease ACRC/GCNA is also thought to be involved in TOP2 resolution since knockout in *C. elegans* shows TOP2-DPC accumulation (Bhargava et al., 2020). Following proteolysis, TDP2 resolves the phosphodiesterase bond between TOP2 remnant and 5' end of DNA (Ledesma et al., 2009). The important role of this enzyme is evident as people with a mutation in TDP2 develop SCAR 23 syndrome (Zagnoli-Vieira et al., 2018), which manifests with intellectual disability, ataxia and seizures. Interestingly, pathway which involves ZATT-TDP2 mechanism allows direct access to the TOP2-DNA bond without prior degradation or need for nucleolysis (J.-M. Park et al., 2023; Schellenberg et al., 2017). However, this has so far been proven only *in vitro*.

Current understanding of TOP1- and TOP2-DPC repair comes mainly from *in vitro* systems and cellular models, while knowledge at the organismal level is limited. Although knock-out mouse models exist for TDP1 and TDP2, TOP1- and TOP2-DPC repair has not been investigated in these models because they were established (Gómez-Herreros et al., 2013; Hirano et al., 2007; Katyal et al., 2007; Zeng et al., 2012) before the existence of specialised DPC repair pathways was discovered in 2014 (Stingele et al., 2014, 2015; Stingele & Jentsch, 2015). For this reason, we have focused on creating adequate animal models to study DPC repair pathways. Our model of choice is zebrafish (*Danio rerio*), a well-established vertebrate model used to study cancer, neurodegenerative and metabolic human diseases due to similar physiology, major organs and signalling pathways to humans (Dawes et al., 2020; Kent et al., 2012) Most importantly, zebrafish is the only vertebrate whose genome is sequenced and assembled with similar quality to those of human and mouse (Varshney et al., 2015), gene conservation with mammals is substantial (70 %), genes involved in DNA repair pathways are 99 % conserved and 84 % of genes known to be associated with human diseases have orthologues in zebrafish (Abugable et al., 2019). Furthermore, external fertilisation simplifies experiments such as gene editing, embryo manipulation and DPC analysis. In particular, the cost-effectiveness and high reproductive capacity allow for more robust statistical analyses of DPC formation in embryonic and adult stages. This makes zebrafish an excellent model for understanding DNA repair pathways, their interplay, and regulatory mechanisms in different cellular contexts. Ultimately, this model offers valuable insights into how organisms cope with disrupted DPCR pathways.

The aim of this study was to establish a zebrafish model with deficiencies in TDP1 and TDP2 proteins, and then to investigate the effects of these alterations on TOP1- and TOP2-DPC repair, and on DPC repair as a whole. In addition, the upstream repair factor, SPRTN protease, known for its contribution to the repair of TOP1- and TOP2-DPCs in cell culture, was investigated, and alternative repair pathways for TOP2-DPCs involving MRE11 nuclease and ZATT SUMO ligase were examined. These factors were specifically silenced by morpholino oligonucleotide mediated silencing. This study also shows how targeted gene manipulations affect (1) the accumulation of total DPCs and specific TOP1- and TOP2-DPCs, (3) zebrafish phenotypes, and (3) formation of DSBs. The potential role of TDP1and SPRTN in the repair of histone-DPCs was also investigated.

The working hypothesis is that TOP1-DPCs are repaired *in vivo* by the SPRTN-mediated proteolytic pathway, followed by TDP1-mediated hydrolysis of the remaining peptide residue. For TOP2-DPCs, , it is proposed that they are repaired *in vivo* through either (1) SPRTN-mediated proteolysis followed by TDP2-mediated hydrolysis of the peptide residue, or (2) a nucleolytic pathway involving the MRE11 nuclease. It is also hypothesized that TOP2-DPCs could be repaired *in vivo* via the ZATT/TDP2-mediated pathway.

2. RESEARCH OVERVIEW

2.1. DNA damage and repair

DNA damage can arise from various sources, including exposure to environmental agents, natural metabolic processes, and errors during DNA replication (Ciccia & Elledge, 2010). If not repaired properly, DNA damage can lead to harmful mutations, genomic instability, and various diseases, including cancer, neurodegenerative disorders, and immune deficiencies. For this reason, eukaryotic cells have a DNA Damage Response (DDR), a crucial defence mechanism that constantly monitors and repairs DNA damage to maintain the genome stability. The DDR is a complex and tightly regulated process involving a network of proteins and signalling pathways that coordinate cell cycle arrest, DNA repair, or apoptosis to address the damage (Nastasi et al., 2020).

There are two main sources of DNA damage. Endogenous DNA damage arises from the interaction between DNA and reactive oxygen and nitrogen species (ROS and RNS) which emerge as by-products of the electron transport chain (ETC) during cellular respiration of aerobic organisms or as a result of redox reactions associated with the catalytic actions of peroxisomal enzymes and inflammatory signalling. Another endogenous source of DNA damage originates from errors during DNA replication. In addition to the high-fidelity replicative polymerases (δ and ε), human cells also have other DNA polymerases (α, β, σ, γ, λ, REV1, ζ, η, ι, κ, θ, ν, μ, Tdt, and PrimPol) that display a higher tendency to make errors, resulting in a lowered replication fidelity. Replication slippage events occurring within repetitive DNA sequences further contribute to genomic rearrangements such as insertions and deletions. Another important cause of mutations is the deamination of DNA bases, particularly cytosine (C) and 5-methylcytosine (5mC), resulting in the loss of their exocyclic amine group (Nakamura & Nakamura, 2020). Exogenous sources of DNA damage originate from external factors such as UV radiation from the sun, ionizing radiation from X-rays and gamma rays and exposure to environmental toxins and genotoxic chemicals. UV radiation primarily induces two types of DNA lesions known as cyclobutane pyrimidine dimers (CPDs) and pyrimidine-pyrimidone (6-4) photoproducts, which distort the DNA helix, affecting replication and transcription processes (Rastogi et al., 2010). Another source of damage coming from industrial chemicals or environmental contaminants are alkylating agents which can modify DNA bases, leading to the formation of alkylated adducts that can interfere with DNA replication and repair and potentially lead to mutations (Soll et al., 2017). Additionally, bulky DNA lesions, like thymine dimers and adducts formed by environmental carcinogens

(like exposure to UV light), cause structural distortions in the DNA helix, affecting normal DNA metabolism (Katerji & Duerksen-Hughes, 2021). Therefore, DNA breaks, both SSBs and DSBs, can arise from ionizing radiation, oxidative stress, or errors in DNA replication (Cannan & Pederson, 2016).

The Nobel Prize in Chemistry was awarded to pioneers of DNA repair research Tomas Lindahl, Paul Modrich, and Aziz Sancar in 2015 for their discoveries of DNA repair mechanisms that demonstrates the importance of understanding cellular DNA repair pathways. Their groundbreaking work has shed light on how cells continuously monitor and repair DNA, ensuring the chemical stability necessary for life's existence and evolution (Lindahl et al., 2016).

DDR is a multi-faceted process involving sensor, transducer, and effector proteins. Sensor proteins, such as ATM (Ataxia telangiectasia mutated), ATR (Ataxia telangiectasia and Rad3 related), and DNA-PK (DNA-dependent protein kinase) detect DNA damage and initiate the DDR signalling cascade. Transducer proteins, such as CHK1 (Checkpoint kinase 1) and CHK2 (Checkpoint kinase 1), transmit the damage signal via the phosphorylation of further downstream kinases and activate the cell cycle checkpoints. Effector proteins, such as p53, play a pivotal role in controlling cell fate decisions, by either enabling DNA repair or inducing apoptosis if the damage is irreparable (Nikfarjam & Singh, 2023).

Cells have developed specialized DNA repair pathways to address various forms of DNA damage, with each pathway playing a crucial role in safeguarding genome integrity, as depicted in Figure 1. Base Excision Repair (BER), Mismatch Repair (MMR), and Nucleotide Excision Repair (NER) are primarily responsible for the repair of smaller DNA lesions. BER addresses small base lesions, including oxidized bases and base alkylations (Figure 1). These lesions can arise from exposure to reactive oxygen species (ROS) during normal cellular metabolism or from exposure to chemical agents such as cisplatin. Specific DNA glycosylases identify and eliminate the damaged base, creating an apurinic/apyrimidinic (AP) site, also known as abasic (AB) site which is further processed by endonucleases, polymerases, and ligases to restore the missing base and complete the repair process (Figure 1) (Krokan & Bjørås, 2013). Considering that AP sites are the most frequent DNA lesions (10,000 AP sites/genome/day) (“DNA Damage,” 2005), BER is particularly vital in preventing the accumulation of mutagenic and cytotoxic DNA lesions and thus ensures the stability of the genome. Intermediates of BER repair are SSBs, which can occur following exposure to ionizing radiation, oxidative stress, or due to aberrant activity of cellular enzymes (e.g., DNA topoisomerase 1). Accurate BER repair is critical to prevent the progression of

these breaks into the most damaging lesions, DSBs (Hossain et al., 2018). DNA mismatch repair (MMR) is a highly conserved pathway that repairs base–base mismatches and small insertions/deletions caused by misincorporation errors during DNA replication. The key players in this process are MSH2-MSH6 and the MSH2-MSH3 (MutS homologs) detection complexes which detect DNA mismatches that occurred during replication, followed by recruitment of downstream repair proteins that excise the error-containing DNA strand and resynthesize it correctly (G.-M. Li, 2008). A disrupted MMR pathway leads to accumulation of mutations and can lead to cancer development (Pećina-Šlaus et al., 2020).

NER is responsible for eliminating bulkier DNA lesions, such as cyclobutane pyrimidine dimers (CPDs) , as well as pyrimidine-pyrimidone (6-4) photoproducts induced by UV radiation and lesions caused by specific chemical carcinogens such as cisplatin or etoposide (Figure 1) (Schärer, 2013). NER functions via two different subpathways: global genome NER (GG-NER) and transcription-coupled NER(TC-NER). In GG-NER, damaged DNA is recognized and excised by the XPC-HR23B (xeroderma pigmentosum group C protein complex) complexes, followed by gap-filling synthesis and ligation. TC-NER, on the other hand, is triggered when RNA polymerase II stalls at a lesion during transcription, ensuring rapid repair by the same XPC protein to maintain proper gene expression (Schärer, 2013).

The most severe form of DNA damage is DSBs which can result in the loss of genetic information or chromosomal rearrangements if not properly repaired. DSBs are repaired via NHEJ (Non-Homologous End Joining), MHEJ (Microhomology-Mediated End Joining) and HR (Homologous Recombination) (Povirk, 2012) (Figure 1). NHEJ, which occurs mainly during the G1 phase of the cell cycle and in post-mitotic cells directly joins the broken DNA ends together. The Ku70/80 heterodimer rapidly recognizes broken DNA, protects the ends from nuclease activity, and orchestrates the recruitment of various NHEJ effectors, such as nucleases, polymerases, and DNA ligase 4 (Chang et al., 2017).While NHEJ is a rapid and efficient repair mechanism and is the dominant DSB repair pathway in human cells, it is error-prone and can lead to small insertions or deletions (indels) at the repair site. These indels have the potential to disrupt gene function and contribute to genomic instability. Nevertheless, NHEJ plays a crucial role in preserving genome integrity in resting and non-dividing cells. It is especially important in cells that never divide including neurons and muscle cells (McKinnon, 2013). In contrast to NHEJ, Homologous Recombination (HR) is active during the S and G2 phases of the cell cycle, when a sister chromatid is available as a template for repair (X. Li & Heyer, 2008). HR ensures high-fidelity repair of DSBs that can occur during DNA replication (Figure 1). In this process, the broken DNA strand invades the

intact sister chromatid, and DNA synthesis occurs using the sister chromatid as a template, restoring the original DNA sequence. HR is vital for maintaining genomic stability, as errors in this pathway can lead to chromosomal rearrangements and loss of genetic information (Noda et al., 2011).

Microhomology-mediated end joining (MMEJ), also known as alternative nonhomologous end-joining (Alt-NHEJ), is a DNA repair pathway that functions when DSBs escape detection by Ku70/Ku80 heterodimers. MMEJ uses short microhomologous sequences to align and connect broken ends, often resulting in deletions around the break site (H. Wang & Xu, 2017). This repair mechanism is associated with complex chromosome alterations, including deletions, translocations, and inversions.

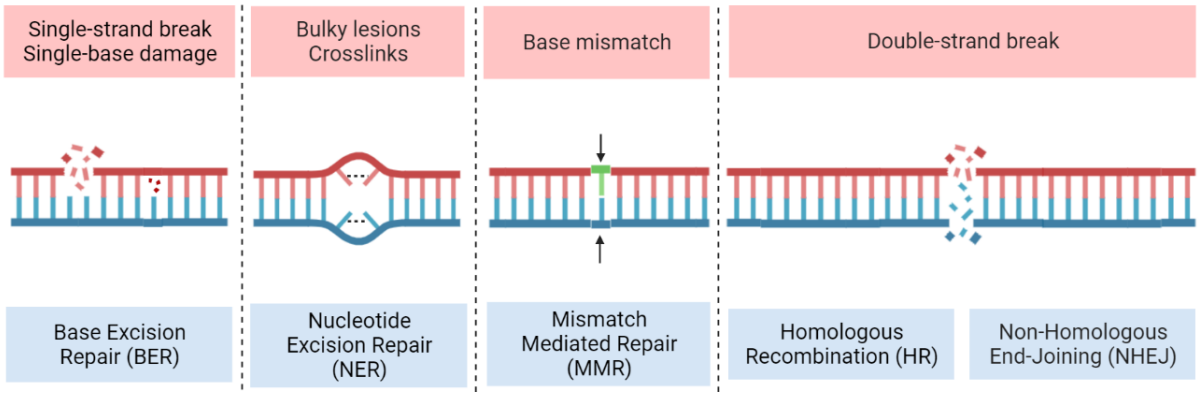

Figure 1. Canonical DNA repair pathways and types of DNA damage they deal with. These pathways include BER, NER, MMR, HR, and the NHEJ pathway (Biorender).

DDR has significant implications for human health and disease. Inherited deficiencies in DDR pathways, as seen in Ataxia Telangiectasia (AT), Nijmegen Breakage Syndrome (NBS), and Fanconi Anemia (FA), lead to immunodeficiencies, neurodegenerative disorders, and increased cancer susceptibility (Jackson & Bartek, 2009). Dysregulation of DDR mechanisms can lead to chromosomal instability and oncogenic mutations that contribute to the development and progression of tumours, while the accumulation of DNA damage during ageing has been linked to age-related diseases, including neurodegeneration and metabolic disorders (Jackson & Bartek, 2009).

In tumorigenesis, the DDR plays a vital role in tumour suppression by preventing the growth of cells with damaged DNA that could lead to malignancies. The tumour suppressor protein p53 is central to this process, activating cell cycle arrest and apoptosis in response to DNA

damage. Dysfunctional p53 or alterations in other DDR components can lead to the evasion of cell cycle checkpoints, promoting genomic instability and cancer development (Kastan & Bartek, 2004). Germline mutations in DDR genes, such as in BRCA1 (BReast CAncer gene 1) and BRCA2 (BReast CAncer gene 2), are associated with an increased risk of breast and ovarian cancer (Casaubon et al., 2023). Targeting DDR pathways in cancer therapy has emerged as a promising approach, using inhibitors to sensitize cancer cells to DNA-damaging treatments. PARP (Poly (ADP-ribose) polymerases) inhibitors, for instance, have shown promising results in treating BRCA-deficient cancers (Lord & Ashworth, 2017).

In neurodegenerative disorders, the accumulation of DNA lesions in neurons is associated with diseases such as Alzheimer's, Parkinson's, and Huntington's (Jeppesen et al., 2011). High mitochondrial respiration in neurons leads to increased DNA damage, and defects in DNA repair pathways have been linked to the pathogenesis of these diseases. Understanding the role of the DDR in neurodegeneration could lead to new therapeutic strategies to preserve neuronal function and prevent disease progression (T. Lu et al., 2004). For instance, mutations in genes encoding DNA glycosylases and other DNA repair proteins have been linked to the early-onset of Alzheimer's disease (X. Lin et al., 2020).

Ageing is associated with an accumulation of DNA damage that contributes to age-related diseases such as cardiovascular disease, metabolic disorders and sarcopenia (Schumacher et al., 2021). Cellular senescence, a state of permanent cell cycle arrest, is a hallmark of aging and is associated with persistent DDR activation due to unrepaired DNA damage or dysfunctional telomeres (Fumagalli et al., 2014). Senescent cells secrete pro-inflammatory factors, promoting inflammation and tissue dysfunction, contributing to age-related pathologies (Schumacher et al., 2021). Strategies that target senescent cells, such as senolytics, may offer potential interventions to mitigate age-related diseases by eliminating harmful cells and reducing inflammation (von Kobbe, 2019).

In conclusion, the DNA Damage Response is an intricate and finely regulated network that protects cells from the harmful consequences of DNA damage. It orchestrates a series of events, from detection to repair, to ensure genome integrity and cellular homeostasis. Understanding the mechanisms underlying the DDR has far-reaching implications for human health and disease, with potential therapeutic applications in cancer treatment and the development of targeted interventions to enhance DNA repair efficiency. Furthermore, exploring the roles of the DDR in neurodegenerative disorders and age-related diseases opens up new avenues for improving the health span and quality of life in an ageing population.

2.2. DNA-protein crosslinks

DNA-protein crosslinks (DPCs) are complex and pervasive DNA lesions that can significantly impact essential chromatin processes including transcription and replication. DPCs form when proteins become irreversibly covalently attached to DNA molecules, either as a result of endogenous cellular processes or due to exposure to various exogenous agents, including chemotherapeutic drugs and radiation. DPCs are structurally very complex because proteins of various sizes can be crosslinked, ranging from small proteins such as histones to large protein complexes (Wei et al., 2021). The nature of crosslinked binding can vary depending on whether DPC formation is triggered by the action of agents such as aldehydes or whether enzymatic DPCs are immobilised on DNA (Kiianitsa & Maizels, 2020; Permana & Snapka, 1994). Furthermore, DPCs can vary based on the DNA to which they are crosslinked: they can develop on both intact and disrupted DNA, which include SSBs and DSBs (Yudkina et al., 2018; Wei et al., 2021; Kiianitsa & Maizels, 2020; Permana & Snapka, 1994). Understanding the formation and repair of DPCs is essential as their persistence can lead to severe consequences, including the formation of DSBs, genomic instability and/or cell death at the cellular level (Fielden et al., 2020; Halder et al., 2019; Stingele et al., 2016; Vaz et al., 2016) and cancer, ageing and neurodegenerative phenotypes at the organismal level (Lessel et al., 2014; Maskey et al., 2014; Takashima et al., 2002; Zagnoli-Vieira et al., 2018).

DPCs can be broadly categorized into two types based on their formation principles: nonenzymatic (or general) DPCs and enzymatic DPCs (Figure 2). Nonenzymatic DNA-protein crosslinks (DPCs) are covalent adducts that form between DNA and a protein located in the vicinity of DNA, such as histones, often triggered by chemical reactions with reactive substances (H. Zhang et al., 2020). Unlike enzymatic DPCs, which involve specific proteins forming covalent intermediates during their normal enzymatic functions, such as topoisomerases, nonenzymatic DPCs are induced by various reactive agents that can crosslink proteins to DNA in a non-specific manner. These reactive agents can arise both, endogenously as byproducts of cellular metabolism such as ROS, NOS and aldehydes, and exogenously through exposure to environmental contaminants such as UV light, gamma irradiation and chemotherapeutic drugs such as camptothecin (CPT) and etoposide (ETO).

One of the most common endogenous sources of nonenzymatic DPCs is formaldehyde (FA) (Ide et al., 2018) that is produced in cells as a part of normal metabolic processes, including histone demethylation, DNA repair, and lipid peroxidation (Lai et al., 2016). FA can readily react with nucleophilic amino acid residues, such as lysine and cysteine, in proteins, resulting in the formation of irreversible covalent crosslinks with DNA. Another common endogenous

source of nonenzymatic DPCs are reactive oxygen species (ROS). These radicals can react with both DNA bases and amino acids in proteins, leading to the formation of various DNA-protein adducts, including DPCs (Kühbacher & Duxin, 2020). DNA helical modifications, including abasic sites, as well as structural-base modifications like base deamination, are central to DPC formation (Guan & Greenberg, 2010; Kroeger et al., 2003; Verdine & Norman, 2003). Most frequent non-enzymatic DPCs are histones, and High-Mobility Group (HMG) proteins (Kiianitsa & Maizels, 2020). Exogenous agents, such as certain chemotherapeutic drugs and environmental toxins, can also induce nonenzymatic DPCs. For example, platinum-based chemotherapeutics, like cisplatin and carboplatin, are commonly used to treat cancer by inducing DNA damage, including DPCs, in rapidly dividing cancer cells (Dasari & Tchounwou, 2014). These drugs can crosslink DNA and proteins, ultimately triggering apoptosis in cancer cells. Similarly, exposure to ionizing radiation generates highly reactive fee radical like ROS and reactive nitrogen species (RNS) that, among other DNA lesions, lead to the formation of DPCs. The diversity of nonenzymatic DPCs arises from the different types of reactive agents and the wide range of proteins that can become crosslinked. Among the 50 most abundant proteins identified in isolated DPCs are nuclear RNA binding proteins (RBP), histones, HMG proteins, topoisomerase 1 and 2, DNA-(cytosine-5)-methyltransferase 1 (DNMT1), and Ku 70/80 (XRCC5/6) (Kiianitsa & Maizels, 2020).

Unlike nonenzymatic DPCs, which involve reactive agents that non-specifically crosslink proteins to DNA, enzymatic DPCs are formed when a DNA transaction enzymes become irreversibly linked to DNA during their normal enzymatic functions in which it transiently binds DNA (Vaz et al., 2017) (Figure 2). A prominent example is the topoisomerase family of enzymes - specifically, topoisomerase 1 and 2 that induce SSBs and DSBs to facilitate DNA relaxation (Figure 2). Further insights into these enzymes and their trapping to DNA is explained in the chapter Topoisomerases. Another example of enzymatic DPCs is DNA methyltransferase 1 (DNMT1), an enzyme responsible for maintaining DNA methylation patterns during DNA replication. DNMT1 covalently binds to its DNA substrate during the methylation process, and this covalent intermediate is essential for efficient methylation. Therefore, the cytidine analogue 5-aza-2'-deoxycytidine (5azadC or decitabine), which is used as a chemotherapeutic agent to treat myelodysplastic syndromes, can be incorporated into DNA during replication (Weickert et al., 2023). When DNMT1 attempts to methylate the incorporated 5azadC, it forms a stable DPC that traps the enzyme on the DNA. This leads to global DNA hypomethylation, which has a beneficial therapeutic effect by reactivating tumour suppressor genes that have been silenced by aberrant DNA methylation in cancer cells

(Weickert et al., 2023). During transcription initiation, RNA polymerases form transcription initiation complexes with the DNA template through covalent interactions. These complexes are vital for the accurate initiation of transcription. However, under certain conditions like exposure to DNA-damaging agents or oxidative stress, the transcription machinery can stall, resulting in the formation of persistent DPCs consisting of RNA polymerases (Quiñones et al., 2015). DNA helicases are enzymes that unwind the double helix during various cellular processes, including DNA replication, repair, and recombination. Some DNA helicases can become covalently crosslinked to DNA during their unwinding activities, leading to the formation of enzymatic DPCs (Klages-Mundt & Li, 2017). Another common enzymatic DPC is DNA polymerase β (Polβ). Polβ plays an essential role in BER repair by replacing missing nucleotides, forming a covalent Schiff base intermediate with DNA which is subsequently resolved by hydrolysis (Quiñones & Demple, 2016). But when AP residues undergo oxidation, typically caused by exposure to free radicals such as ROS, they generate 2-deoxyribonolactone (dL), which captures Polβ DNA intermediates formed during the BER repair (DeMott et al., 2002). Therapeutic stabilization of this intermediate makes Polβ a potential target in cancer treatment (Goellner et al., 2012).

Extensive research has also focused on the creation of PARP1-DPCs. Poly (ADP-ribose) polymerase 1 (PARP1) is a crucial ADP-ribosylation enzyme that initiates various DNA repair processes. As a primary responder, it detects DNA damage and controls the selection of repair pathways. PARP1 binds to damaged DNA through its N-terminal zinc finger motifs, activating its catalytic C-terminal domain to hydrolyse NAD^+ and generate linear and branched PAR chains that span over hundreds of ADP-ribose units (Ray Chaudhuri & Nussenzweig, 2017). Upon binding to the AP site, PARP1 establishes a Schiff base intermediate, forming a linkage between the C1' atom of deoxyribose and one of its primary amine-containing amino acids. If this Schiff base is reduced, potentially by the intrinsic redox capacity of PARP1, triggered by PARP inhibitors, it results in DNA nicking, with PARP1 now covalently trapped at the 3' end of DNA (Prasad et al., 2014). Additionally, PARP1 can crosslink to the 5' end of a DNA nick after APE1 cleavage during the BER repair process. Trapping PARP1 to DNA in cancer cells disrupts the DNA damage response, and ultimately leads to cancer cell death (Murai et al., 2012).

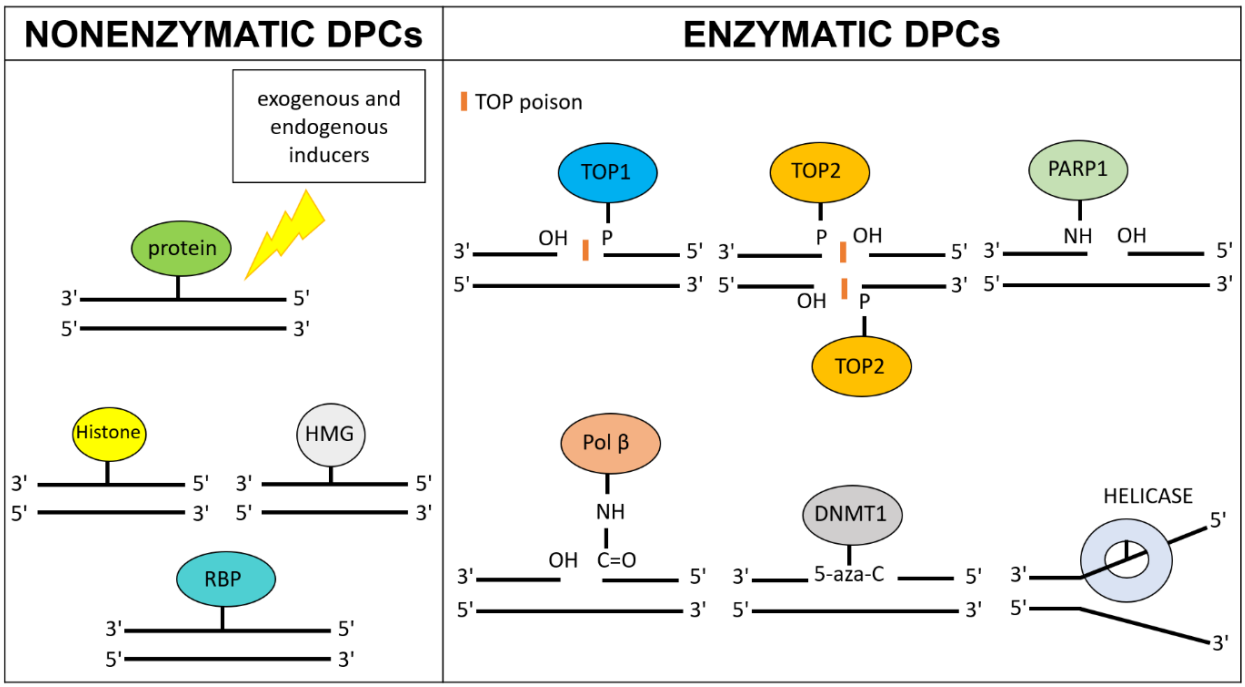

Figure 2. Categorization of DPCs into non-enzymatic and enzymatic. The scheme was created with Biorender.

Interestingly, some enzymatic DPCs are essential intermediates in specific cellular processes. In meiotic recombination, for example, the enzyme SPO11 (SPO11 initiator of meiotic DSBs) introduces DSBs into DNA as part of the homologous recombination (Paiano et al., 2020). These breaks are covalently trapped by SPO11 and form transient covalent complexes which are essential for proper chromosome segregation and recombination in meiosis.

In conclusion, DPCs are highly complex DNA lesions that can arise from various endogenous and exogenous sources. They are divided into nonenzymatic and enzymatic categories according to the protein type that forms DPC. Understanding the mechanisms of DPC formation and repair is critical for developing targeted therapeutic strategies to combat diseases associated with defective DPC repair and for improving cancer therapies, as well as for gaining insights into the intricate processes that safeguard the integrity of the genetic material in our cells. Another interesting area besides DNA adducts are RNA-protein crosslinks which are also very abundant in the cell (Glumac et al., 2023; Kiianitsa & Maizels, 2020) and have not been investigated at all.

2.3. DNA-protein crosslinks repair

Distinct characteristics of DPCs including size, structure, chemistry of the crosslinks, DNA topology, and the phase of the cell cycle in which they arise, will determine how the crosslink will be repaired. The field of DPC repair (DPCR) is very new and was only recognized as a DNA Damage Repair (DDR) pathway in its own right in 2014, when a first protease was found in yeast (Wss1) to initiate DPC removal from the DNA backbone (Stingele et al., 2014). After the discovery of its mammalian counterpart SPRTN, which plays a central role in DPCR, in 2016 (Lopez-Mosqueda et al., 2016; Stingele et al., 2016; Vaz et al., 2016), the field has gradually expanded, with more than 20 publications per year since 2018, and many research groups have joined the DPCR field.

Multiple mechanisms are involved in DPCR, including proteolytic and nucleolytic pathways, as well as specialized repair enzymes, all working together to maintain genomic stability and cellular homeostasis (Figure 3) (Weickert et al., 2023). Efficient repair of DPCs is crucial, as failure to do so results in genomic instability and/or cell death, which in turn can lead to the development of various human diseases including Ruijs-Aalfs syndrome (RJALS), Spinocerebellar ataxia with axonal neuropathy type 1 (SCAN1) or Spinocerebellar ataxia type 23 (SCA23) (Katyal et al., 2007; Maskey et al., 2017; Ruggiano & Ramadan, 2021; Vaz et al., 2016; Zagnoli-Vieira et al., 2018).

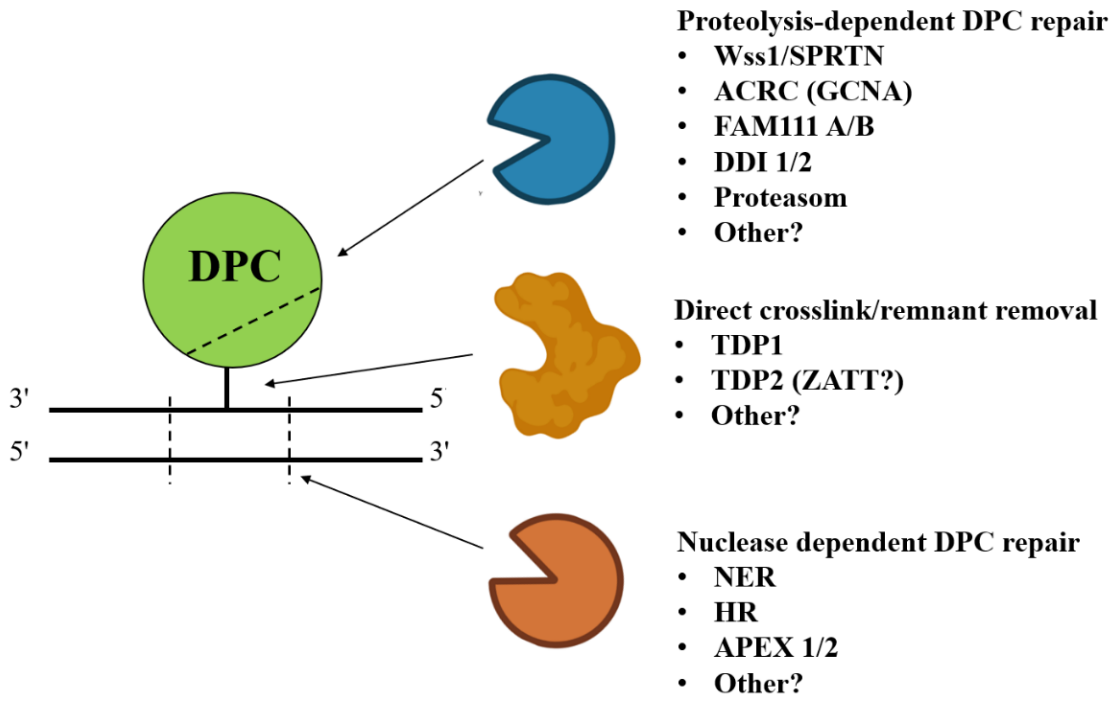

Figure 3. A schematic representation of the DPC repair pathways. The scheme was created using Biorender.

The proteolytic pathway was first discovered in yeast, where the metalloprotease Wss1 (Weak Suppressor of Smt3 1) was identified as the initiator of DPCR through proteolysis (Stingele et al., 2014). Subsequent studies in *Xenopus* egg extracts (Duxin et al., 2014) confirmed a similar pathway in metazoans, which was later attributed to the SPRTN protease (SprT-Like N-Terminal Domain) (Vaz, 2016, Lopez-Mosqueda *et al.*, 2016; Stingele *et al.*, 2016; Maskey *et al.*, 2017). While Wss1 and SPRTN share similarities in the proteolytic core, they are not orthologues but functional homologs with limited sequence identity (Vaz et al., 2017). Both Wss1 and SPRTN play critical roles in DPCR and demonstrate the ability to process various DPCs, including histones, topoisomerase 1 and 2 (TOP2) (Fielden et al., 2020; Lopez-Mosqueda et al., 2016; Maskey et al., 2017; Stingele et al., 2014; Vaz et al., 2016).

The proteolytic activity of DPC proteases must be tightly regulated to prevent uncontrolled proteolysis. Wss1 and SPRTN are activated by binding to single-stranded (ss) and double-stranded (ds) DNA, respectively, providing protection against unwanted proteolysis of soluble nuclear proteins (Vaz, 2016, Li *et al.*, 2019; Reinking, Hofmann and Stingele, 2020). Additionally, both proteases can undergo self-cleavage in trans in the presence of DNA, acting as a regulatory mechanism to downregulate protease activity when localised to chromatin (Vaz, 2016). Furthermore, post-translational modifications, such as phosphorylation, ubiquitylation, SUMOylation, and acetylation, of the proteases and/or their substrates, as well as their interactions with partner proteins like PCNA (proliferating cell nuclear antigen), the ATPase p97/Vcp, and the TOP1-1 binding protein TEX264 (testis expressed 264), further regulate the activity of the DPC proteases (Fielden et al., 2020; Y. Wang et al., 2016).

Recently, several other proteases have been implicated in DPCR. These include ACRC/GCNA (acidic repeat containing/germ cell nuclear acidic peptidase), FAM111A (Family with sequence similarity 111 member A), Ddi1/DDI1 (DNA damage inducible homolog 1), and DDI2 (DNA damage inducible homolog 2) in humans and their respective orthologues (Bhargava et al., 2020; Borgermann et al., 2019; Dirac-Svejstrup et al., 2020; Dokshin et al., 2020a, 2020b; Fielden et al., 2018; Kojima et al., 2020; Otten et al., 2023; Quispe, 2023; Serbyn et al., 2020). Their direct involvement in DPC repair remains to be confirmed, but indirect evidence places them into DPCR pathways. For instance, ACRC is involved in the resolution of TOP2-DPCs (Dokshin et al., 2020b) and cellular DPCs in zebrafish (Otten, 2023), while Ddi1 in yeast has been shown to cooperate with Wss1 in resolving CPT and FA-induced DPCs (Svoboda et al., 2019). Similarly, FAM111A, a serine protease, has been linked to the repair of TOP1-DPCs and trapped PARP-1(Hoffmann et al.,

2020; Kojima et al., 2020). Currently evidence of direct DPC proteolysis for these emerging proteases is currently lacking, their recruitment to the DPC lesions, (Bhargava et al., 2020; Kojima et al., 2020; Nowicka et al., 2015; Otten et al., 2023) argues for their involvement in DPCR.

Following proteolysis, the remaining crosslinked peptide residues remain covalently attached to the DNA backbone. These remnants could be further repaired by the nucleotide excision repair (NER) pathway which can remove peptides up to 38 kDa in size (Chesner & Campbell, 2018). In addition, specialized repair enzymes, Tyrosyl-DNA Phosphodiesterase 1 (TDP1) and Tyrosyl-DNA Phosphodiesterase 2 (TDP2) are involved in resolving specific TOP1- and TOP2-DPC remnants (Ledesma et al., 2009; Yang et al., 1996). The TDPs are described in detail in the chapter ‘’Tyrosyl DNA phosphodiesterases 1 and 2.

In the intricate process of DPCR, repurposing canonical DNA repair enzymes is a vital mechanism. The MRN complex plays a pivotal role in the DSB repair and can also sense and potentially remove protein adducts at DNA ends (Deshpande et al., 2016). This mechanism is proposed to be important for the processing of TOP2-DPCs (Hoa et al., 2016). Moreover, other nucleases, such as XPF/ERCC1 (DNA excision repair protein 1) and Mus81 (Structure-specific endonuclease subunit), have been implicated in TOP1-DPC repair (Deng et al., 2005) as well as APEX2 (also known as Apn2, apurinic/apyrimidinic end deoxyribonuclease 2) which has been identified as a nuclease capable of removing TOP1-DPCs at 3' DNA ends (H. Zhang et al., 2022). The exact contributions of these nucleases to the DPCR and their specific substrate preferences require further investigation to confirm singular studies and to understand the relationship between the nucleolytic and the proteolytic pathways.

Besides these two main DPCR pathways, it has been shown that the Sumo ligase ZATT/ZNF451 (Zinc finger protein Associated with TDP2 and TOP2/ Zinc finger protein 451) has been shown to alter the conformation of TOP2-DPCs, enabling TDP2 to approach the crosslink and remove TOP2 from the DNA backbone *in vitro*. (Lee et al., 2018; Schellenberg et al., 2017). Further investigations are needed to validate this mechanism in mammalian cells and animal models.

The repair of DNA-protein crosslinks is a critical process for maintaining genomic integrity and cellular function. Understanding the intricate interplay between proteolytic and nucleolytic repair mechanisms in DPCR has significant implications for developing therapeutic strategies to target DPC-related diseases and improve cancer therapies. Further research is needed to fully comprehend the regulation and individual contributions of each repair mechanism and how DPCs are repaired in non-dividing cells.

2.4. Methods for the isolation of cellular DPCs

Three methods are used in the majority of studies for isolation of DPCs : (1) SDS/KCl precipitation assay (Zhitkovich & costa, 1992) which allows for the isolation of DPCs along with other chromatin-bound proteins, (2) caesium chloride (CsCl) method (Barker et al., 2005), and (3) the RADAR (rapid approach to DNA adduct recovery) assay (Kiianitsa & Maizels, 2013) which are specific for DPC isolation. Recently, a new method, the STAR assay, has been reported, which is a modification of the RADAR method with an additional step involving the removal of RNA-crosslinked proteins (Glumac et al., 2023).

In the SDS/KCl precipitation assay, the oldest known method for DPC isolation (Zhitkovich & costa, 1992), cells are lysed in a buffer containing 0.5% SDS which disrupts the non-covalent bonds between proteins and DNA, while covalently linked proteins and DPCs remain intact. To fragment the DNA, the lysate undergoes freezing and thawing. Following this, KCl is added to the lysate and the mixture is centrifuged in order to precipitate the DPCs and covalently linked proteins from the rest of the solution containing non-crosslinked proteins, RNA, free DNA and small molecules. To release DNA, both fractions are treated with proteinase K, and the DNA content is quantified. The amount of DPCs is determined by calculating the ratio of crosslinked DNA to the total DNA (including both soluble and cross-linked forms. The SDS/KCl precipitation assay is relatively simple, straightforward, and easy to perform, making it accessible to researchers with limited resources. However, there are significant disadvantages that should be considered. First, the method captures all covalently bound proteins, not exclusively the irreversibly covalently bound DPCs and second, its sensitivity is lower when compared to the RADAR assay. Most importantly, it does not allow for the visualisation and analysis of proteins in the DPC isolate, nor do the detection of specific DPCs, as all proteins are digested upon treatment with proteinase K and the method rely on the quantification of crosslinked DNA fragments. Finally, the method has only been optimised for cell cultures and has not been studied for tissue analysis.

The CsCl isolation method, which is based on density gradient centrifugation, allows the specific purification of DNA crosslinked proteins (Barker et al., 2005; Hu et al., 2020; Shoulkamy et al., 2012). Cells are lysed using a 6 M guanidinium that disrupts all bonds except for crosslinks (Barker et al., 2005). DNA fragmentation is achieved by shearing with a syringe, and then CsCl is added to establish a density gradient for isolating DPC-containing DNA fractions. DNA molecules move to a position in the gradient where their buoyant density matches that of the surrounding CsCl solution, and distinct bands or fractions containing DPC-containing DNA are collected. The collected fractions are dialysed to remove

CsCl and other contaminants, and a second round of CsCl density gradient centrifugation is performed to ensure thorough removal of any remaining free proteins. The purified DNA containing DPCs are subjected to dialysis to replace the CsCl buffer with an appropriate benzonase buffer. Subsequently, they are treated with benzonase to release the DPCs, which can then be detected using immunostaining. The CsCl isolation method provides high purity of DPC-containing DNA, allowing extensive downstream analysis, but requires technical expertise and specialized equipment for density gradient centrifugation including a ultracentrifuge capable of reaching 100,000 g. The method can also be time-consuming, results in significant sample loss and only a small number of samples can be processed in a single experiment (up to six).

The RADAR assay was developed to specifically isolate DPCs and avoid other chromatin-bound proteins by Kiianitsa & Maizels in 2013 and was further improved by the same authors in 2014 and 2020 (Kiianitsa & Maizels, 2013, 2014, and 2020). The main differences from the KCl/SDS assay were (1) the use of 6M guanidinium instead of SDS in the lysis, disrupting all protein-DNA interactions apart from crosslinks and (2) the use of reducing agents to solubilize DPCs. The main improvement from the CsCl assay was higher processivity and the fact that no expensive equipment was needed (ultracentrifuge).

In the RADAR assay, after cell lysis in 6 M guanidinium buffer, which disrupts all protein-DNA interactions apart from crosslinks, DPCs along with nucleic acids are precipitated with ethanol, and the resulting mixture is centrifuged to pellet the crosslinked proteins along with the DNA. After pelleting, the DPCs are resuspended in a slightly alkaline buffer. To quantify the amount of DNA, a small sample aliquot is treated with proteinase K, and the DNA concentration is measured using a fluorescent DNA-binding dye. Meanwhile, the rest of the sample is normalised by DNA content and then treated with benzonase to remove any residual DNA. The isolated proteins are then pelleted using TCA (2-trichloroacetic acid) and extensively washed for downstream analysis. The RADAR assay exhibits high specificity and sensitivity for DPC detection but can be time-consuming due to multiple steps involved in the detection process. After many washing steps following TCA protein precipitation, significant sample loss is often observed, resulting in moderate intra- and inter-experimental reproducibility. Additionally, the processing of a big number of samples is limited, typically to a maximum of ten. One advantage of this method is the gel separation and visualization of total cellular DPCs, which can be achieved by silver staining or even by the less sensitive Coomassie staining. The major advantage of this method is that it allows the study of specific

DPC-associated proteins; therefore, it is commonly used to study enzymatically created DPCs.

The STAR assay introduces an initial step of dissolving cells in RIPA (Radioimmunoprecipitation assay) buffer (Glumac et al., 2023). This buffer contains 50 mM Tris–HCl (pH: 7.4), 1 mM EDTA, 150 mM NaCl, 1% Triton X-100, 0.5% deoxycholate (DOC), and 0.1% sodium dodecyl sulfate (SDS). After lysis, DNA containing crosslinked protein are separated from DNA, RNA and soluble proteins through centrifugation. The resulting pellet is then dissolved in 6M guanidinium buffer. Subsequently, DPCs are precipitated, and the DNA concentration is determined from a portion of the sample treated with proteinase K. The remaining portion of the sample undergoes treatment with benzonase to release DPCs. After this step, the concentration of DPCs is determined with the Bicinchoninic acid (BCA) assay. In addition, the total DPCs present can be visualized by subjecting the sample to SDS-PAGE, followed by Coomassie staining. Alternatively, specific DPCs can be visualized using western blotting. A significant advantage of this method is the effective removal of RNA and RNA crosslinked proteins during the DPC isolation process. This modification of the RADAR assay addresses a notable issue observed in the original method, where a substantial portion of isolated DPCs were found to be RNA binding proteins (Kiianitsa & Maizels, 2020). Indeed, this improvement enhances the precision and selectivity of DPC detection. Nevertheless, a notable drawback of this modified RADAR technique is its demand for a substantial initial sample size. In conclusion, the RADAR method appears to be the most effective technique for isolating DPCs. It enables the specific isolation of DPCs from cell cultures. However, this method is not widely used due to its multiple steps, limited sample processing in each experiment, high variability, and low reproducibility. Further optimisation of the method is needed to address these challenges. Additionally, it is worth noting that all current methods are limited to cell models, leaving the question of how to isolate DPCs from tissue samples yet to be answered.

2.5. Topoisomerases

The human topoisomerase family consists of six enzymes (TOP1 and mitochondrial TOP1, TOP2A and TOP2B and TOP3A and TOP3B) that play crucial roles in maintaining genome stability and organization. There are two major families of topoisomerases: type 1 enzymes that introduce transient single-strand cuts into DNA and type 2 enzymes, which make double-strand cuts in DNA (Pommier et al., 2022).

The type I enzymes include two isoforms: type 1A (TOP3A and TOP3B) and type IB (TOP1 and mitochondrial TOP1). Type 1A enzymes are involved in DNA decatenation and disentanglement, while type IB enzymes are mainly responsible for relaxing DNA supercoils. Human topoisomerase 1 (TOP1) is the most extensively studied among cellular type 1B enzymes (Pommier et al., 2022).

Human topoisomerase 1 is a monomeric protein with a molecular weight of 90.7 kDa, comprising four distinct domains (Champoux, 2001) (Figure 4). The N-terminal domain (first 214 amino acids) is hydrophilic and unstructured, and contains nuclear localization signals (NLSs) and interaction sites for various cellular proteins, including transcription factors, p53, and the WRN (Werner protein) protein (Albor et al., 1998; Bharti et al., 1996). The core domain (421 amino acids) is highly conserved and contains all the catalytic residues (Arg488, Lys532, Arg590, and His632) except the active site tyrosine (Tyr723). The linker domain (77 amino acids) connects the core domain to the C-terminal domain, which has 53 amino acids and contains the active site tyrosine (Tyr723) which is crucial for cleavage and religation reactions during the catalytic cycle (Czubaty et al., 2005).

The catalytic mechanism of human topoisomerase I involves several steps. Initially, the enzyme non-covalently binds to DNA, clinging tightly around the DNA with contacts between the protein and the DNA phosphate backbone spanning 14 base pairs (Figure 4B). During DNA binding and release, the enzyme undergoes conformational changes (Fiorani et al., 1999). It prefers supercoiled DNA over relaxed DNA, recognizing DNA junctions where two duplexes cross. The catalysis occurs through nucleophilic attack of Tyr723 on the scissile phosphate, forming a transient covalent enzyme-DNA intermediate called the cleavage complex. A triad of basic amino acids (Arg314, Arg410 and His453) stabilizes the transition state during the reaction. After cleavage, the enzyme facilitates the controlled rotation of the helical duplex downstream of the cleavage site, relieving torsional stress within the substrate DNA (Champoux, 2001). This rotation occurs while the enzyme is open, and it may adopt a conformation that resembles the DNA-free form. Finally, the DNA strands are religated, and the enzyme is released from the DNA.

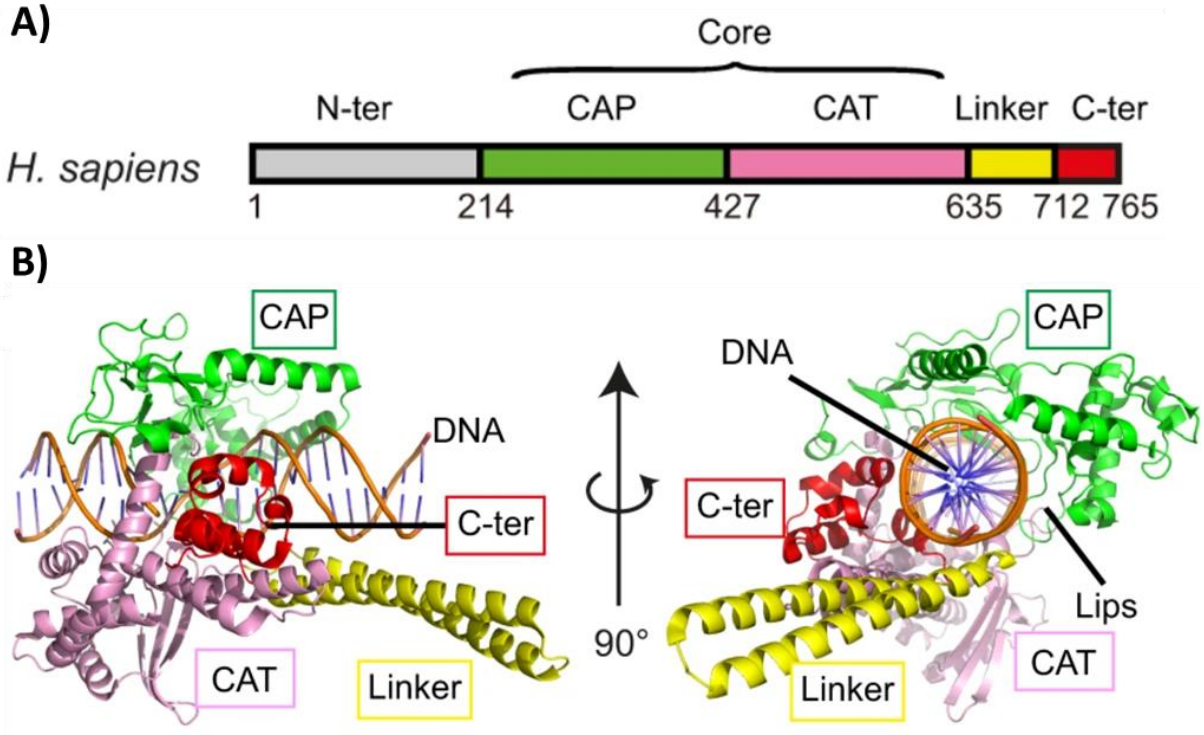

Figure 4. A) The schematic view presents the domain organization of the eukaryotic TOP1B. In this representation, the domains CAP (capping), CAT (catalytic), linker, and C-terminal domain are shown as green, pink, yellow, and red boxes, respectively. Additionally, the N-terminal domains are shown in grey. B) Human TOP1 (HsTOP1) crystal structure: The cartoon representation of the Human TOP1 crystal structure (PDB 1K4T) was adapted from Takahashi *et al.*, 2022 and Redinbo et al., 1998.

Type 2 topoisomerases include type 2A (TOP2A and TOP2B) and type 2B (DNA topoisomerase 6). Type 2A topoisomerases, such as human topoisomerase 2 (TOP2), generate transient DSBs in DNA and play essential roles in DNA replication, transcription, and chromosome condensation (Pommier et al., 2022). Type 2A topoisomerases operate as dimers, with each subunit containing an ATPase domain and a DNA binding/cleavage domain (Figure 5). Subunit A contains the DNA binding/cleavage domain and is responsible for cleavage and rejoining of DNA strands. It contains the active site tyrosine, which is essential for the catalytic reaction. Subunit B is responsible for ATP binding and hydrolysis, as it contains an ATPase domain involved in DNA capture and gating (Champoux, 2001) (Figure 5B). The ATPase and DNA capture domains form the N-gate, which acts as a DNA gate for type 2A enzymes, opening and closing during the DNA transport process. DNA gyrase, a type 2A topoisomerase, wraps the bound G-segment around the enzyme, generating a right-handed

supercoil to introduce negative supercoils. The enzymatic cycle of type 2A topoisomerases involves binding to a G-segment of DNA and an ATP molecule, closing the DNA gate, ATP-dependent DNA cleavage leading to a transient covalent enzyme-DNA intermediate, passage of the T-segment of DNA through the DNA gate, closing of the gate, DNA religation, and release of the products: ADP and inorganic phosphate (Dalvie & Osheroff, 2021) (Figure 5B). Type 2B topoisomerases, such as DNA topoisomerase 6 in humans, are involved in meiotic recombination and chromosome segregation. Unlike type 2A enzymes, they lack a well-defined exit gate, which raises questions about the mechanism of T-segment release after DNA transport (Takahashi et al., 2020).

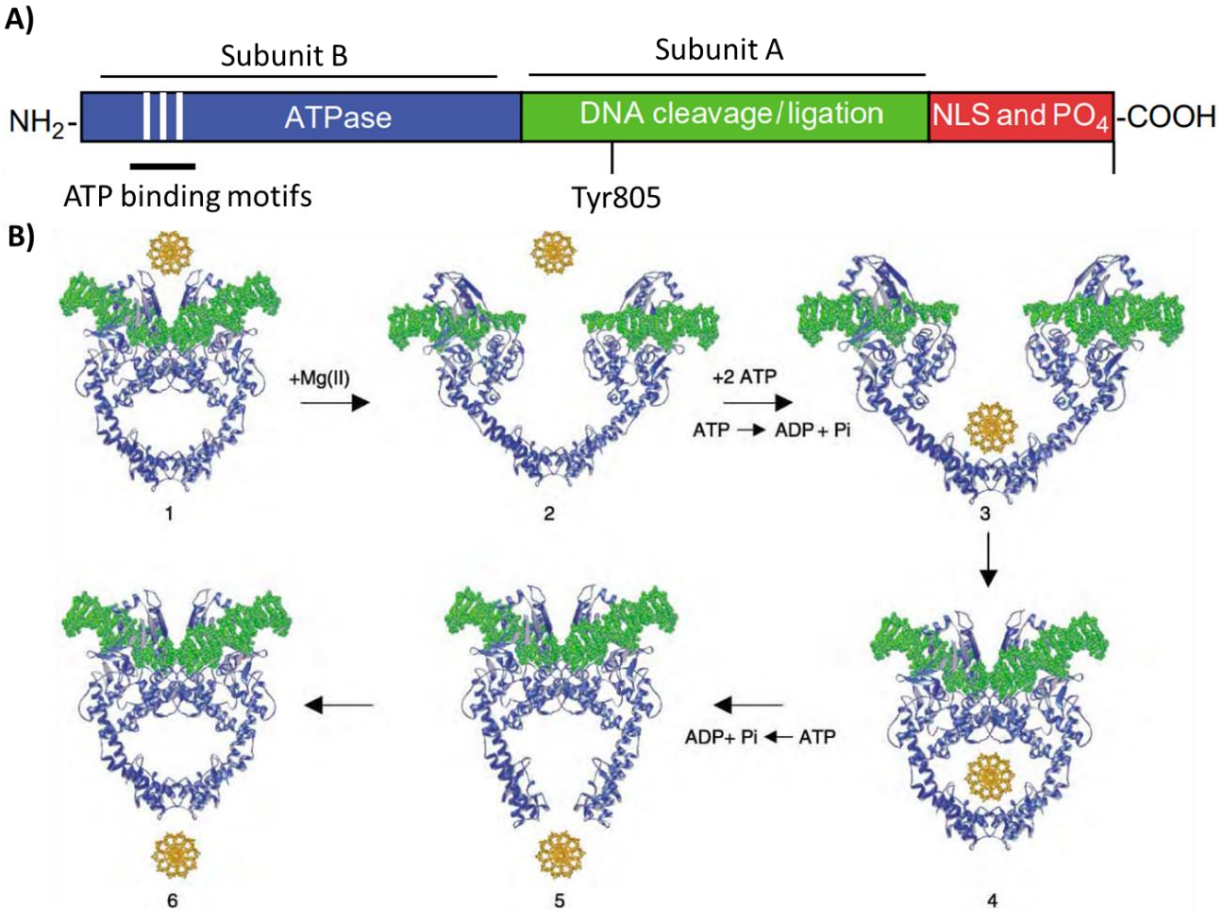

Figure 5. A) Domain structures of type 2A topoisomerases B) Catalytic cycle of type 2A topoisomerases: The complete dsDNA passage reaction is shown as a series of discrete steps, including enzyme-DNA binding, DNA cleavage (formation of cleavage complex), dsDNA passage, DNA ligation, gate opening, release of the translocated DNA helix, and enzyme recycling. Figure is adapted from Dalvie and Osheroff, 2021 and Graille et al., 2008.

TOP1 and TOP2 have been a primary focus in cancer therapy for a long time (Delgado et al., 2018; Martino et al., 2017; Nitiss, 2009; Pommier, 2006; Vann et al., 2021). The most effective approach for targeting topoisomerases is to stabilise their transient DNA intermediates, known as Topoisomerase DNA covalent complexes by forming DNA-protein crosslinks: TOP-DPCs. When stabilised, these complexes hinder DNA replication, ultimately leading to the formation of DNA DSBs and causing the death of cancer cells (Delgado et al., 2018; Fengzhi Li, 2017; Martino et al., 2017; Pommier, 2006).

One well-known class of topoisomerase inhibitors is camptothecin (CPT) and its derivatives, irinotecan and topotecan. These compounds act as TOP1 poisons, stabilizing TOP1-DPCs and causing DNA strand breaks when the replication or transcription machinery encounters the trapped enzyme (Martino et al., 2017). Despite the fact that CPT was discovered over 60 years ago, only two analogues, irinotecan and topotecan, have been approved for cancer treatment, despite extensive studies and synthesis of numerous derivatives over the years. Induction of TOP1-DPCs is used to treat ovarian, colorectal, and recurrent small cell lung cancer (Laev et al., 2016).

TOP2 poisons, such as anthracyclines (e.g., doxorubicin) and epipodophyllotoxins (e.g., etoposide), stabilize the covalent TOP2-DNA complex, preventing DNA religation and resulting in DSBs which are highly toxic to rapidly dividing cancer cells (Nitiss, 2009). Etoposide, known for inducing TOP2-DPCs, received approval for cancer therapy in 1983. The TOP2 crosslinkers are used for the treatment of systemic cancers and solid tumours, including breast cancer, lung cancers, neuroblastoma, sarcomas, leukaemia's, lymphoma and germ-cell malignancies (Vann et al., 2021).

2.6. The repair of topoisomerase 1- and topoisomerase-2 DPCs

To repair TOP1-DPCs, an initial proteolysis step is required to remove the bulk of the protein from the DNA, thus making the remaining crosslinked peptide accessible to the repair enzymes. The ubiquitin-proteasome pathway plays a crucial role in this process by targeting the covalent complex for degradation, marking it with ubiquitin molecules for destruction (C. P. Lin et al., 2008; Meroni et al., 2022; Sciascia et al., 2020). Debulking of TOP1-DPCs exposes the phosphotyrosyl bonds, allowing tyrosyl-DNA phosphodiesterase 1 (TDP1) to access and cleave the bonds. Non-proteasomal proteolytic pathways involving several proteases, including SPRTN, also contribute to the repair of TOP1-DPCs. SPRTN functions as a versatile DNA repair protein, cleaving TOP1 *in vitro*, and cells lacking SPRTN accumulate TOP1-DPCs indicating its importance in resolving these complexes (Fielden et

al., 2020; Maskey et al., 2017; Vaz et al., 2016). Another protease called DDI1 also plays a role in removal of TOP1 from the DNA covalent complex during S phase, aiding in the eviction of crosslinked proteins from DNA (Serbyn et al., 2020). Additionally, the protease FAM111A protects replication forks from stalling at both PARP1-DNA nucleoprotein complexes and TOP1-DPCs, suggesting its involvement the removal of DPC during DNA replication (Hoffmann et al., 2020; Kojima et al., 2020). It is not known why there are so many apparently redundant pathways for TOP1-DPC repair and which pathways are dominant under which conditions.

The key player in the downstream repair of the TOP1 peptide remnant is TDP1, an enzyme that hydrolyses the phosphodiester linkages between the tyrosine residue of TOP1 and the 3'-phosphate of DNA, effectively removing the TOP1 adduct (Kawale & Povirk, 2018). However, recent discoveries in TDP1-KO (Knock-Out) HeLa cells reveal a TDP1-independent mechanism for repairing TOP1-DPCs through the nuclease activity of APEX1/APEX2 (apurinic/apyrimidinic endodeoxyribonucleases 1 and 2) (H. Zhang et al., 2022). This finding is also supported by the increased expression of Apex1 in Tdp1-deficient zebrafish embryos (Zaksauskaite et al., 2021).

In contrast to TOP1-DPC repair, TOP2-DPC removal is a less explored area. TOP2-DPC can be repaired by several pathways: (1) proteolysis followed by the removal of the TOP2-remnant by TDP2 which has been showed *in vitro* and in human cells (Lopez-Mosqueda et al., 2016; Vaz et al., 2016) (2) removal of the entire TOP2-DPC by the action of MRE11 nuclease, which has also been shown *in vitro* and in cell culture (Aparicio et al., 2016; Deshpande et al., 2016; Hoa et al., 2016) , and (3) through the action of Sumo ligase ZATT and TDP2 which has been shown *in vitro* in one study (Schellenberg et al., 2017). Since 2016/2017, there have been no follow-up studies in cell cultures and no *in vivo* studies.

SPRTN efficiently cleaves TOP2-DPCs *in vitro* (Lopez-Mosqueda et al., 2016; Vaz et al., 2016) and cells lacking SPRTN accumulate TOP2-DPCs, indicating its importance in the resolution of these complexes (Lopez-Mosqueda et al., 2016; Vaz et al., 2016). Furthermore, recent research has associated the protease ACRC/GCNA to the removal of TOP2-DPC. Studies in *C. elegans* have demonstrated that gcna-1 mutants exhibit hypersensitivity to TOP2 poison, providing evidence for the role of GCNA in the resolution of TOP2-DPCs (Bhargava et al., 2020). After proteolytic debulking, TDP2 removes TOP2 remnants from the DNA backbone via hydrolysation of the 5'-tyrosyl bond between TOP2 and DNA (Ledesma et al., 2009).

Interestingly, TOP2-DPCs share similarities with SPO11 trapping, a process which occurs during the cell division in which SPO11 generates DSBs, which are essential for the chromatid crossover (Keeney et al., 1997), while MRE11 endonuclease is involved in resolving trapped SPO11. The similarity between TOP2-DPC and trapped SPO11 supports the notion that the MRE11 may also play a role in the removal of TOP2-DPCs *in vivo* by DNA resection (Hoa et al., 2016; Sun et al., 2022).

Interestingly, a compelling alternative repair mechanism for TOP2 removal has recently been suggested, involving the SUMO ligase ZATT (ZNF451) and TDP2. ZATT is a member of the zinc-finger family enzymes, a novel class of SUMO 2/3-specific E3 ligases which are crucial for maintaining cell homeostasis by regulating protein functions through SUMOylation, a process carried out by the hierarchical action of E1, E2, and E3 enzymes, with E3 ligases ensuring substrate specificity (Cappadocia et al., 2015; Streich & Lima, 2014). When ZATT interacts with TOP2-DPC, it induces a conformational change in TOP2, thus allowing TDP2 to access the bond between TOP2 and DNA (Schellenberg et al., 2017). Through hydrolysis, TDP2 effectively removes TOP2 from DNA, ensuring efficient repair of the complex. This mechanism eliminates the need for prior degradation or nucleolytic activity.

Current knowledge focuses mainly on the repair of TOP1 and TOP2-DPCs in cell models. However, there is a lack of data from animal models, not only for this specific repair pathway but also for other DPC repair processes. Moreover, multiple pathways for repair of TOP1- and TOP2-DPCs have been described, raising questions about their redundancy, dominance, and timing of their occurrence (replicative vs. non-replicative phase). A significant question remains regarding how this repair orchestration takes place in non-replicative cells such as neurons.

2.7. Tyrosyl DNA phosphodiesterases 1 and 2

Tyrosyl DNA phosphodiesterases 1 and 2 (TDP1 and TDP2) play a crucial role in the repair of DNA damage caused by abnormal topoisomerase activity. TDP1 resolves phosphotyrosyl peptides formed by trapped topoisomerase 1 (TOP1) at 3' DNA ends, whereas TDP2 manages 5'-phosphotyrosyl residues induced by topoisomerase 2 (TOP2). Despite having distinct roles, TDP1 and TDP2 share some structural similarity. Mutations in the genes encoding these enzymes lead to severe neurodegenerative conditions (Takashima et al., 2002; Zagnoli-Vieira et al., 2018) due to the accumulation of TOP-DPCs, underscoring their critical importance (Pommier et al., 2014).

The discovery of TDP1 was accidental, revealing an enzyme capable of hydrolysing the phosphodiester bond linking TOP1 tyrosyl residue to the 3' end of DNA (Yang et al., 1996). Subsequent studies uncovered the crystal structure of TDP1, exposing its 'HKN' catalytic motifs and an asymmetric substrate-binding channel (Figure 6A) (Davies et al., 2002). TDP1 uses a 'ping pong'-type phosphoryl transfer reaction mechanism to efficiently process the 3'-phosphotyrosyl binding and release 3'-phosphate-ended DNA (Gottlin et al., 1998) (Figure 6B).

The mechanistic journey of TDP1 begins with its recruitment to sites of DNA damage where TOP1 is trapped in a covalent complex with DNA. The N-terminal regulatory domain of TDP1 is instrumental in directing the enzyme to damaged chromatin (Figure 6B). The catalytic mechanism involves a nucleophilic attack on the phosphotyrosyl bond by a conserved histidine residue (H263) within TDP1 N-terminal HKN motif. This attack leads to the formation of a covalent phosphoenzyme intermediate, linking the DNA 3'-phosphate to TDP1 histidine residue (Figure 6B). The following step involves a second conserved histidine residue (H493), located in the C-terminal HKN motif of TDP1, which acts as a general acid catalyst. This histidine residue protonates the departing TOP 1 peptide's tyrosine moiety, preparing it for hydrolysis (Figure 6B). Hydrolysis is executed through the activation of a water molecule by H493, acting as a general base catalyst. The activated water molecule then attacks on the phosphoenzyme intermediate, breaking the phosphotyrosyl bond and liberating the 3'-phosphate-ended DNA (Figure 6B). Post-hydrolysis, the repaired DNA is released from the active site of TDP1, making it available for further processing by other cellular DNA repair enzymes, ultimately restoring genomic integrity (Kawale & Povirk, 2018).

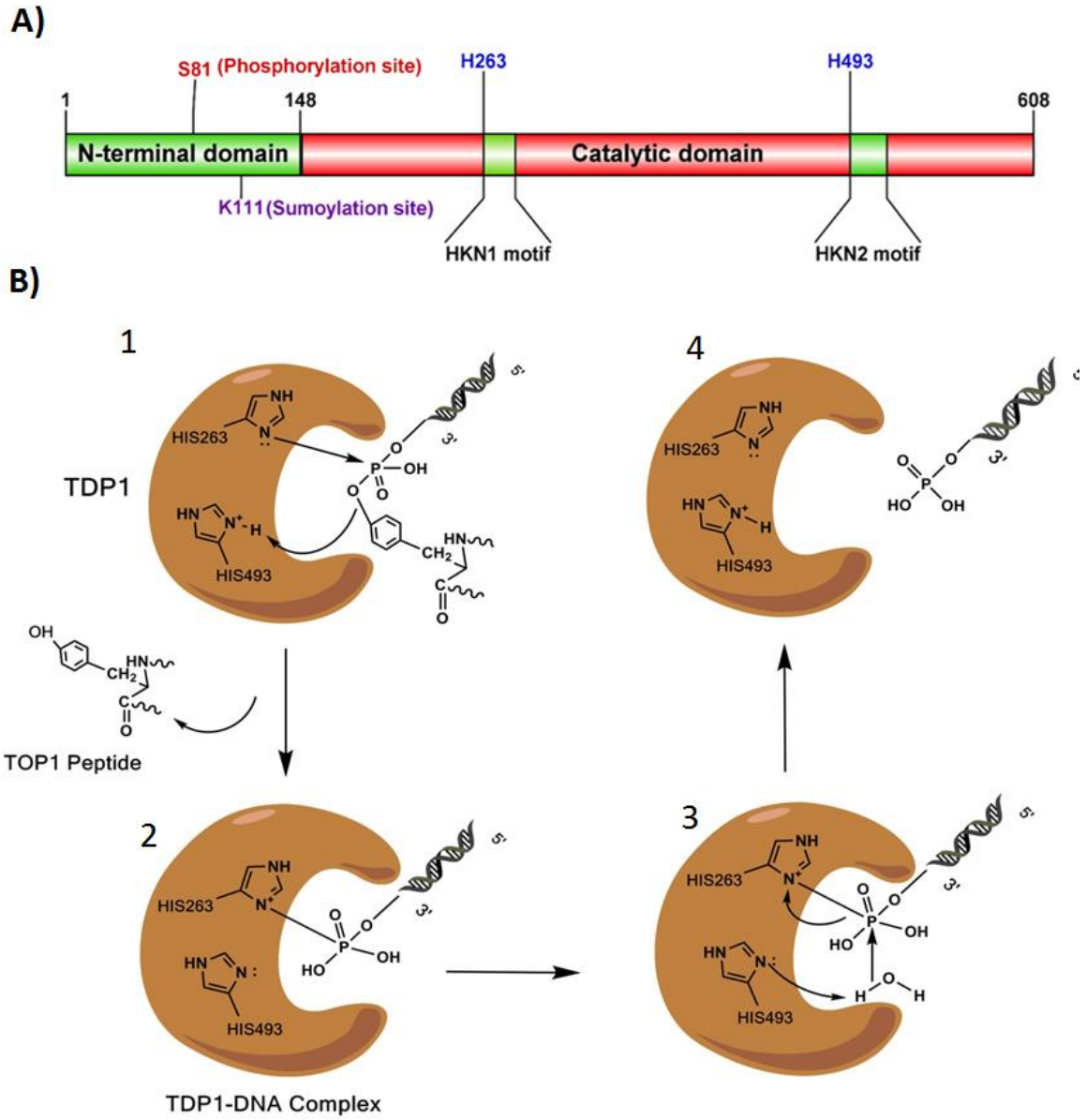

Figure 6. A) Domain structure of human TDP1. The sites shown in blue are key residues in the active site of TDP1 B) Mode of action of TDP1: 1. Initiation of nucleophilic attack on the tyrosyl–DNA 3′-phosphate via the imidazole N2 atom of H263, while H493 provides a proton to the departing TOP1 peptide. 2. Formation of the covalent TDP1-DNA intermediate. 3. Activation of a water molecule by H493, leading to an attack on the 3′-P, causing the N-P bond to break and consequent hydrolysis of the phosphoenzyme intermediate. 4. Release of the DNA 3′-phosphate from TDP1. Figure adapted from Kawale and Povirk, 2018.

A specific missense mutation in the TDP1 gene (A1478G) results in TDP1 H493R mutant, in which the histidine 493 is substituted with an arginine residue (Takashima et al., 2002). This genetic alteration underlies Spinocerebellar Ataxia with Axonal Neuropathy (SCAN1), an

extremely rare autosomal recessive neurodegenerative disorder. The TDP1 H493R mutant patient exhibits a significantly reduced hydrolysis rate of the tyrosyl-containing peptide from DNA, resulting in impaired enzymatic activity (Interthal, Chen, Kehl-Fie, et al., 2005). Intriguingly, the mutant protein becomes covalently trapped with a half-life of approximately 13 minutes. SCAN1 cells harbouring the TDP1 H493R change are hypersensitive to CPT, which induces TOP1-DPCs and subsequently DNA breaks (Hirano et al., 2007). Consequently, the inability of the mutant TDP1 to repair SSBs resulting from oxidative stress and stalled TOP1 responses becomes the molecular basis for the development of this disease in post-mitotic neurons (Povirk, 2012).

TDP1 assumes a pivotal role in correcting TOP1-DPC lesions, actively removing tyrosyl-containing peptides to prevent their accumulation and potential cytotoxic consequences. Apart from its ability to untangle tyrosyl-3′-phosphodiester crosslinks, TDP1 can resolve diverse substrates at the 3' terminus of DNA including 3'-phosphoglycolate, 3'-phosphoamid or 3' abasic sites (Interthal, Chen, & Champoux, 2005; Raymond et al., 2004). It has been shown *in vitro* that it cannot excise full-length crosslinked TOP1 protein, but can effectively cleave only a fragment of TOP1 up to 108 amino acids in size (Interthal & Champoux, 2011). Beyond its primary function in TOP1-DPC repair, it was recently shown *in vitro* that TDP1 can remove histone H2B- and H4-DNA crosslinks at the specific 3' end of SSBs (Wei et al., 2022); however this remains to be confirmed in human cells and in animal models.

In the line with 3'end DNA processing, TDP1 is shown to be a part of chromosomal single-strand break repair pathway arising from abortive TOP1 activity or oxidative stress. TDP1 directly interacts with DNA ligase IIIα (Lig3α), which plays a role in rejoining SSDBs in collaboration with XRCC1 (X-Ray Repair Cross Complementing 1). (El-Khamisy et al., 2005). In addition to its involvement in SSB repair, TDP1 plays a role in the BER repair in mitochondria (Das et al., 2010). Due to ongoing oxidative stress in mitochondria, mitochondrial TOP1 (TOP1mt) is more likely to form DNA adducts. Nuclear TDP1, known to be recruited to mitochondria, could potentially play a role in maintaining the integrity of the mitochondrial genome since cells lacking TDP1 have an abnormal accumulation of oxidative mtDNA damage which can lead to mitophagy (Huang & Pommier, 2019; H. Zhang & Pommier, 2008).

The therapeutic targeting of TDP1 has been attracting interest for several years. TDP1 inhibitors have potential as therapeutic agents to sensitize cancer cells to various DNA damage-inducing treatments, such as TOP1 inhibitors, radiation, radiomimetic drugs, nucleoside analogues, or alkylating agents (Laev et al., 2016; Pearl et al., 2015). Inhibition of

TDP1 can trigger synthetic lethality in cancer cells with dysregulated DNA repair pathways, making them highly dependent on compensatory mechanisms for survival (Ashworth, 2008). TDP1 inhibitors have been proposed as a strategy to enhance the sensitivity of cancer cells to TOP1 inhibitors like CPT and its derivatives, irinotecan and topotecan. Certain cancers, such as non-small cell lung cancer (NSCLC), develop resistance to CPT through overexpression of TDP1, making TDP1 inhibition an attractive approach to overcome this resistance (C. Liu et al., 2007). Several specific TDP1 inhibitors have been developed, including chemically synthesized compounds and naturally occurring plant and fungal metabolites (Antony et al., 2007; P. Wang et al., 2017). Some of these inhibitors, such as modified indenoisoquinolines (P. Wang et al., 2017), have shown potent cytotoxicity in cancer cell lines. However, none of the inhibitors have advanced to clinical trials yet, and future preclinical studies and evidence are needed to confirm their potential as therapeutic agents. This emerging field holds great promise in the fight against cancer and for improving existing treatments.

TDP2 plays a crucial role in TOP2-DPC repair processes. It was first discovered to be associated with TRAF (TNF receptor-associated factors) and TTRAP (TNF receptor-associated protein) (Pype et al., 2000), recognized for its role in orchestrating nuclear factor-kappa beta (NF-κB) signalling. (Pype et al., 2000; J. Zhang et al., 2009). Further investigation unveiled its actual function: as a member of the Mg^{+2}/Mn^{+2}-dependent family of phosphodiesterases, bearing a structural similarity with another DNA repair enzyme, APE1 (Apurinic/apyrimidinic endonuclease 1) (Rodrigues-Lima et al., 2001), TDP2 contributes to DNA repair by resolving 5′-phosphotyrosyl residues, which arise from abortive DNA processes involving TOP2 (Pommier et al., 2014).

TDP2 has an N-terminal domain similar to the ubiquitin-associated domain (UBA-L) that allows it to interact with ubiquitin, and a C-terminal catalytic domain known as the exonuclease/endonuclease/phosphodiesterase (EEP) (Figure 7A) (Hornyak et al., 2016; Rao et al., 2016). Eight well-preserved motifs (M1-M8) in the catalytic domain enable the binding of TDP2 to 5′ DNA end (Figure 7A). M7, which includes the DNA binding motif β-2helix-β (β2Hβ) is particularly important because it holds the last three nucleotides at the exposed 5′ end of the DNA (Schellenberg et al., 2012). In addition, residues W307, F325, and L315, a part of M7, hold the terminal 5′ nucleoside (N1) of the DNA substrate via Van der Waals forces (Schellenberg et al., 2012).

Functionally, the catalytic mechanism of TDP2 involves a carefully orchestrated series of events (Figure 7B) (Kawale & Povirk, 2018; Schellenberg et al., 2012). The reaction starts with the nucleophilic attack on water, which is stabilised by specific residues including D272

and N274 within the catalytic site (Figure 7B). When the 5'-phosphotyrosyl group of the substrate is proximal to the water (around 2.18 Å), D272 activates the water molecule, triggering a nucleophilic attack on the 5'-phosphate of the tyrosyl–DNA adduct (Figure 7B). This gives rise to a penta-covalent transition state intermediate, where the 5'-phosphate is coordinated by H236, S239, H359, and a divalent Mg^{+2} ion is stabilized by E162 (Figure 7B). As the reaction progresses, the O-P bond between the water and the substrate stretches and eventually breaks, resulting in the release of the topoisomerase II (Top II) crosslinked peptide and DNA 5'-phosphate. This process includes the transfer of a proton from water to D272 (Figure 7B). The end result is DNA with a 5'-phosphate end, which is subsequently processed by DNA ligases (Schellenberg et al., 2012)

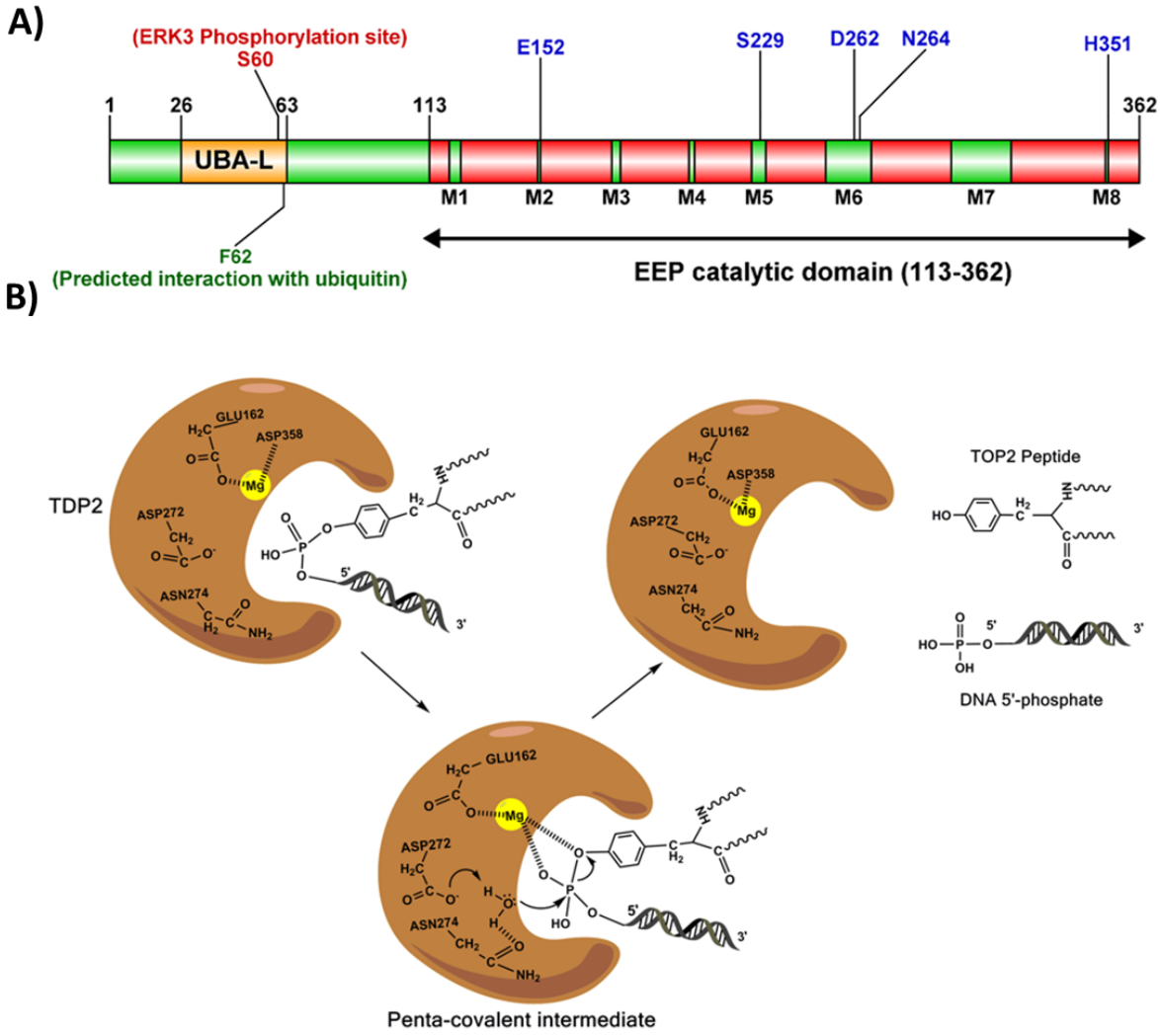

Figure 7 A) Domain structure of human TDP2. The sites shown in blue are key residues in the active site of TDP2. Catalytic Cycle of TDP2: 1. The active site of TDP2 accommodates the 5′-phosphotyrosyl–DNA adduct. 2. Activation of the nucleophilic water molecule by

D272. Formation of the ‘O–P’ bond between the oxygen ('O') of water and the phosphate ('P') of DNA leads to the creation of the penta-covalent intermediate. A yellow Mg^{2+} ion stabilizes the 5′-phosphate of the DNA. 3. The phosphotyrosyl bond is cleaved, resulting in the liberation of the Top II peptide and the 5′-phosphate of DNA. The figure is adapted from Kawale and Povirk, 2018.

TDP2 is not an essential gene but it is crucial for the repair of TOP2-DPCs. It hydrolyses 5'-phosphotyrosyl bonds, thereby resolving trapped TOP2 or its fragments from the 5' end of DSBs caused by aberrant TOP2 activity. Depletion or mutations in TDP2 have been associated with a neurological condition known as Spinocerebellar ataxia autosomal recessive type 23 (SCAR 23) (Errichiello et al., 2020; Zagnoli-Vieira et al., 2018), a rare hereditary ataxia characterized by an early onset symptomatic generalized epilepsy, progressive cerebellar ataxia resulting in walking difficulties or wheelchair dependence, and severe intellectual disability. The substrate specificity of TDP2 includes 5'-phosphotyrosine adducts in single-stranded or 5'-overhanging dsDNA substrates. It retains activity in DNA substrates ranging from short five-nucleotide strands to larger 37-nucleotide substrates, and its efficiency in processing 5'-phosphotyrosyl adducts varies with the size of the DNA substrate (Gao et al., 2012).

TDP2, despite its lack of sequence or structural similarity to TDP1, is involved in repairing DNA damage induced by abortive TOP1 activity. In cells lacking TDP1, TDP2 can rescue the sensitivity of these cells to the TOP1 poison, CPT(Ledesma et al., 2009). Furthermore, $TDP2^{-/-}$ cells are hypersensitive to CPT, and the additional deletion of TDP1 exacerbates this sensitivity. Overexpression of TDP2 can partially complement the defect caused by loss of TDP1, suggesting that TDP2 contributes to TOP1-DPC repair in the absence of TDP1 (Zeng et al., 2012).

TDP2 exhibits a specific substrate preference at 5' DNA end, as it acts exclusively on substrates containing 5'-phosphotyrosyl bonds. It shows no activity on other non-phosphotyrosyl substrates, such as synthetic 5'-fluorescein, 5'-biotin, 5'-digoxigenin, abasic sites, or 5'-AMP substrates (Gao et al., 2012). Besides it role in TOP-DPC repair, TDP2 has also been linked to the life cycle of certain viruses. It can act as a host cell protein know asVPg (Virus Protein genome-linked) which cleaves the 5'-tyrosyl–DNA phosphodiester bond in the RNA genome of picornaviridae viruses (Langereis et al., 2014). Additionally, TDP2 has been shown to play a role in the replication of coxsackievirus B3 (CVB3) and Hepatitis B virus (HBV), making it a potential target for antiviral agents (Cui et al., 2015; Königer et al.,

2014). Apart from these described roles, TDP2 has been independently identified as EAPII (ETS1-Associated Protein II) and TTRAP, which functions as a transcriptional regulator involved in the NF-κB, MAPK, and TGF-β signal transduction pathways (Gao et al., 2012; C. Li et al., 2011; Pommier et al., 2014; Pype et al., 2000).

As for TDP2 inhibition, some inhibitors have been identified, including deazaflavin derivatives, isoquinoline-1,3-dione, and NSC111041 (Kankanala et al., 2016). These inhibitors show promising results in *in vitro* studies which showed that it can enhance the efficacy of TOP2 poisons in cancer cells and cause cell death. However, the development of effective and safe TDP2 inhibitors is still at an early stage and requires further preclinical evidence before clinical trials can be considered. The potential of TDP2 inhibitors as anti-cancer agents and anti-viral agents against specific infections is an exciting area of investigation.

In conclusion, TDP1 and TDP2 play critical roles in the repair of specific types of DNA damage, and their functions have been extensively studied since their discovery. However, there are still many unanswered questions about their role in DPC repair. Most importantly, how is the repair of TOP1- and TOP2-DPCs coordinated at the level of the organism? Can TDP1 and TDP2 repair other types of DPCs (besides TOP1 and TOP2) Are TDP1 and TDP2 partially redundant *in vivo* and to what extent?

2.8. Rodent models deficient in TDP1 and TDP2

Mouse models for TDP1, TDP2, and double TDP1/TDP2 knockout mice have been established. To generate Tdp1 knockout mice, three separate research groups used a similar method involving plasmid gene trap cassette insertion to disrupt the *Tdp1* gene (Hawkins et al., 2009; Hirano et al., 2007; Katyal et al., 2007). This approach resulted a complete absence of TDP1 protein (Hawkins et al., 2009; Katyal et al., 2007) or a truncated form of TDP1 (Hirano et al., 2007). Interestingly, all three groups observed no significant phenotypic changes in TDP1-deficient mice (Hawkins et al., 2009; Hirano et al., 2007; Katyal et al., 2007) and one group reported a progressive reduction in cerebellar size similarly to age-related cerebellar atrophy in SCAN1 patients (Katyal et al., 2007). However, after exposure to CPT or TPT, TDP1-deficient mice exhibited extensive tissue damage, necrosis, and apoptosis (Hirano et al., 2007; Katyal et al., 2007). Tissues with slower proliferation rates, such as intestines, kidneys, and liver, exhibited necrosis, while rapidly proliferating lymphoid and haematopoietic tissues suffered apoptosis and tissue loss (Katyal et al., 2007). Despite these tissue alterations, mice did not develop muscle weakness or ataxia, typical symptoms of

SCAN1 patients (Hawkins et al., 2009; Hirano et al., 2007). Behavioural assessments of these mice revealed no significant differences in grip strength, stride length, or other SCAN1-related metrics when compared to WT mice (Hawkins et al., 2009). Neither their central nervous system (cerebrum, cerebellum, spinal cord) nor peripheral nervous system (dorsal root ganglia, peripheral nerve) showed apparent atrophy or apoptosis (Katyal et al., 2007). On the other hand, mouse embryonic fibroblasts (MEF) and neurospheres derived from TDP1-deficient mice, showed increased sensitivity to CPT, similar to SCAN1 patient cells (Hirano et al., 2007). In order to investigate the potential role of TDP1 in the repair of DSBs resulting from stalled TOP2, mice were treated with the TOP2-DPC inducer, etoposide. Surprisingly, both TDP1-deficient and WT mice showed similar sensitivities to etoposide treatment, with no apparent pathological differences between the two groups (Hirano et al., 2007). These findings indicate that TDP1 is not directly involved in resolving TOP2-associated DNA-protein crosslinks.

TDP2-deficient (*Tdp2*$^{-/-}$) mice and double TDP1/TDP2-deficient (*Tdp1*$^{-/-}$/*Tdp2*$^{-/-}$) mice were generated by the previously mentioned research group (Zeng et al., 2012) using a *Tdp1* mutant mouse line from Katyal et al., 2007. Surprisingly, *Tdp2*$^{-/-}$ mice did not exhibit any phenotypic changes either at the cellular level or *in vivo*. However, after exposure to ETO, significant and dramatic effects were observed, indicating that TDP2 has a vital role in alleviating TOP2-induced DNA damage (Gómez-Herreros et al., 2013). Notably, the study demonstrated that ETO treatment of 8-week-old *Tdp2*$^{-/-}$ mice caused increased mortality due to intestinal damage, substantial weight loss, and enhanced toxicity in lymphoid tissue (Gómez-Herreros et al., 2013; W. Zhang et al., 2021). The observed hypersensitivity to ETO was directly linked to a deficiency in repairing ETO-induced DSBs, as indicated by the accumulation of γH2AX in MEF cells derived from *Tdp2*$^{-/-}$ mice. Furthermore, MEFs from *Tdp2*$^{-/-}$ mice exhibited elevated levels of HR-mediated DSB repair, evidenced by an increase in the frequency of RAD51 foci and sister chromatid exchange exchanges following ETO treatment (Gómez-Herreros et al., 2013). To investigate whether TDP2 might compensate for the loss of TDP1 in MEFs, WT, *Tdp1*$^{-/-}$, *Tdp2*$^{-/-}$, and *Tdp1*$^{-/-}$/*Tdp2*$^{-/-}$ cells, DNA break accumulation was measured after TOP1-DPC induction with CPT using alkaline comet assays (Zeng et al., 2012). As expected, *Tdp1*$^{-/-}$ cells were very sensitive to CPT-induced DNA breaks compared to WT cells. Interestingly, DNA breaks did not accumulate in CPT-treated *Tdp2*$^{-/-}$ MEF cells. However, the simultaneous knock-out of both TDP1 and TDP2 led to a significant accumulation of DNA breaks compared to the deletion of either gene alone (Zeng et al., 2012). These results are consistent with clonogenic survival data, where *Tdp2*$^{-/-}$ MEFs

show normal survival following CPT treatment, but *Tdp1*$^{-/-}$/*Tdp2*$^{-/-}$ MEFs were more sensitive to CPT than *Tdp1*$^{-/-}$ MEFs (Zeng et al., 2012). Strikingly, while all WT, *Tdp2*$^{-/-}$, and *Tdp1*$^{-/-}$ mice survived for over 100 days after CPT treatment, while none of the *Tdp1*$^{-/-}$/*Tdp2*$^{-/-}$ mice survived beyond 10 days. These observations strongly suggest that TDP2 significantly contributes to the repair of TOP1-induced DNA damage *in vivo*, particularly in the absence of TDP1 (Zeng et al., 2012).

The TDP mouse models highlight the importance of TOP1 and TOP2-DPC repair and the involvement of TDPs in these repair processes. The absence of TDPs and that ultimately result of DSBs lead to severe phenotypes, ultimately resulting in the death of the mice due to the accumulation of DSBs. However, none of the described research papers which were published before 2013 investigated the DPCs at this point, as the mouse models were created before the DPC repair pathways was recognised as a separate DDR pathway. Therefore, DPC accumulation, and specifically TOP1- and TOP2-DPCs were not analysed in these animal models, nor in SCAN1 and SCAR23 patient-derived cells. Since it was only later found that DPCs can be repaired via multiple pathways, it is still unclear which repair mechanism prevails at the organism level. Furthermore, the discrepancy between the human syndromes and the mouse models is still unresolved in respect to the TDP deficiencies. It is even more surprising that there were no follow-up studies on animal models since 2013.

2.9. Zebrafish animal model in life sciences

The zebrafish (*Danio rerio*) (Figure 8), a small freshwater teleost fish indigenous to South Asia, has solidified its position as a versatile and useful model organism in the field of molecular biology since the 1960s. Initially gaining prominence due to its distinctive attributes such as external fertilization and optical transparency of embryos, zebrafish quickly became a cornerstone in developmental biology research since early 1980s (Veldman & Lin, 2008). The transparency of the embryo up to the fifth day of life enables direct visualisation of embryonic development and organogenesis, setting the stage for groundbreaking insights into biological processes. Furthermore, a remarkable fecundity of zebrafish (up to 500 eggs per female) and its rapid development, with larvae emerging within 72 hours of fertilisation, greatly improve the accuracy and reproducibility of results, while allowing for much faster experimental setups compared to rodent models (Y. M. Bradford et al., 2017). Significance of the model goes beyond embryogenesis and developmental biology and extends to genetic manipulation and modelling of human diseases. In contrast to traditional rodent models, zebrafish possess several distinct advantages, such as their light-responsive ovulation that

allows precise reproductive control, and cost-effective microinjection techniques for genetic modifications (C. Y. Lin et al., 2016). Gene conservation with mammals is substantial (70%), genes involved in DNA repair pathways are 99 % conserved and 84 % of genes known to be associated with human disease have orthologues in zebrafish (Abugable et al., 2019). Zebrafish embryos, being transparent and easy to maintain (Figure 8A), provide a unique window into studying genetics, gene function, and human disease (Khan & Alhewairini, 2018). The vast majority of human tumours can be studied in zebrafish. By inducing various genetic mutations or triggering signalling pathways with chemicals, tumours can emerge in numerous organs, including the liver, pancreas, intestines, skin, muscles, blood vessels, and testes (Dang et al., 2016). Additionally, the xenotransplantation of mammalian tumour cells into zebrafish embryos and adults has been recently used to study how tumour cells interact with the vascular and immune systems, thus enabling better understanding of metastatic processes (White et al., 2008).

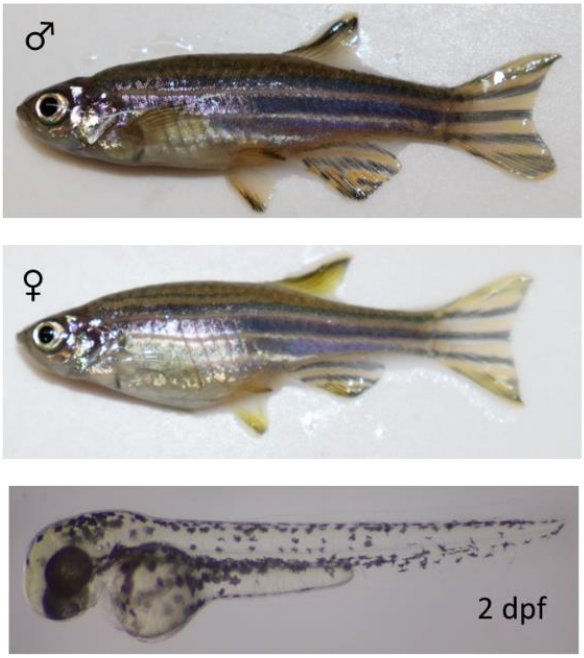

Figure 8. Images show adult male and female zebrafish and transparent 2-day old embryo (Cecile Otten, IRB, unpublished results).

Molecular mechanisms, cell development, and organ physiology including heart, kidney, liver, pancreas, intestinal tract, brain and gonads are similar to those in humans, and the zebrafish has been used as a model to study cancer, neurodegenerative, cardiovascular and metabolic diseases. (Y. Liu, 2023). Recent advances in genome editing techniques have

significantly improved research on the zebrafish model. Techniques like Zinc Finger Nucleases (ZFNs), Transcription Activator-Like Effector Nucleases (TALENs), morpholino oligonucleotide mediated silencing and Clustered Regularly Interspaced Short Palindromic Repeats (CRISPR)/CRISPR-associated protein 9 (Cas9) have enabled targeted genetic modification, allowing researchers to investigate molecular pathways and phenotypic outcomes. In this regard,, CRISPR/Cas9 stands out for its simplicity and versatility, enabling multiplexed gene editing and precise genome modifications (Hwang et al., 2013; P. Liu et al., 2019; Varshney et al., 2015). A lot of mutant strains is already created and are used for numerous studies, while majority of the strains is stored at EZRC (European Zebrafish Resource Centre, Geisler et al., 2016) and available to the research community. Despite all its advantages, the zebrafish is not without limitations. In particular, it lacks certain anatomical structures such as the ventricular septum, lungs, mammary glands, prostate, and limbs, which may restrict the scope of some studies (d'Amora & Giordani, 2018; Jiang et al., 2021; Ribas et al., 2017). The presence of duplicated genes in its genome can middle with genetic analyses and requires careful consideration when designing knockout experiments (J. Lu et al., 2012; Ravi & Venkatesh, 2008).

In summary, the unique characteristics of the zebrafish, its genetic proximity to humans and its ease of genetic manipulation have made it one of the most important model organisms in the life sciences. Its contributions span developmental biology, genetics, disease modelling, and beyond. While certain limitations exist, such as anatomical differences and duplicated genes, ongoing advances in genome editing and research methodologies continue to unlock the full potential of zebrafish as an indispensable tool in advancing our understanding of biological mechanisms and human health.

2.10. CRISPR gene editing

Genetic manipulations have been significantly improved by CRISPR genome editing technology. Discovered by Emmanuelle Charpentier and Jennifer A. Doudna, winners of the 2020 Nobel Prize in chemistry, this revolutionary tool enables relatively easy and fast gene manipulation(Uyhazi & Bennett, 2021).

The journey of CRISPR-Cas9 began in the late 1980s when scientists discovered a cryptic microbial defence mechanism in the bacterial genome. The bacterial genomes showed interesting patterns: they contained groups of repetitive DNA sequences mixed with unknown "spacer" sequences taken from viruses or plasmids. This sequence was called CRISPR, short

for Clustered Regularly Interspaced Short Palindromic Repeats. However, the importance of these repeats remained unclear for a long time.

Emmanuelle Charpentier researched the bacteria *Streptococcus pyogenes* and uncovered a new molecule: tracrRNA (trans-activating CRISPR RNA). This molecule plays an important role in the CRISPR/Cas bacterial defence system, which uses CRISPR arrays and Cas proteins to cut out viral DNA from their genome (Figure 9). In collaboration with Jennifer Doudna, they simplified and adapted this bacterial defence system for easier use across different species (Uyhazi & Bennett, 2021). The result of their collaboration is the RNA-directed CRISPR-Cas9 tool. The RNA-driven Cas9 protein searches for a specific DNA sequence that matches the 'guide' RNA (Figure 9). This target sequence of Cas9 is positioned immediately after a unique recognition site on the DNA, called the PAM sequence (protospacer adjacent motif) which is a sequence of three nucleotides, NGG (Figure 9). Once sgRNA binds to the DNA, Cas9 works as molecular scissors and cuts both DNA strands 3-5 nucleotides upstream of NGG (Nishimasu et al., 2014). After the DSB is formed, repair occurs via either NHEJ or HR. NHEJ rejoins the DNA ends directly, often causing small changes that can affect gene function and is therefore useful for creating mutants with loss of function for the target protein (Figure 9). On the other hand, HR is a precise repair process that needs a matching DNA template for accurate repair and therefore can be useful for introduce precise genomic alterations such as point mutations in the gene of interest if sgRNA/Cas9 complex is injected along with the template carrying the target mutation (Figure 9) (Su et al., 2016; C. Xue & Greene, 2021; Zhu et al., 2015).

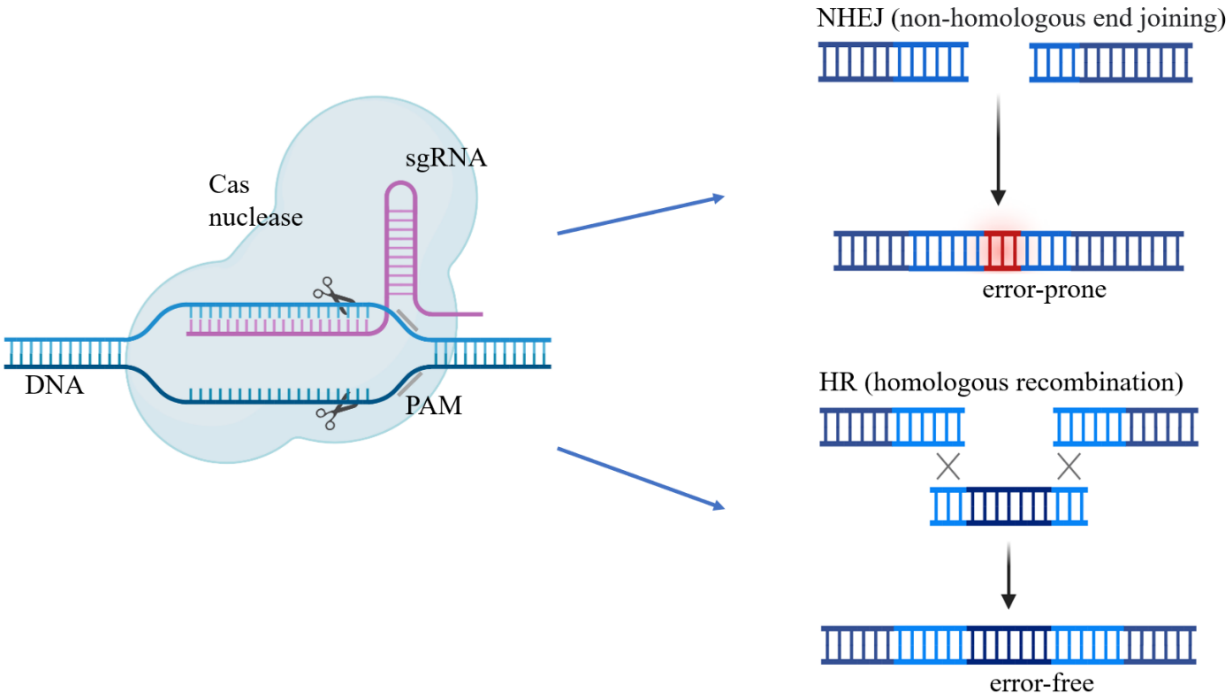

Figure 9. This schematic illustrates the CRISPR/Cas system. The Cas nuclease is guided to the target sequence in the gDNA by a 20-nt guide RNA. The single guide RNA (sgRNA) anneals to the target DNA before the PAM sequence. DSB is introduced upstream of the PAM. Repair of the break occurs via NHEJ which can introduce indels, disrupting the target site (error-prone), while HR repairs using a donor template (error-free). The scheme was created with Biorender.

It's important to note that while Cas9 is the most well-known enzyme in the CRISPR-Cas system, other enzymes can also be used for genome editing. For example, Cpf1 (also known as Cas12a) is another enzyme that functions similarly to Cas9. Cpf1 recognizes a different DNA PAM sequence than Cas9, expanding the range of target sites that can be edited. This diversity of enzymes provides researchers with a broader toolkit for genetic manipulation (P. Liu et al., 2019). One of the most remarkable features of CRISPR technology is its versatility. Unlike previous genetic manipulation techniques, which required time-consuming redesign for each new target, CRISPR-Cas systems only require creating a new guide RNA sequence.

3. MATERIALS AND METHODS

3.1. Materials

3.1.1. Biological models

Competent DH5α E. coli cells (Life Technologies, CA, USA) were used for cloning. These cells were grown on agar plates (Sigma-Aldrich, Taufkirchen, Germany) and in liquid Luria-Bertani medium (Becton, Dickinson and Company, Sparks, USA) supplemented with 100 µg/ml ampicillin (Sigma-Aldrich, Taufkirchen, Germany).

Human embryonic kidney cells (HEK293T) (ATCC, CRL-1573) were used for protein overexpression, siRNA-mediated silencing, and Tdp1 activity assay due to their short amplification time (< 24 h), high protein yield and high transfection efficiency (Tom et al., 2008).

Human Retinal pigment epithelium-1 (RPE-1) cells, a kind gift from Dr. sc Iva Tolić (Ruder Boskovic Institute, Croatia), were used in all experiments for DPC isolations. This cell line was chosen as a non-transformed alternative to cancer cell lines with low endogenous levels of DNA damage (Ghetti et al., 2021).

Zebrafish (*Danio rerio*) AB strain were purchased from the European Zebrafish Resource Centre (EZRC, Karlsruhe, Germany). All handling and experiments were conducted in accordance with the EU Guide for the Care and Use of Laboratory Animals, Council Directive (86/609/EEC), and the Croatian Constitutional Act on the Protection of Animals (NN 135/06 and 37/13) under the project license HR-POK-023.

Frozen mouse tissues from single individuals of both genders (129S1/SvImJ WT, Stock No: 002448, 4-month-old) used for qPCR analysis were kindly provided by dr.sc. Tihomir Balog (Ruder Boskovic Institute, Croatia).

3.1.2. Non- biological materials

Chemicals, enzymes, molecular biology kits, and oligonucleotides used in this study were as follows: standard chemicals (Table 1), enzymes (Table 2), commercial kits (Table 3), oligonucleotides used for quantitative PCR (qPCR), High-Resolution Melting (HRM) analysis, generation of repair template, creation of sgRNAs (Table 4). Oligonucleotides with modifications, used for activity assay and morpholino oligonucleotide mediated zebrafish embryos silencing of *sprtn*, *tdp2a*, *tdp2b*, *zatt* and *mre11* genes are listed in Table 5. Additionally, small interfering RNAs (siRNAs) used to silence target genes in RPE1 cells are

listed in Table 6. Antibodies used in the western blot and dot blot analysis are listed in Table 7. All equipment used in this study is listed in Table 2.8.

Table 1. Standard chemicals used in the study.

CHEMICAL	SOURCE	CAT. NO.
Agarose	Sigma-Aldrich, Germany	A9535
APS (ammonium persulfate)	Sigma-Aldrich, Germany	A3678
Acrylamide/bis-acrylamide	Sigma-Aldrich, Germany	A8887
β-mercaptoethanol	Sigma-Aldrich, Germany	63689
BSA (bovine serum albumin)	Carl Roth, Germany	8076.4
Camptothecin	Alfa Aesar, USA	J62523
Clarity Western ECL Substrate	Bio-Rad Laboratories, USA	1705061
Dig-DNA Marker VII	Merck Millipore, USA	11669940910
DharmaFECT tranfection reagent	Dharmacon, USA	T-2001-02
DMEM	Capricorn Scientific, Germany	DMEM-HPA
DNase/RNase-free water	Invitrogen, USA	10977035
Etoposide	Alfa Aesar, USA	J63651
Ethanol	Kemika, Croatia	505655
FBS (fetal bovine serum)	Capricorn Scientific, Germany	FBS-GI-12A
Formaldehyde	Kemika, Croatia	0633501
GeneRuler DNA ladder mix	Thermo Fisher Scientific, USA	SM1551
Glycine	Alfa Aesar, USA	J16407.A1
Hepes	Sigma-Aldrich, Germany	75277-39-3
Methanol	Kemika, Croatia	P140500
NaCl	Kemika, Croatia	123-54-6
Opti-MEM	Gibco, USA	31985070
Powdered milk	Carl Roth, Germany	t145.1
Precision plus protein ladder	Bio-Rad Laboratories, USA	1610374
SDS Sigma-Aldrich	Sigma-Aldrich, Germany	2326.2
TEMED	Sigma-Aldrich, Germany	D8900
Tris-HCl	Thermo Fisher Scientific, USA	1930809
Trypsin-EDTA	Sigma-Aldrich, Germany	T4049
Tween 20, Ultrapure	Alfa Aesar, USA	J20605.AP

Table 2. List of enzymes used in this study.

ENZYME	SOURCE	CAT. NO.
BamHI, restriction enzyme	New England Biolabs, USA	R0136S
Benzonase, Nuclease	Sigma-Aldrich, Germany	71205-3
Cas9 endonuclease	New England Biolabs, USA	19897
Eco RI, restriction enzyme	New England Biolabs, USA	R0101S
GoTaq qPCR mix	PROMEGA, USA	A6001
MeltDoctor HRM Master mix	Applied Biosystems, USA	4415440
NotI, restriction enzyme	New England Biolabs, USA	R0189S
PCR DIG Probe Synthesis Kit	Roche, Switzerland	11636090910
Phusion polymerase	New England Biolabs, USA	M0530L
Power SYBR Green PCR Master mix	Applied Biosystems, USA	4367659
Proteinase K	Thermo Fisher Scientific, USA	Bp1700-100 FSH
Reverse transcriptase	New England Biolabs, USA	4374966
SalI, restriction enzyme	New England Biolabs, USA	R0138S
SceI, restriction enzyme	New England Biolabs, USA	R0694S
T4 DNA ligase	New England Biolabs, USA	M0202S
Taq DNA poymerase	HighQu, Germany	PCE0201
XholI, restriction enzyme	New England Biolabs, USA	R0146S

Table 3. List of commercial kits used in this study.

MOLECULAR BIOLOGY KIT	SOURCE	CAT NO.
CloneJET PCR Cloning Kit	Thermo Fisher Scientific, USA	K1232
DIG Luminescent Detection Kit	Roche, Switzerland	11363514910
In-fusion cloning kit	Takara, Japan	638947
MEGAshortscript T7 Transcription Kit	Thermo Fisher Scientific, USA	am1354
Monarch DNA Gel Extraction Kit	New England Biolabs, USA	19783
Monarch Genomic DNA Purification Kit	New England Biolabs, USA	T3010S
Monarch PCR & DNA Cleanup Kit	New England Biolabs, USA	T3010S
Monarch RNA Cleanup Kit	New England Biolabs, USA	T2040L
Monarch Total RNA Miniprep kit	New England Biolabs, USA	T2010S-50
Pico Green	Invitrogen, USA	P7581
Power SYBR Green PCR Master Mix	Thermo Fisher Scientific, USA	4367659
ProtoScript II First Strand cDNA Synthesis kit	New England Biolabs, USA	E6560l
ProteoSilver Silver Stain Kit	Sigma-Aldrich, Germany	PROTSIL1-1KT
QuantiFluor ONE dsDNA System	PROMEGA, USA	E4870
Zyppy Plasmid Miniprep Kit	Zymo research, USA	D4036

Table 4. List of oligonucleotides used in this study. All oligonucleotides were purchased from Macrogen EU.

OLIGONUCLEOTIDE NAME	SEQUENCE	PURPOSE
IVT-T7- F	GGATCCTAATACGACTCACTATAG	sgRNA creation
OLIGO-SCAFF-R	AAAAAAGCACCGACTCGG	guide creation
SCAFFOLD	AAAAAAGCACCGACTCGGTGCCACTTTTTCAAG TTGATAACGGACTAGCCTTATTTTAACTTGCTAT TTCTAGCTCTAAAAC	guide creation
DrTdp1-guide-premature STOP	GGATCCTAATACGACTCACTATAGGAATGTGGG GGTCTCTTCGTTTTAGAGCTAGAA	guide creation
DrTdp1-genotype-F-premature STOP	GTGAAACCAGATTCGCAAAGCA	genotyping
DrTdp1-genotype-R-premature STOP	GTTTTGGACTCAGTCTGGGCT	genotyping
DrTdp1-guide-catalytic mutant	GGATCCTAATACGACTCACTATAGGGTAGAGTG CGTACTCCAGGTTTTAGAGCTAGAA	guide creation
DrTdp1-LA_F	AGGGTAATGGCGGCCGCACCAGTTTGGAGGGCT ATCCAG	cloning left homology arm
DrTdp1-LA-R	GCAGCCCGGGGGATCCTGTTTTAGGGCAGACTG TGCAGAC	cloning left homology arm
DrTdp1-RA-F	TATCGATACCGTCGACCCAGCTCTCTGCACCTGC	cloning right homology arm
DrTdp1-RA-R	GTAATGGCGGCTCGAGATCAGCCTTTAGGTTCG ATAGTCAG	cloning right homology arm
DrTdp1-H501A	ACGTTACTGATAGGAGCAACGCGATGCCTGCCA TTAAAACC	mutagenic primer, catalytic site
DrTdp1-NGG	ATTCAATCTTAGTCTCACTCTGGAGTACGCAC	mutagenic primer, NGG change

DrTdp1-probe -F	TAGGTCAGGAGGTTTAGGGGG	DIG-DNA probe creation
DrTdp1-probe -R	TGGCAGCCGTATGAAATCAGT	DIG-DNA probe creation
M13-F	TGTAAAACGACGGCCAGT	pKHR5 sequencing
M13-R	CAGGAAACAGCTATGAC	pKHR5 sequencing
DrTdp1-seq-F-LA	GGTGATTAGTACAACACGAGGG	LA Sequencing
DrTdp1-seq-R-LA	TTCAGGTTCAGGGGGAGGTG	LA Sequencing
DrTdp1-seq-F1-23676-RA	TGGGCTTAGATTGACAGACTGC	RA Sequencing
DrTdp1-seq-R1-25009-RA	ATTCAACAAGCTTGGCACAGT	RA Sequencing
DrTdp1-seq-F2-24639-RA	GTTACAGTGTAACCTGCTCACCTAT	RA Sequencing
DrTdp1-seq-R2-25574-RA	ACCTGAGCTGAATTTAGAGC	RA Sequencing
DrTdp1-seq-F3-25928-RA	GTCTCCGATGAACTCATCAAC	RA Sequencing
DrTdp1-seq-R3-26969-RA	GGTAAGCGATGGTGTACAGCC	RA Sequencing
DrTdp1-seq_F4-26986-RA	TGGCTGTACACCATCGCTTAC	RA Sequencing
DrTdp1-seq-R4-27050-RA	CACAAGCTTGGCACACCTG	RA Sequencing
DrTdp1-seq-F-insert	TGGCCTCAATTTCGCTAAG	RA Sequencing
DrTdp1-seq-R-insert	TTGATCATTCCAACCTTGTG	RA Sequencing
DrTdp2a-guide	GGATCCTAATACGACTCACTATAGGGTTGTGCTA CTGCAAGAGCGTTTTAGAGCTAGAA	guide creation
DrTdp2a-genotype-F	GCAGGTACCGTGCAGATGT	genotyping
DrTdp2a-genotype-R	CATACCTTCCAGAAATTGATCA	genotyping
DrTdp2b-guide	GGATCCTAATACGACTCACTATAGGGTGACACT GCTGAAGCTTCGTTTTAGAGCTAGAA	guide creation
DrTdp2b-genotype-F	GCAGAGAAAACTGAAGTGACTGG	genotyping
DrTdp2b-genotype-R	TCCGCATTGTCCGTCTTCAA	genotyping
HsTDP1-F-qPCR	GGGACGCTTGTTTCTTCAGC	human qPCR
HsTDP1-R -qPCR	TCACCATGCACAAGCAGGAT	human qPCR
HsSPRTN-F-qPCR	GAGGTGGATGAGTATCGGCG	human qPCR
HsSPRTN-R-qPCR	GGGTTCCCTGTTAGTAGCTCG	human qPCR
HsTDP2-F-qPCR	CCAGTATACATGGGATACACAAATG	human qPCR
HsTDP2-R-qPCR	TCTGCTGCTGCTCTGAAAAATA	human qPCR
HsATP50-F-qPCR	ATTGAAGGTCGCTATGCCACAG	human qPCR
HsATP50-R-qPCR	AACAGAAGCAGCCACTTTGGG	human qPCR
DrTdp1-F-qPCR	ACAGATGCTCCTGATTTACCCA	zebrafish qPCR
DrTdp1-R-qPCR	TGTGCCGTCTGTATGCTGTA	zebrafish qPCR
DrSprtn-F-qPCR	AATGACAAGTTCTTCTGGGGG	zebrafish qPCR
DrSprtn-R-qPCR	AAACACCAGCACATAGCGTCA	zebrafish qPCR
DrTdp2a-F-qPCR	CAGAGTCTCTCCAATGTCAATCCA	zebrafish

		qPCR
DrTdp2a-R-qPCR	TGGGTGCACTTGGTTTCTGT	zebrafish qPCR
DrTdp2b-F-qPCR	ATGGATTCAGTCTTCGATGAGG	zebrafish qPCR
DrTdp2b-R-qPCR	CTGTCAAGTCAATGCAATCCGC	zebrafish qPCR
DrAtp50-F-qPCR	CTTGCAGAGCTGAAAGTGGC	zebrafish qPCR
DrAtp50-R-qPCR	ACCACCAAGGATTGAGGCAT	zebrafish qPCR
MmTdp1-F-qPCR	TTGGAACACACCACACGAAA	mouse qPCR
MmTdp1-R -qPCR	GGGTTTTCTGGTGCCAGTCT	mouse qPCR
MmAtp50-F-qPCR	TATGCAACCGCCCTGTACTC	mouse qPCR
MmAtp50-R-qPCR	CCTTCAGGAGTTGCCCTACG	mouse qPCR
Mm18SrRNA-F-qPCR	GATGGTAGTCGCCGTGCCTA	mouse qPCR
Mm18SrRNA -R-qPCR	CCTGCTGCCTTCCTTGGA	mouse qPCR
DrSprtn-MO-F	ACTGTCCGTCCAGTAAGAGG	Silencing efficiency
DrSprtn-MO-R	CCACTTGCTTGGTTGATTCTGT	Silencing efficiency
DrTdp2aMO-F	CAGCGCAAGAAGCAATCATC	Silencing efficiency
DrTdp2aMO-R	CAGAGATACCATCCGGCAAC	Silencing efficiency
DrTdp2bMO-F	TCCAACACTGTTTTGTCAGGT	Silencing efficiency
DrTdp2bMO-R	CAGTAATAGAGCAGGTGGGC	Silencing efficiency
DrZatt/Znf451-MO-F	ATTCAGGCTCTCTGTGGAAG	Silencing efficiency
DrZatt/Znf451-MO-R	CCGATGTCTTTACAGAGAGC	Silencing efficiency
Complementary oligo	GCATGATGGTAGGCAACGATG	Tdp2 activity assay
Competitor_oligo	ATGGTAGGCAACGATG	Tdp2 activity assay

Table 5. List of modified oligonucleotides used in this study.

NAME	SEQUENCE	MODIFICATION	PURPOSE	SOURCE
Tdp1 activity	GATCTAAAAGACT	3′-pY, 5′-Cy5.5	Tdp1_activity	Midland TX, USA
Tdp2 activity	CATCGTTGCCTACCAT	5′-pY, 3′-Cy5.5	Tdp2_activity	Midland TX, USA
DrSprtnMO-1	TCGGTCTGCTTTAGTAACAA CAGTT	Morpholino oligonucleotide	5′ UTR blocking zebrafish *sprtn*	Genetools LLC, USA?
DrSprtnMO-2	AGAGAGGCATATTTAACCA ACCTGA	Morpholino oligonucleotide	ex2-in2 splice blocking, zebrafish *sprtn*	Genetools LLC
DrTdp2aMO	TGCGATCTTTGACATACCTT CCAGA	Morpholino oligonucleotide	ex3-in3 splice blocking,zebra fish *tdp2a*	Genetools LLC
DrTdp2b-MO	ATATGGAGACAATACCAAT CCGCAT	Morpholino oligonucleotide	ex2-in2 splice blocking, zebrafish *tdp2b*	Genetools LLC

DrZatt-MO	TGAATGAAGGAAAACCTTG GACTGC	Morpholino oligonucleotide	ex7-in8 splice blocking, zebrafish *zatt/znf451*	Genetools LLC
DrMre11-MO	AGCTGATGCCATACTAGGA GACTGC3'	Morpholino oligonucleotide	ATG blocking, zebrafish *mre11*	Genetools LLC

Table 6. Small interference RNA (siRNA) used in this study, with corresponding concentrations, manufacturers, and catalogue numbers.

siRNAs	SEQUENCE	c(nM)	SOURCE
HsTDP1-1	CACAAAUGGUCAGCUGAGA	25	Sigma-Aldrich (PDSIRNA2D)
HsTDP1-2	CGAUGAAUCAAAGUGGUUA GGACCAGUUUAGAAGGAUA CUGGGGUGUUGUAUGUAUU GCUAAGGCCUAGAAGGUUA	10	Horizon Discovery(E-016112-00-0005)
HsTDP2-1	GCCAAGAGAUUAUUCCUUU	5	Horizon Discovery (D-017578-02-005)
HsTDP2-2	GCAAGAGGCUCCAGAGUCA	5	Horizon Discovery (D-017578-01-005)
HsSPRTN-1	CAUCAAAGUCAAAAGCGAA	5	Horizon Discovery (L-015442-02-0005)
HsSPRTN-2	CAAGGAUAAGUGUAACAGUTT	5	Thermo Fisher (4392420)
siCTRL	AAGUGGAGCGUGCGAAUGA	10	Santa Cruz Biotechnology (sc-37007)

Table 7. List of antibodies used for western blot and slot blot analysis.

ANTIBIDY	HOST	PRODUCER	CAT. NO.
Mouse Anti-ds DNA monoclonal primary antibody	Mouse	Santa Cruz, Biotechnology, USA	sc-58749
Rabbit Histone H3 polyclonal primary antibody	Rabbit	Cell Signalling Technology, USA	CST-9715S
Mouse Anti-Tubulin monoclonal primary antibody	Mouse	Santa Cruz, Biotechnology, USA	sc-134238
Mouse Anti-TOP1 monoclonal primary antibody	Mouse	Santa Cruz, Biotechnology, USA	sc-271285
Rabbit Anti-TOP1 polyclonal primary antibody	Rabbit	Bethyl Laboratories USA	A302-589A-M
Rabbit Anti-gamma H2A.X (phospho S139) monoclonal primary antibody	Rabbit	Abcam, UK	ab81299
Rabbit Anti-Tdp1 polyclonal primary antibody	Rabbit	Genosphere, UK	Custom made
Anti-Mouse IgG polyclonal secondary antibody	Rabbit	Sigma-Aldrich, Germany	A9044
Anti-Rabbit IgG polyclonal secondary antibody	Goat	Sigma-Aldrich, Germany	A0545

Table 8. List of all equipment used in this study.

EQUIPMENT	PRODUCER	PURPOSE
Hybridization oven	Biometra, Germany	Southern blot
Hybridization tube	Labe-Line, Germany	Southern blot
PCR, T100 Thermal Cycler	Bio-Rad Laboratories, USA	PCRs, incubations
StepOnePlus™ Real-Time PCR	Applied Biosystems, USA	HRM analysis

System		
BInocular lupa	Motic, China	Lens fluorescence detection
Centrifuge Mikro 120	Hettich, Germany	Sample preparation
Centrifuge Universal 32R	Hettich, Germany	Sample preparation
Tecnomara 270	Rockomat, Switzerland	Membrane incubations
Rocking Platform	Labnet, USA	Membrane incubations
Ultra Turrax T25	IKA, Germany	Homogenization
Real-Time PCR System	Applied Biosystems, USA	qPCR analysis
ChemiDoc™ XRS+ System	Bio-Rad Laboratories, USA	Western, Slot and Souther blot dettection
ChemiDoc MP	Bio-Rad Laboratories, USA	Cy-5 fluorescence detection
Royal Blue Fluorescence Viewing System	NIGHTSEA, USA	mVenus detection
Infinite 200	Tecan, Switzerland	Multimode microplate reader
FemtoJet® 4x, Microinjector	Eppendorf, USA	Microinjections

3.2. Methods

3.2.1. Cell culture

Cells (HEK293T and RPE1) were cultured in DMEM-FBS medium, a high-glucose Dulbecco's Modified Eagle Medium (DMEM) (Capricorn Scientific, Germany), supplemented with 10% fetal bovine serum (FBS) (Capricorn Scientific, Germany). They were maintained at 37°C in an incubator within an atmosphere containing 5% CO_2. Cells were passaged twice weekly; first, they were detached from the culture surface using a trypsin-EDTA solution (Sigma-Aldrich, Germany) prewarmed to 37°C. Following a brief incubation in trypsin-EDTA, the reaction was stopped by introducing four ten times the volume of DMEM-FBS. A portion of the resulting cell suspension was returned to either a 25 or 75 cm^2 culture flask to support ongoing cell cultivation, while the remaining portion was used for experimental purposes.

3.2.2. Zebrafish husbandry

Zebrafish (*Danio rerio*) AB were purchased from the European Zebrafish Resource Centre (EZRC, Karlsruhe, Germany). Fish were maintained at a constant temperature of 28 °C and on a 14-hour light and 10-hour dark cycle, with water quality (temperature, pH, and conductivity) monitored daily (Aleström et al., 2020). Embryos were maintained in E3 media (5 mM NaCl, 0.17 mM KCL, 0.33 mM $CaCl_2$, and 0.33 mM $MgSO_4$) in petri dishes in the incubator at 28 °C until 5-dpf stage. Fish that were 30 days old (post-hatch) were fed once a day with high marine protein Gemma 300 (300 Gemma Micro, Zebcare, Netherlands) food. Meanwhile, smaller fish, aged 15 to 30 days post-hatch, were fed three times a day with Gemma 150, and from 6 to 15 days post-hatch, they were fed with Gemma 75. All handling

and experiments were performed in accordance with the directions given in the EU Guide for the Care and Use of Laboratory Animals, Council Directive (86/609/EEC), and the Croatian Federal Act on the Protection of Animals (NN 135/06 and 37/13) under the project license HR-POK-023.

3.2.3. Phylogenetic and syntenic analyses and structural modelling

Protein sequences were retrieved from the National Centre for Biotechnology Information (NCBI) database (Benson et al., 2013) using the blast algorithm (Altschul et al., 1990) with human TDP1 or TDP2 as the query sequences, followed by alignment of the full-length protein sequences using the Multiple Alignment using Fast Fourier Transform (MAFFT, online software) algorithm (Katoh et al., 2002). Alignment quality score was assessed using the Guidance 2 server (Penn et al., 2010). Phylogenetic analysis was performed with the Maximum Likelihood method in SeaView software (Gouy et al., 2010) using the PhyML program with the following parameters: LG model, 8 rates of categories, tree searching operation best of NNI&SPR (Nearest Neighbor Interchange & Subtree Pruning and Regrafting) (Guindon & Gascuel, 2003). Tree node confidence is expressed as Alrt values (Approximate likelihood-ratio test) on a scale of 0-1, where 1 represents the maximum node confidence (Anisimova & Gascuel, 2006). Synteny analyses of human and mouse and zebrafish *TDP1* and *TDP2* genes, were performed using Genomicus, a browser for conserved synteny synchronized with genomes from the Ensembl database (Louis et al., 2013).
Zebrafish Tdp1 was modelled using the Phyre2 workspace (Kelley et al., 2015) and human TDP1 (PDB: c1nopB) as a template. The degree of protein disorder was predicted using the PONDR-FIT software (B. Xue et al., 2010).

3.2.4. Chemical exposure of cells and embryos

HEK293T cells were seeded at a density of 1.3 x 10^3cells/cm^2 in a 10 cm^2 cell culture dish and allowed to grow for two days until they reached 80 - 90% confluence. Cells were cultured at 37°C in Dulbecco's Modified Eagle's medium (Capricorn, DMEM-HPA) containing 10% FBS (Capricorn, FBS-11A) serum under 5% CO_2. For exposure experiments, cells were treated with 1 mM formaldehyde (FA, Kemika: 0633501) for 20 minutes in ice-cold serum-free media.
RPE1 cells were seeded at a density of 1.3 x 10^3 cells/cm^2 in 75 cm^2 cell culture plates and incubated for 72 hours until they reached 80 - 100% confluence. Prior to collection, the cells were treated with 50 nM camptothecin (CPT, Alpha Aesar: J62523) for 1 hour, 25 µM

etoposide (ETO, Alfa Aesar, J63651) or with 1 mM FA for 20 minutes in serum-free media at 37°C in incubator with 5% CO_2.

Two-day-old zebrafish embryos were manually dechorionated using tweezers and treated with 10 µM CPT for 1 hour or 5 mM formaldehyde for 30 minutes at 28 °C in incubator.

3.2.5. Gene silencing by transfection of small interfering RNAs

Gene silencing using small interfering RNA (siRNA) transfection was used to target three genes: *TDP1*, *TDP2*, and *SPRTN*. To assess the efficiency of gene silencing, quantitative polymerase chain reaction (qPCR) was performed using gene-specific primers (Table 2.4). As a negative control, siCTRL (scrambled or randomly rearranged RNA sequence) was used, which should have no effect on the cells because it does not target any mRNA (Table 2.6). qPCR is typically the initial step in validating silencing and is often sufficient to detect the absence of a protein (Tsai & Chang, 2014; Tuzmen et al., 2007). The results of the qPCR experiments are presented in Figures 23 and 41A. Retinal pigment epithelium cells (RPE1) were seeded at a density 1.3 x 10^3 cells/cm^2 (75 cm^2 cell culture flasks) on the day of transfection. The commercially available reagent DharmaFECT from Dharmacon (USA) was used for siRNA transfection according to the manufacturer instructions. Briefly, solution A was prepared by mixing siRNA with opti-MEM (31985070, Gibco), and solution B was prepared by mixing Dharmafect transfection reagent with opti-MEM. The transfection mixture (solution A + solution B) was added to the cells to achieve final siRNA concentrations indicated in Table 6. The cells were then incubated at 37°C (5% CO_2) for 72 hours and collected for subsequent DPC isolation using the RADAR assay. A small aliquot of the cells was also collected for qPCR analysis to check the efficiency of gene silencing.

3.2.6. RNA isolation, reverse transcription, and qPCR analysis

Analysis of gene expression in adult and embryonic zebrafish tissues and mice tissues was performed by quantitative real-time polymerase chain reaction (qPCR). For adult tissues, RNA isolation was carried out using the Monarch Total RNA Miniprep Kit (NEB, T2040L). Tissue samples were homogenized using an Ultra Turrax T25 homogenizer (medium intensity for 60 seconds (13500 rpm)), and incubated with proteinase K at 55 °C for 5 min. Following the incubation, the RNA was purified according to the manufacturer's instructions. Tissue specimens of three animals (8 months old) were pooled together for the qPCR analysis due to small organ size as previously described (Glisic et al., 2015; Lončar et al., 2010, 2016;

Popovic, Zaja, & Smital, 2010; Popovic, Zaja, Loncar, et al., 2010). To ensure minimal RNA degradation, organs were carefully dissected on ice, and all surfaces and equipment were thoroughly cleaned with RNAse away solution. Frozen mouse tissues from single individuals of both genders (129S1/SvImJ WT, Stock No: 002448, 4-month-old) were used. Tissues from three females and three males were analysed. To quantify the expression of *tdp1*, *sprtn*, *tdp2a* and *tdp2b* genes during zebrafish embryonic development, 5 embryos per condition were collected at specific developmental stages: 6 hours post-fertilization (hpf), 1, 2-, 3-, 4-, and 5-days post-fertilization (dpf). Embryos were lysed with proteinase K in DNA/RNA protection buffer (NEB, T2040L) at 55 °C for 30 minutes and RNA was isolated using the Monarch Total RNA Miniprep Kit (NEB, T2040L). RNA samples were aliquoted and stored at -80 °C, while a portion of them was immediately reverse transcribed using the ProtoScript II First Strand cDNA Synthesis Kit (NEB, E6560L) yielding cDNA with concentrations above 50 - 100 ng/µL, which is suitable for subsequent gene expression analysis. The qPCR analysis was performed using the GoTaq qPCR mix (PROMEGA, A6001) and custom-designed primer pairs that span exon-exon boundaries, thereby eliminating any interference from genomic DNA amplification. The housekeeping ATP synthase peripheral stalk subunit OSCP, *atp50* (Gene ID: 335191) was used as a reference gene for normalization, because it shows similar expression in all samples analysed. The Qgene method (Simon, 2003) was used for quantification, and gene expression levels were expressed as Mean Normalized Expression (MNE). MNE values were calculated based on the primer efficiencies (E) and mean Ct values for both the housekeeping gene and the target gene, using the following formula: $MNE = E(HKG)^{Ct(HKG)} / E(gene)^{Ct(gene)} \times 10^6$. The Ct (cycle threshold) is the count of cycles needed for the fluorescent signal to surpass background levels. A lower Ct value indicates higher gene expression.

RNA isolation and qPCR analysis were performed on mouse tissues (129S1/SvImJ WT, 4-months old) to allow a comparative study. The same RNA isolation and cDNA synthesis protocols used for zebrafish samples were applied to mouse tissues. Tissues from three females and three males were analysed. The housekeeping gene *18S rRNA* was used for normalisation.

3.2.7. MTT viability test

The colorimetric MTT assay was used as an indicator of cell viability as previously described (P. Wang et al., 2010). This colorimetric method involves the reduction of a yellow tetrazolium salt (MTT) to form purple formazan crystals by metabolically active cells. Cells

with NAD(P)H-dependent oxidoreductase enzymes reduce MTT to formazan. The resulting solution is analysed by measuring absorbance at 500-600 nM with a spectrophotometer, where a darker solution indicates more viable, metabolically active cells. In brief, RPE1 cells were seeded in 24-well plates at 1.3 x 10^3 cells/cm^2 density and transfected with siRNA. After 72 hours, cells were incubated with 100 µL of a 5 mg/mL MTT solution (Alfa Aesar, L11939) for 3 hours. The solution was removed and 500 µL isopropanol (Kemika, 1622601) was added, followed by shaking at 350 rpm for 15 minutes (BioSan, PST -60HL-4, Plate Shaker-Thermostat). Absorbance was measured at 570 nm using a microplate reader (Tecan, Infinite M200).

3.2.8. Tdp1 activity assay

The Tdp1 activity assay was performed as described in Zaksauskaite *et al.* 2021. In brief, two-day-old mutant and WT embryos were deyolked in ice-cold PBS, and pelleted embryos were homogenized twice for 10 seconds (Ultra Turrax T25, IKA - Janke & Kunkel) in 200 µL of lysis buffer (200 mM Hepes, 40 mM NaCl, 2 mM MgCl2, 0.5% Triton X-100 with protease inhibitors (leupeptin, aprotinin, chymostatin, pepstatin at a concentration of 1 µg/mL and PMSF at a concentration of 1 mM) and incubated on ice for 30 minutes. Embryo lysates were incubated with a TDP1 oligonucleotide substrate (Table 5) containing a tyrosine at the 3' DNA end and Cy5 at the 5' end for visualization, which was purchased from Midland Certified Reagent Company. If TDP1 is active, a shift in the size of the oligonucleotide substrate becomes visible, indicating the removal of the tyrosine from the substrate. After incubation, the embryos lysates were centrifuged at 10,000 g for 5 minutes at 4°C. The resulting supernatant was collected, and the protein concentration was determined using the Bradford assay (M. M. Bradford, 1976). 600 ng total lysates of embryos were incubated with 2.5 µM labelled oligonucleotide substrate (Midland Certified Reagent Company) in activity buffer (25 mM Hepes (pH 8.0), 130 mM KCl, and 1 mM dithiothreitol (DTT)) in a final reaction volume of 10 µL. The reaction was incubated at 37 ºC for 1 hour in the PCR machine (T100 Thermal Cycle, Bio-Rad), and stopped by adding loading buffer (80% (w/v) deionized formamide, 1 mg/mL xylene cyanol, 1 mg/mL bromophenol blue, and 10 mM EDTA (pH 8.0)), followed by boiling at 90 ºC for 10 minutes. All samples were loaded onto a pre-run 20% homemade urea gel (pre-run on 80 V for 1 h) and run at constant voltage of 150 V for 1 hour. Reaction products were visualised using the ChemiDoc MP imaging system for detection of Cy 5 fluorescence (651 nm/emis 670 nm) (Bio-Rad, 1708280).

3.2.9. Tdp2 activity assay

The Cy5-labeled substrate (100 pmol) (Table 5) was mixed with a 20-bp complementary oligonucleotide (Table 4) containing a 5' overhang, in 33.3 µl dH2O. The mixture was denatured at 95 °C for 5 minutes and then reannealed by gradually reducing the temperature at a rate of 2 °C/s for 5 seconds, followed by 0.1 °C/s for 600 seconds using the gradient PCR (T100 Thermal Cycler, Biorad). This process generated a 3 µM dsDNA substrate oligomer with a 5' overhang, which is a model *in vitro* substrate for TDP2 (Gao et al., 2012). The TDP2 activity assay was performed as previously described (Zagnoli-Vieira et al., 2018; Zaksauskaite et al., 2021) with some modifications. Along with zebrafish samples, a control reaction consisting of human HEK293T cell lysate containing functional human TDP2 protein was used, as previously described (Zaksauskaite et al., 2021). Zebrafish embryos were deyolked in deyolking buffer (55 mM NaCl, 1.8 mM KCl and 1.25 mM $NaHCO_3$, pH 8.5) and washed twice with deyolking wash buffer (110 mM NaCl, 3.5 mM KCl, 2.7 mM $CaCl_2$ and 10 mM Tris-HCl, pH 8.5). The deyolked embryos and HEK cells were lysed in a solution containing 40 mM Tris/HCl pH 7.5, 100 mM NaCl, 0.1% Tween-20, 1 mM DTT, 1 mM PMSF, and protease inhibitors (leupeptin, aprotinin, chymostatin, pepstatin at a concentration of 1 µg/mL). The lysates were then sonicated for 30 seconds using a sonde sonicator with 3 µm peak-to-peak amplitude. Following sonication, the lysate was incubated for 30 minutes on ice and then centrifuged at 10,000 g for 5 minutes at 4 °C. The supernatant was collected, and protein concentration was determined using the Bradford assay (Bradford, 1976). Subsequently, supernatant containing 10 µg total proteins was mixed with 1 × activity buffer (50 mM Tris/HCl pH 8.0, 10 mM MgCl2, 80 mM KCl, 1 mM DTT,0.01% Tween-20), Cy5-labeled substrate oligomer (40 nM) and a competitor oligo (3 µM) (Table 4). The reaction was incubated for 1.5 hours at 37°C in a PCR machine, and stopped by the addition of 2x formamide loading buffer (80% (w/v) deionized formamide, 1 mg/mL xylene cyanol, 1 mg/mL bromophenol blue, and 10 mM EDTA (pH 8.0)) and incubating at 95 °C for 5 minutes. Samples were separated in a 20% polyacrylamide gel containing 8 M urea that had previously been run at 80 V for 1 hour. The gel was run for 2 hours at 100 V to achieve optimal sample separation and was visualized using the ChemiDoc MP imaging system.

3.2.10. Zebrafish mutant line creation

To generate a zebrafish line deficient in both Tdp1 and Tdp2 proteins, we chose to target the first exon of *tdp1*, as well as both *tdp2* orthologues, *tdp2a* and *tdp2b*. Fish lines were created using the gRNA/Cas9 (guide RNA/CRISPR-associated protein 9) system, with

target regions selected before important amino acid residues of all proteins (Figures 12A, 13 and 35). Fortunately, during the creation of the *tdp2a* premature stop line, we were able to remove the catalytically important E231, resulting in the generation of an additional zebrafish strain.

In addition to the creation of the *tdp1* premature stop line, we also generated a *tdp1* catalytic mutant line by targeting the catalytic residue H501. This point mutation was introduced using the *knock-in* system of gRNA/Cas9, where a template with the desired changes was introduced along with the complex. This allows for the repair of a DSB and the incorporation of the desired mutation.

3.2.11. sgRNA synthesis and microinjecting procedure

To generate a Tdp1-deficient mutant line, we introduced a mutation that resulted inin premature stop in Tdp1 protein sequence. For this purpose, first exons of zebrafish Tdp1 were searched for a PAM sequence (protospacer adjacent motif, NGG) where sgRNA/Cas9 complex would bind, using CRISPR scan algorithm (Moreno-Mateos et al., 2015). We chose 5'GAATGTGGGGGTCTCTTC3' as the DNA template for sgRNA with the highest score of 54 and a low off-target effect of 4.63 CFD (cutting frequency determination). Score numbers represent the chance of on-target cleavage efficiency of Cas9, with a higher score indicating greater specificity on a scale of 1 - 100, and CFD reflects the cutting efficiency of potential off-targets, with lower CFD indicating lower chance of off-target effect on a scale of 1-100 (Doench et al., 2016).

The gRNA was generated as previously described (Modzelewski et al., 2018). In brief, the short DNA oligo (guide DNA template) complementary to the sgRNA sequence was synthesised by Macrogen Europe, amplified by PCR, and inserted between two short DNA sequences, one containing the T7 promoter and the second sequence complementary to the scaffold template which were ordered from Macrogen (Figure 10). In the PCR mixture, we combined the guide DNA template, the IVT-T7- F primer annealing at the beginning of the template (T7 promoter), the scaffold template, and the OLIGO-SCAFF-R primer that sits at the end of the scaffold sequence (Table 4). The PCR product was resolved on 1% agarose gel, purified using monarch PCR & DNA cleanup kit (New England Biolabs, T3010) and reversely transcribed *in vitro* using the MEGAshortscript™ T7 Transcription Kit (Invitrogen™, AM1354). *In vitro* transcription was performed according to the manufacturer's instructions, and the transcribed RNA was purified using the Monarch® RNA Cleanup Kit (NEB, T2040L), RNA concentration was measured using nanodrop (BioSpec-nano,

Shimadzu), and the sgRNA was aliquoted and stored at -80 °C. On the day of injection, guide RNA was incubated with Cas9 protein in a 1:1 ratio for 5 min at 37 °C. The sgRNA/Cas9 complex was diluted in 0.015% Phenol-red / 300 mM KCl solution and pipetted into a Femtotips needle (Eppendorf, 5242957000) and needle was connected to a microinjector (Eppendorf, FemtoJet® 4x).

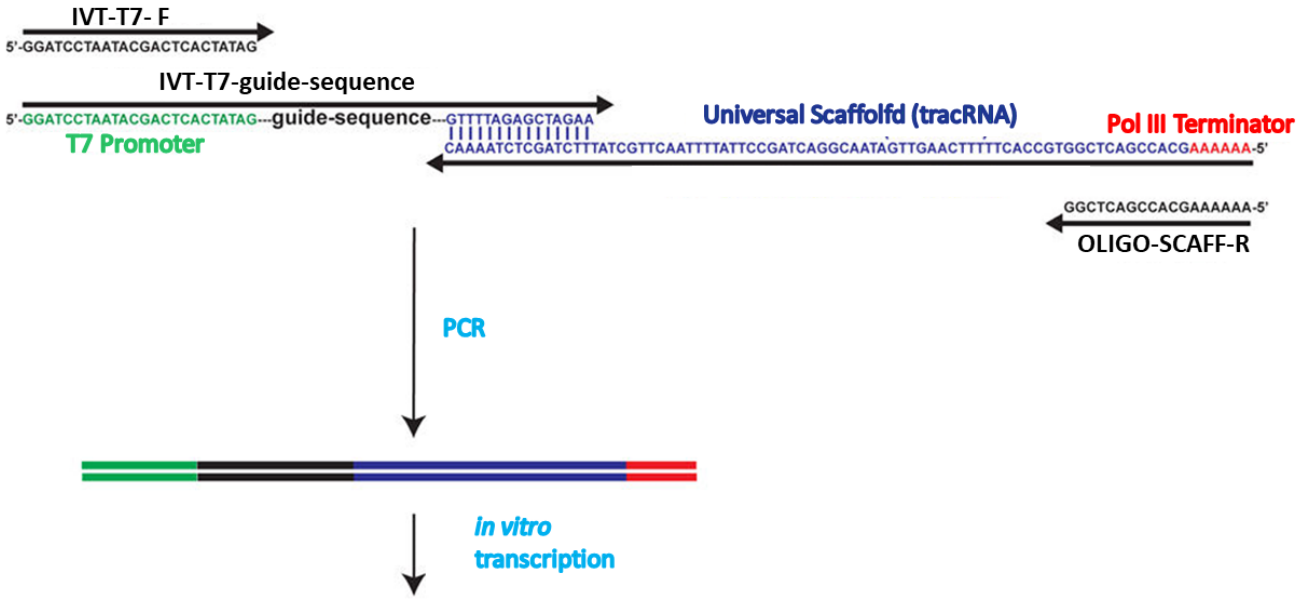

Figure 10: Schematic Illustration of sgRNA generation. The guide generated using with a set of PCR primers (depicted in black: IVT-T7-F and OLIGO-SCAFF-R), a shared reverse template oligo (depicted in blue/red: Universal-Scaffold), and an oligo carrying a 5' T7 promoter alongside a gene specific target sequence (shown in green/black/blue: IVT-T7-guide). Adapted from (Modzelewski et al., 2018).

In order to create a mutant strain bearing catalytically inactive Tdp1 (C23572G and A23573C, resulting in H501A alteration at the protein level), a *knock-in* approach was followed according to the protocol of Hoshijima et al., was followed. In brief, a DNA donor template was co-injected with the gRNA/Cas9 system in order to introduce the desired mutations after induction of DSB. This DNA template is referred to as the "repair template" (RT) and included a fluorescent reporter gene for easier screening of positive introduction events. In this study, the mVenus reporter was used under the control of the α-crystalline promoter. This promoter triggers the expression of the fluorescent reporter protein specifically in the zebrafish lens, indicating successful genomic integration of the RT carrying target mutation. A 5'GGTAGAGTGCGTACTCCAG3' guide targeting intron 12 was selected, based on a high

score of 74 and a low theoretical off-target effect of 7.23 CFD using a CRISPR scan software (Moreno-Mateos et al., 2015). 2 µL of microinjection mixture containing sgRNA (Table 2.4), Cas9 (600 ng) in a 1:1 molar ratio, RT at a final concentration of 50 ng/µl, 0.015% Phenol-red and 300 mM KCl was pipetted into Femtotips needle and approximately 1 nL of solution was injected into one cell stage embryos with Eppendorf microinjector.

To create a Tdp2a-deficient zebrafish line, a mutation resulting in a premature stop codon was induced by targeting exon 3 using a guide with a score of 27 and a low CFD of 4.30. The procedures for guide preparation and microinjection were identical to those used to generate the Tdp1-deficient line. Furthermore, using the same guide, a Tdp2a-deficient zebrafish line with a catalytic mutation ΔE231 (delAGC at positions 3122/3/4 on genomic DNA) was also successfully established.

For the creation of the Tdp2b-deficient zebrafish line, a mutation which led to the introduction of premature stop in Tdp2b protein sequence was introduced as described above. The guide 5'GGTGACACTGCTGAAGCTTC3' targeting exon 2 was selected with a high score of 48 and a low CFD of 8.62.

3.2.12. Repair template creation

To generate a catalytically inactive mutant of zebrafish Tdp1 with two point mutations in the active site (C23572G and A23573C, resulting in H501A alteration at the protein level), a repair template was created following the protocol described by Hoshijima, Jurynec and Grunwald, 2016. The repair template was designed with left and right homology arms flanking the mVenus reporter gene, regulated by the α-crystallin promoter. First, a 600 bp long left homology arm (LA) was generated from genomic DNA isolated from 3-dpf zebrafish embryos, using primers listed in Table 4. These primers were designed to integrate *NotI* (R0189S, NEB) and *BamHI* (R0136S, NEB) cutting sites at the ends of LA, to ensure precise integration into the pkHR5 plasmid. A similar procedure was followed to construct the right homology arm (RA) using primers listed in Table 4, where *SalI* (R0138S, NEB) and *Xhol* (R0146S, NEB) restriction sites were introduced at the ends of the 600 bp long RA. To incorporate the LA into the pkHR5 plasmid InFusion recombinant cloning was used (J. Park et al., 2015). InFusion cloning is based on the annealing of complementary ends of a cloning insert amplified with the primers carrying a part of the host plasmid sequence and a linearized cloning vector. To incorporate LA, *NotI* and *BamHI* restriction enzymes were used to linearize the plasmid following manufacturer instruction, and the generated linear plasmid was then combined with the LA with sticky ends, generated by In-Fusion primers specific to

the *NotI* and *BamHI* sites. Ligation was performed according to the instructions for In-Fusion® HD Cloning (102518, Takara Bio USA). Following ligation, the pkHR5 plasmid with the integrated LA was transformed into Dh5α *E. coli* cells (Life Technologies, CA, 18265017). Only clones harbouring the circular plasmid survived ampicillin selection (100 µg/ml). These clones were subsequently amplified, and plasmid was isolated using the Zyppy plasmid miniprep kit (Zymo research, D4036). Integration of LA was confirmed by sequencing with the primer listed in Table 4. A similar approach was used for introducing the RA into the pkHR5 plasmid with confirmed LA integration. *SalI* and *Xhol* restriction enzymes were used to linearize the plasmid. The resulting linearized plasmid was then combined with the RA via sticky end ligation, generated by In-Fusion primers for *SalI* and *Xhol* restriction sites (Table 4). The circular plasmid, now containing both the LA and RA, flanking the mVenus reporter gene regulated by the α-crystallin promoter, was transformed into Dh5α cells. Positive clones were identified and amplified, followed by plasmid isolation and sequencing using the primers listed in Table 4. Site-directed mutagenesis was used to introduce the catalytic changes C23572G and A23573C (location of changes is shown on gDNA) were introduced into the RA. To prevent undesired Cas9 cleavage of the repair template itself, a point mutation G23273A was introduced that effectively converted the NGG site of Cas9 cleavage (in this case CGG) to NNG (in this case CAG) (Figure 15A). These modifications were introduced using the primers listed in Table 4 and a Site-directed mutagenesis kit (200523, Agilent) following manufacturer's instructions. The repair template was then amplified in *E. coli* Dh5α cells, and the recombinant plasmid was sequenced (Macrogen). Before the injection, the plasmid was linearized with the *SceI* restriction enzyme (R0694S, NEB) (Figure 15B) following manufacturer's instructions, followed by DNA purification.

3.2.12.1. Founder fish identification

3.2.12.1.1. High resolution melting curve (HRM) analysis

HRM analysis is a post-PCR method used to identify genetic variations in nucleic acid sequences. The process begins with a PCR reaction amplifying the target region in the presence of a fluorescent dye that binds to dsDNA. Amplification is followed by a high-resolution melting step occurs, where the dsDNA dissociates into single strands, leading to changes in fluorescence due to the release of the dye. As the temperature increases, denaturation of the dsDNA takes place, resulting in a decrease in fluorescence. The largest

decrease in fluorescence is observed near the melting temperature (T_m) of the PCR product. The T_m indicates the temperature at which 50% of the DNA is double-stranded and 50% is single-stranded (melted), and it depends on the properties of the PCR product: GC content, length, and sequence (Lay & Wittwer, 1997). The outcome of HRM analysis is a specific melting curve profile for the amplicon, that enables mutation screening, genotyping, methylation analysis, and other applications (Słomka et al., 2017). In this study, HRM analysis was used to genotype injected zebrafish embryos, as well as adults of F0, F1 and F2 generation. Primers for HRM analysis were designed using Primer-BLAST software (NCBI, National Centre for Biotechnology Information) to amplify a 90-130 bp product around the gRNA target site in genomic DNA. To predict and select a single melting curve sequence of the desired product, uMELT software was used, which calculates the T_m temperature and predict the melting curve (Dwight et al., 2011). The reaction mixture consisted of 5 μL of the commercial MeltDoctor™ HRM Master Mix Kit, 0.6 μL of forward and reverse primers (5 μM each), 0.5 μL of genomic DNA, and 3.3 μL of ultrapure water. The prepared reaction mixtures were loaded into a 96-well microplate and briefly centrifuged (5 min, 4°C, 500 g). The PCR reaction was then conducted with an initial incubation at 95°C for 10 minutes, followed by 40 cycles of: 95°C for 15 seconds, 60°C for 1 minute, and 95°C for 10 seconds, a single cycle of 60°C for 1 minute, and a final high-resolution melting step at 95°C for 15 seconds and 60°C for 15 seconds using the StepOnePlus™ Real-Time PCR System (7300 Real Time PCR System Applied Biosystems) . The obtained results were analysed using High Resolution Melt Software v3.2 (Słomka et al., 2017).

3.2.12.1.2. Genotyping using cloning and sequencing

To confirm the presence of inserted mutations, individuals that tested positive in HRM analysis, were analysed by sequencing of the genomic region of interest. The first step consisted of amplifying the region of interest using Phusion® High-Fidelity DNA Polymerase (NEB) and the primers used in the HRM analysis (Table 4.). The PCR reaction mixture was prepared by combining 5 μL of 5x Phusion HF buffer, 0.5 μL of 10 mM dNTPs, 1.25 μL of 10 μM forward and reverse primers, 1 μL of genomic DNA, 0.25 μL of Phusion DNA polymerase, and 15.75 μL of ultrapure water. The PCR reaction was subjected to the following incubation: 98°C for 30 s, followed by 35 cycles of: 98°C for 10 s, annealing at a temperature specific to the primers used for 30 s, 72°C for 15 s, and a final extension at 72°C for 10 min. Phusion DNA polymerase generated a blunt-ended PCR product, which was cloned into the pJET1.2 vector using the CloneJET PCR Cloning Kit (Thermo Fisher

Scientific, K1232). The efficiency of the PCR reaction was confirmed by agarose gel electrophoresis, and DNA amplicons were purified from the PCR mixture using the DNA/PCR clean-up kit (NEB). For ligation, the linearized cloning vector pJET1.2/blunt was used, which accepts inserts ranging from 6 bp to 10 kb. This vector contains a lethal gene that is disrupted upon ligation of a DNA insert into the cloning site, ensuring that only cells with recombinant plasmids can replicate. Additionally, the vector harbours an ampicillin resistance gene, allowing only transformed cells to survive in the presence of this antibiotic. The amount of PCR product added to the ligation reaction was determined based on the size of the PCR product according to the manufacturer's instructions (CloneJET PCR Cloning Kit, Thermo Fisher Scientific) and the ligation mixture was incubated at 22°C for 30 minutes followed by transformation into bacterial competent *Escherichia coli* DH5α cells according to the manufacturer's instructions (Invitrogen, 18265017). In brief, 1 µl of the ligation reaction was mixed with 25 µl of competent cells, the cells were subjected to heat shock at 42°C for 30 s, and then incubated on ice for 2 min. Cells were then incubated in LB medium at 37°C for 1 hr and shaken with a shaker at 225 rpm (Eppendorf, New Brunswick Innova 40/40R). Transformed cells were then plated onto agar plates containing ampicillin (100 µg/ml) and incubated overnight at 37°C. The following day, bacterial colonies were transferred to 5 ml tubes containing 3 ml of LB medium with ampicillin (100 µg/ml) for overnight incubation in a shaker incubator at 37°C (225 rpm).

Plasmid DNA was isolated from the obtained bacterial cultures using the commercial Zyppy™ Plasmid Miniprep Kit (D4019, Zymo research). The isolated plasmids containing the integrated DNA amplicon were sent for sequencing using sequencing primer (pJET1.2 Forward Sequencing Primer: 5' CGACTCACTATAGGGAGAGCGGC 3') and the EZ-seq DNA sequencing service from Macrogen (Amsterdam, The Netherlands). The obtained sequencing results were analysed using BioEdit Sequence Alignment Editor software (Hall, 1999).

3.2.12.1.3. Detection of fluorescent reporter of RT integrated embryos

After microinjection of embryos with RT and sgRNA/Cas9, embryos were grown in Petri dishes containing E3 media at 28°C for 2 days. One day before the detection, casting molds were prepared using zebrafish microinjection and transplantation molds (Z-MOLDS) with 3% agarose in water. Prior to imaging, the two-day-old embryos were anesthetized with tricaine methanesulfonate (MS-222) (0.02% in E3 media) for 10 minutes and then placed in an agarose mold in a lateral orientation so one lens of the eye is visible. If the repair template

which bears homology arms and α-crys::Venus gene was incorporated, the eye lens will fluoresce green, as the Venus gene (expression peak at 475 nm (blue) and emission peak at 509 nm (green)) is located under the α-crystallin promoter in the pkHR5 plasmid and is specifically expressed in the lens (Hesselson et al., 2009). Embryos were imaged on a binocular (SMZ-171, Motic) using a green filter (Royal Blue Fluorescence Viewing System,NIGHTSEA) with an attached Full HD Camera (Moticam 1080) after excitation at 475 nm (blue). Embryos with green fluorescence in the lens were grown to adulthood and used for further experiments.

3.2.12.1.4. Detection of the repair template in zebrafish genome using sequencing

Confirmation of the precise integration of repair template at the exact genomic location was achieved by sequencing. Integration of the left homology arm (LA) was confirmed using primers DrTdp1-seq-LA from Table 4. The forward (F) primer was positioned downstream of the genomic region outside the RT, while the reverse primer (R) was placed in the plasmid backbone of the RT (Supplement 4). A PCR was conducted using genomic DNA isolated from two positively fluorescent female F0 embryos, and the resulting PCR mixture was analysed on a 1% agarose gel. The DNA fragment, encompassing a portion of the genomic part, LA and the plasmid backbone, was extracted from the gel using a kit, subsequently cloned into pJET, and sequenced with the pJET-F primer listed in Table 4. The same approach was applied to confirm the integration of the right homology arm (RA). For the validation of RA integration, the F primer was positioned at the start of the RA, while the R primer was placed upstream of the RA in the genomic region (Table 4, Supplement 5). Following PCR, the DNA fragment containing RA and a part of the gDNA was purified, cloned into pJET, and sequenced. In addition, the middle part of the RT which includes the mVenus reporter gene, promoter, and plasmid backbone, was also sequenced. The same genomic DNA used to determine the genomic position of LA and RA was used to detect the middle part of RT. PCR was performed using the primers listed in Table 4, with the forward primer (F) positioned within the plasmid backbone and the reverse primer (R) positioned in the middle of RA (Figure 15, Supplement 6).

3.2.12.1.5. Southern blotting

To investigate whether the repair template was integrated into the genome at one site, we performed Southern blot analysis. Southern blotting involves transferring of DNA

fragments from an agarose gel to a solid support, usually a nylon membrane. Once the DNA fragments are immobilized on the membrane, they can be hybridized with specific probes to detect the target sequence (Tofano et al., 2006).

Genomic DNA, from lens positive embryos, was analysed after the digestion with the *Eco RI* (R0101S, NEB) restriction enzyme which was chosen due to its high cutting frequency of gDNA. To design the experiment, Clone manager software (Clone Manager 9.0) was used to predict target sequence. We selected 10,000 base pairs upstream and downstream from the predicted *knock in* integration site. The selected sequence was then analysed to identify cutting sites for the *Eco RI* enzyme. For the experimental procedure, 10 µg of genomic DNA isolated from wild-type and lens positive embryos was digested with the *Eco RI* enzyme overnight at 37°C in a PCR machine and separated on a 0.8 % agarose gel in TAE buffer (40 mM Tris-HCl, pH 8, 20 mM acetic acid, and 1 mM EDTA) containing 1 µl of GelRed for DNA visualization. Electrophoresis was performed at 60 V for 5 h to ensure optimal separation of DNA fragments according to size. The separated DNA fragments were visualized using a ChemiDoc™ For the alkaline capillary transfer, the DNA depurination step was carried out by incubating the gel in 0.25 M HCl for 10 minutes with gentle agitation, followed by neutralization with 0.5 M Tris-HCl pH 7.5 for 2 x 15 minutes with gentle agitation. The DNA fragments were then transferred onto a positively charged nylon membrane, which had previously been soaked in distilled H_2O and carefully placed on top of the gel to facilitate the transfer. To ensure a stable transfer setup, two filter papers were arranged to match the gel size, and a stack of paper towels (6 cm heigh) was used to apply gentle pressure. A long filter paper was placed over the carrier tray, with both sides immersed in 0.4 M NaOH. The gel was placed face down on the wet filter paper, then the nylon membrane was carefully placed on top of the gel. Two additional filter papers and the stack of paper towels were then added on top of the membrane, and everything was covered with a glass plate. A weight of about 250 g was placed on the glass plate to apply an even pressure. The transfer was left to proceed overnight.

The efficiency of the transfer was confirmed by visualizing the DNA on the nylon membrane under the UV light. To permanently immobilize the DNA on the membrane, the gel was exposed to UV light for 10 minutes. Now that the DNA was firmly immobilized on the nylon membrane, it was prepared for the next step, probe hybridization. The probe was generated through DIG-DNA labelling following the manufacturer's instructions (Roche, cat. no. 11636090910) and using the primer pair listed in Table 2.4. The probe sequence can be found in Supplement 4. To ensure proper hybridization, probe was designed to be approximately

500 bp in size, following the recommended size for DIG-labelling. Additionally, the specificity of the probe sequence was checked by blasting it against the whole zebrafish genome. The GC percentage of the probe sequence was also monitored, as the hybridization temperature depended on it, aiming for a range between 60°C and 68°C. To determine the optimum hybridization temperature (T_{hyb}), the T_{hyb} temperature was calculated using the formula $T_{hyb} = T_m - 25°C$. The Tm value was obtained by applying the formula $T_m = 16.6 \log c\ (Na^+) + 0.41\ (\%\ (G+C)) + 81.5$, where c ($Na^+$) is molar concentration of Na^+ in the hybridization buffer (kept at -20°C until use) and % (G+C) is the percentage of guanine and cytosine bases in the probe sequence. The hybridization buffer used in this study contained 0.25 M phosphate buffer (pH 7.2), 1 mM EDTA (pH 8.0), 200 g/dm^3 SDS, and 5 g/dm^3 blocking reagent (Roche, 11363514910). The hybridization temperature of the mVenus probe was 68°C.

For the hybridization process, the nylon membrane was placed in a hybridization tube (308-9, Labe-Line) with the "DNA-bound" side up. Then,10 mL of hybridization buffer without the DNA probe was added to the tube, which was then closed and placed in a hybridization oven (Biometra OV3) for 2 hours at the hybridization temperature of 68°C. For the hybridization step itself, the DIG-labelled DNA probe was denatured by heating at 100°C for 10 minutes in a thermoblock (Thermomixer 5436, Eppendorf), following by fast cooling on ice (5 minutes) and then prompt spin down to ensure homogeneity. Next, 2 µL of the denatured probe was added per 1 mL of hybridization buffer, resulting in a final probe concentration of 10 ng/mL. The prepared probe was added to the hybridization buffer that had been preheated to the specified hybridization temperature of 68°C. This allowed for the hybridization of the probe with the immobilized DNA fragments on the nylon membrane. To proceed with probe hybridization, the pre-hybridization buffer was removed from the tube and replaced with the hybridization buffer containing the DNA probe. The membrane was then hybridized overnight so that the probe could bind to its complementary DNA sequences on the membrane. To wash off excess DNA probe, the membrane was washed 3 x 20 minutes in 15 mL preheated washing buffer (20 mM Na_2HPO_4, 1 mM EDTA, pH 8.0, 10 g/dm^3 SDS at a temperature 5°C lower than the hybridization temperature.

The DIG luminescence detection kit (Roche, 11363514910) was used to detect the DIG - labelled DNA probes. The detection procedure began by transferring the membrane to a plastic tray with buffer 1 (0.1 M maleic acid, pH 8, 3 M NaCl, 0.3% (v/v) Tween 20), 5-minutes incubation with gentle agitation and incubation in buffer 2 (prepared by dissolving blocking reagent from the kit (1% (m/V)) in buffer 1) for 60 minutes. Next, the anti-DIG

antibody conjugated with AP was diluted in buffer 2 at a 1:10,000 ratio, and the membrane was incubated in this solution for 30 minutes, transferred to a clean plastic tray with buffer 1 and washed 5 x 10 minutes in buffer 1. The membrane was then incubated twice for 5 minutes in buffer 3 (0.1 M Tris-HCl, pH 9.5, 0.1 M NaCl) before being transferred to a clear plastic bag (office bag) for the remaining steps. The hybridized probes are immunodetected with anti-digoxigenin, Fab fragments conjugated to alkaline phosphatase and visualized with the chemiluminescence substrate CSPD. CSPD (3-{5-chloro-3'-methoxyspiro [adamantane-2,2'-[1,4] dioxetane]-3'-yl}phenoxyphosphonic acid) is a chemiluminescent substrate used with alkaline phosphatase for sensitive detection of biomolecules which decomposes and emits light at a maximum wavelength of 477 nm. The emitted light is captured on X-ray film or luminescence imager systems (Martin et al., 1995). Within the DIG system, digoxigenin is introduced during probe amplification, functioning as an epitope recognized by anti-DIG-Fab. This anti-DIG-Fab is conjugated with alkaline phosphatise (anti-DIG-AP).This system enzymatically dephosphorylates the CSPD substrate, to form anions that eventually decompose, resulting in light emission at 477 nm. All the steps involving CSPD substrate were done under red light conditions to prevent any exposure to UV or bright light. CSPD substrate (Roche, 11363514910) was diluted at a 1:100 ratio in 1 mL of buffer 3. The substrate was spread evenly on the membrane and incubated for 10 minutes. After the incubation, the excess CSPD solution was carefully squeezed out from the bag and cleaned to avoid any potential background signal. The hybridization signal was detected with chemiluminescence on a ChemiDoc™.

3.2.13. Gene silencing in zebrafish embryos using morpholino oligonucleotides

Morpholino oligonucleotides are synthetic oligonucleotides that act by binding to the complementary RNA sequence of a target gene. They are introduced to either interfere with mRNA translation by binding to the 5'-UTR region or the ATG site of the mRNA, or to prevent splicing of the pre-mRNA by targeting the exon-intron boundaries. They are known to be very stable, allowing gene silencing for several days (up to 6 days) (Moulton, 2007). Two morpholino oligonucleotides, one targeting the 5'-UTR region and the other targeting the exon 2-intron 2 boundary were designed were designed to block transcription of the *sprtn* gene in zebrafish (Table 5). The morpholino oligonucleotides were ordered from Genetools (USA) and were used as described in Nasevicius and Ekker, 2000. In brief, for microinjection, a mixture containing 250 µM of each morpholino oligonucleotide, 300 mM KCl, and 0.015% phenol red was injected into one-cell stage zebrafish embryos. Two-day-old morphants were

collected for qPCR and RADAR experiments. Total RNA was extracted from the embryos using the Monarch Total RNA Kit (NEB, T2040), and equal amounts of RNA were reverse transcribed using the High-Capacity cDNA Kit (Applied Biosystems™, 4368814). The efficiency of the splicing blocking morpholino was verified using PCR on cDNA samples, and the silencing efficiency was quantified using ImageJ (Abràmoff et al., 2004). For the *tdp2a* and *tdp2b* genes, splice-blocking antisense morpholino oligonucleotides were designed and ordered from Genetools LLC (Table 5). The morpholino oligonucleotide targeted the exon 3 - intron 3 boundary of *tdp2a* and the exon 2 - intron 2 boundary of *tdp2b*. Each morpholino oligonucleotide was diluted in a 0.015% Phenol-red / 300 mM KCl solution to obtain specific injection mixtures. For *tdp2a*, the injection mix contained 500 µM *tdp2a*MO, for *tdp2b*, it contained 200 µM *tdp2b*MO, and for the double knockdown, it contained 500 µM of *tdp2a*MO and 200 µM of *tdp2b*MO. The morpholino oligonucleotides were injected into zebrafish eggs between the one and four-cell stage. To verify the efficiency of the silencing, RNA was extracted from the injected embryos at 2 dpf, and reverse-transcribed to cDNA. PCR reactions were then performed on these cDNA samples using specific primer pairs targeting the respective genes (Table 4). The resulting amplified DNA fragments were separated using 1% agarose gel electrophoresis. Changes in the size of the amplicons derived from morpholino oligonucleotide injected embryos indicated successful splice-blocking activity of the morpholino oligonucleotide. Similar approach was used to silence the *zatt/znf451* and *mre11* genes. Given that zebrafish have two isoforms of the *zatt* protein (long and short), splice-blocking morpholino oligonucleotides were designed to target both isoforms (Figure 50A). The splice-blocking morpholino oligonucleotide for *zatt/znf451* targets exon 7 - intron 7 boundary in the long isoform and exon 2 - intron 2 boundary in the short isoform. This morpholino oligonucleotide was injected into zebrafish eggs at the one-cell stage with two different concentrations: 100 µM and 300 µM. To assess the efficacy of *zatt/znf451* silencing, RNA was extracted from injected embryos at 2 dpf and reverse-transcribed into cDNA. Subsequent PCR reaction using specific primers for the *zatt/znf451* gene (Table 4) was performed on these cDNA samples. PCR amplicons were separated using 1% agarose gel electrophoresis. The size changes of the morpholino oligonucleotide injected embryos indicated successful splice-blocking activity. Silencing of the *mre11* gene was achieved using a morpholino oligonucleotide targeting the ATG region on the mRNA to prevent translation. Similar to *zatt/znf451* protein silencing, two different concentrations of morpholino oligonucleotide (100 µM and 300 µM) were injected into one-cell stage embryos

for *mre11* silencing with 300 mM KCl and 0.015% phenol red. Embryos were monitored for 5 days, and resulting phenotypes were documented by imaging.

3.2.14. The characterization of embryonic phenotypes in zebrafish

Phenotypes of zebrafish embryos were observed and recorded throughout the development from 1-dpf until 5-dpf. Embryos were manually dechorionated using tweezers and imaged using a Samsung 13-megapixel camera with an f/1.9 aperture applied to the ocular of Motic SMZ-171 binocular. Phenotypes were observed in all mutant lines in this study (*tdp1*$^{-/-}$, *tdp2a*$^{\Delta E231}$, and *tdp2b*^{97STOP}), as well as in embryos subjected to gene silencing (*sprtn*, *tdp2a*, *tdp2b*, *tdp2a/2b* combination, *zatt* and *mre11*). Deviations from WT controls were documented alongside representative images and marked with arrows. We focused on the changes in the brain and eye size, which were already observable by 2-dpf and serve as indicators of neurological issues (Sakai et al., 2018). Additionally, on the second day after dechorionation, we monitored their ability to stretch and twitch, indicating muscular problems (Snow et al., 2008). By 5-dpf, we searched for edema as a sign of heart issues (Narumanchi et al., 2021; Werdich et al., 2012) and observed the presence of a swim bladder, enabling water movement. Continuous 5-day monitoring showed whether the embryos were “using" the yolk efficiently, reflecting developmental progress.

3.2.15. DPC isolation using modified RADAR Assay

In this study, we modified and improved for the DNA adduct recovery assay (RADAR) (Kiianitsa & Maizels, 2013, 2020) in human cells to increase processivity and reduce variability within and between experiments. In addition, we developed a DPC isolation protocol specifically for 2-day-old zebrafish embryos, as published in Anticevic *et al.*, 2023.
For DPC isolation, we used two distinct biological models: human cells (RPE1) and zebrafish embryos. Human RPE1 cells were lysed in 1 mL of prewarmed DPC lysis buffer (6M guanidinium isothiocyanate, 10 mM Tris-HCl (pH 6.8), 20 mM EDTA, 4% Triton X-100, 1% N-lauroylsarcosine sodium, 5% β-mercaptoethanol) at 55°C for 10 minutes in 1.5 mL tubes in a water bath. The lysate was subjected to DNA precipitation by adding an equal volume of 100% ethanol, followed by centrifugation at 10,000 x g for 10 minutes at 4°C. The resulting DNA pellet was washed three times with wash buffer (20 mM Tris HCl pH 7.5, 50 mM NaCl, 1 mM EDTA, 50% ethanol) and dried for 5 minutes at 55°C in a thermoblock. After drying, the DNA was dissolved in 1 mL of 8 mM NaOH. For zebrafish embryos, we collected 2-day-old embryos and lysed 30 embryos per condition using prewarmed lysis buffer at 50°C for 10

minutes in a water bath. The subsequent steps of DNA precipitation and washing were as described above for RPE1 cells.

To quantify the DNA content in the isolated DPC samples, we treated a 25 µL aliquot of each sample with proteinase K (20 mg/mL) for three hours at 55°C, and subsequently analysed it using the Pico Green assay following the manufacturer's instructions (Invitrogen, P7581). The DNA content in the DPC samples was normalized based on the sample with the lowest amount of DNA. After normalization, the DPC samples were treated with DNAse (Millipore, E1014) for 1 hour at 37°C in thermoblock to remove DNA. The treated samples were then snap-frozen in liquid nitrogen and subjected to overnight lyophilization using a FreeZone 2.5 lyophilizer (Labconco, USA) under a freeze-drying condition of -48°C (5 Pa vacuum). The lyophilized DPC samples were then dissolved in 50 µL of SDS loading buffer containing 4 M urea, 62.5 mM Tris-HCl (pH 6.8), 1 mM EDTA, and 2% SDS.

3.2.16. Detection and quantification of DPCs

To detect total DPCs, we used SDS-PAGE (Sodium dodecyl-sulfate polyacrylamide gel electrophoresis) gradient gel (5-18%) to resolve the isolated DPCs. The resolved DPCs were visualised using the ProteoSilver™ Silver Stain Kit according to the manufacturer's protocol (Sigma Aldrich, PROTSIL1). For specific DPC detection from human cells, we used dot blot analysis on nitrocellulose membranes (GE Healthcare, 10-6000-02) or western blot with protein-specific antibodies. For DPCs isolated from zebrafish embryos, samples were resolved using SDS-acrylamide gradient gel (5-18%) and transferred to PVDF membranes (Roche, 03010040001) for Western blotting. To detect specific proteins, we performed immunostaining using antibodies targeting histone H3, TOP1 and TOP2. For detection of histone H3, 200 ng of DNA-normalized DPCs were subjected to either dot blot or Western blotting and immunostained with anti-H3 antibody (Cell Signaling, #9715, 1:3000). For detection of TOP1 and TOP2 detection, we used 500 ng of DNA-normalized DPCs for dot blot analysis and quantified them with anti-TOP1 antibody (Cell Signaling, #38650, 1:1000) or with anti-TOP2 antibody (Abcam, ab52934. 1:1000). An equivalent of 1 µg of DNA-normalized DPCs from embryos was first separated on SDS-acrylamide 4M urea gradient gel, then transferred to aPVDF membrane and detection with anti-TOP1 Antibody (Bethyl, A302-589A, 1:1000). In addition, the equivalent of 1 µg of DNA-normalized DPCs from both, HEK WT cells and ETO-treated HEK cells, and1 µg of DNA-normalized DPCs from WT embryos and tdp2- morpholino oligonucleotide silenced embryos, were resolved on an SDS-acrylamide gradient gel (5-18%) containing 2.5 M urea. The gel was pre-run for 30 minutes at

80 V, and the DPCs were allowed to resolve for 1 hour at 100 V. After wet transfer and subsequent blocking, the membranes were incubated with the anti-TOP2 antibody (Abcam, ab52934. 1:1000) overnight.

To verify the accuracy of DNA quantification and DPC normalization, 10 ng of DNA from the sample treated with proteinase K was diluted in 1 mL TBST buffer. A nylon membrane was pre-wetted in TBST for 1 min, placed on a dot blot apparatus and sealed. Wells were washed with 200 µL of TBST buffer which passed through the dots by vacuum-induced aspiration (Vacuum pump, Buchi B-177, 1000 hPa) and 200 µL of the sample was added. Following this step, the wells were washed once more with 200 µL of TBST. After this step, the wells were washed again with 200 µL of TBST. Then, only the parts of the membrane containing the sample were carefully cut off, air-dried for 15 minutes, and the DNA was crosslinked by exposing the membrane to UV light (UV-Transilluminator (312 nm), Bachofer for 5 minutes. After a two-hour blocking step, the membrane was incubated overnight with α-dsDNA antibody (Abcam ab27156, diluted 1:7000).

3.2.17. DSB quantification using yH2AX Western blot analysis

Wild type (WT) zebrafish embryos and embryos with silenced *tdp2a*, *tdp2b*, and both *tdp2a* and *tdp2b* as well as $tdp2a^{\Delta E231}$ and $tdp2b^{97STOP}$ mutants were collected at different developmental time points: 6 hours post fertilization, 1 day post fertilization, and 2 days post fertilization. Each condition included 15 embryos for detection. All samples were treated as previously described in Anticevic et al., 2023. In brief, embryos were subjected to lysis using RIPA buffer (150 mM NaCl, 1% Triton X-100, 0.50% Na-deoxycholate, and 50 mM TrisHCl (pH 8)) containing 0.5% SDS and sonicated for 20 sec (sonde sonicater with 3 µm peak-to-peak amplitude). Lysates were then incubated on ice for 30 minutes. Protein concentrations were determined using Bradford assay (M. M. Bradford, 1976), and embryo lysates containing 15 µg of proteins were subjected to Western blot analysis. For the analysis, the samples were boiled for 5 minutes at 95°C in 5x Laemmli buffer (50 mM Tris-HCl (pH 6.8), 2% SDS, 10% w/v glycerol, 0.05% bromophenol blue, and 5% β-mercaptoethanol). Total proteins were separated on homemade gradient gels (5-18%) using SDS-PAGE and Mini-PROTEAN 3 Cell electrophoresis chamber (Biorad). Blocking was performed with 5% lowfat milk (T145.1, Carl Roth) in TBST (10 mM Tris-HCl (pH 7.5), 150 mM NaCl, 0.02% Tween 20) for 2 hours with gentle rocking at room temperature. The membranes were then washed and incubated with anti-yH2AX antibody (Abcam, ab81299, 1:2500) in 2.5% BSA TBST

buffer overnight at 4°C (gentle rocking, Labnet, ProBlot™ 35). Anti-Tubulin antibody (Santa Cruz, sc-134238, 1:7000) was used as a loading control. The following day, the membranes were washed three times for 5 minutes with TBST buffer and then incubated with a secondary antibody, goat anti-rabbit IgG-HRP (Sigma-Aldrich, a0545, 1:100,000) for yH2AX and goat anti-mouse IgG-HRP (diluted 100,000-fold) for tubulin, with gentle shaking at RT for 1 hour (Tecnomara 270, Rockomat). Membranes were then washed three times for 15 min with TBST buffer and once with TBS (10 mM Tris-HCl (pH 7.5), 150 mM NaCl) buffer. Proteins were detected using ECL blotting substrate and visualized using the ChemiDoc.Protein size was estimated by use of protein marker (1610374, Biorad).

3.2.18. Western blotting and Dot blotting

Western blotting was used to analyse protein expressions in zebrafish embryos and adult tissues. Embryos were lysed in RIPA buffer (containing 150 mM NaCl, 1 mM EDTA, 25 mM Tris, and 0.5% SDS) with the addition of protease and phosphatase inhibitors (leupeptin, aprotinin, chymostatin, pepstatin at a concentration of 1 µg/mL, and PMSF at a concentration of 1 mM) for 30 minutes on ice. After brief sonication (sonde sonicater with 3 µm peak-to-peak amplitude and centrifugation at 1,000 x g for 10 minutes at 4°C, the supernatants were collected and used for subsequent analysis. Protein concentration was measured using the Bradford assay (Bradford, 1976), after preparing the Bradford reagent by dissolving 100 mg Coomassie Brilliant Blue G250 (Sigma-Aldrich, Taufkirchen, Germany) in 50 mL ethanol (96%; Kemika, Zagreb). To this solution, 100 mL of phosphorous acid was added, followed by the addition of 850 mL of mQ water. The mixture was then filtered through a membrane filter (pore diameter 0.2 µm; TPP Techno Plastic Products AG, Switzerland).

Zebrafish tissues including liver, brain, intestine, kidney, testis, and ovary, were placed in RIPA lysis buffer containing protease inhibitors (leupeptin, aprotinin, chymostatin, pepstatin at a concentration of 5 µg/mL, and PMSF at a concentration of 5 mM) and kept on ice. The tissues were homogenized using an Ultra Turrax T25 homogenizer (3 x 20 sec). After homogenization, SDS was added at a final concentration of 0.8%, and the tissues were incubated on ice for 15 minutes. Samples were then centrifuged at 8,000 x g for 10 minutes at 4°C, and the supernatant containing the protein extract was collected, aliquoted, and stored at -80°C. Because of the small size of the tissue samples, three pools, each consisting of three individuals, were used for analysis.

For the Western blot analysis, lysate solutions containing 10 - 30 µg of proteins were loaded per lane and separated by SDS PAGE (5-18% homemade gradient gel) using Mini-PROTEAN 3 Cell electrophoresis chamber (Bio-Rad Laboratories, CA, USA). Precision plus protein ladder spanning 10 to 250 kDa (Biorad, 1610374) was used to determine protein size. The separated proteins were then transferred to a PVDF (Millipore, MA, USA) with wet transfer using Mini Trans-Blot system (Bio-Rad, 1703935). Membranes were blocked with 5% nonfat dry milk (Bio-Rad, 1610374) diluted in TBST buffer (20 mM Tris, 150 mM NaCl, 0.1% Tween) for 2 hours at room temperature to prevent nonspecific binding. After blocking, the membranes were washed in TBST buffer for 5 minutes and then incubated overnight with the primary antibody at 4°C in 2.5% BSA/TBST with gentle rocking. Custom-made zebrafish Tdp1 antibody (Genosphere, UK) with the epitope N-GALEKNNTQIMVRSYE-C was selected to detect both zebrafish and human proteins. It was used at a dilution of 1:1000 for immunoblotting, while anti-H3 antibody (Cell Signaling, #9715, 1:3000) served as a loading control. The following day, membranes were incubated in the secondary antibodies in 2.5% BSA/TBST using rabbit anti-mouse or goat anti-rabbit IgG peroxidase (1:10,000) (Sigma-Aldrich, Taufkirchen, Germany) for 45 minutes at RT with gentle rocking, followed by washing (3x for 15 minutes in TBST and 1X min in TBS).

Specific DPCs were detected using dot blot and a protein-specific antibody using the Bio-dot microfiltration device (Bio-Rad Laboratories, CA, USA). For this analysis, a nylon membrane was used for dsDNA blotting, because its positive charge enhances the binding of negatively charged DNA molecules, whereas a nitrocellulose membrane was used for protein blotting. To perform slot blot analysis 200 µL of DPC sample was loaded onto the membranes per slot, and the samples were vacuumed using vacuum pump at 700 mbar. For dsDNA detection, the DNA was crosslinked to the nylon membrane by exposure to UV light for 5 minutes at UV-Transilluminator (312 nm) (Bachofer) Membranes were blocked for 2 hours in 5% nonfat dry milk diluted in TBST buffer (20 mM Tris, 150 mM NaCl, 0.1% Tween), washed for 5 minutes to remove any unbound molecules and incubated overnight with the primary antibody at 4°C in 2.5% BSA/TBST with gentle rocking. The following day, membranes were incubated with Horseradish Peroxidase (HRP) - labelled secondary antibodies, rabbit anti-mouse or goat anti-rabbit IgG peroxidase (1:10,000) (Sigma-Aldrich, Taufkirchen, Germany) for 45 min at RT with gentle agitation, washed 3X for 15 min in TBST and 1X for 5 min in TBS. HRP conjugates generate a signal by oxidizing a chemiluminescent substrate, luminol, resulting in the emission of light.

Proteins or dsDNA were detected using Clarity Western ECL Substrate containing luminol and chemiluminescence signal was detected with the ChemiDoc™ XRS+ System.

3.2.19. Development and verification of a custom-made zebrafish Tdp1 antibody

The peptide N-GALEKNNTQIMVRSYE-C was specifically selected to recognize both zebrafish and human TDP1 proteins and was used to immunize two rabbits followed by affinity purification of rabbit sera (Genosphere, UK). To test the specificity of the antibody, we performed western blotting using samples from WT and tdp1 mutant zebrafish, as well as HEK293T cells WT and HEK293T cells overexpressing human TDP1. Cells were transfected with the recombinant plasmid carrying the human TDP1 gene (GenScript, OHU22350D) using the PEI transfection reagent as described previously (Popovic et al., 2013; Tom et al., 2008). Cells were collected after 72 hours and lysed in RIPA buffer (150 mM NaCl, 1% Triton X-100, 0.50% Na-deoxycholate, 0.10% SDS, 50 mM TrisHCl (pH 8)) followed by a 10-second sonication (sonde sonicater with 3 µm peak-to-peak amplitude 2-day old zebrafish embryos were lysed in RIPA buffer and sonicated twice for 10 seconds. Cell lysates containing 30 µg of proteins and embryos lysates containing 50 µg of proteins were loaded on 5-18% homemade gradient acrylamide gel, resolved with SDS-PAGE and transferred to a PVDF membrane (wet transfer). The membrane was blocked with 5% milk for 2 hours and incubated overnight with the custom-made anti-Tdp1 antibody (1:1000). The blot was visualised by incubating the membrane with an HRP-labelled anti-rabbit antibody followed by detection using ECL (Biorad) at the ChemiDoc™ XRS+ System.

3.2.20. Statistical Analysis

Quantification of dot blots, western blots, and morpholino oligonucleotide mediated silencing efficiency in zebrafish was performed using the ImageJ software (Abràmoff et al., 2004) and Microsoft Excel (Microsoft Office 2013). For graphical representation and statistical analysis, an unpaired two-sided Student's t-test was conducted using GraphPad Prism 8 Software. Significance was declared when $p < 0.05$ for differences between two independent variables. To ensure the accuracy of the results obtained, all experiments were repeated three to six times (biological replicates) for RADAR isolation from cells and embryos and qPCR analysis and the data is presented as means ± standard deviation (SD).

4. RESULTS

4.1. Comparison of zebrafish, mouse and human TDP1 proteins: phylogeny, synteny, sequence and structure

A phylogenetic tree of Tdp1 orthologues in multicellular organisms, yeast, and bacteria was constructed by aligning protein sequences using the MAFFT algorithm (Katoh et al., 2002) and a phylogenetic tree was built using the Maximum Likelihood method (Guindon & Gascuel, 2003). The Tdp1 protein is very conserved in all kingdoms of life, from bacteria and yeast to plants and animals and is always present as a single orthologue (Figure 11A and Supplement 1). Interestingly, the Tdp1 orthologues in invertebrates form two distinct clusters: one which is phylogenetically very close to the vertebrate cluster, the another which is closer to the yeast and bacterial orthologues (Figure 11A, Supplement 1). Human and zebrafish Tdp1 are phylogenetically very close (Figure 11A, Supplement 1) and structurally very similar (Figure 12A).

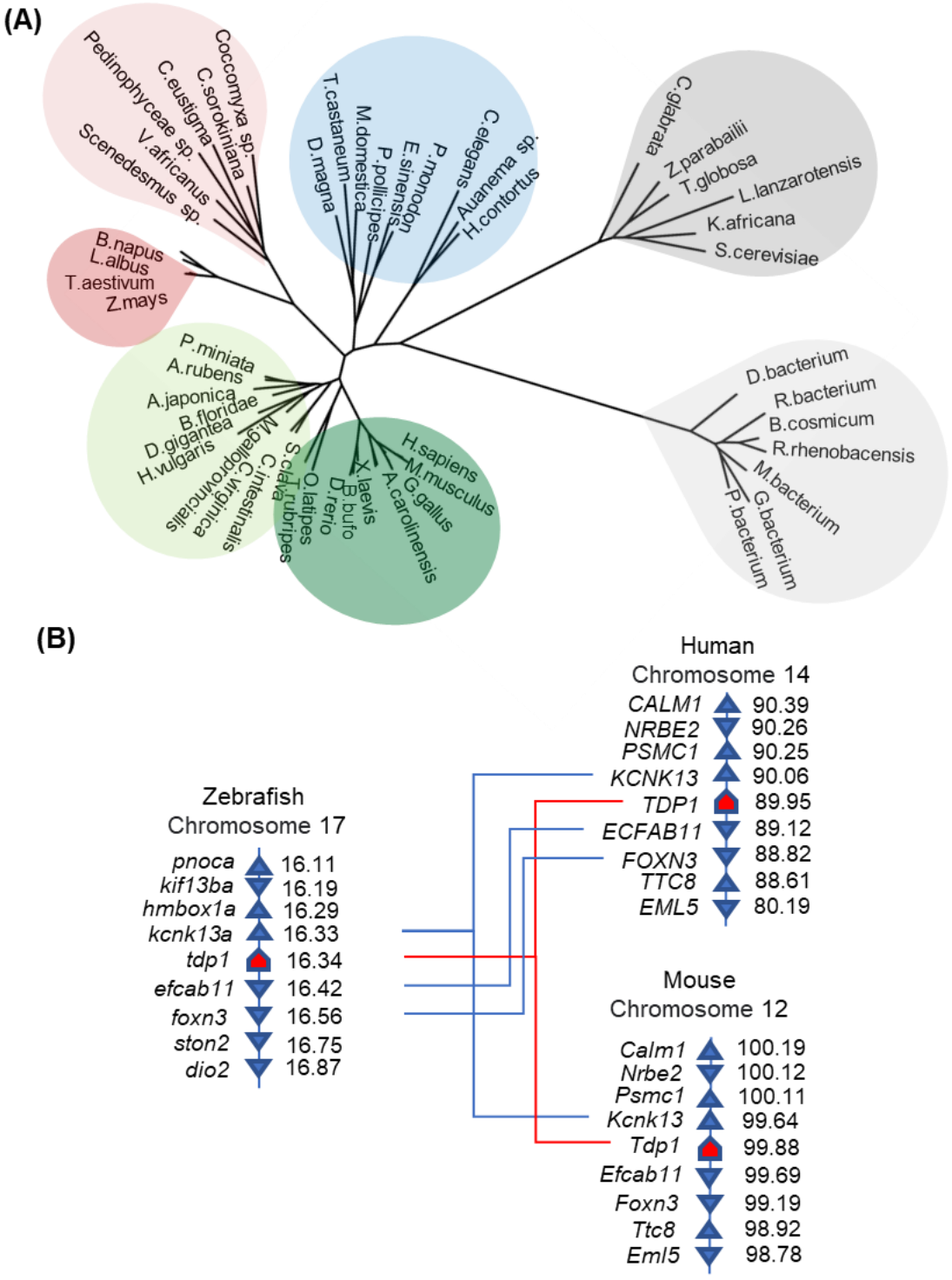

Figure 11. Phylogenetic and syntenic analysis of zebrafish Tdp1 (A) Phylogenetic tree of TDP1 orthologues. The vertebrate TDP1 cluster is shown in dark green, one invertebrate cluster, which is phylogenetically closely related to the vertebrate orthologues, is shown in light green, the second invertebrate cluster is shown in blue. Plant and algae clusters are shown in dark and light red, respectively, while fungi and bacterial orthologues are shown in

dark and light grey, respectively. (B) Synteny analysis of zebrafish, human, and mouse *TDP1* was performed using Genomicus browser. The numbers next to the gene names represent the megabase pair (Mbp) of each gene position on the chromosome.

The structure of zebrafish Tdp1 was modeled using the crystal structure of human TDP1 (PDB: c1nopB) (Davies et al., 2002) in the Phyre2 workspace (Kelley et al., 2015). These orthologues share a very similar structure of N and C domains with a remarkable degree of conservation (Figure 12A). N domain (164. – 358. amino acid) and C domain (359. – 616. amino acid) form a pseudo-2-fold axis of symmetry with each domain contributing the histidine, lysine and asparagine to the active site: H263, K265, and N283 in the N domain and H493, K495, and N516 in the C domain (Davies et al., 2002; Flett et al., 2018) (Figure 12A). Upstream of the N domain is an N terminal portion which is heavily disordered in both zebrafish and human TDP1 (1-163. and 1-144. amino acids, respectively) (Figure 12B) This part is highly variable among species, and its structure has not yet been solved. The amino acid sequence similarity between human and zebrafish Tdp1 is 66% (identity 55%), whereas the similarity between mouse and human Tdp1 is 83% (identity 77%). If we exclude the variable N terminus, similarities between orthologues are much higher: 76% between human and zebrafish Tdp1 (identity 66%) and 92% between human and mouse Tdp1 (identity 88%). After determining the phylogenetic, structural, and sequence similarities between the human, mouse, and zebrafish Tdp1 proteins, we analysed the gene environment of the orthologues and found that it is partially conserved. Zebrafish *tdp1* on chromosome 17 is surrounded by the upstream neighbouring gene *kcnk13a* and the downstream neighbouring genes *efcab1*1 and *foxn3* similarly as in human and mouse *TDP1* genes located on chromosomes 14 and 12, respectively (Figure 11 B). Apart from the aforementioned neighbouring genes, the gene environment between zebrafish on one side and human and mouse *TDP1* on the other side is not conserved. In contrast, the gene environment of *TDP1* in humans and mice exhibits preserved genomic order that was presumably passed down from a common mammalian ancestor (Figure 11 B).

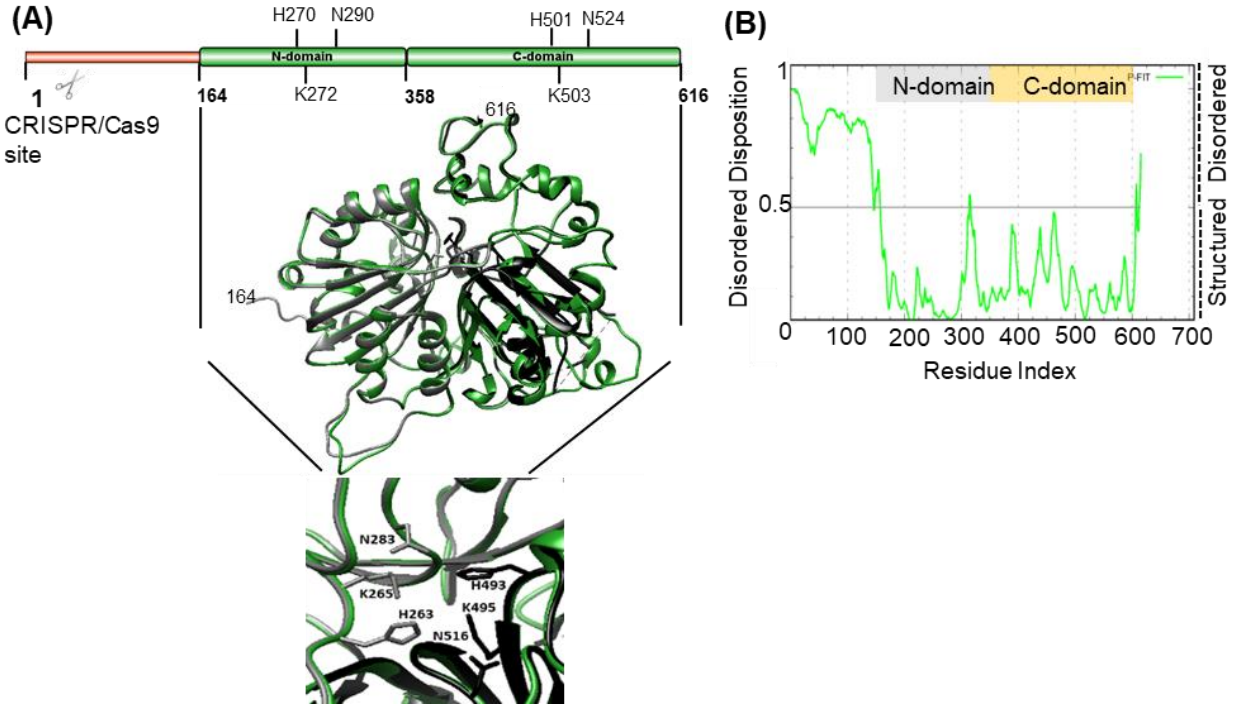

Figure 12. Structural comparison between zebrafish and human Tdp1. A) The zebrafish Tdp1 structural model (in green) is overlapped with the human TDP1 crystal structure (PDB: 1jy1) (Davies et al., 2002), shown in grey (N domain) and black (C domain). Zebrafish Tdp1 was modelled using the Phyre2 workspace (Kelley et al., 2015) according to the human TDP1 (PDB: c1nopB). N domain and C domain form a pseudo-2-fold axis of symmetry where each domain contributes to the active site: H263, K265 and N283 in the N domain and H493, K495 and N516 in the C domain. The CRISPR/Cas9 cutting site in exson 2 is marked with scissors. B) The plot of disorder disposition for zebrafish Tdp1 protein predicted by PONDR-FIT software. Values above 0.5 indicate likely disordered regions (N-terminal), while structured N- and C-domains are labelled in grey and yellow, respectively.

4.2. Creation and characterization of zebrafish line lacking Tdp1 protein

The CRISPR/Cas9 system was used to create zebrafish strains with deficient Tdp1. To this end, we tried two different strategies: (1) introducing mutations which lead to a frame shift and a premature STOP at the beginning of the Tdp1 protein sequence, and (2) creating a zebrafish line with an enzymatically inactive Tdp1 by introducing a mutation (H501A) into the catalytic core of the Tdp1 protein. The premature stop line was created using a guide RNA (gRNA) that targeted exon 2 (Figure 12A). The result was a frameshift mutation, causing a premature STOP codon at amino acid position 44 (Figures 13A and B and Supplement 2). This stop codon occurred upstream of the catalytic residues H270, K272, and N290 in the N

domain (Figure 12A). In particular, the gRNA/Cas9 complex was injected into one-cell stage embryos and fish were grown to adulthood. Identified founder fish in the F0 generation that transmitted frameshift mutations which resulted in premature stop at amino acid position 44 were crossed and the F1 generation was raised. When the F1 generation reached adulthood, individuals were genotyped based on fin tissue and allele changes were sequenced (Figure 13 B and Supplement 2). Female and male carrying the described frameshift mutations (Figures 13A and B, Supplement 2) were further crossed to produce a Tdp1-deficient F2 generation. The lack of functional Tdp1 was confirmed by enzyme activity assay (Figure 13C) and Western blot using a custom-made antibody against zebrafish Tdp1 (Figures 13D and 13E). For the activity assay, we used a model substrate of Tdp1: a 3'-phosphotyrosyl-DNA probe (3'pY) with a fluorescent reporter Cy-5 at the 5' end. When Tdp1 is active, tyrosine (Y) is removed from the substrate, resulting in the oligonucleotide form (3'p) (Figure 13C). Lysates from WT embryos (with active TDP1) were incubated with the labelled substrate and very efficient tyrosine removal was observed; in contrast, no reaction occurred after incubation with the lysates from *tdp1* mutant embryos demonstrating the absence of Tdp1 in the mutants (Figure 13C).

The absence of the Tdp1 protein in the *tdp1* mutant line was demonstrated using a custom-designed Tdp1 antibody (Figure 13D). Notably, when creating the Tdp1 zebrafish antibody, a conserved protein region that overlaps between zebrafish and human TDP1 was deliberately selected. Within this region, an epitope was chosen to enable the detection of both zebrafish and human TDP1 proteins. To validate its specificity in human cells, the antibody was tested on both HEK293 WT cells and HEK293 cells transfected with a recombinant plasmid containing human TDP1 (Figure 13E). The detected signal in cells overexpressing human TDP1 served as a positive control for subsequent western blot analyses.

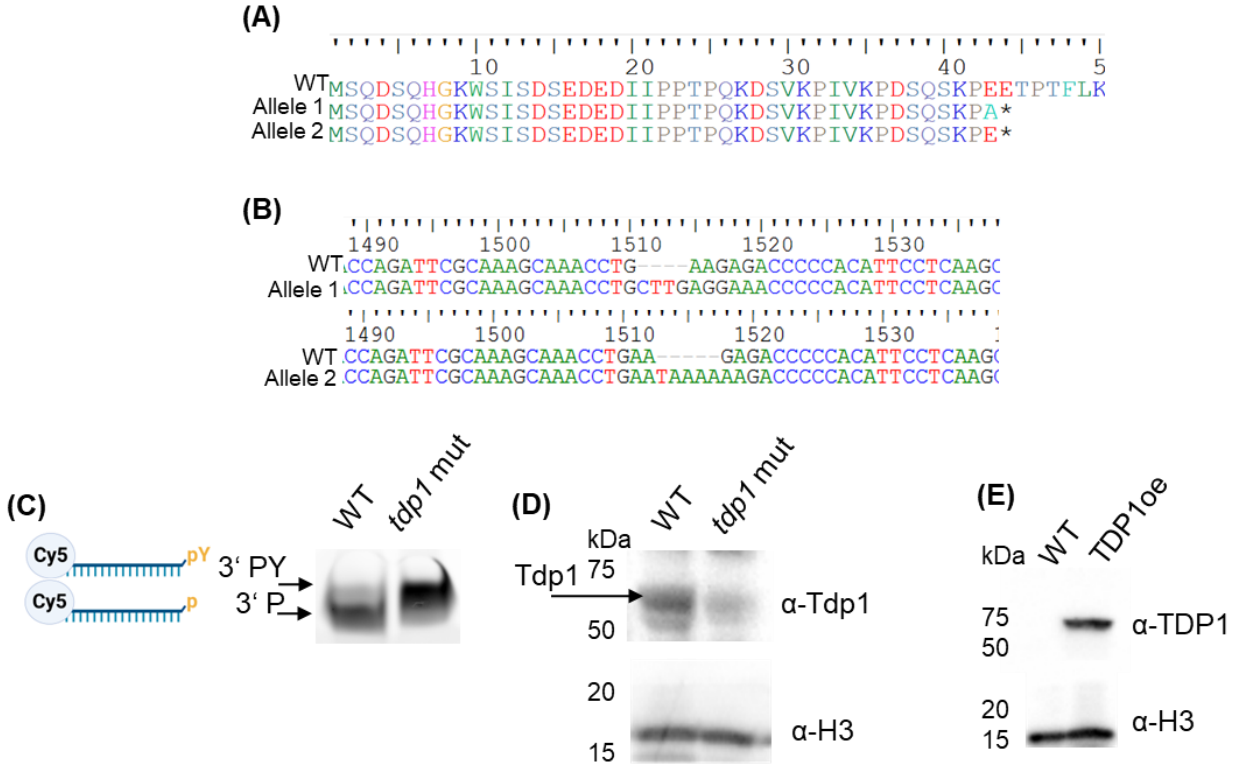

Figure 13. Validation and characterization of the zebrafish *tdp1* premature STOP mutant line. A) Amino acid sequence of Tdp1 in *tdp1* mutant fish line: frameshift and introduction of a premature stop codon in *tdp1* mutant fish line is deduced from DNA sequencing (*, premature STOP). B) Sequencing od *tdp1* mutant fish line that contains Tdp1 allele 1 bearing the insertion of CTTG after position 1510 (Gene ID: 571485). on gDNA and allele 2 bearing the TAAAA insertion after position 1512. on gDNA. C) TDP1 activity assay performed with 600 ng of lysate from 2-dpf WT and *tdp1* mutant embryos. Left panel: scheme created of TDP1 substrate oligonucleotide with tyrosine (pY) on 3' end and Cy5 fluorescent reporter on 5' end and a reaction product after TDP1-mediated removal of tyrosine (p); right panel: TDP1 activity assay reactions resolved on a 20% homemade urea gel and visualized using Cy-5 fluorescence D) Western blot using a custom-made antibody against zebrafish Tdp1 shows the absence of a specific Tdp1 signal (68 kDa, indicated by arrow) in *tdp1* mutant embryo lysate. Histone H3 was used as a loading control. E) Western blot showing that the custom-made Tdp1 antibody recognizes the overexpressed recombinant human TDP1 protein in HEK293 cells. Histone H3 is shown as the loading control.

After determining that the Tdp1 protein was indeed absent in the *tdp1* mutant line (Figure 12D), the animals were examined to observe whether Tdp1 deficiency resulted in phenotype changes in embryos and adult zebrafish. There were no obvious morphological differences between WT and *tdp1* mutant embryos or in adult zebrafish that are now 12 months old (Figure 14). Future studies are needed to investigate specific phenotypes in adult Tdp1-deficient zebrafish, particularly with regard to neurodegeneration in old fish (> 2 years old).

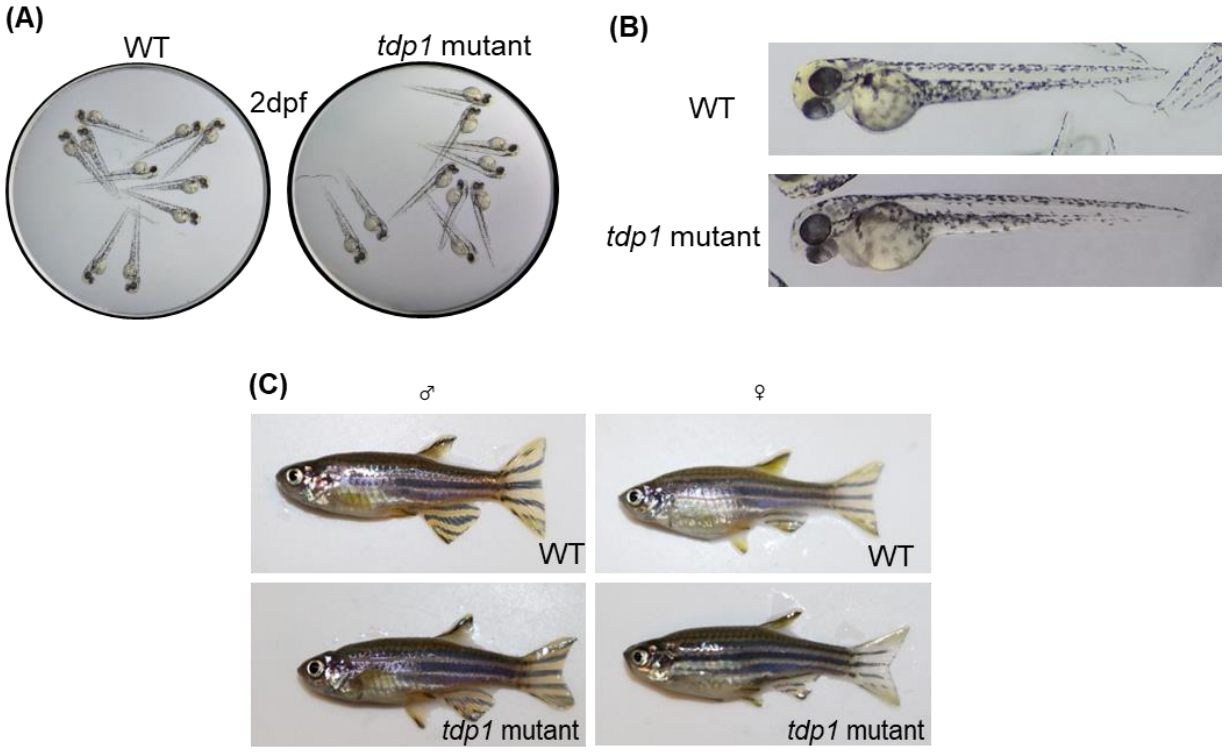

Figure 14. Images of WT and *tdp1* mutant embryos and adult fish. A) Overview of WT and *tdp1* mutant embryos (2-dpf) B) individual images of WT and *tdp1* mutant embryos. C) Live, anesthetized WT and *tdp1* mutant adult fish (6 months old, males left and females right). Prior to imaging, adult fish were anesthetized with tricaine methanesulfonate (MS -222) (0.02% in aquarium water) for 10 minutes and left to recover afterwards. Images were captured using a Canon 250D DSLR camera and Samsung 13-megapixel camera (Cecile Otten, IRB, unpublished results).

4.3. Generation of the inactive H501A mutant *tdp1* zebrafish line

In order to create a Tdp1 catalytic mutant we aimed to replace catalytic histidine 501 with an alanine. Histidine 501 is a conserved amino acid that corresponds to human Tdp1 H492 and plays a crucial role in the activation of a water molecule, the subsequent protonation of

the phosphotyrosyl bond, and the release of the 3'-phosphate end of the DNA from the TOP1 remnant. To generate a inactive mutant, we used the CRISP /Cas9 *knock in* approach, in which we used the Tdp1 repair template (RT) with two modifications, A23,573C and C23,572G, as the donor sequence for repairing Cas9-mediated DSBs (Figures 15A and B). This template was co-injected along with Cas9 protein and sgRNA targeting exon 12, with the aim of inducing a DSB near the catalytic site and providing an artificial RT bearing the desired mutation and a reporter gene mVenus, which serves as a template for homology-directed (HR) repair. The repair template was created following the protocol published by Hoshijima, Jurynec and Grunwald, 2016. The left arm (LA) was a 600 bp DNA fragment spanning region from 22,800 to 23,400 of the *tdp1* gene from WT zebrafish AB strain carrying the guide RNA binding site was cloned into the pKHR5 plasmid (Figures 15A and B). In order to prevent Cas9 cutting of the LA, after the microinjection of the Cas9/gRNA complex with RT, a G 23,273A modification was introduced to alter the NGG sequence in RT (Figures 15A and B). The right arm was a 600 bp DNA fragment spanning the region 23,401 to 24,000 in *tdp1* gene and was amplified from the gDNA of WT zebrafish AB strain and carried the catalytic modifications (Figure 15A). In the final step of the preparation of RT, the recombinant pKHR5 plasmid containing left and right arms along with the desired mutation was linearized using the *SceI* restriction enzyme. This enzyme cleaves the recombinant plasmid into two fragments: one fragment contains the RT with homology arms and the reporter gene, while the second fragment contains other parts of the plasmid such as the ampicillin resistance gene, primer sequencing regions, and restriction sites (Figure 15B). After restriction, these two fragments were separated using agarose gel electrophoresis. However, due to their comparable size, they could not be effectively separated. As a result, they were purified together and subsequently injected.

The mVenus reporter, together with its α-crystalline promoter and a 500 bp plasmid backbone derived from the pKHR5 plasmid, is enclosed between the left and right arms of the RT (Figures 15A and B). This middle part of the RT is designed to be integrated into intron 12 of the *tdp1* gene during the HR repair (Figure 15A). The mVenus reporter gene encodes a fluorescent mVenus protein and is controlled by the α-crystalline promoter, ensuring that the reporter gene is specifically expressed in the fish lens which is easily detected using a binocular fluorescence microscope. This allows for the florescence selection of individuals with the integrated repair template.

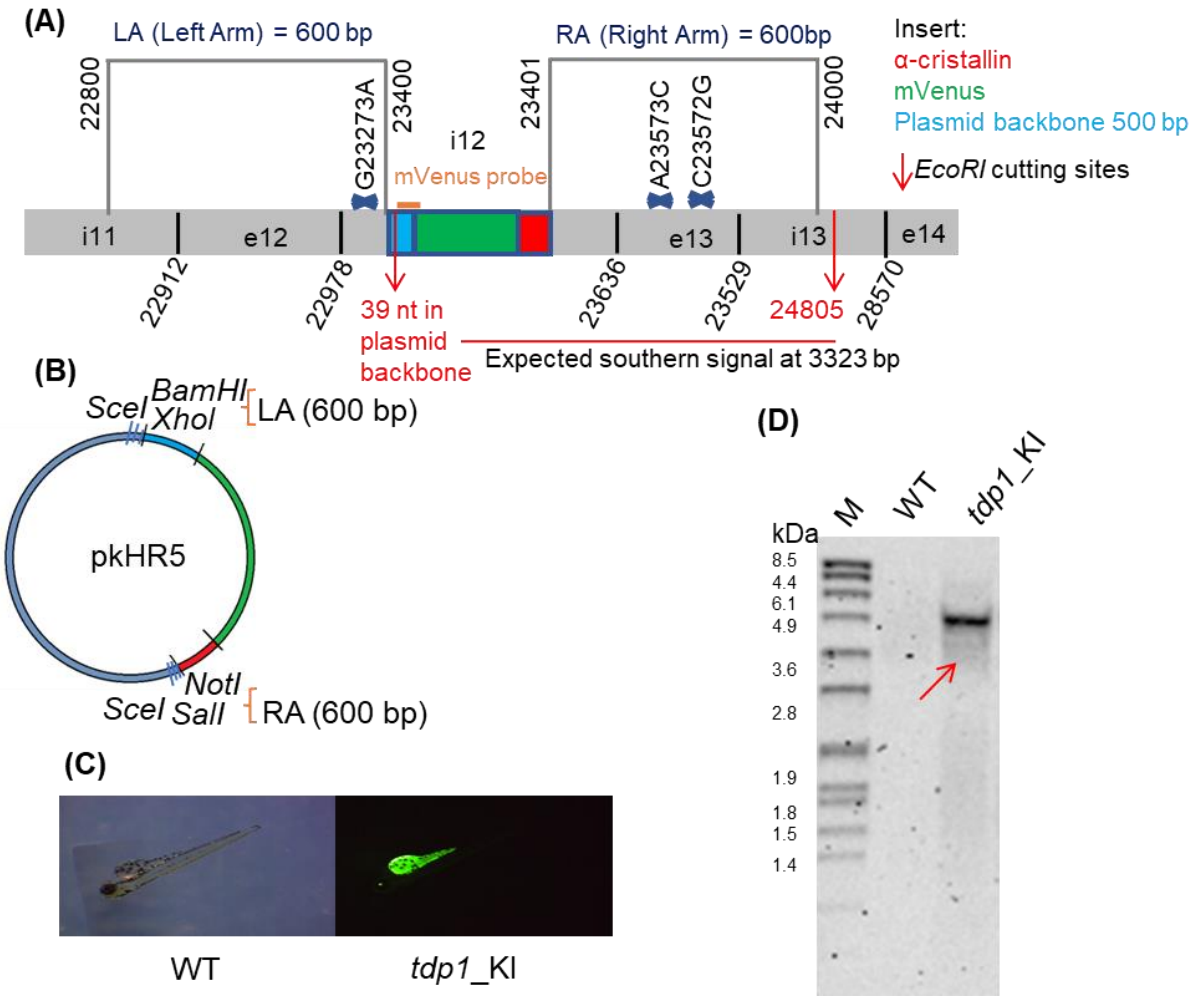

Figure 15. Characterization of the zebrafish *tdp1* catalytic mutant fish line. A) Schematic representation of the repair template construction and southern blot design. Both left and right arms, each spanning 600 bp, are numbered to indicate their positions on the genomic DNA. Between the arms, inserts containing the plasmid backbone (blue), the mVenus florescence gene (green), and its α-crystalline promoter (red) are designed for integration into intron 12 of the *tdp1* gene. PAM and catalytic mutations are marked with crosses. The orange mark signifies the location of the mVenus-specific probe, while red arrows indicate *EcoRI* restriction sites and the anticipated southern blot signal after hybridization with the mVenus probe. B) Schematic representation of the pKHR5 plasmid and cloning design: the left arm (LA) was incorporated into the plasmid using *BamHI* and *XhoI* restriction enzymes, while the right arm (RA) were introduced using *NotI* and *SalI* enzymes. Upon confirming accurate integrations, the plasmid was linearised via *SceI* enzyme, resulting in two fragments - one containing the reporter gene flanked by homology arms and the other one containing the remaining half of the plasmid. C) An image of *tdp1* lens-positive embryo. Images of 2-day

old *tdp1* mutant embryo after exposure to blue light and detection with a green lens filter. Fluorescence in the lens indicates incorporation of the RT including the mVenus reporter gene into the genome. D) Southern blot analysis of WT and *tdp1* lens-positive embryos: 10 µg of genomic DNA from WT and *tdp1* RT-injected embryo embryos were digested with the restriction enzyme *EcoRI*. The resulting restricted DNA fragments were subjected to hybridization using a mVenus DIG labelled probe (Supplement 3). The band in the *tdp1* lens-positive embryo sample was approximately 2500 bp higher than expected (red arrow indicate expected bend size).

The injected embryos were raised for two days and screened for the green fluorescence in the eye lens (Figure 15C). Embryos with fluorescent lens were selected and raised to adulthood (Figure 15C). Adult fish at 2.5 months of age were genotyped using PCR and sequencing of the target region in the gDNA isolated from the fin tissue. Two female fish were identified in which both the left arm segment (LA) and the right arm segment (RA) were correctly integrated (Supplements 4 and 5). Unexpectedly, while one fish carried the catalytic modification, the other did not (Supplement 5). In order to check if the RT was integrated only at the intended place in the genome, the female carrying all the desired integrations was further analysed by southern blot. In brief, the female was outcrossed with a WT male to get enough material for the analysis (20 embryos) and the embryos were analysed by southern blot. In brief, 10 µg of gDNA from a pool of florescence positive embryos was hybridized with the mVenus probe (Supplement 3)**.** Indeed, only one specific band was detected in the whole genome, but the size of the fragment was again 2.5 kb larger than expected (Figure 15D). Sequencing of the inserted segment revealed an unexpected integration of the part of the pKHR5 plasmid backbone in the middle of RT, which was not originally intended as part of the repair template (Supplement 6). This was probably a consequence of co-injection of the linearized RT bearing homology arms with the linearized plasmid backbone, but this remains to be confirmed in future studies. In conclusion, we observed unexpected outcomes of the KI approach, and therefore, we could not confidently create a clean mutant line carrying a catalytic mutation in *tdp1* at this point. The method warrants further optimization which is very time consuming and therefore we have chosen to proceed with the analysis of DPCR in the successfully created and validated *tdp1*-deficient animal model.

4.4. *Tdp1* is highly expressed throughout embryonic development and in adult tissues

It was demonstrated that *tdp1* is strongly expressed throughout embryonic development from 6 hours post-fertilization (hpf) to 5 days post-fertilization (dpf) (Figure 16A). WT embryos were collected at different time points, starting at 6 hpf, when the maternal transcriptome is degraded and transcription from the embryonic genome is fully developed (Laue et al., 2019). Expression levels are highest at early stages, at 6 hpf and 1 dpf stage, followed by a 5-fold decrease at later stages (2-5 dpf). Overall, the expression levels remain high from 6 hpf to 5 dpf (Figure 16A). To facilitate comparison of expression levels, we set arbitrary thresholds following previous publication (Loncar et al., 2016): high expression when MNE is > 60 x 10^6 (Ct values < 22), moderate when MNE is 2 x 10^6 – 60 x 10^6 (Ct = 23 - 26), and low when MNE is < 2 x 10^6 (Ct > 27). To compere *tdp1* expression me measured and *sprtn* expression which shows a similar expression pattern to *tdp1* at later stages, with high and stable expression levels from 2 to 5 dpf (Figure 16B). *Sprtn* expression is particularly high at 6 hpf, when mRNA levels are 33-fold higher than those of *tdp1* (Figure 16A).

In adults, *tdp1* is highly expressed in all analysed tissues, with the highest expression in testis and ovaries, followed by a 3.3-fold lower expression in brain and kidney and a 14.7-fold lower expression in liver and intestine (Figure 16B). Small gender differences were observed in gonads, but they were not statistically significant (Figure 16B). To compare *tdp1* expression in zebrafish with the most commonly used animal model, the laboratory mouse, *Tdp1* expression was determined in the corresponding mouse tissues (Figure 16C). The expression pattern is generally similar to that of the zebrafish with the highest expression in the gonadal expression, although *Tdp1* in mice shows higher expression in the testes than in the ovaries (although not statistically significant) (Figure 16B).

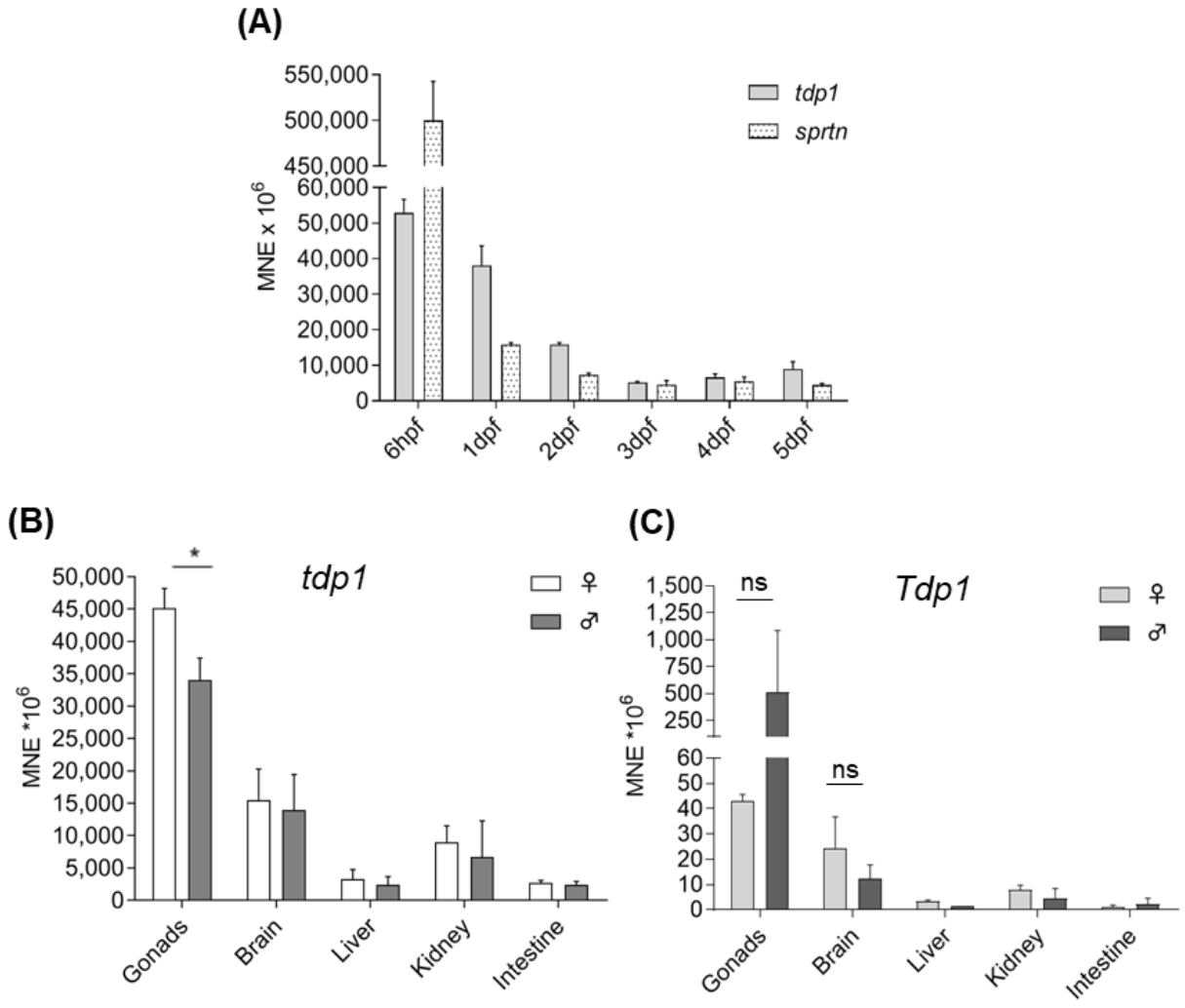

Figure 16. *Tdp1* expression profiles in zebrafish embryos and zebrafish and mouse adult tissues. A) *Tdp1* and *sprtn* expression patterns during embryonic development from 6-hpf to 5-dpf stages. Data represent MNE (mean normalized expression) ± SD (n = 3) normalized to the housekeeping gene *atp50*. B) Tissue expression pattern of *tdp1* in male and female zebrafish, with statistically significant differences between expression in ovaries and testes (*$p < 0.05$) determined by unpaired t-test. Data are presented as MNE (mean normalized expression) ± SD (n = 3) normalized to the housekeeping gene *atp50*. C) Tissue expression pattern of *Tdp1* in male and female mice (ns, non-significant, $p > 0.05$). Data represents MNE (mean normalized expression) ± SD (n = 3) normalized to the housekeeping gene *Atp50*.

Tdp1 protein levels in zebrafish tissues corresponded to some extent to mRNA expression levels (Figures 16B and 17). In females, Tdp1 expression was highest in the ovaries, followed by the liver, kidney, and brain, whereas the expression in the intestine was almost undetectable with this antibody (Figures 17A and B). In males, the pattern was partially similar to that in females, except for a higher expression in the brain and intestine (Figures 17D and E).

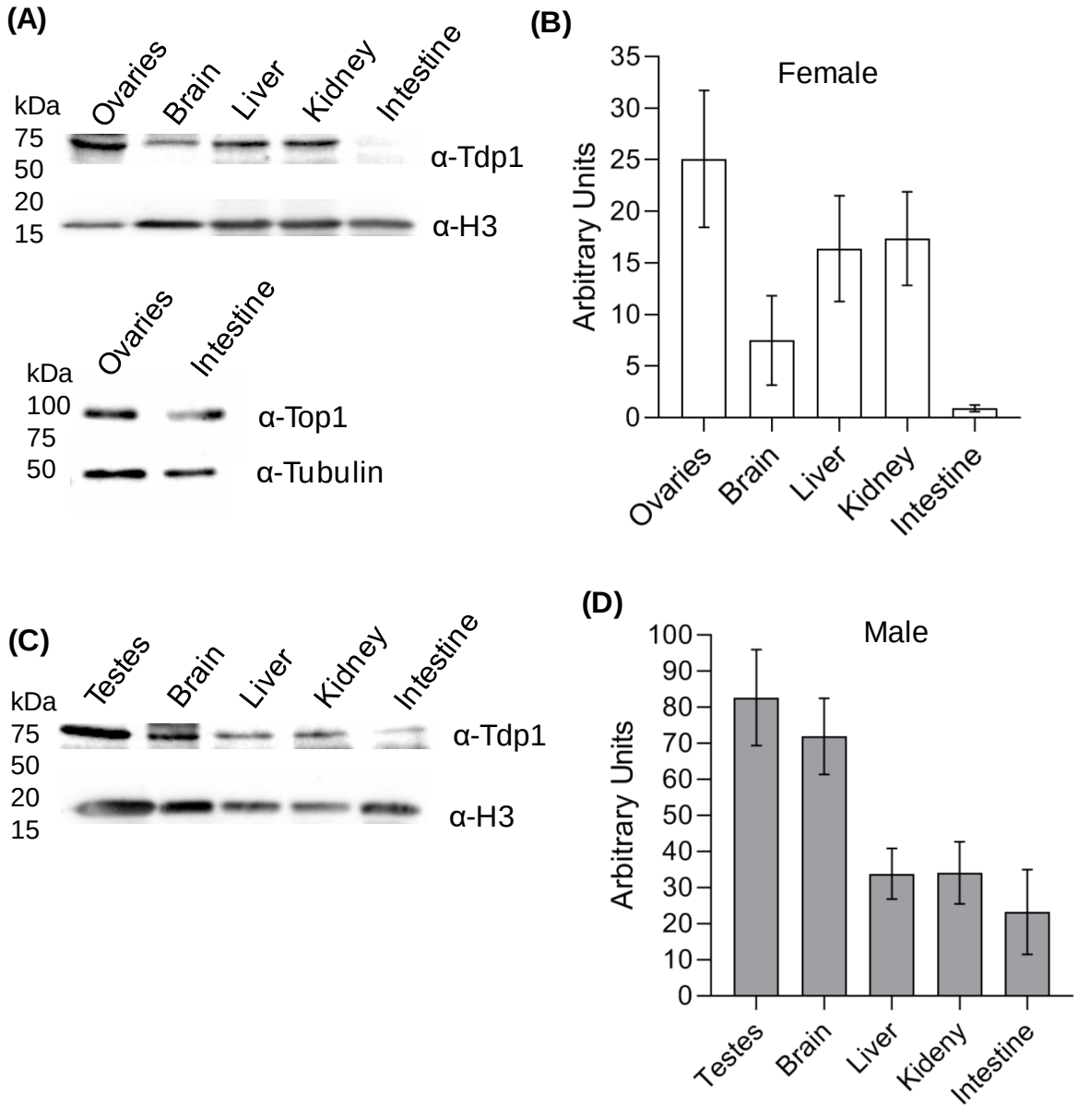

Figure 17. Western blot analysis of zebrafish Tdp1 protein in adult tissues. A) Western blot showing expression of Tdp1 in adult zebrafish female tissues 50 μg total protein lysate was loaded per well) and histone H3 as a loading control. In the right panel, tubulin and Top1 are detected in the intestine and ovaries as additional controls to show that intestinal sample was not degraded. B) Quantification of Tdp1 protein levels in females using Image J software

(mean ± SD; n = 3 independent experiments). C) Western blot showing Tdp1 expression in adult male zebrafish tissues of (50 µg of total protein lysate was loaded per well) and histone H3 as a loading control. D) Quantification of Tdp1 protein levels in males using Image J software (mean ± SD; n = 3 independent experiments). Data represent mean fold change to WT ± SD (n = 3).

4.5. Tdp1 repairs Top1- and histone H3-DPCs *in vivo*

To examine the effects of TDP1 loss of function on DPCs in both *in vivo* and cellular models, DPC isolates were analysed for the presence of TOP1- and histone H3-DPCs by Western blot and dot-blot using protein-specific antibodies. Top1- and H3-DPCs were detected in 4 biological replicates in zebrafish embryos and three biological replicates in RPE1 cells. Tdp1-deficient embryos had greatly increased Top1-DPC levels under physiological conditions (4.8-fold more than WT) (Figure 18). In comparison, the effect of the Top1-DPC inducer, camptothecin (CPT, 10 µM, 1 hour) was weaker in WT embryos: 2.6-fold increase compared to WT (Figures 18A, B and E), and CPT further increased Top1-DPC levels in *tdp1* mutants (6.2-fold) (Figures 18A, B and E). Formaldehyde (FA) treatment (5 mM, 30 min) had a much stronger effect on Top1-DPC induction than CPT in both WT and mutant embryos: FA induced Top1-DPC levels by 7.1-fold in WT and by 9-fold in *tdp1* mutant embryos (Figures 18A, B and E).

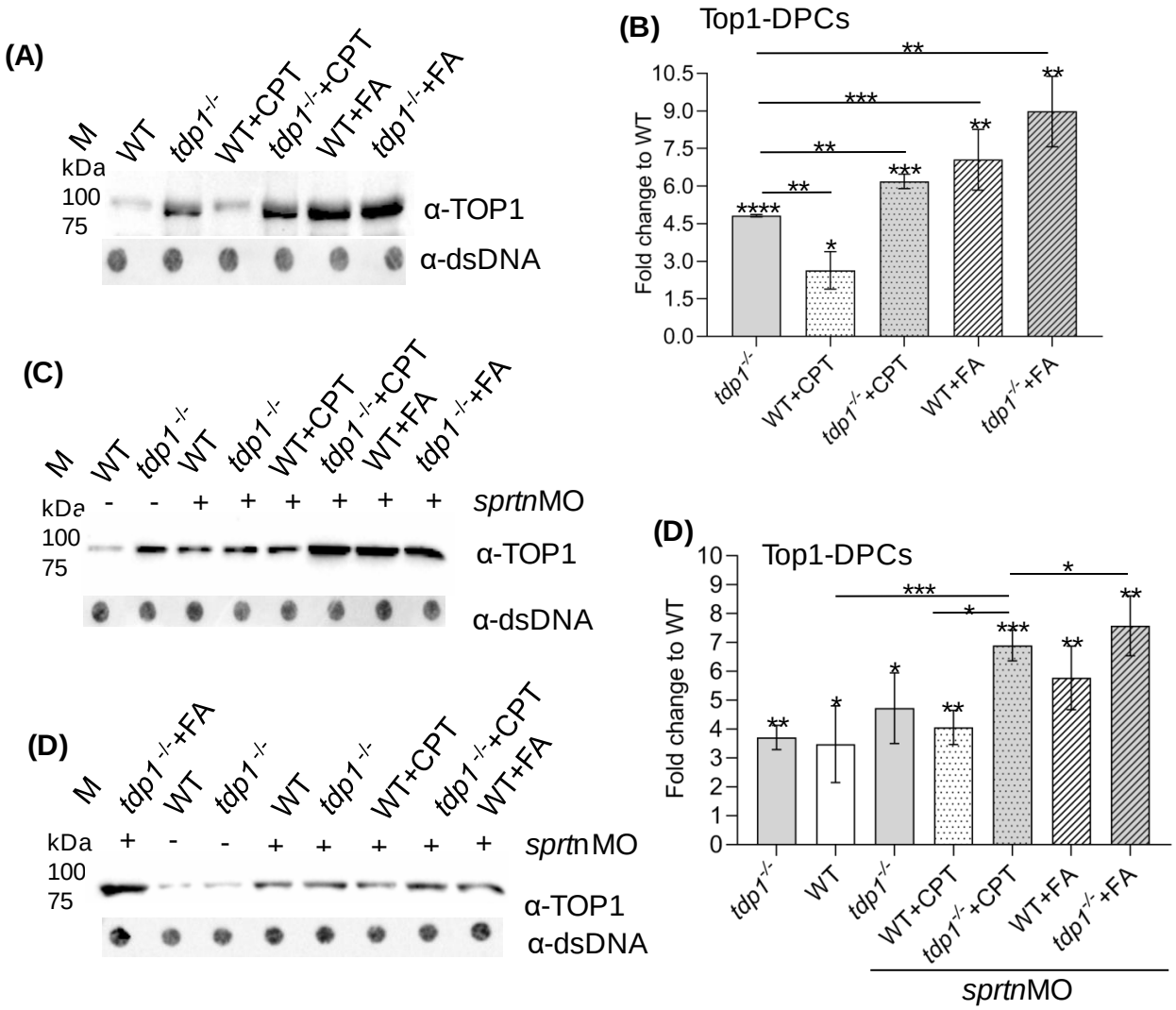

Figure 18. Tdp1 deficiency causes strong accumulation of endogenous and chemically induced Top1-DPCs in embryos. A) Western blot showing zebrafish Top1-DPCs in *tdp1* mutant embryos before and after camptothecin (CPT) (10 µM, 1 hour) or formaldehyde (FA) treatment (5 mM, 30 min) (DPC equivalent of 1 µg DNA was loaded per well) and B) corresponding quantification (n = 4). C) Western blot showing zebrafish Top-1 DPCs in *tdp1* mutant embryos before and after *sprtn* silencing and CPT (10 µM, 1 hour) or FA treatment (5 mM, 30 min) and D) corresponding quantification. E) Additional Western blot showing zebrafish Top1-DPCs in *tdp1* mutant embryos before and after silencing of *sprtn* and treatment with CPT (10 µM, 1 hour) and FA (5 mM, 30 min) used for quantification in Figure 18D. The equivalent of 1 µg DNA of total DPCs was loaded per sample. Results represent mean fold change ± SD of three different experiments. Statistically significant changes as a result from unpaired one sample Student's t-test are shown as * ($p < 0.05$), **($p < 0.01$), *** ($p < 0.001$) or **** ($p < 0.0001$).

In RPE1 cells, the pattern of TOP1-DPC induction (Figure 19) was to some extent similar to that in embryos. TOP1-DPCs strongly accumulated in RPE1 cells after *TDP1* silencing with 3.7-fold increase compared to endogenous levels (Figures 19A, B, and C). CPT caused a 2.2-fold increase in WT cells (Figures 19A and B). When cells were further challenged by the combination of TDP1 deficiency and CPT treatment, TOP1-DPC levels also further increased 7.1-fold compared to nontreated WT cells (Figures 19A and B), confirming that TDP1 is critical for TOP1-DPC removal in human cells. In comparison, FA treatment (1 mM, 20 min) had a very strong effect on TOP1-DPC increase in WT cells, and this induction did not further increase with *TDP1* or/and *SPRTN* silencing (Figures 19C and D).

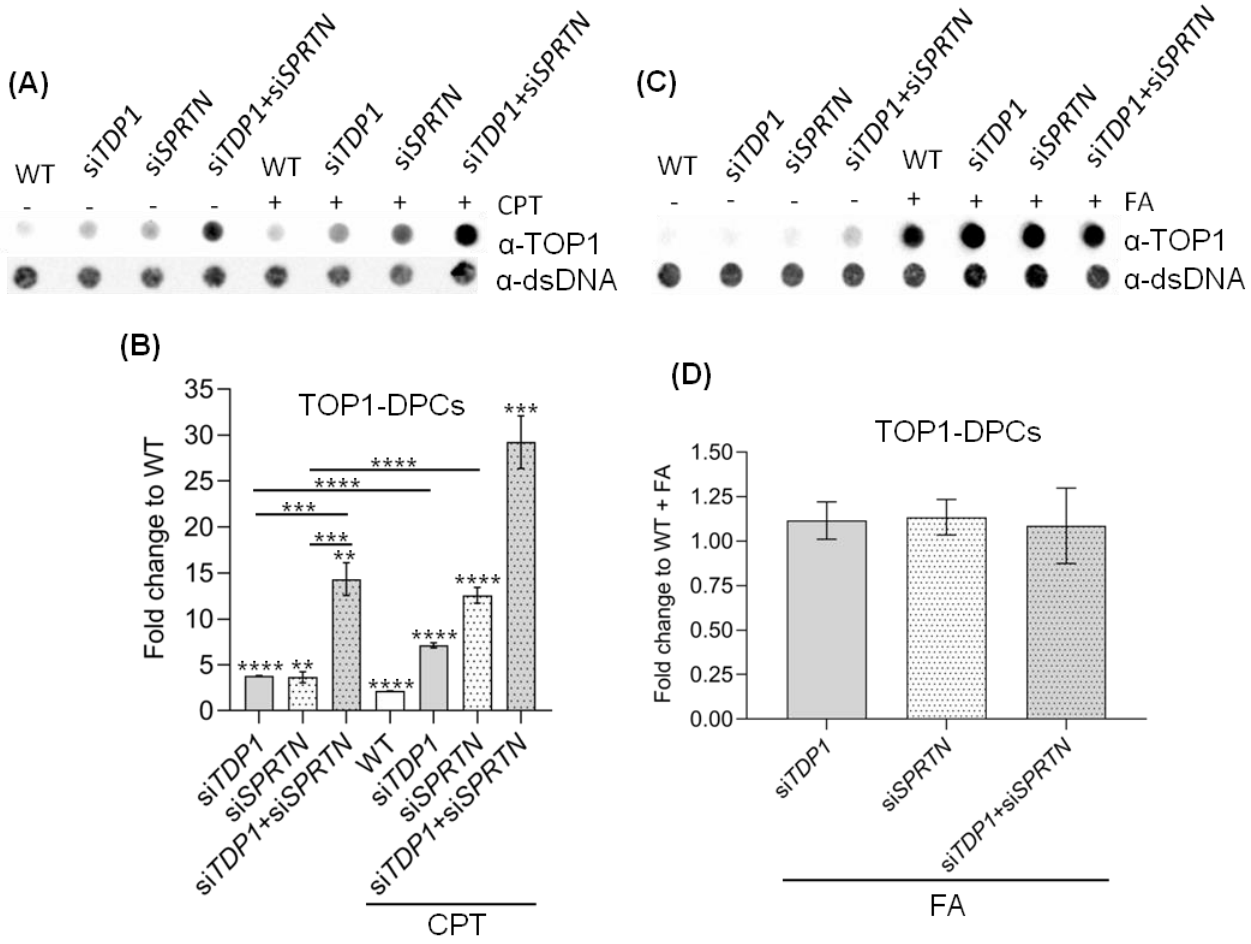

Figure 19. TDP1 deficiency causes strong accumulation of endogenous and chemically induced TOP1-DPCs in human RPE1 cells. A) Dot blots showing human TOP1-DPCs detected with TOP1-specific antibody before and after CPT treatment of RPE1 cells (50 nM, 1 hour) with corresponding DNA loading controls (DPC equivalent of 500 ng DNA was loaded per well). B) Quantification of E from three different biological replicates normalized to untreated WT cells. C) Dot blots showing human TOP1-DPCs detected with TOP1-specific

antibody before and after FA treatment of RPE1 cells (1 mM, 20 min) with corresponding DNA loading controls (DPC equivalent of 500 ng DNA was loaded per well). D) Quantification of G (n = 3). Results represent mean fold change ± SD of three different experiments. Statistically significant changes as a result from unpaired Student's one- sample t-test are shown as * ($p < 0.05$), **($p < 0.01$), *** ($p < 0.001$) or **** ($p < 0.0001$).

To investigate whether TDP1 is involved in the repair of DPCs other than TOP1-DPCs, examination of histones as potential TDP1 substrates was chosen based on recent *in vitro* data from Wei et al. (2022), who showed that purified TDP1 removes H4 and H2B crosslinked at abasic sites of the DNA. Histone H3 was selected as a representative of the core histones because optimized protocols and a sensitive antibody for its detection in the DPC isolates were available. In embryos, Tdp1 deficiency caused very strong accumulation of endogenous H3-DPCs: a 4.2-fold increase compared with WT embryos (Figure 20). This is very similar to what was observed for the canonical substrate of Tdp1, Top1-DPC, in *tdp1* mutants (4.8-fold increase) (Figure 18). CPT treatment caused a 4.7-fold increase in H3-DPCs in WT and an even greater 7.3-fold increase in *tdp1* mutants (Figures 20A and B), again consistent with the pattern of Top1-DPC accumulation after CPT treatment (Figures 18A and B). The FA treatment had a similarly strong effect in WT and *tdp1* mutant embryos, namely a 5.3- and 5.1-fold increase in H3-DPCs (Figures 20C and D).

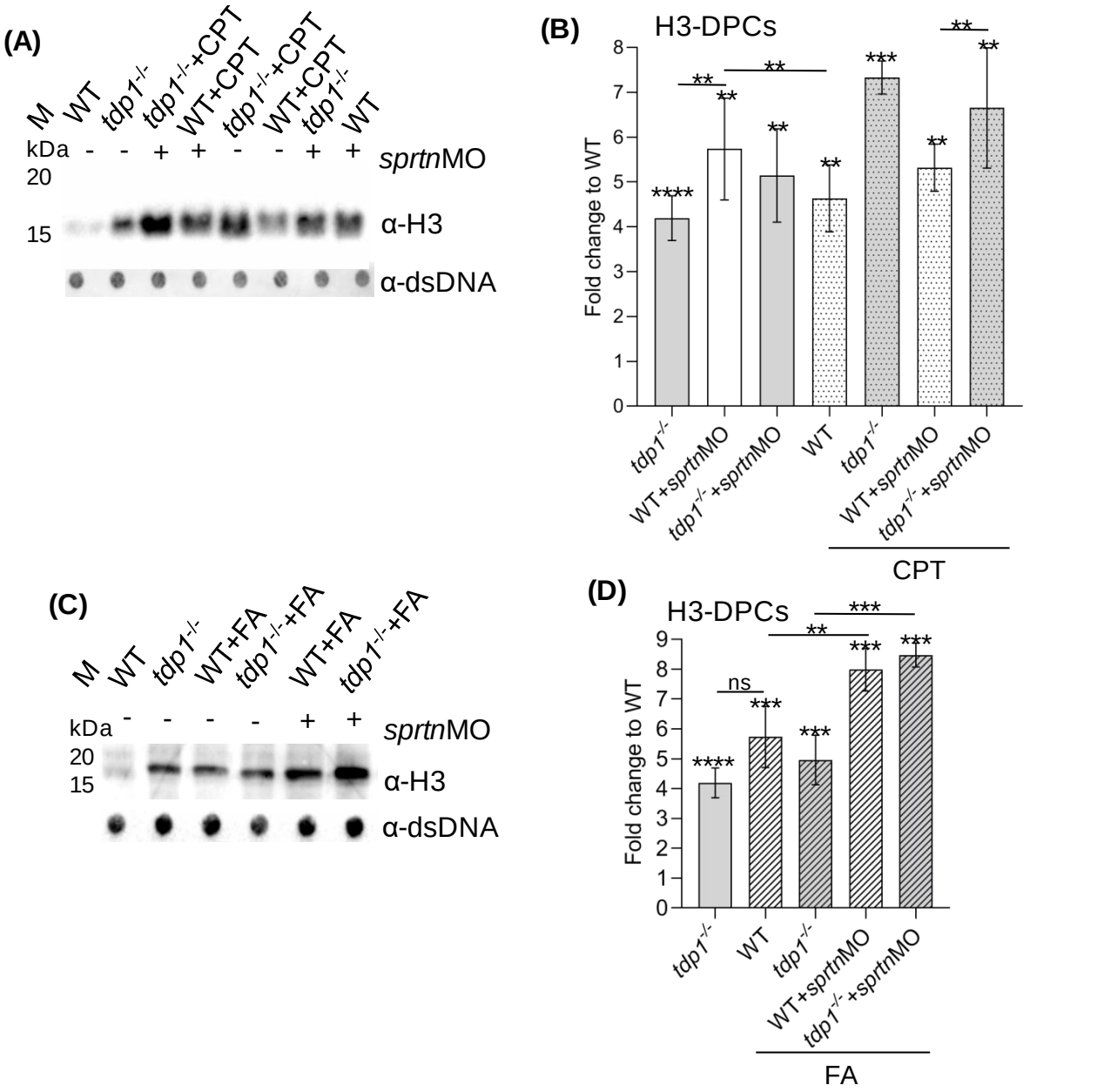

Figure 20. H3-DPC levels are increased in vivo in the *tdp1* mutant fish line. A) Western blot showing H3-DPC levels in *tdp1* mutant embryos in combination with *sprtn* knockdown and CPT (10 µM, 1h) treatment. Total DPCs were isolated from 2-day old embryos, separated by SDS-PAGE (DPC equivalent of 200 ng DNA per well) and detected with H3-specific antibody. B) Quantifications of H3-DPCs from four biological replicates with mean (± SD) fold change to endogenous H3-DPCs in WT embryos. C) Western blot analysis of H3-DPCs in zebrafish embryos and (D) corresponding quantification after FA treatment (5 mM for 30 min) (n = 4). Results are presented as mean ± SD with statistically significant changes, determined using an unpaired one-sample Student's t-test, indicated with *($p < 0.05$), **($p < 0.01$), ***($p < 0.001$), and ****($p < 0.0001$).

In RPE1 cells, *TDP1* silencing induced H3-DPC levels by 2.5-fold compared to untreated WT cells (Figure 21). It is important to note that CPT, although previously known to be a specific TOP1-DPC inducer, increased H3-DPCs 2.9-fold in WT cells (Figures 21A, B, E and F). H3-DPC levels were comparably affected when WT or *TDP1*-silenced cells were exposed to CPT: 2.9-fold and 2.8-fold increase, respectively (Figures 21A, B, E and F). In contrast, CPT induced many more H3-DPCs in *tdp1* mutants (7.3-fold) than in CPT-treated WT embryos (4.6-fold increase) (Figure 20). FA caused a remarkable 15.7-fold increase in H3-DPCs in WT cells and a 25.8-fold increase in *TDP1*-silenced cells compared with WT untreated cells (Figures 21C and D).

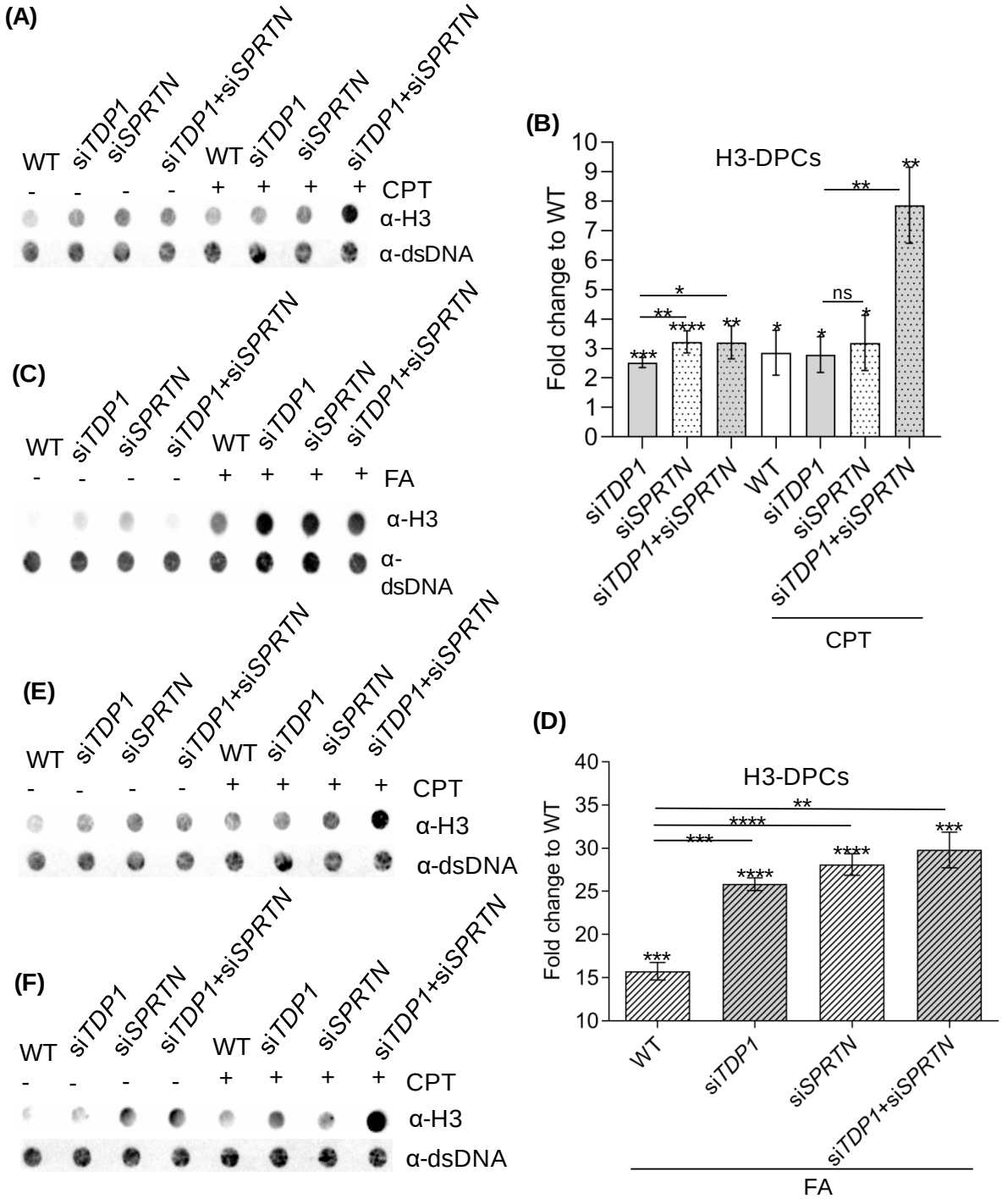

Figure 21. H3-DPC levels are increased in *TDP1* silenced RPE1 cells. A) Dot blots showing H3-DPCs after silencing *TDP1* and/or *SPRTN* before and after CPT exposure in RPE1 cells (50 nM CPT, 1h) and DNA loading controls. Equivalent of 200 ng DNA of total DPCs was loaded per sample. (B) Quantification of H3-DPC analysis in RPE1 cells (n = 3). C) Dot blots showing H3-DPCs after silencing *TDP1* and/or *SPRTN* before and after FA exposure (1 mM FA, 20 min) in RPE1 cells and DNA loading controls and D) Corresponding

quantification (n = 3). (E) and (F) Dot blots of H3-DPCs from two independent experiments after *TDP1* and *SPRTN* silencing before and after exposure to CPT (50 nM, 1h) with corresponding DNA loading controls used for quantifications shown in C. Results are presented as mean ± SD with statistically significant changes, determined using an unpaired one-sample Student's t-test, indicated with *($p < 0.05$), **($p < 0.01$), ***($p < 0.001$), and ****($p < 0.0001$).

4.6. SPRTN proteolysis is necessary for TOP1 and H3 DPC repair *in vivo*

To test the hypothesis that upstream proteolysis by SPRTN is required for the subsequent action of TDP1 in removing TOP1-DPCs, we quantified TOP1-DPC levels in embryos and RPE1 cells under different conditions. In WT embryos, *sprtn* knockdown was accomplished by combining two morpholino oligonucleotides: one aimed at the UTR to block transcription and the second at the exon 2-intron 2 boundary, which prevents splicing (Figures 22A, B and C). This splice-blocking morpholino oligonucleotide triggered exon-skipping, leading to an 80% reduction in *sprtn* mRNA levels. (Figures 22A, B and C). Remarkably, this knockdown did not yield any apparent phenotypic changes (Figure 22D) but resulted in a significant 3.5-fold increase in Top1-DPC levels (Figures 18C, D and E). In *tdp1* mutant embryos, the increase in Top1-DPCs with or without concomitant *sprtn* knockdown was 3.5 and 4.7-fold, respectively (Figures 18C, D and E). Surprisingly, CPT treatment (10 µM, 1 hour) did not result in an additional increase in Top1-DPC levels in *sprtn*-silenced embryos (with functional Tdp1) (Figures 18C, D and E). Compared with untreated WT embryos, CPT exposure of embryos deficient in both Tdp1 and Sprtn increased Top1-DPC levels 6.9-fold which is a significant increase compared with *tdp1* mutants and *sprtn*-silenced mutants (Figures 18C, D and E). FA treatment (5 mM, 30 min) of *sprtn*-silenced embryos with functional Tdp1 caused a significant 5.8-fold increase in Top1-DPC levels compared with untreated WT embryos (Figures 18C, D and E) which is an additional increase in comparison to *sprtn*-silenced embryos (3.5-fold). In *sprtn*-silenced *tdp1* mutants, exposure to FA, significantly increased Top1-DPC levels compared with nontreated *sprtn*-silenced *tdp1* mutants ($p < 0.005$) (Figures 18C, D and E).

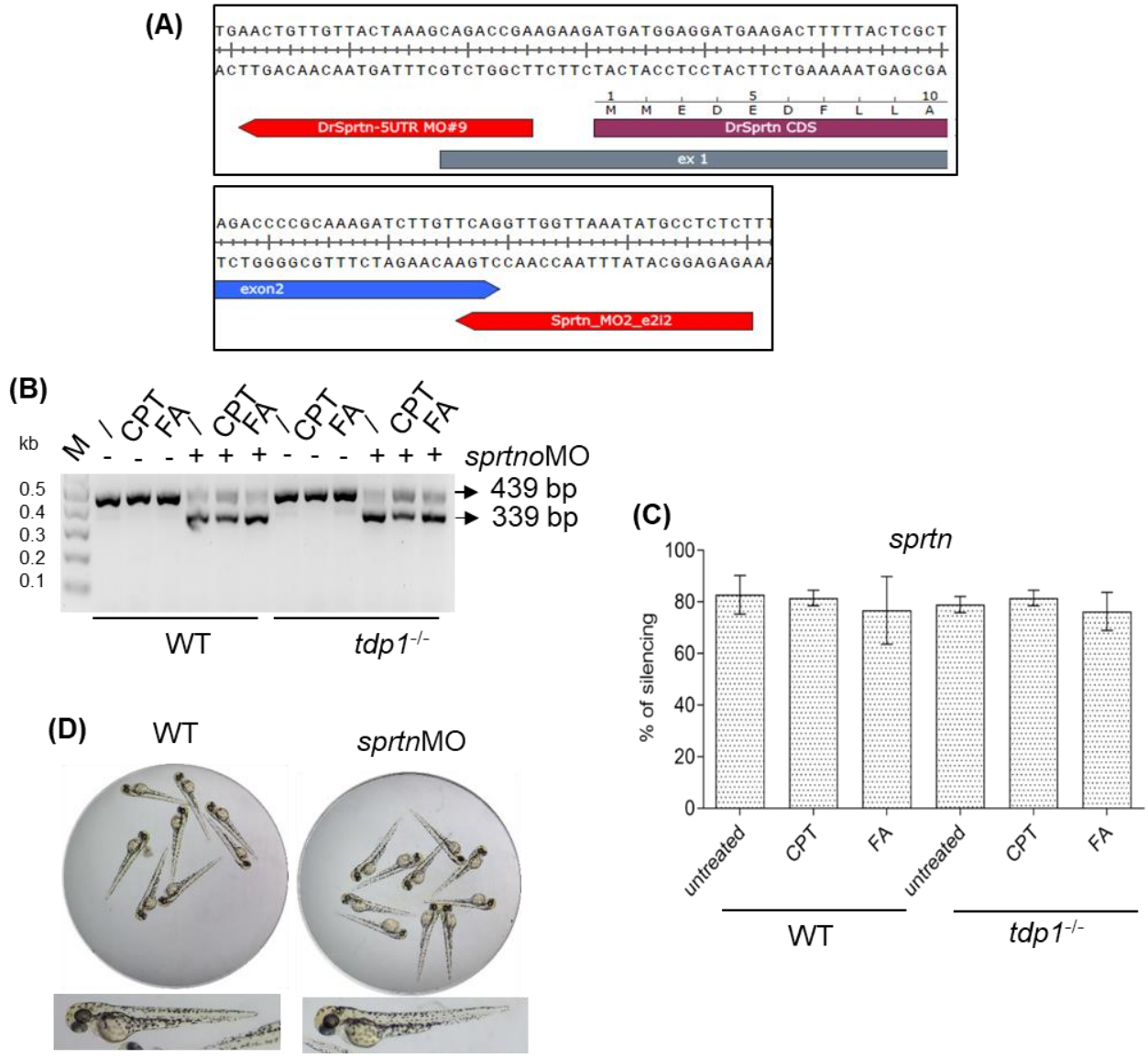

Figure 22. Silencing of *sprtn* using morpholino oligonucleotides in zebrafish embryos. (A) Schematic representation of ATG and splice-blocking zebrafish *sprtn* morpholino oligonucleotide binding sites. The ATG-blocking morpholino oligonucleotide targets the *sprtn* UTR region, while the splice-blocking morpholino oligonucleotide targets the exon 2 intron 2 boundary. (B) DNA gel electrophoresis showing the resolution of PCR reactions performed on cDNA isolated from 2-dpf stage embryos after injection of exon-skipping morpholino oligonucleotide at the one cell stage. (C) Quantification of *sprtn* silencing from (B): *sprtn* silencing efficiency was approximated as a reduction in WT band, quantified using Image J and presented as a fold change to WT (mean ± SD) (n = 4). (D) Overall and individual images of 2-dpf stage WT and *sprtn*-silenced embryos. No phenotypic changes were observed.

Optimization of *TDP1* silencing was conducted in RPE1 cells, utilizing scrambled siCTRL as a control to validate silencing specificity (Figure 23A). Throughout the experiments, SPRTN siRNAs were used alongside *TDP1* siRNAs to silence the human *SPRTN* gene (Christina

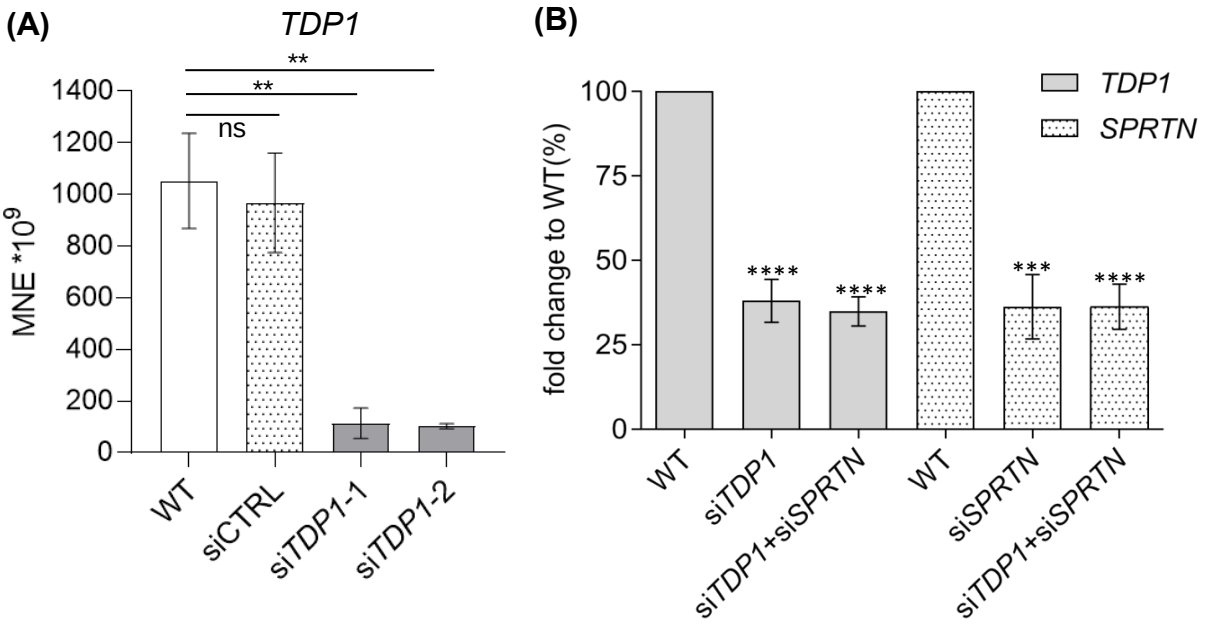

Supina Pavic, 2023) Silencing of *SPRTN* with 65% efficiency (Figure 23B) resulted in a significant increase in TOP1-DPC levels (3.6-fold), which is a similar effect to silencing of *TDP1* (3.7-fold) (Figures 19A and B).

Figure 23. Optimization of *TDP1* silencing in RPE1 cells and assessment of *TDP1* and SPRTN gene silencing efficiency in DPC experiments. A) The optimization of *TDP1* silencing in human RPE1 cells was achieved through siRNA-mediated approaches. Cells were treated with siRNAs as detailed in Table 6 for a duration of 72 hours. The presented results represent the mean ± SD, with statistically significant changes, identified through an unpaired two-sample Student's t-test, marked with **($p < 0.01$). B) The quantification of silencing efficiency was performed via qPCR. The results depict the mean percentage reduction in expression compared to untreated WT cells, presented as mean ± SD (n = 9, one-sample Student's t-test, statistically significant changesindicated with ***($p < 0.001$), and ****($p < 0.0001$))

When both *SPRTN* and *TDP1* were silenced (Figure 23B), TOP1-DPCs accumulated dramatically (14.3-fold increase), suggesting that both proteins are involved in TOP1-DPCs removal (Figures 19A and B). The same setup after CPT exposure (50 nM, 1h) showed a

somewhat different pattern: *SPRTN* silencing caused a 12.6-fold increase, *TDP1* silencing 7.1-fold increase, whereas double silencing additionally increased TOP1-DPC levels by 29.2-fold (Figures 19A and B). FA treatment (1 mM, 20 min) dramatically increased TOP1-DPC levels to a similar extent under all conditions (Figures 19C and D).

In embryos, *sprtn* knockdown had a tremendous effect on H3-DPC levels in both, WT and *tdp1* mutants with 5.7- and 5.1-fold increase, respectively (Figures 20A and B). CPT (10 μM, 1 hour) caused a different pattern of H3-DPC induction in the same backgrounds: a 4.8-fold increase in *sprtn*-silenced embryos and a 6.6-fold increase in *sprtn*-silenced *tdp1* mutants (Figures 20A and B). Both inductions were weaker than in CPT-treated mutant embryos with functional Sprtn (7.3-fold) (Figures 20A and B). The levels of H3-DPCs observed in *tdp1* mutants after exposure to CPT show a significant increase compared to the endogenous levels of H3-DPCs in *tdp1* mutants ($P < 0.0001$). Moreover, this increase is even greater than the increase caused by *sprtn* silencing in *tdp1* mutants ($P < 0.0001$) (Figures 20A and B). At the same time, H3-DPC levels were similarly induced after *sprtn* silencing in WT and mutant embryos before and after CPT treatment (Figures 20A and XB). Compared with CPT-treated WT or *tdp1* mutant embryos, knockdown of *sprtn* had no further effect on the increase in H3-DPCs ($p < 0.05$) (Figures 20A and B). *Sprtn* knockdown in FA-treated embryos (5 mM, 30 min) further increased H3-DPC levels compared in embryos with functional Sprtn: 8- and 8.5-fold increase in WT and mutants, respectively, versus 5.3- and 5.1-fold increases in WT and mutants with functional Sprtn, respectively (Figures 20C and D).

In RPE1 cells, SPRTN deficiency caused a very strong accumulation of H3-DPCs (3.2-fold increase) (Figures 21A, B, E and F). No additional effects on H3-DPC levels were observed when both *SPRTN* and *TDP1* were silenced. *SPRTN* silencing in untreated and in CPT-treated cells increased H3-DPCs similarly: by 3.2- and 3.2-fold, respectively (Figures 21A, B, E and F). However, simultaneous silencing of *TDP1* and *SPRTN*, followed by exposure to CPT had an additive effect on H3-DPC levels resulting in a 7.9-fold increase (Figures 21A, B, E and F). This increase is not as strong as in TOP1-DPC levels, where CPT treatment after simultaneous silencing dramatically increased TOP1-DPCs: from 14.3-fold to 29.2-fold (Figures 19A and B). When exposed to FA (1 mM, 20 min), *SPRTN*-silenced cells, as well as *SPRTN*- and *TDP1*- silenced cells exhibited a 1.8- and 1.9-fold increases in H3-DPCs, respectively, compared with FA-treated WT cells (Figures 21C and 21D).

4.7. *Sprtn* silencing increases *tdp1* expression in zebrafish embryos and human cells

To investigate the interplay between TDP1 and SPRTN at the gene expression level, we quantified their mRNA levels under different conditions of gene silencing and DPC induction. In zebrafish embryos, knockdown of *sprtn* resulted in a strong 2.2-fold increase in *tdp1* expression (Figure 24A), whereas this induction was much weaker in RPE1 cells where *SPRTN* silencing increased *TDP1* expression by 1.2-fold (Figure 24C). Furthermore, the increase in *tdp1* mRNA levels after *sprtn* knockdown led to an increase in Tdp1 protein levels (1.25-fold compared to WT embryos) (Figures 24A and B).

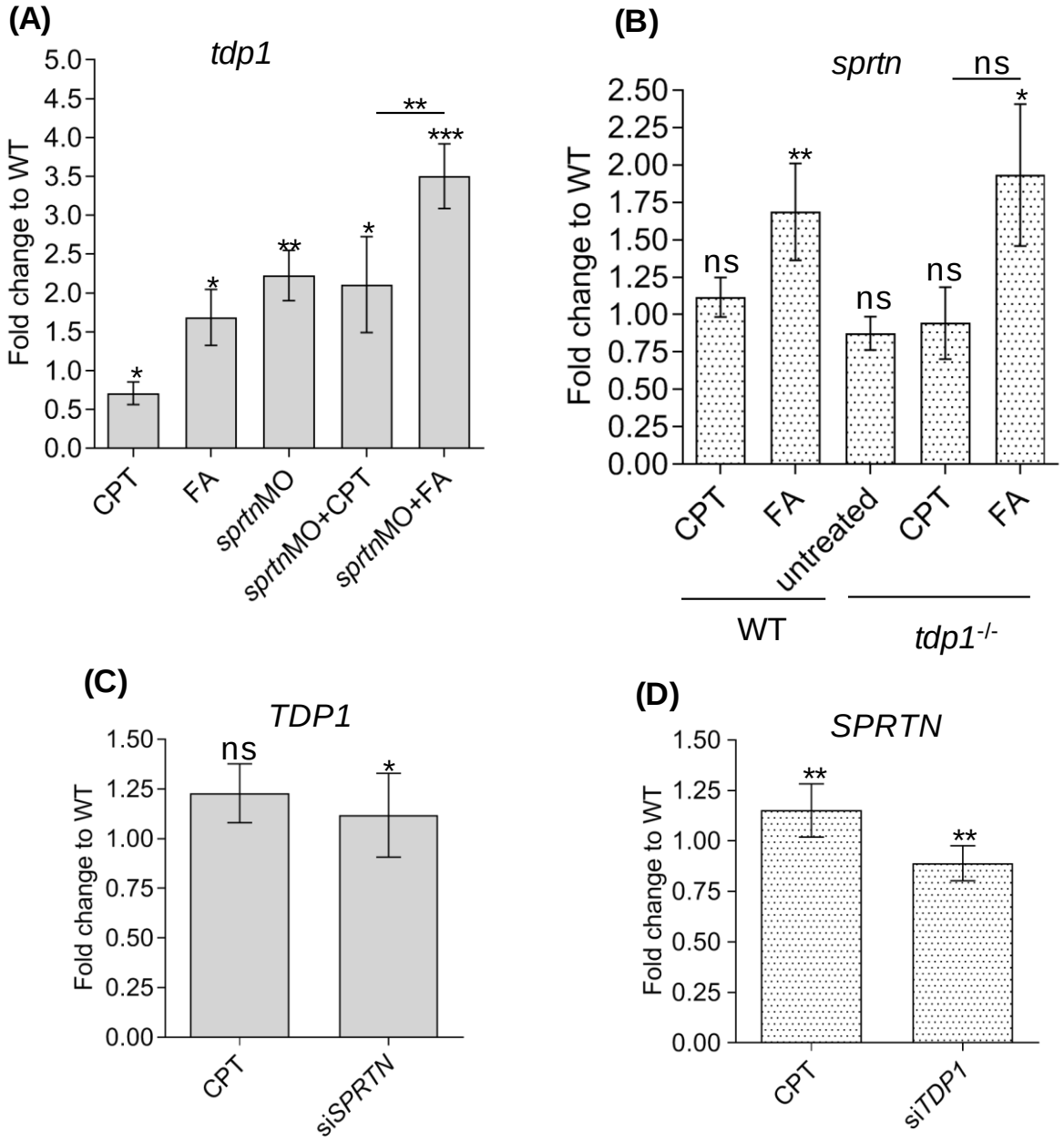

Figure 24. Effects of TDP1 and SPRTN deficiency on *tdp1* and *sprtn* mRNA expression levels in zebrafish embryos and RPE1 cells. A) Zebrafish *tdp1* expression levels *sprtn*

knockdown and CPT and FA treatment. B) *Sprtn* expression in WT and *tdp1* mutant embryos before and after CPT (10 µM, 1h) and FA (1 mM, 20 min). C) Expression levels of *TDP1* in RPE1 cells after *SPRTN* silencing and CPT exposure (50 nM, 1 hour) D) *SPRTN* levels decrease after *TDP1* silencing and increased in CPT-treated RPE1 cells. Corresponding silencing efficiencies are shown in Figures 22 and 23 (mean ± SD; n = 3 independent experiments). Unpaired one-sample t-tests were performed with GraphPad Prism, with significant shown as * ($p < 0.05$), ** ($p < 0.01$), or *** ($p < 0.001$).

Brief acute exposure of embryos to CPT (10 µM, 1h) which strongly induced Top1-DPCs (2.8-fold) (Figures 19A and B) resulted in a 29% (0.7-fold) decrease in *tdp1* expression (Figure 24A). In contrast, a lower dose of CPT (1 h, 50 nM) in RPE1 cells, which induced TOP1-DPCs by 2-fold (Figures 20A and B), did not significantly alter *TDP1* expression (Figure 24C). The combination of *sprtn* silencing and CPT treatment had no further effect on *tdp1* expression compared to *sprtn*-silenced non-treated embryos (Figure 24A). In contrast to the effects caused by CPT, treatment of WT embryos with FA (30 min, 5 mM) increased *tdp1* expression by 1.7-fold (Figure 24A). This effect was even more pronounced in FA-treated *sprtn*-silenced embryos, in which a 3.5-fold increase in *tdp1* expression was observed (Figure 24A). In contrast to the increase in *tdp1* mRNA levels, brief acute exposure to FA (5 mM, 30 min) had no effect on Tdp1 protein levels, probably because 30 min is too short to cause such an increase (Figures 24A and B).

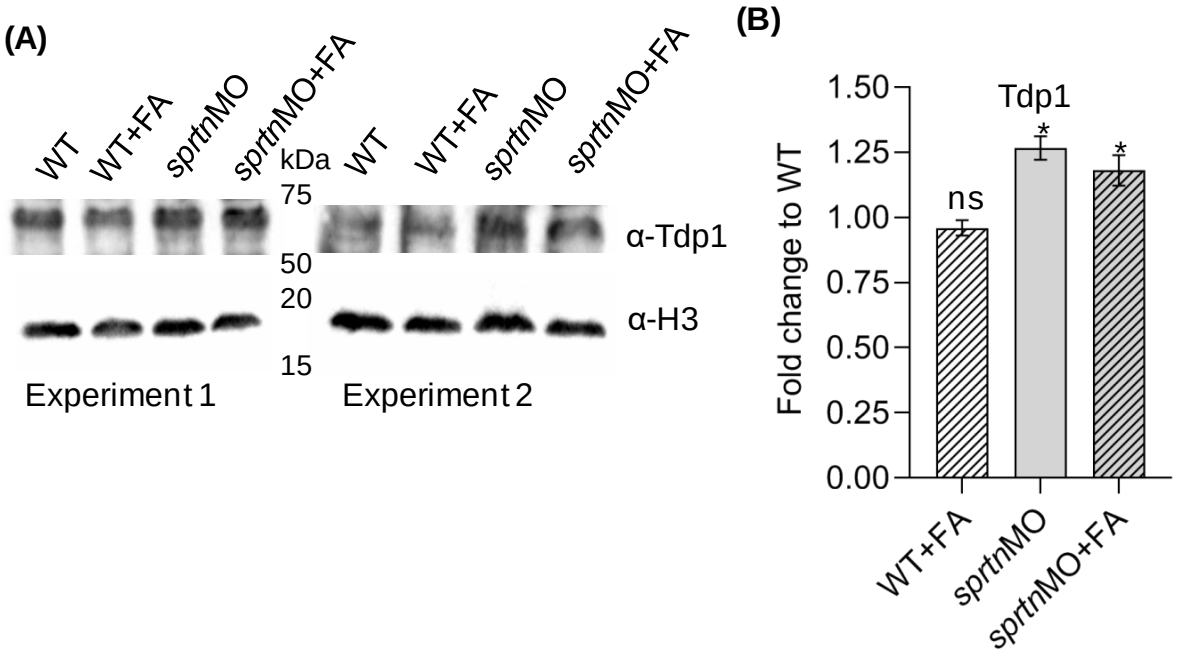

Figure 25. Western blot analysis of zebrafish Tdp1 after *sprtn* silencing and treatment with FA A) Western blot showing Tdp1 protein levels in 2-day- old zebrafish embryos after *sprtn* silencing and exposure to FA (5 mM, 30 min). Histone H3 is included as a loading control. B) Quantifications of A. Data represent mean fold change to WT ± SD (n = 3), statistical significance was determined using an unpaired one-sample Student's t-test (* ,$p < 0.05$).

The expression levels of *sprtn* in embryos were similar in WT and mutant embryos and did not change significantly after CPT exposure. However, FA increased *sprtn* expression 1.5-fold and 1.8-fold in WT and *tdp1* mutant embryos, respectively (Figure 24B). In RPE1 cells, *TDP1* silencing caused a 10% decrease in *SPRTN* expression (Figure 24D), whereas CPT exposure increased *SPRTN* expression by 1.2-fold (Figure 24D). Silencing and knockdown efficiencies are shown in Figures 22 (*sprtn* MO) and 23 (RPE1 silencing).

4.8. *Tdp2* expression increases in TDP1-deficient RPE1 cells and zebrafish embryos

In the absence of TDP1, it was observed that TDP2 can participate in the repair of TOP1-induced DNA damage in cultured avian leukosis virus (ALV) induced bursal lymphoma DT40 cells, and in biochemical experiments using purified proteins (Ledesma et al., 2009b; Zeng et al., 2012). Therefore, qPCR experimentes were carried out to determine whether *TDP2* expression increases when TDP1 is depleted in cells and embryos. In RPE1 cells, *TDP2* expression remained the same after silencing *TDP1* and *SPRTN* without exposure to DPC inducers. Control siRNA (siCTRL) did not affect *TDP1*, nor *TDP2* expression levels (Figures 23A and 41A). However, when cells were treated with CPT (50 nM, 1 h) *TDP2* expression increased strongly (1.8-fold) in *TDP1*-silenced cells and moderately (1.3-fold) in *SPRTN*-silenced cells (Figure 26A). These data suggest that TDP2 may help overcome CPT-induced DNA damage in the absence of TDP1 in human cells. Next, *tdp2* expression was tested in zebrafish. Because zebrafish has two *tdp2* orthologues, *tdp2a* (gene ID: 101887157) and *tdp2b* (gene ID: 553516), both genes were analysed. In the absence of Tdp1, the expression of both genes increased significantly: *tdp2a* by 3.7-fold and *tdp2b* by 1.6-fold (Figures 26B and 26C). Expression of *tdp2a* also increased after *sprtn* knockdown (*sprtn*MO) in WT (1.6-fold) and in *tdp1* mutants (2.3-fold). The effect of *sprtn* silencing on *tdp2b* expression is similar to the pattern observed for *tdp2a*, with a 1.4-fold increase in WT and a 2.1-fold increase in *tdp1* mutants (Figure 26C). In contrast, the expression pattern of the two *tdp2* orthologues in *tdp1* mutants is different: silencing of *sprtn* in mutants strongly decreased

tdp2a expression compared with non-silenced mutants (Figure 26B), whereas the pattern was reverse with respect to *tdp2b* expression, where silencing of *sprtn* caused an increase in *tdp2b* mRNA levels (Figure 26C).

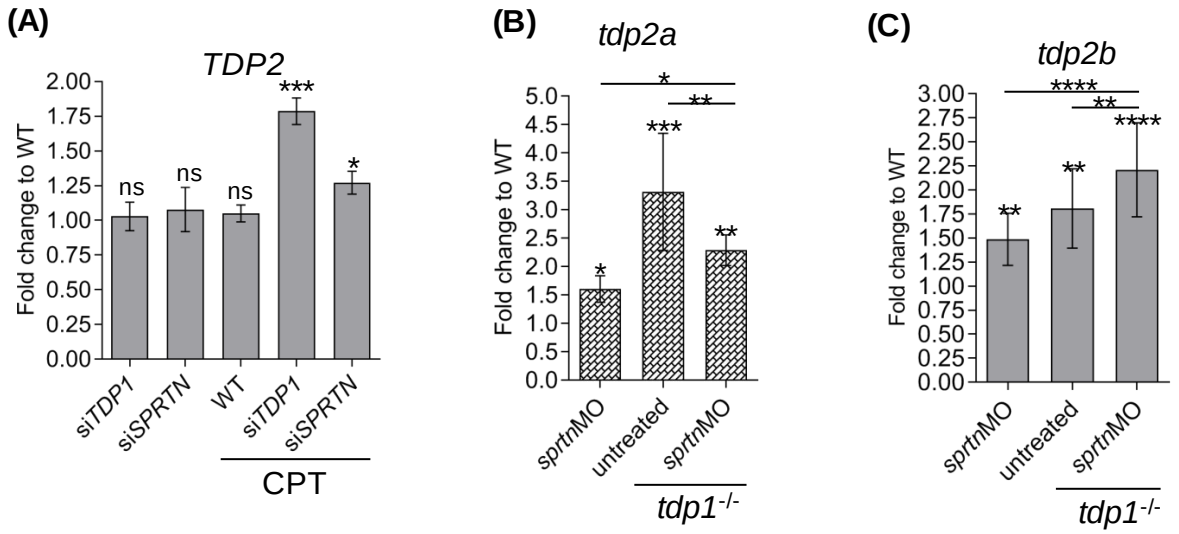

Figure 26. Effects of *TDP1* and *SPRTN* deficiency on *TDP2* expression in human RPE1 cells and embryos. A) *TDP2* significantly increases after *TDP1* silencing in CPT-treated RPE1 cells. B) *Tdp2a* expression is significantly increased in *tdp1* mutants with or without *sprtn* silencing and in *sprtn* morphants. C) *Tdp2b* expression significantly increases in *tdp1* mutants with or without *sprtn* silencing and in *sprtn* morphants. Results are presented as fold changes to WT (mean ± SD) from four biological replicates. One-sample, unpaired t-tests were performed with GraphPad Prism, with significant shown as * ($p < 0.05$), **($p < 0.01$), ***($p < 0.001$), or ****($p < 0.0001$).

4.9. TDP1 and SPRTN deficiency affects cell viability

Significant reduction was observed a in cell density after silencing of *TDP1* and *SPRTN* in RPE1 cells, so we quantified this effect using the MTT [3-(4,5-Dimethylthiazol-2-yl)-2,5-Diphenyltetrazolium Bromide] assay (P. Wang et al., 2010). Considering that TDP2 could compensate for the loss of TDP1 *in vitro* and in DT40 cells when cells are challenged with CPT (Ledesma et al., 2009; Zeng et al., 2012), the effects of TDP2 deficiency was investigated in combination with the lack of TDP1 and SPRTN on cell survival. Individual silencing of *TDP1*, *TDP2*, or *SPRTN* decreased cell viability by 50% (Figure 27A). Simultaneous silencing of *TDP1* and *SPRTN* further decreased cell viability by 68% ($p < 0.0001$). Interestingly, the effect was most pronounced when both *TDP1* and *TDP2* were

silenced, where viability decreased by 80%. Similar effect was obsered, an 84% decrease in viability, after all three genes were silenced (Figure 27A). The experiment was performed with three independent biological replicates, silencing efficiencies were measured for each condition and control siRNA (siCTRL) did not affect cell viability (Figures 27B, C, D and E).

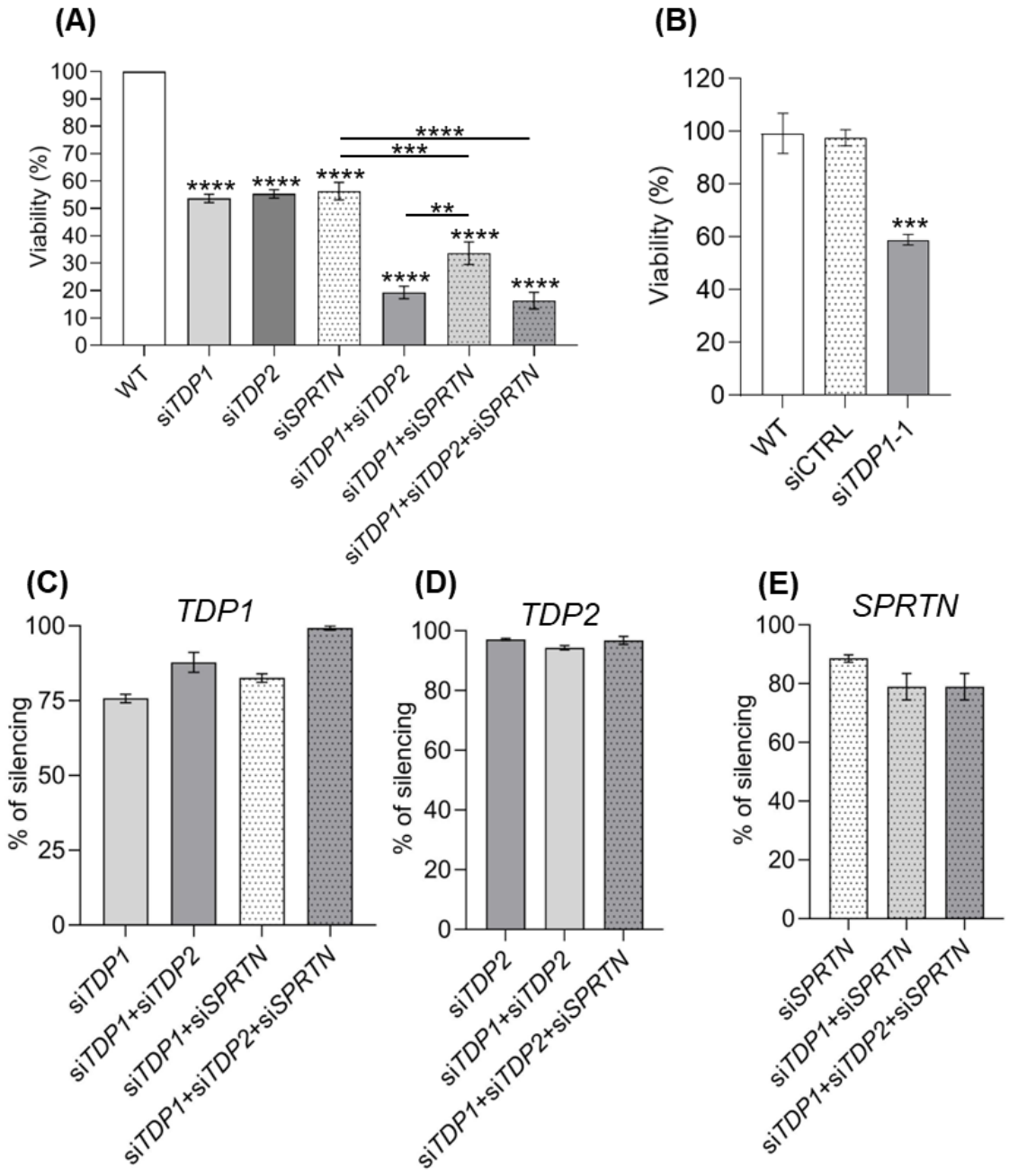

Figure 27. MTT viability assay after *TDP1*, *SPRTN* and *TDP2* gene silencing. A) RPE1 cell were incubated with siRNA listed in Table 6 for 72 h. All measurements were normalized to WT from three different experiments. B) Control MTT experiment to show that silencing conditions do not affect cell viability. C-D) In parallel with the seeding of

cells for the MTT viability assay, cells were seeded for silencing verification using the same experimental conditions. Silencing efficiencies were determined using qPCR analysis and presented as the percentage reduction in expression to WT ± SD from three technical replicates. Unpaired one –sample t-tests were performed with GraphPad Prism, with significant shown as *** ($p < 0.001$) and **** ($p < 0.0001$).

4.10. A lyophilization step replaced TCA protein precipitation and increased RADAR reproducibility

The RADAR method was used in this study mainly because it is currently the only available technique for specific isolation of DPCs that is sensitive enough to visualize both total and specific DPCs, and doesn't require expensive equipment (Kiianitsa & Maizels, 2013, 2014, 2020). This approach involves several steps: initially, cells are lysed in a guanidinium-based buffer; then, DNA and DPCs are precipitated, and the resulting pellet is washed. Subsequently, the pellet is dissolved, with one portion dedicated to DNA detection and the other portion normalized based on DNA content. Next steps include benzonase treatment to release DPCs, followed by precipitating the DPCs using trichloroacetic acid (TCA) and subsequent extensive washing to remove TCA traces. Unfortunately, the method results in significant sample loss, especially during protein precipitation and subsequent washing steps, which leads to low experimental reproducibility, both within the same experiment, and between different experiments. To address this concern, the lyophilization step was introduced, which effectively replaces the TCA-mediated protein precipitation. After the initial steps, in which both DNA and DNA-associated DPCs are pelleted, they are dissolved in an 8mM NaOH solution. Following this, the DPCs are released by treatment with benzonase. The aqueous solution containing dissolved DPCs is then subjected to the overnight lyophilization. This results in a powder consisting of DPCs and RNA adducts, which are dissolved in an SDS loading buffer and subsequently subjected to analysis using silver staining or slot/western blot techniques. Silver staining results (Figures 43, 44, 45, and 46) show significant improvement in consistency across different biological triplicates and different experimental isolations, including different mutant strains (Figure 43), gene silencing (Figures 44, 45A and B, 46) and chemical exposure (Figures 44 and 45C).

4.11. Loss of Tdp1 leads to DPC accumulation in zebrafish embryos

Tdp1 mutants have significantly higher endogenous DPC levels than WT embryos. The change is 1.4-fold increase and is statistically significant (Figure 28, n = 4). All experiments

in embryos were repeated 4 - 6 times (biological replicates), because the results showed higher variability compared to experiments in RPE1 cells. CPT treatment had no effect on total DPC levels in WT embryos but caused a significant increase (1.7-fold) in *tdp1* mutants (Figure 28). In contrast, the general DPC inducer, FA, caused a similar increase in total DPCs independent of Tdp1 deficiency: 2.2-fold in WTs and 2.1-fold in *tdp1* mutants (Figure 28). Exposure to CPT or FA had no effect on embryonic phenotype up to 2-dpf stage (data not shown) when embryos were collected for DPC analysis.

Following the analysis of the endogenous and chemically induced total DPC levels in *tdp1* mutants, the interplay of Tdp1 and Sprtn in DPC removal was investigated *in vivo*. Knockdown of *sprtn* resulted in a strong and significant increase in total DPC levels in both WT and *tdp1* mutant embryos (2.4-fold and 2.5-fold, respectively) (Figure 28). Compared with untreated WT embryos, CPT exposure increased total DPCs in *sprtn*-silenced embryos 2.6-fold in and 3.1-fold in *tdp1* mutant *sprtn*-silenced embryos (Figure 28). Also, *sprtn* silencing caused a significant additive effect on total DPC increase ($p < 0.001$) in CPT-treated WT and mutant embryos (Figure 28). In contrast, the effect of *sprtn* silencing was not significant in either WT ($p > 0.05$) or mutant embryos ($p > 0.05$) when exposed to the general DPC inducer, FA (Figure 28).

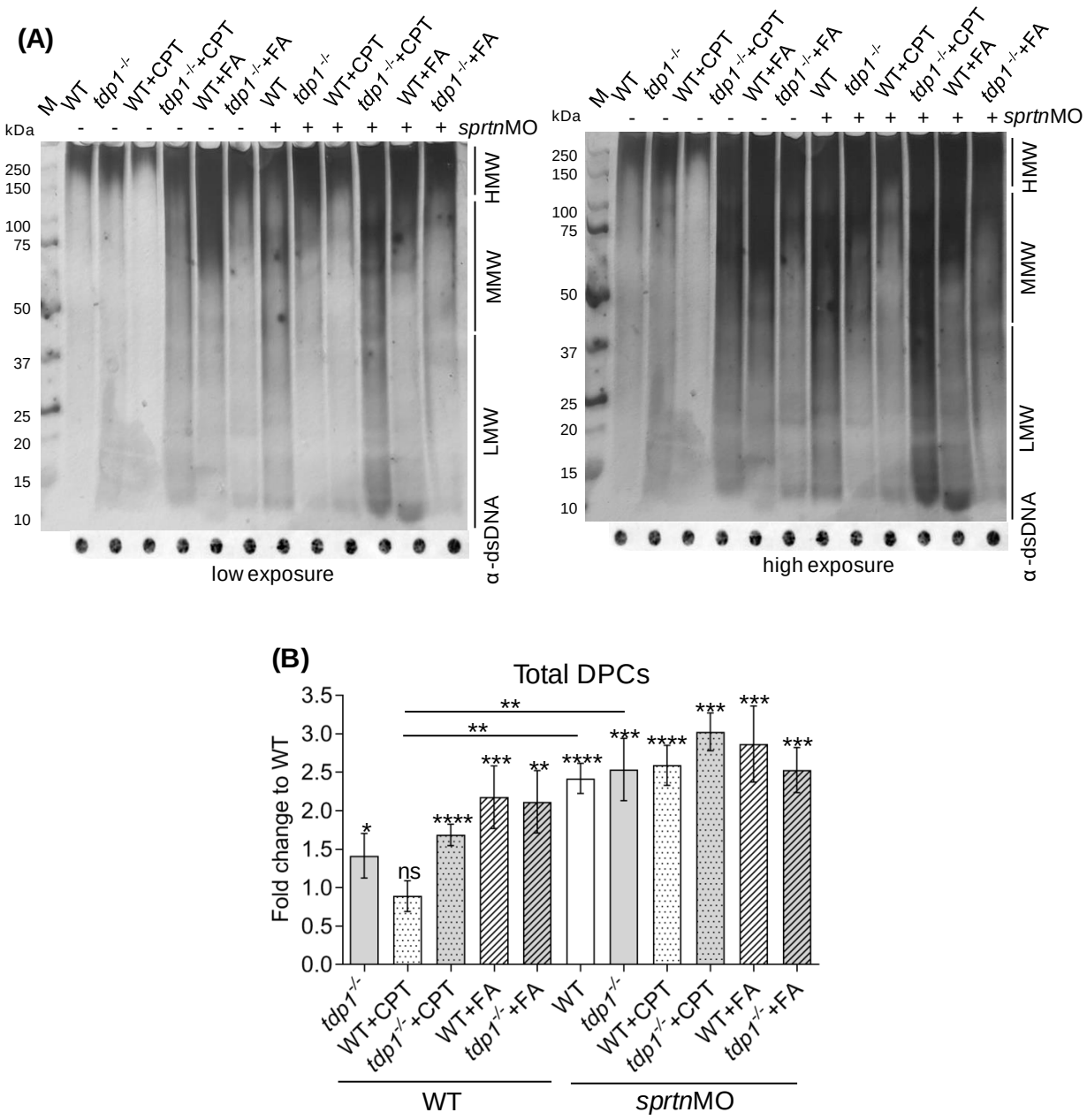

Figure 28. DPC analysis in Tdp1 and Sprtn deficient embryos under physiological conditions and after CPT (10 µM, 1h) and FA (5 mM, 30 min) treatment. A) DPCs were isolated from 2-dpf stage embryos using the RADAR assay (30 embryos per condition, n = 4), resolved on the SDS acrylamide gel, and stained with silver (left panel - low exposure, right panel - high exposure). Dot-blots showing DNA loading controls for DPC analysis prior to benzonase treatment are shown below (DPC equivalent of 200 ng of total DNA was loaded per well). B) Quantification of A. Data represent mean fold change to WT ± SD (n = 4), statistical significance was established using an one-sample unpaired Student's t-test (* (p < 0.05), ** (p < 0.01), *** (p < 0.001), and **** (p < 0.0001)).

Analysis of total cellular DPCs revealed important insights into the functions of TDP1 and SPRTN in DPC removal and about the effects of DPC inducers. However, to determine which DPCs are most affected by targeted perturbations, DPCs were divided into three subgroups: High Molecular Weight (HMW > 151 kDa), Medium Molecular Weight (MMW, 40 kDa to 150 kDa), and Low Molecular Weight (5 - 40 kDa) DPCs. This categorization is not ideal, but it can provide valuable additional information as opposed to only quantifying total DPC levels (Anticevic et al., 2023). Studying the size distribution of DPCs can help us better understand which repair factors are involved in their repair and whether the function of a particular factor depends on the size of the crosslink. More detailed analysis revealed that the 1.4-fold increase in total endogenous cellular DPCs in the *tdp1* mutants was due to the increase in low and medium molecular weight DPCs, whereas high molecular weight DPCs were not affected (Figure 28A, high exposure). Specifically, Tdp1-deficient embryos accumulated 1.7-fold more endogenous LMW DPCs and 1.6-fold more endogenous MMW DPCs than WT embryos (Figures 28A and 29A and B). CPT treatment further increased LMW DPC levels: 3.1-fold in mutants and 1.5-fold in WTs (Figures 28A and 29A). A different pattern was observed after induction of general DPCs by FA, where levels of LMW DPCs increased 2.7- to 2.5-fold in both WT and mutant embryos (Figures 28A and 29A). As expected, treatment with FA had strong effects on LMW DPC levels considering that most of cellular DPCs are histones (Kiianitsa & Maizels, 2020). Unexpectedly, LMW DPCs were also induced by CPT treatment (1.5-fold), although not as strongly as after FA treatment (Figures 28A and 29A). When *sprtn* was knocked down, WT embryos accumulated more LMW DPC (3.1-fold) than mutants (2.4-fold) (Figures 28A and 29A). CPT treatment further increased LMW in mutant embryos (3.1- fold) but had no effect on LMW levels in WT embryos after knockdown of *sprtn*. LMW levels were not further affected by FA treatment when *sprtn* was silenced in WT or *tdp1*-deficient embryos (Figures 28A and 29A).

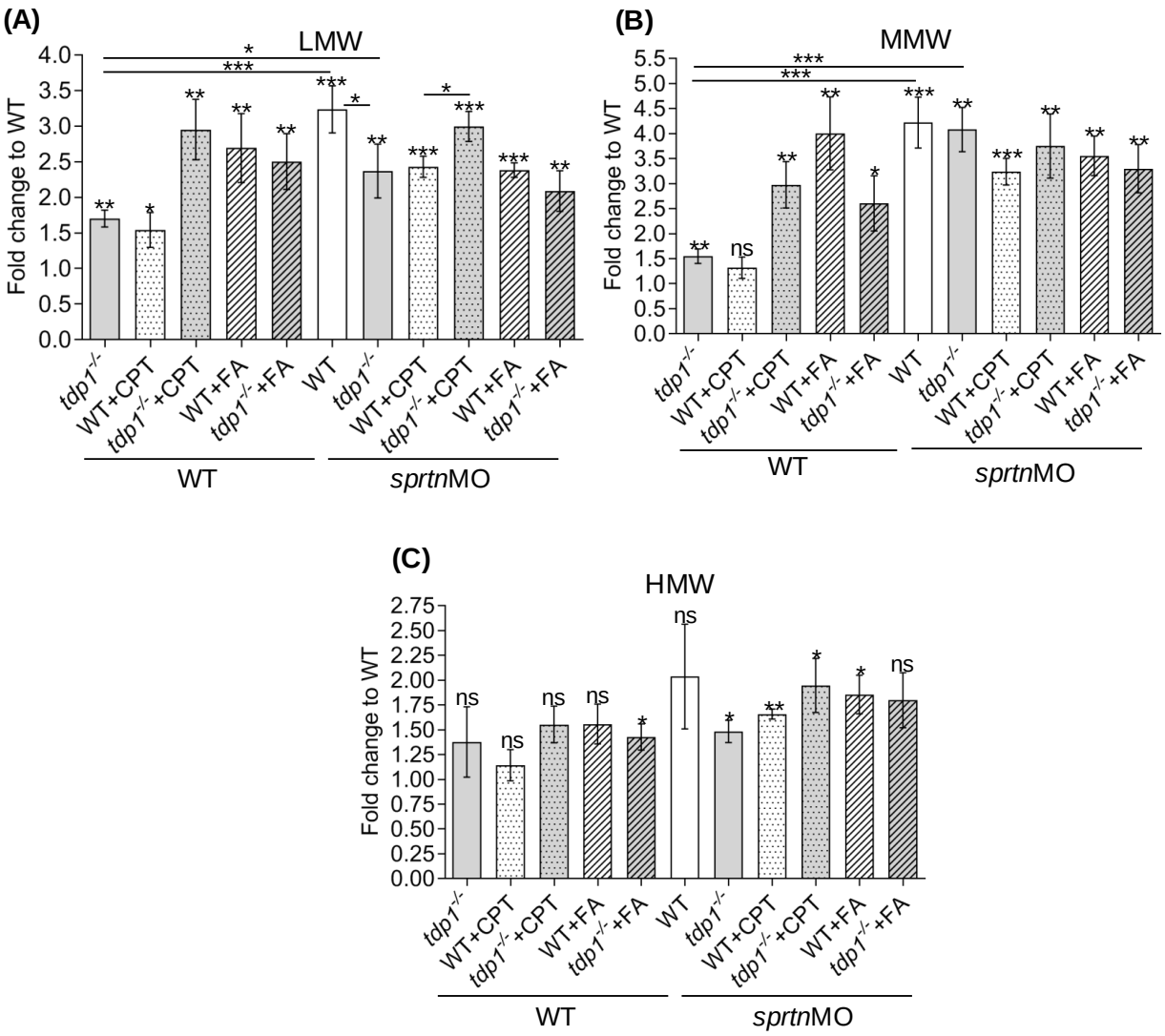

Figure 29. Size dependent DPC analysis in Tdp1 and Sprtn deficient embryos under physiological conditions and after CPT (10 µM, 1h) and FA (5 mM, 30 min) treatment from Figure 28A. Quantifications of LMW DPCs (protein size < 40 kDa) (A), MMW DPCs (40 kDa to 150 kDa) (B) and HMW (>150 kDa) (C) from Figure 28A. Data represent mean fold change to WT ± SD (n = 4), statistical significance was established using an one–sample unpaired Student's t-test (* ($p < 0.05$), ** ($p < 0.01$), *** ($p < 0.001$), and **** ($p < 0.0001$)).

CPT treatment of *tdp1* mutants strongly increased the levels of MMW DPCs (by 2.9-fold), in contrast to a slight statistically nonsignificant change in WT embryos (Figures 28A and 29B). FA increased MMW DPCs by 2.6-fold in mutants and by 4.1-fold in WT embryos, showing a similar pattern of induction as LMW but with much stronger absolute changes. MMW DPCs increased 4.1-fold in both WT and *tdp1* mutants after *sprtn* knockdown treatment (Figures

28A and 29B). MMW DPCs in WT embryos and *tdp1* mutants were not additionally affected by CPT or FA treatment in *sprtn* knockdowns (Figures 28A and 29B).

Tdp1 deficiency, *sprtn* knockdown, and exposure to CPT or FA had the least effect on HMW DPCs. However, some of the effects were still pronounced. HMW DPCs increased following *sprtn* knockdown by 1.5-fold in *tdp1* mutant embryos ($p < 0.05$) and by 2-fold in WT embryos ($p > 0.05$) (Figures 28A and 29C). HMW DPCs increased 1.9-fold in the *tdp1* mutant and 1.6-fold in WT when *sprtn* knockdown was combined with CPT treatment. Independent of Tdp1 deficiency, knockdown of *sprtn* showed a similar induction of 1.8-fold in both *tdp1* mutant and WT embryos which were treated with FA (Figures 28A and 29C). The minor variations in HMW DPCs observed between the *tdp1* mutant and WT embryos with and without CPT or FA treatment were not statistically significant.

4.12. *TDP1* silencing causes DPC accumulation in human cells

DPC levels were quantified in RPE1 cells after *TDP1* and *SPRTN* silencing. The silencing of *TDP1* alone caused a small, but statistically significant increase in total DPCs (1.2-fold) (Figures 30A and B), whereas silencing of *SPRTN* caused a stronger effect: 1.6-fold increase in DPC levels (Figures 30A and B, $n = 4$). When both *TDP1* and *SPRTN* were silenced (Figure 23), additive effect was observed: a 2-fold increase in total cellular DPCs (Figures 30A and B). Considering that SPRTN is involved in the removal of very diverse DPCs, ranging from LMW proteins such as histones to bulky (HMW proteins such as topoisomerases (Vaz et al., 2016), crosslikes were further investigated for the size distribution of the isolated DPCs. *TDP1* silencing increased LMW and MMW DPCs by 1.3- and 1.5-fold, respectively (Figures 30A middle and right panel and 30C). The effect of the increase was not as strong as that of *SPRTN* silencing, which showed an increase of 2.6-fold in the LMW region and 1.9-fold in the MMW region (Figure 30C). The silencing combination showed an additive effect on the increase in LMW and MMW DPCs (3.2- and 2.2-fold, respectively). The silencing combination also showed a 1.7-fold increase in HMW DPCs, in contrast to single gene silencing, where no increase was observed (Figures 30A and C).

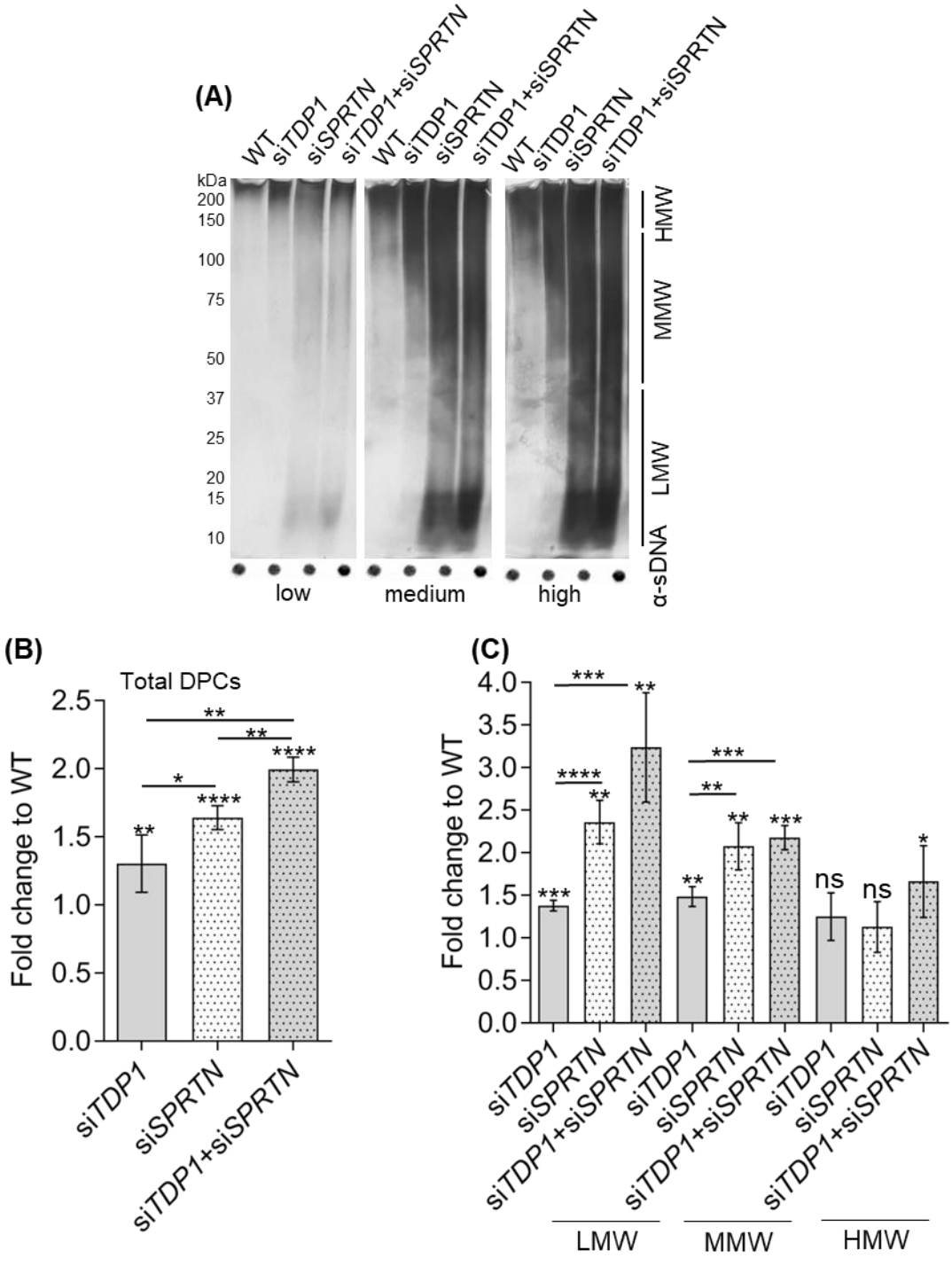

Figure 31. DPC analysis in RPE1 cells after *TDP1* and *SPRTN* gene silencing and after CPT (50 nM, 1h) treatment. A) DPC isolates from CPT-treated cells resolved on the SDS acrylamide gel and stained with corresponding DNA loading controls shown below. B) Total DPC quantification from (A) (n=3). C) HMW, MMW and LMW DPCs (quantification from A). All conditions were normalized to WT and statistical analysis was performed with

GraphPad Prism software using a one-sample unpaired t-test (* ($p < 0.05$), ** ($p < 0.01$), *** ($p < 0.001$), or **** ($p < 0.0001$)).

After analysing DPC accumulation in untreated cells, DPCs were quantified after exposure to CPTor FA. We used 50 nM CPT (1 h, 37 °C) in serum-free medium which induces TOP1-DPCs without the occurrence of DSBs (Ray Chaudhuri et al., 2012) and 1 mM FA in ice cold serum-free medium (20 min, 37 °C) which induces DPCs and probably also SSBs and DSBs based on the data from HEK293 cells (Mórocz et al., 2017). Treatment with CPT had a similar effect on DPC accumulation as did *TDP1* silencing: total DPCs increased by 1.3-fold, with the largest effect on LMW DPCs with a 1.6-fold increase (Figure 31). When CPT was added to *TDP1*-silenced cells, a 1.4-fold increase in total DPCs was observed (Figures 31A and B), again with the largest effect on LMW with a 1.6-fold increase (Figures 31A and C). CPT exposure of *SPRTN*-silenced cells caused very strong DPC accumulation (2.7-fold compared with untreated WT cells), again with the largest effect on LMW DPCs of 2.-fold increase (Figure 31). In contrast to untreated cells, treatment with CPT after double silencing had no additional effect on DPC accumulation (Figure 31). Similar to LMW DPCs, treatment with CPT resulted in a slight 1.3-fold increase in MMW DPCs (Figures 31A and C). Interestingly, MMW DPCs in cells with silenced *TPD1*, *SPRTN*, or *TDP1* and *SPRTN* were equally affected whether CPT was applied or not (Figure 31 A and C). CPT exposure had the least effect on HMW DPCs (Figure 31 A and C).

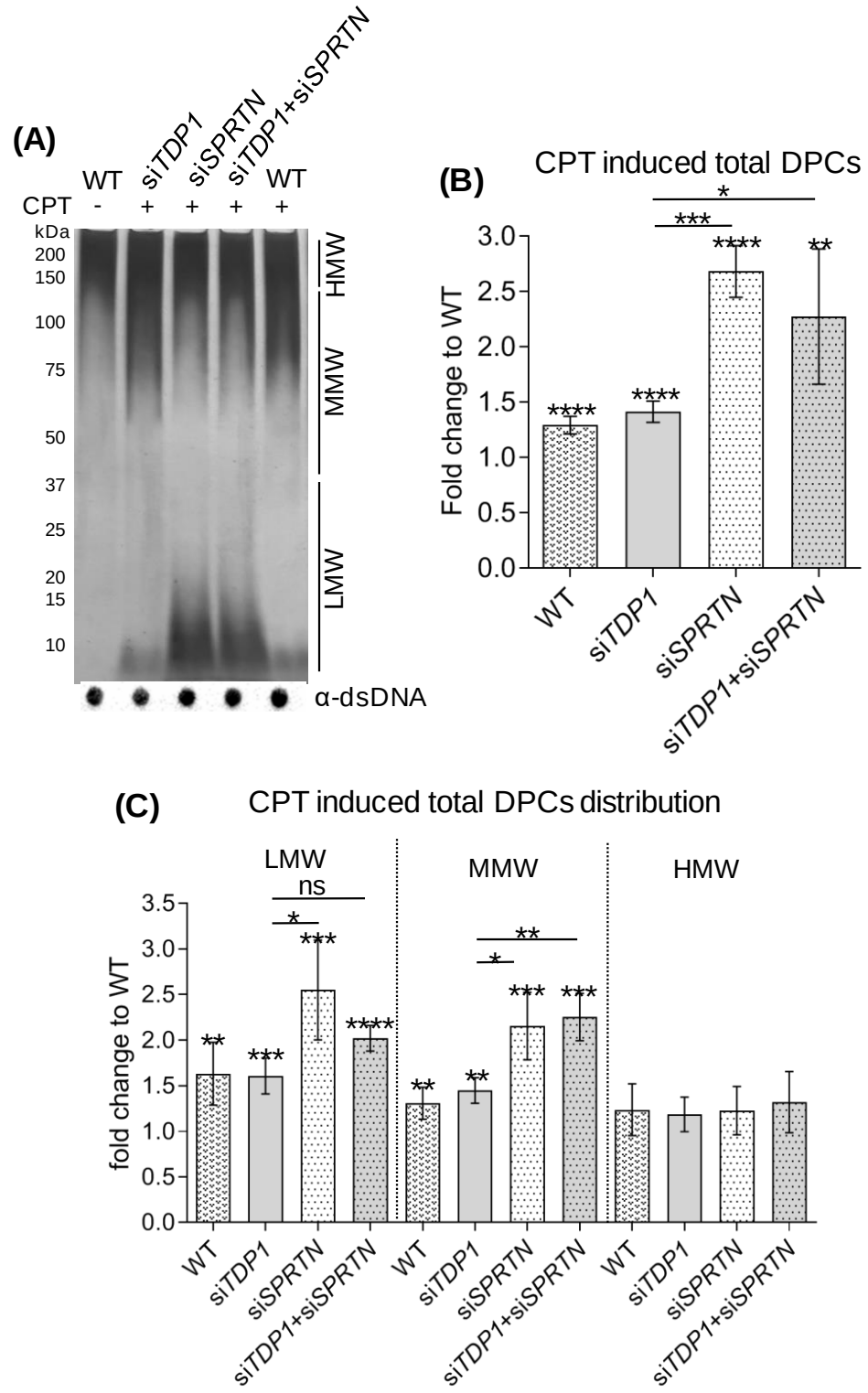

Figure 31. DPC analysis in RPE1 cells after TDP1 and SPRTN gene silencing and after CPT (50 nM, 1h) treatment. A) DPC isolates from CPT-treated cells resolved on the SDS acrylamide gel and stained with corresponding DNA loading controls shown below. B) Total DPC quantification from (A) (n=3). C) HMW, MMW and LMW DPCs (quantification from A). All conditions were normalized to WT and statistical analysis was performed with GraphPad Prism software using an one-sample unpaired t-test (* ($p < 0.05$), ** ($p < 0.01$), *** ($p < 0.001$), or **** ($p < 0.0001$)).

In contrast to the DPC response to CPT treatment, the pattern of DPC accumulation after FA treatment was very different. FA treatment increased total DPC levels by 2-fold in all samples regardless of which gene was silenced (Figure 32). In all samples, FA treatment had the greatest impact on LMW and MMW DPCs, which increased by 2.3 and 2.8-folds on average in comparison to untreated WT cells (Figure 32A and C). Proteins of high molecular weight were least affected by FA treatment and showed no statistically significant difference in comparison to WT (Figure 32C).

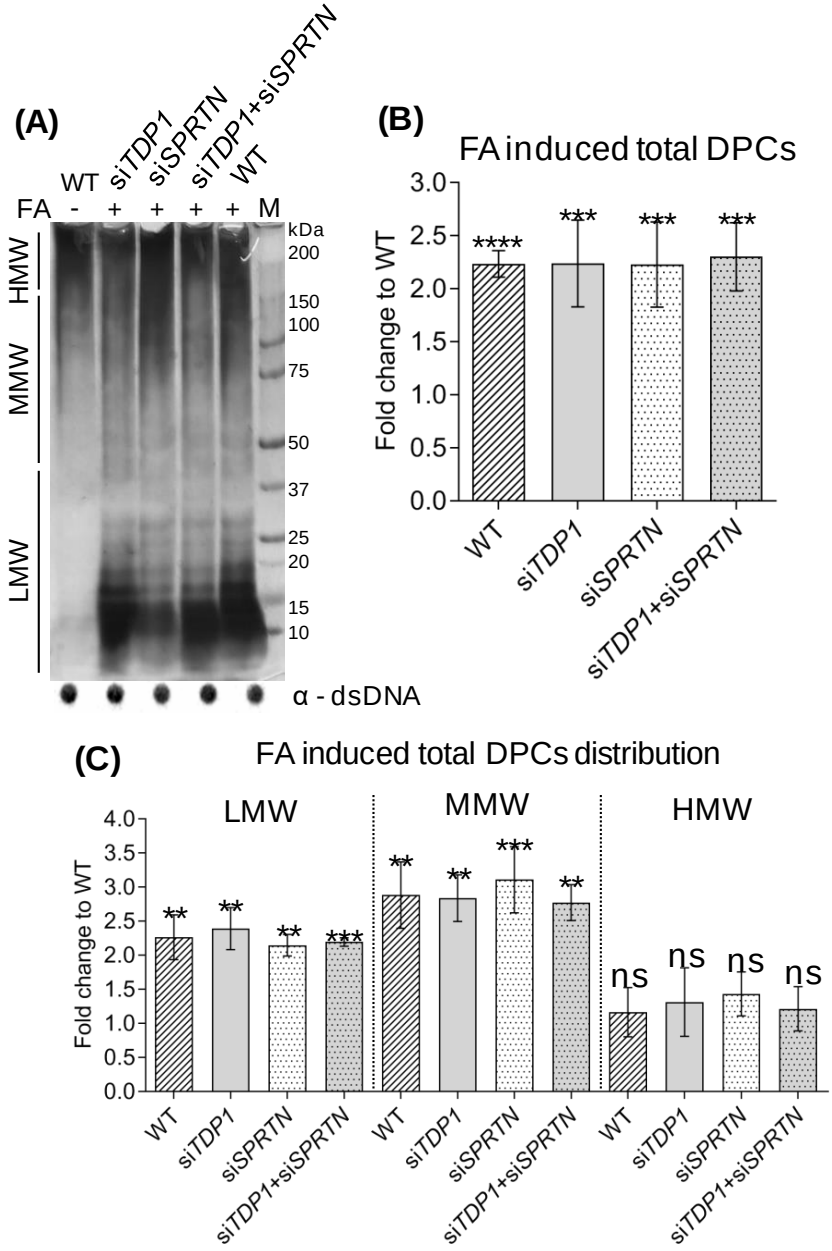

Figure 32. DPC analysis in RPE1 cells after *TDP1* and *SPRTN* gene silencing and after FA (1 mM, 20 min) treatment. A) DPC isolates from FA-treated cells resolved on the SDS

acrylamide gel and stained with silver with corresponding DNA loading controls. B) Quantification of (A) (n = 3). I) HMW, MMW and LMW DPC levels quantified from (A), a DPC equivalent of 200 ng total DNA was loaded per condition. All conditions were normalized to WT and statistical analysis was performed with GraphPad Prism software using an one-sample unpaired t-test (* ($p < 0.05$), ** ($p < 0.01$), *** ($p < 0.001$), or **** ($p < 0.0001$)).

4.13. Phylogenetic and syntenic comparison of human and zebrafish TDP2/Tdp2.

Tyrosyl-DNA phosphodiesterase 2 (TDP2) is a highly conserved genes found in all domains of life from bacteria to fungi, plants, algae, and animals (Figure 33 and Supplement 7). Surprisingly, only yeasts lack TDP2 protein, as was previously reported (Ledesma et al., 2009). Because TDP2 is an evolutionarily ancient protein (Figure 33), it has likely been lost in yeast lineages during evolution. Occasional *TDP2* duplications were observe over the course of evolution, specifically in some cyprinid species, including zebrafish and European carp (*Cyprinus carpio*) (Figure 33) and within the invertebrate group which is phylogenetically closer to vertebrates (Figure 33, in dark green), specifically in tunicates (*Styela clava*), echinoderms (*Anneissia japonica*) and cnidarians (*Dendronephthya gigantea*). Due to the teleost-specific whole genome duplication event (WGD) about 320 million years ago (Jatllon et al., 2004), zebrafish often have two paralogues corresponding to the single gene in other vertebrate species (Ravi & Venkatesh, 2008), and this is indeed the case for the *tdp2* gene which has two paralogues of human *TDP2*: *tdp2a* and *tdp2b* (Figure 33). Phylogenetic analysis showed that *tdp2b* is closer to *TDP2* in mammals and other vertebrates, whereas the *tdp2a* cluster in teleost fish diverged from the main vertebrate cluster (Figure 33, in light blue).

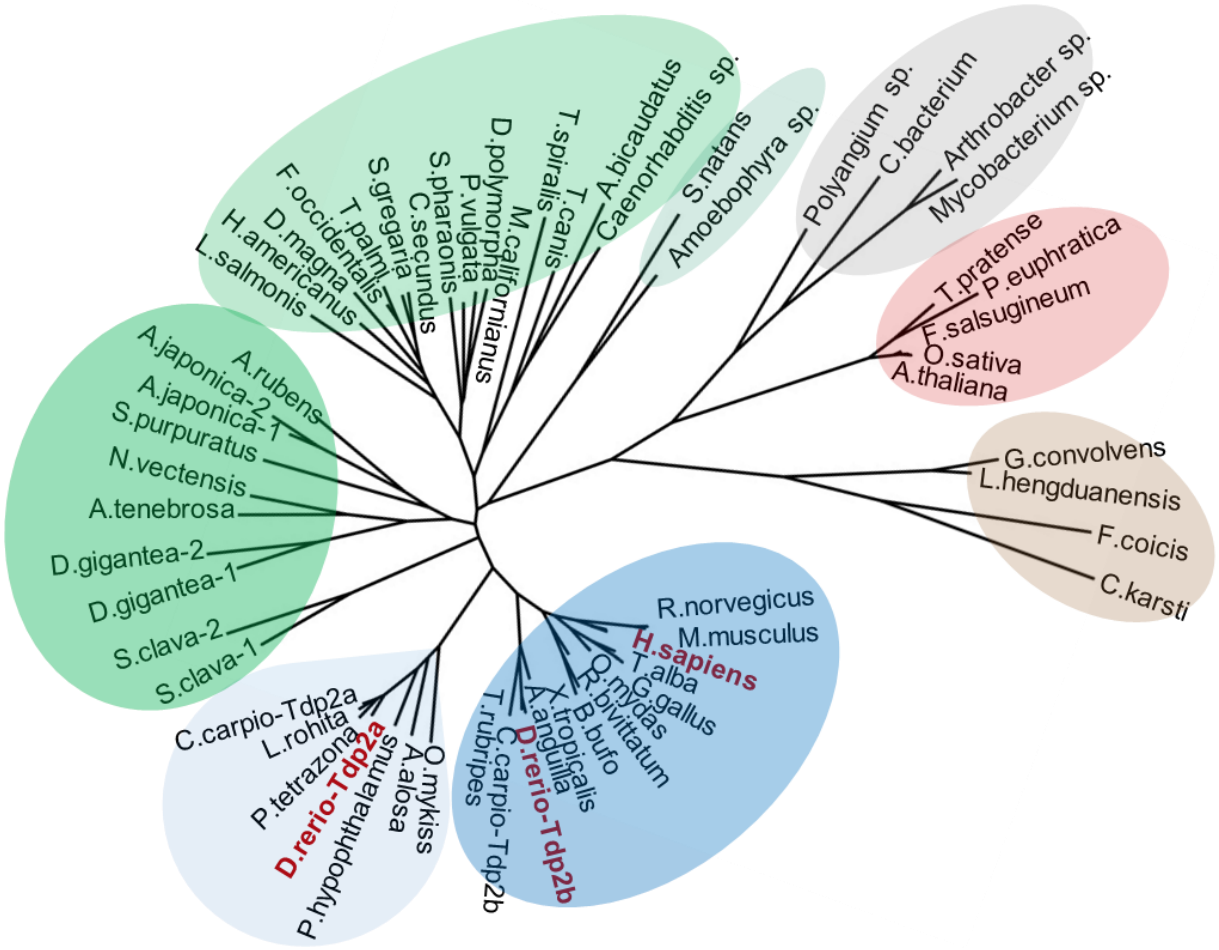

Figure 33. Phylogenetic analysis of Tyrosyl-DNA phosphodiesterase 2 in humans and zebrafish. Phylogenetic tree of tyrosyl-DNA phosphodiesterase 2 (*TDP2*). Vertebrate orthologues are shown in blue, and an additional cluster of *Tdp2* co-orthologues in fish is shown in light blue. Two clusters of invertebrate orthologues are shown in green, algae in light green, plant orthologues in red, fungi in brown and bacterial cluster in grey. Phylogenetic analysis was performed using the Maximum Likelihood method.

Next, synteny was analysed for *TDP2*: the human *TDP2* gene is located on chromosome 16, while in zebrafish *tdp2a* is located on chromosome 16, and *tdp2b* on chromosome 19. Syntenic analysis showed high conservation of gene environment between human and zebrafish *Tdp2* (Figure 34). Comparing the surrounding genes of *TDP2* in humans and zebrafish, we observe that upstream of human *TDP2*, there is a gene cluster consisting of *ACOT13*, *C6orf62*, and *GMNN*, which can also be found surrounding zebrafish *tdp2b* (Figure 34). Additionally, we find *RIPOR2* and *CARMIL*, which are also located upstream of zebrafish *tdp2b* (Figure 34). On the other side, downstream of human *TDP2*, there is a gene

cluster containing *KIAA0319* and *ALDH511*, which is found upstream from zebrafish *tdp2a* (Figure 34). Similarly, downstream of human *TDP2*, we find *MRS2* and *NRSN1*, which are located a bit further downstream from zebrafish *tdp2a* (Figure 34). Interestingly, this small chromosomal region surrounding *TDP2* shows gene duplication, similar to what we observe with the *tdp2* gene. For example, the downstream gene *NRSN1* has two orthologues: *nrsn1* downstream of *tdp2a* and *nrsn1l* downstream of *tdp2b* (Figure 34). The same is true for the downstream gene, *SOX4*, which has two orthologues: *sox4b* downstream of *tdp2a* and *sox4a* downstream of *tdp2b* (Figure 34).

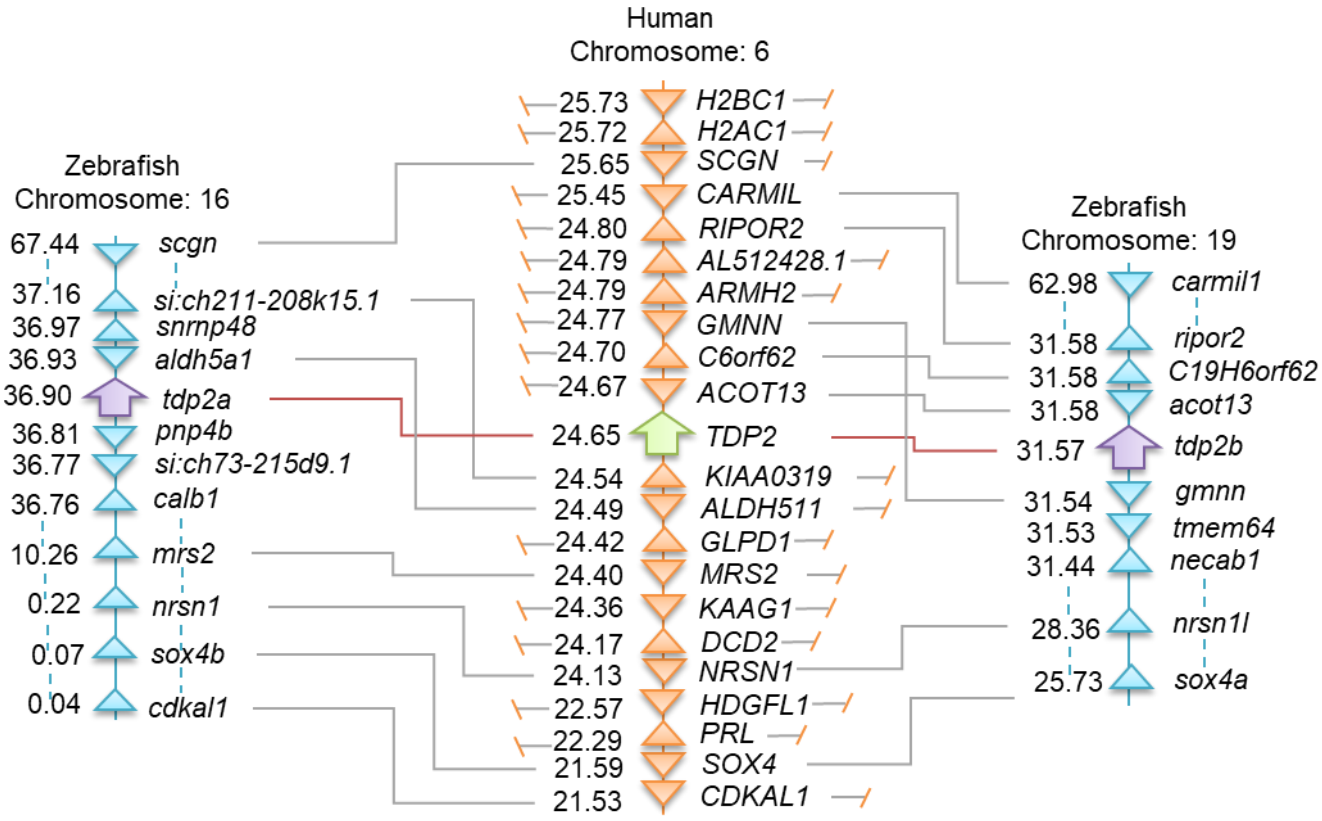

Figure 34. Syntenic analysis of *TDP2* in humans and zebrafish. Synteny analysis of zebrafish and human *TDP2* genes. The scheme shows chromosomal positions of *Tdp2* genes in zebrafish and human determined using Genomicus database. The numbers next to the gene names indicate their respective positions in megabase pairs (Mbp) on the respective chromosome.

Next, domain structures of TDP2 were analysed: domain structures are highly conserved between human and zebrafish *TDP2* orthologues (Figure 35A) and consist of the N-terminal

non-canonical UBA (ubiquitin-associated) domain and the C-terminal catalytic exonuclease/endonuclease/phosphodiesterase (EEP) domain with four conserved catalytic motifs (Figure 35A, in blue) and the residues N120, E152, D262 and H351 forming the magnesium coordination site (Schellenberg et al., 2012; Shi et al., 2012). Zebrafish Tdp2b is more similar to human TDP2 than Tdp2a, which has a longer N-terminal part (Figure 35A) that is mostly unstructured (Schellenberg et al., 2012; Shi et al., 2012) and is a longer protein overall compared to Tdp2b and human TDP2 (Figure 35A).

4.14. Creation of zebrafish Tdp2 deficient zebrafish lines

Given that zebrafish possess two *tdp2* orthologues, *tdp2a* and *tdp2b*, each containing Tdp2 active sites (Figure 35A), both Tdp2a- and Tdp2b-deficient lines were created separately. To create a zebrafish line impaired Tdp2a function using CRISPR/Cas9 system, a sgRNA was designed to target the beginning of the *tdp2a* gene, upstream of crucial catalytic amino acids. The guide chosen (Table 4) targets a site in exon 3 in close proximity to the catalytic residue E231, which is analogous to E162 in human TDP2, D341 and H430 (Figure 35A). This residue stabilizes the Mg^{+2} ion, which is essential for the resolution of the phosphodiesterase bond.

The sgRNA/Cas9 complex was microinjected into one-cell stage WT embryos and induced two separate mutations: a frameshift mutation leading to a premature STOP codon at amino acid position 244 (X244STOP) (Figure 35B), and a deletion of E231 which is essential for catalysis (Figure 35C). F0 fish of both strains were raised to maturity. F0 founders were out crossed with WT to create F1 heterozygous (HET) fish and raised to adulthood, followed by the genotyping of heterozygous fish for the target mutation in the F1 generation. F1 HET females and HET males carrying the ΔE231 change in Tdp2a were crossed to produce the F2 generation. After reaching adulthood, F2 homozygous (HOM) fish for the desired allele were genotyped and incrossed to create the F3 HOM generation of the *tdp2a* $^{\Delta E231}$ line (Supplement 8). In the case of the *tdp2a* fish line with the premature STOP frameshift mutation (*tdp2a* ^{244STOP}), several homozygous fish were identified in the F1 generation, but so far only two homozygous males were identified in the F2 generation (Supplement 8). That is why, a new generation of F2 was initiated, with the goal of raising and identifying homozygous females. In the meantime, zebrafish line with catalytically inactive Tdp2a was used for all subsequent experiments including qPCR and DPC analyses.

In order to establish a Tdp2b-deficient mutant line, a sgRNA targeting exon 2 was chosen

(Table 4) which targets a region upstream of the catalytic residues N129, E161, D271, and H360 (Figure 35A). Following the microinjection of the gRNA/Cas9 complex into embryos, the F0 generation was raised to adulthood. Founder fish were identified in the F0 generation by germline HRMA analysis followed by genotyping by sequencing. Subsequently, one founder fish was outcrossed with a WT fish, leading to the generation of the F1 offspring. Due to the variability in offspring produced by the F0 founder fish, two males and one female heterozygous fish with the same change, frameshift mutations which results in premature stop codons after 96 amino acids were selected through allele-specific genotyping and crossed to generate the F2 generation (Figure 35D). Homozygous female and male fish of the F2 generation were identified by sequencing and crossed to establish the *tdp2b*^{97STOP} mutant line. (Figure 35C and Supplement 8).

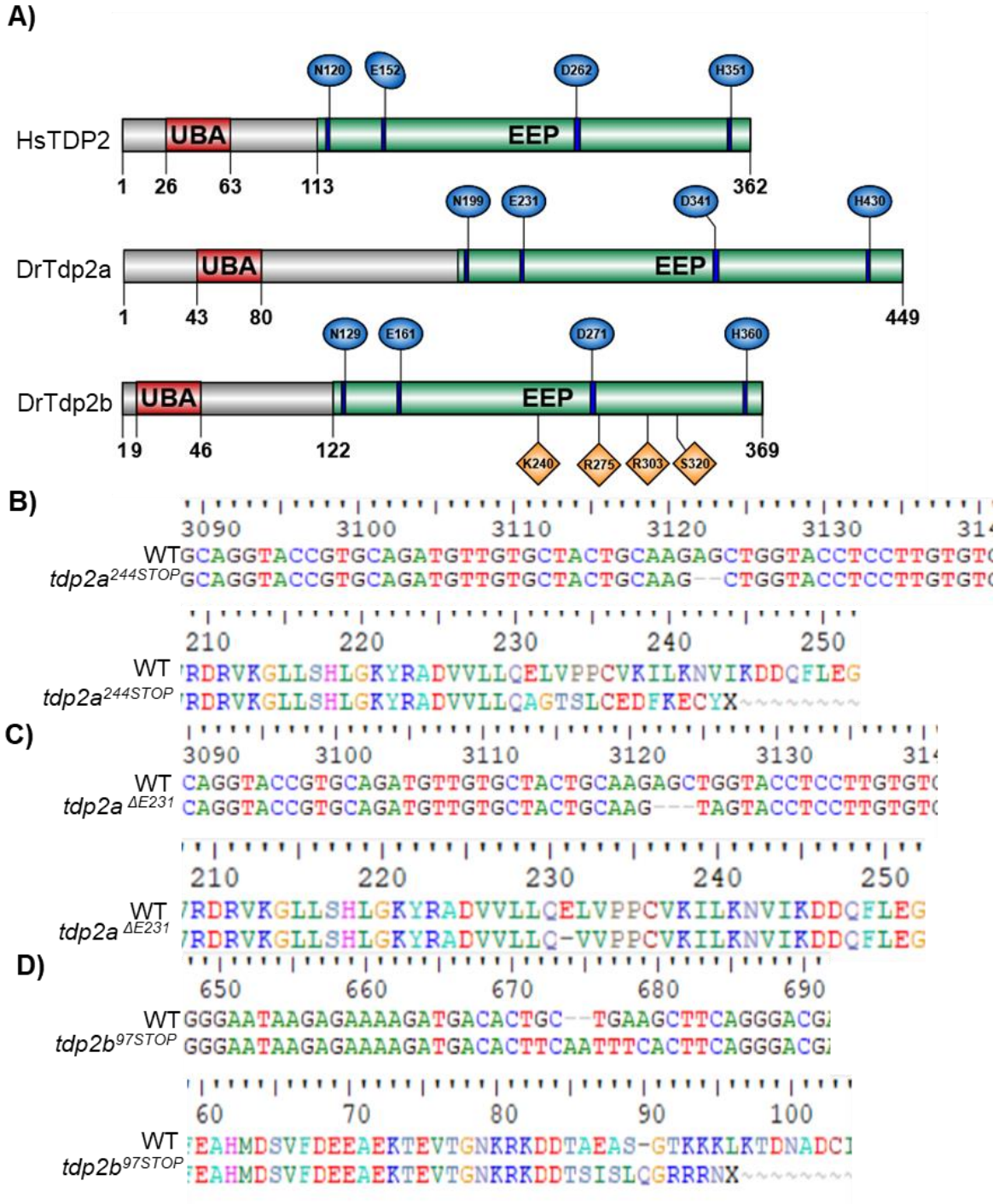

Figure 35. Domain organization of human and zebrafish TDP2 and sequencing validations of the *tdp2* zebrafish mutant strains. A) Domain structures of human and zebrafish tyrosyl-DNA phosphodiesterase 2. UBA - ubiquitin-associated domain; EEP - exonuclease/endonuclease/phosphodiesterase catalytic domain. Conserved catalytic motifs bearing catalytic residues are shown in blue and DNA binding sites in Tdp2b are shown in orange. B) Nucleotide and amino acid sequence of the *tdp2a* gene in the *tdp2a*^{244STOP} fish line. The lower panel shows the protein sequence of Tdp2a of WT and *tdp2a*^{244STOP}, where X

indicates a STOP codon. The upper panel indicates the change induced after Cas9 cutting (deletion of AG on positions 3123 and 3124 on genomic DNA). C) Nucleotide and amino acid sequence of the *tdp2a* gene in the *tdp2a*$^{\Delta E231}$ fish line. The lower panel shows the protein sequence of the Tdp2a protein of WT and *tdp2a*$^{\Delta E231}$. The upper panel indicates the change induced after Cas9 cutting (deletion of AGC on positions 3122, 3123, and 3124 on genomic DNA). D) Nucleotide and amino acid sequence of the *tdp2b* gene in the *tdp2b*^{97STOP} fish line. The lower panel shows the protein sequence of Tdp2b of WT and *tdp2b*^{97STOP} where X indicates a STOP codon. The upper panel indicates the change induced after Cas9 cutting (substitutions G672 to T and 675 to 678 GAAG to TTCA with insertion of AA after 673 positions). Corresponding sequencing histograms are shown in Supplement 8.

4.15. *Tdp2b* is dominantly expressed during embryonic development

In embryos, maternally deposited mRNAs play a crucial role until 4-hpf (Laue et al., 2019; M. Zhang et al., 2014). After 6-hpf, maternal transcripts are degraded, and embryonic transcription is fully active (Laue et al., 2019; Mathavan et al., 2005). To investigate the expression dynamics of the zebrafish *tdp2* orthologues, *tdp2a* and *tdp2,b* at embryonic stages from 6-hpf to 5-dpf qPCR was performed and expression levels were quantified using the previously established thresholds (Figure 16A, Anticevic *et al.*, 2023). Both *tdp2* orthologues showed high expression, but *tdp2b* exhibited 10 to 40 times higher expression compared to *tdp2a* throughout zebrafish embryonic development (Figure 36A). Interestingly, both genes exhibited similar expression patterns, with the highest expression observed at 6 hpf, which gradually decreased and reached a stable and high expression levels from 2 dpf stage onwards (Figure 36A). *Tdp2a* showed three times higher expression at 6 hpf stage compared to the other stages, while *tdp2b* showed eight times higher expression at this stage in comparison to later timepoints (Figure 36A).

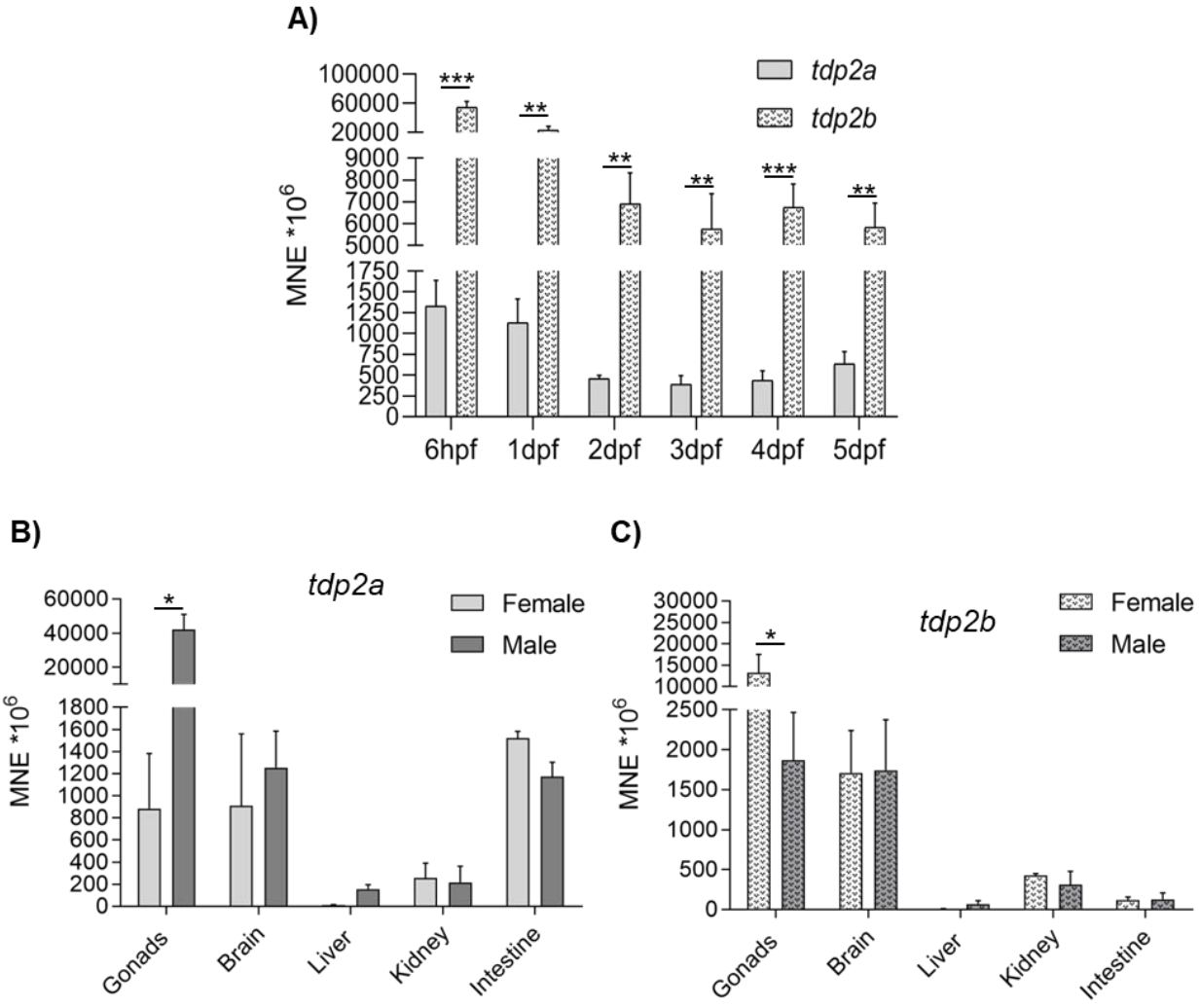

Figure 36. **Tdp2 mRNA expression patterns in zebrafish embryos and adults.** A) mRNA expression profiles of *tdp2a* and *tdp2b* during zebrafish embryonic development from 6 hours post-fertilization (6-hpf) to 5 days post-fertilization (5-dpf). B) Tissue expression pattern of *tdp2a* and C) *tdp2b* in adult zebrafish. Statistically significant differences between expression in embryonal stages and between ovaries and testes (*p<0.05, **p<0.01, ***p<0.001) was determined by unpaired two-sample t-test. Data are presented as MNE (mean normalized expression) ± SD (n = 3), normalized to the housekeeping gene ATP synthase peripheral stalk subunit (*atp50*).

4.16. *Tdp2a* and *tdp2b* are both expressed in adult tissues

Both *tdp2a* and *tdp2b* are highly expressed in adult tissues including gonads, brain, kidney, and intestine, while their expression is moderate in liver (Figure 36B and C). Notably, both genes showed highest expression in gonads with pronounced gender differences. *Tdp2a* is very highly expressed in testes, with expression levels 58 times higher than in ovaries (p <

0.1) (Figure 36B). In contrast, *tdp2b* is very highly expressed in ovaries: 10 times higher than in testes ($p < 0.1$) (Figure 36C). Another difference in expression between the two paralogues was observed in the intestinal tissue where *tdp2a* is dominantly expressed in both genders (10 times higher than *tdp2b*). In the brain, both orthologus exhibited very high expression, followed by high expression in kidney and moderate expression in liver (Figures 36B and C).

4.17. Embryonic phenotypes of zebrafish *tdp2* mutant lines and of *tdp2* morphants

Upon the successful establishment of the zebrafish *tdp2a*$^{\Delta E231}$ and *tdp2b*^{97STOP} lines, homozygous mutant embryos were monitored until 5-dpf stage and no discernible phenotypic alterations were observed (Figure 37).

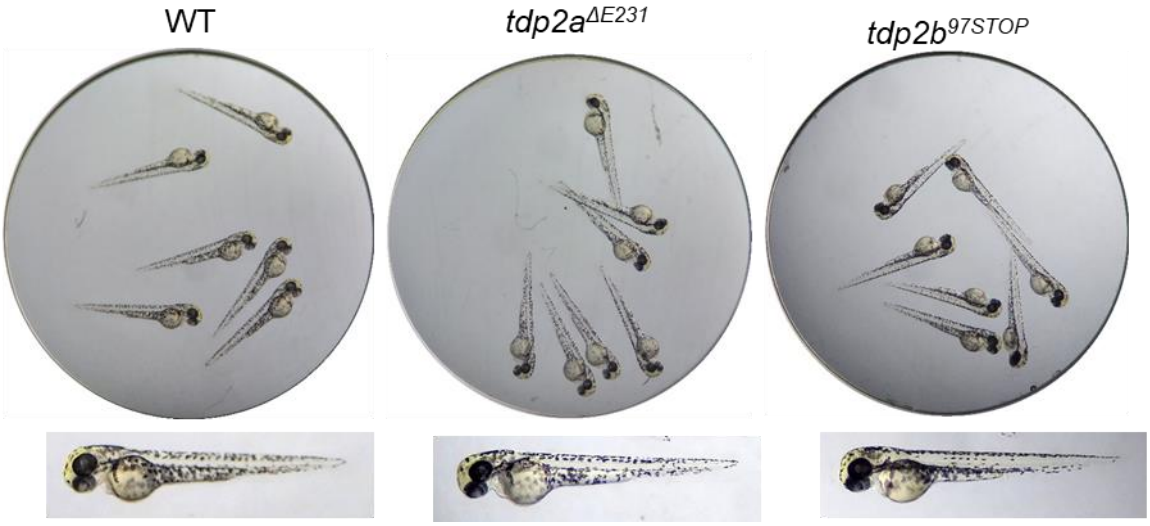

Figure 37. Images of WT and *tdp2* mutant embryos showing overview and individual images of WT, *tdp2a*$^{\Delta E231}$, and *tdp2b*^{97STOP} embryos. No detectable phenotypic changes were observed (Cecile Otten, IRB, unpublished results).

Consequently, in order to confirm redundant functions of *tdp2a* and *tdp2b* in zebrafish embryos, splice-blocking morpholino oligonucleotides were designed to specifically silence gene expression and compared the morphant with the mutant phenotypes. Firstly, silencing efficiencies were determined by injecting the morpholino oligonucleotides into embryos at the one-cell stage, followed by the collection of embryos at 2 dpf stage for subsequent PCR analysis on cDNA derived from these embryos (see Materials and Methods) (Figure 38). The reduction of PCR amplicon in the morphant samples, revealed a silencing efficiency of 100%

for *tdp2a*MO and of 50% for *tdp2b*MO (Figure 38B and C). Since Tdp2a and Tdp2b might have redundant functions, morpholino oligonucleotides combination was used to silence *tdp2a* and *tdp2b*; moreover, *tdp2a*MO morpholino oligonucleotides was injected into *tdp2b*^{97STOP} mutant and *tdp2*bMO into *tdp2a*$^{\Delta E231}$ mutant to uncover potential functional redundancies. This approach was chosen as the analysis of double mutants will require raising them for another 1-2 years. Also, silencing approach is different than complete protein deficiency present in the mutants, and therefore provides a valuable additional insight into the protein function.

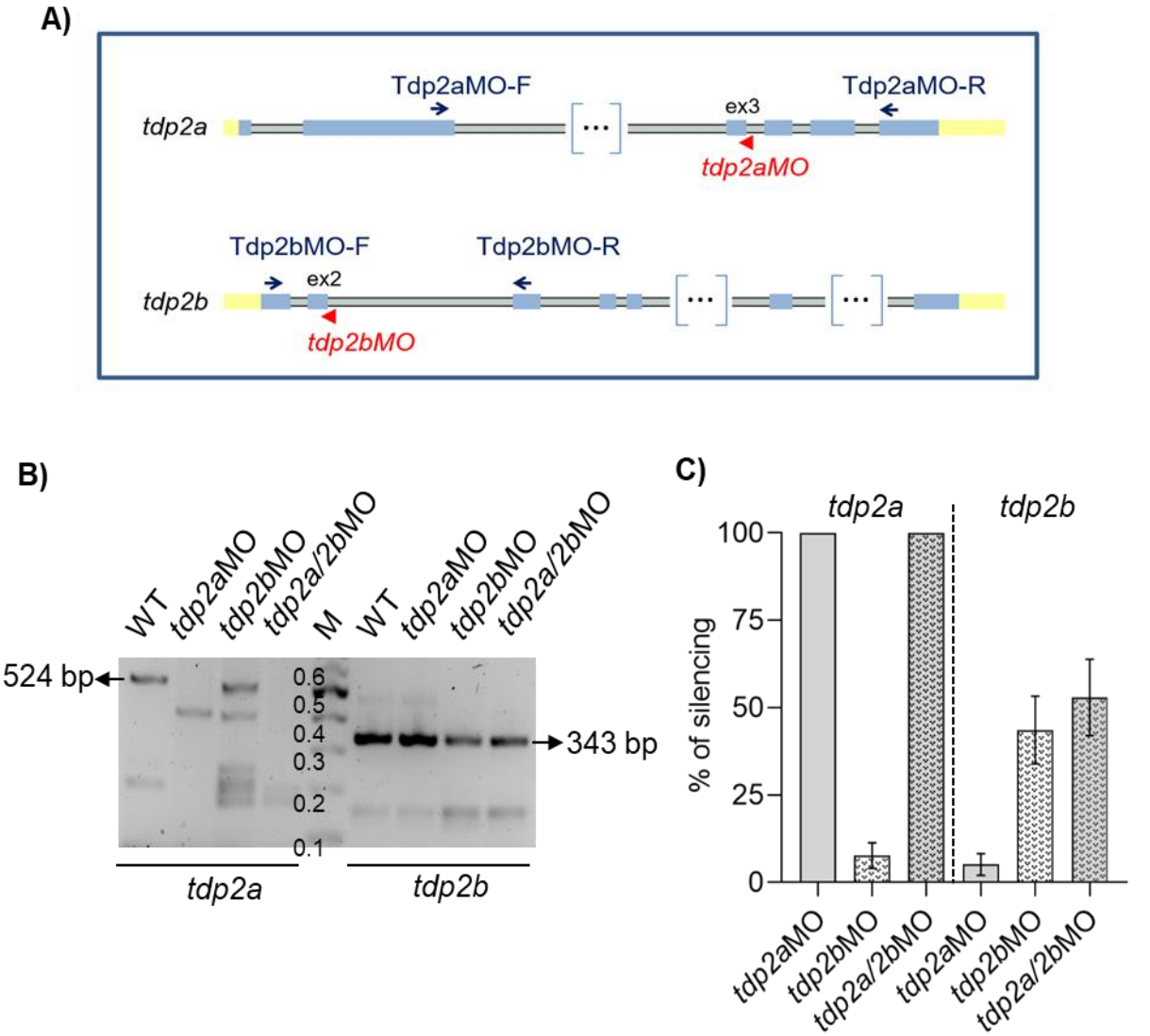

Figure 38. *Tdp2a* and *tdp2b* morpholino-mediated silencing efficiencies. A) Scheme of the zebrafish *tdp2a* and *tdp2b* genes indicating the sequences targeted by the morpholinos (red, arrowhead) and by the primers used to determine the morpholino efficiencies (blue, arrows). Exons are shown as blue squares and UTR regions as yellow squares. As some introns are

very long, their representation is shortened as indicated by brackets. The *tdp2a* morpholino targets the exon3-intron3 boundary, the *tdp2b* morpholino targets the exon2-intron2 boundary. B) DNA gel electrophoresis displaying the resolution of PCR reactions conducted on cDNA derived from 2-days old morphant embryos. PCRs were performed using primers listed in Table 4; a 524bp band and a 343bp band are expected for PCRs on WT for *tdp2a* and *tdp2b*, respectively (arrows). Numbers next to the marker bands represent sizes in kilobases (kb). C) Quantification of B).

Tdp2a morphant embryos were monitored at 1 dpf, 2 dpf and 3 dpf and they had no visible phenotype (Figure 39). In contrast, *tdp2b* morphants displayed slightly reduced head and eye size and a still prominent yolk ball with concomitant underdeveloped yolk extension at 2 dpf and 3 dpf (Figure 39). Since *tdp2a* and *tdp2b* are duplicated genes, they might have redundant functions, thet why *tdp2a* and *tdp2b* morpholino oligonucleotides were co-injected in embryos. The resulting phenotype was similar to *tdp2b*MO alone, and no further worsening of the phenotype was observed in the double morphants (Figure 39).

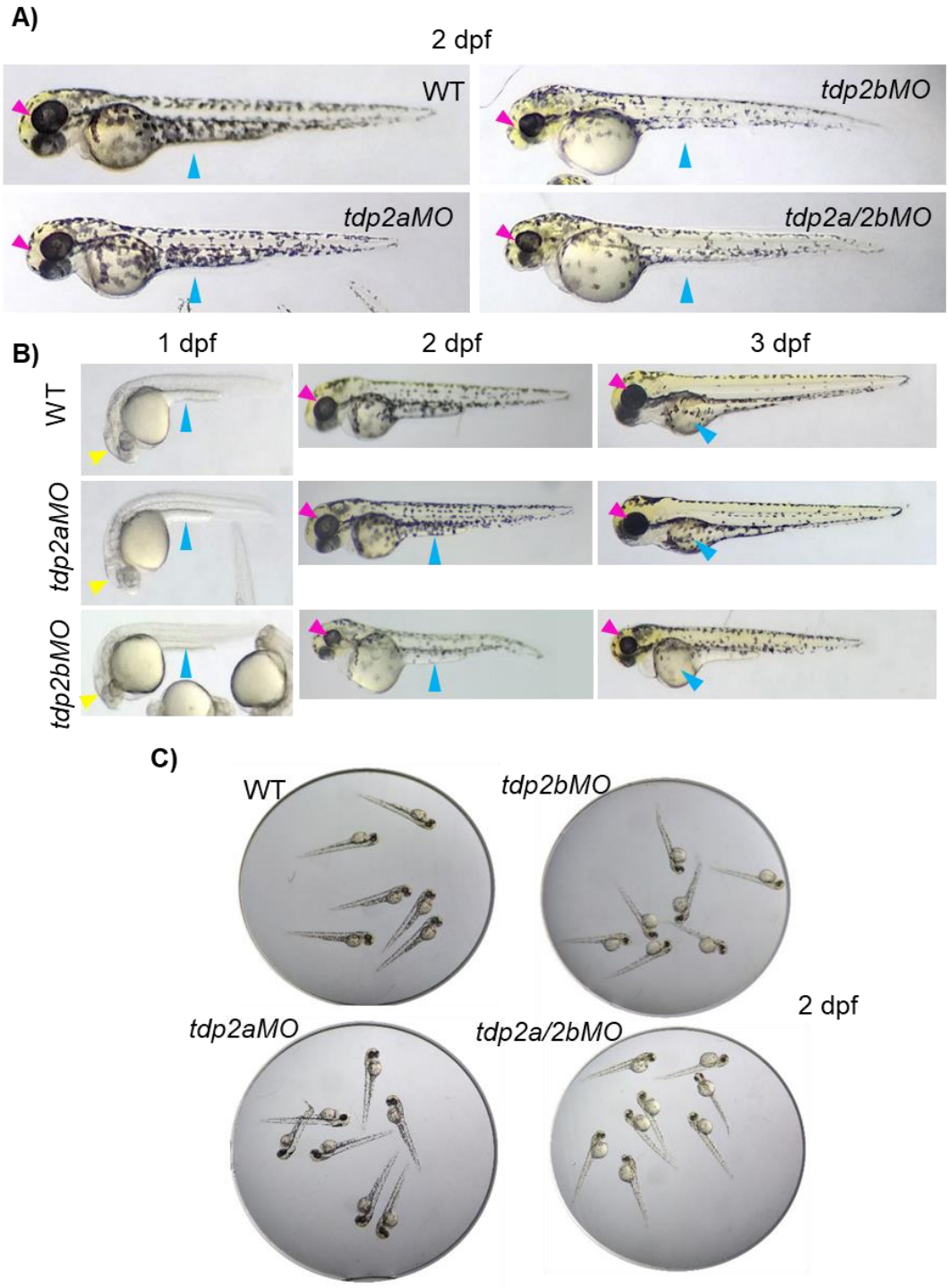

Figure 39. **Representative images of live zebrafish embryos after *tdp2* silencing**. A) Shown are images of 2-dpf stage embryos for: WT, *tdp2a*MO, *tdp2b*MO, and *tdp2a/2b*MO. Magenta arrowheads highlight the eyes, while cyan arrowheads point to the yolk extension. B) live zebrafish embryos at 1-dpf, 2-dpf, and 3-dpf stages. Yellow arrowheads indicate the brain, magenta arrowheads mark the eyes, and cyan arrowheads indicate the yolk extension

(1-dpf, 2-dpf) or the yolk ball (3-dpf). C) An overall view of 2-dpf stage embryos after *tdp2a*, *tdp2b*, or *tdp2a*/*2b* silencing (Cecile Otten, IRB, unpublished results).

4.18. Deficiency in Tdp2b leads to an increase in *tdp2a* expression in zebrafish embryos

To understand the inter-dependency of the two *tdp2* orthologues, the mRNA expression of *tdp2a* was measured when *tdp2b* is mutated or silenced and vice versa. The results revealed that when *tdp2b* was absent or silenced, the expression of *tdp2a* significantly increased, with a 2.5-fold increase in *tdp2b*^{97STOP} embryos and a 2.4-fold increase in *tdp2b* silenced embryos, compared to the expression levels in WT embryos (Figure 40A). Intriguingly, the silencing or impaired activity of *tdp2a* did not trigger a corresponding induction in *tdp2b* (Figure 40B).

4.19. Morpholino oligonucleotide mediated silencing of *tdp2b* leads to an increase in *tdp1* expression in zebrafish embryos

TDP1 and TDP2 are involved in apparently distinct DNA repair pathways, with TDP1 repairing 3' DNA blocks and TDP2 repairing 5' DNA blocks (Ledesma et al., 2009; Shimizu et al., 2023; Zeng et al., 2012). Furthermore, it has been reported that TDP2 can compensate for the loss of function of TDP1 and contribute to overcoming TDP1-dependent repair *in vitro* (Shimizu et al., 2023; Zeng et al., 2012). In results shown in Figure 26A it is reported that *TDP2* expression is induced when *TDP1* is silenced in RPE1 cells challenged with camptothecin, a specific TOP1 inducer. Additionally, both *tdp2* zebrafish orthologues, *tdp2a* and *tdp2b*, were found to be upregulated in our *tdp1*$^{-/-}$ zebrafish line, with *tdp2a* showing a 3.7-fold increase and *tdp2b* a 1.6-fold increase in gene expression (Figures 26B and C). Building on these findings, it is obsereved that loss of function of both *tdp2* orthologues impacts *tdp1* expression in zebrafish embryos. Intriguingly, *tdp2a*$^{\Delta E231}$ catalytic mutants and *tdp2b*^{97STOP} mutants did not exhibit changes in the expression of the *tdp1* gene. Remarkably, *tdp1* expression was not changed in tdp2a morphants, whereas *tdp2b* silencing led to a 2-fold increase in *tdp1* expression compared to that in WT embryos (Figure 40C). Notably, a similar increase was noted when both orthologues were simultaneously silenced (Figure 40C). Intriguingly, the most substantial increase of 2.4-fold was observed when *tdp2b* was silenced in the *tdp2a*$^{\Delta E231}$ catalytic mutant (Figure 40C).

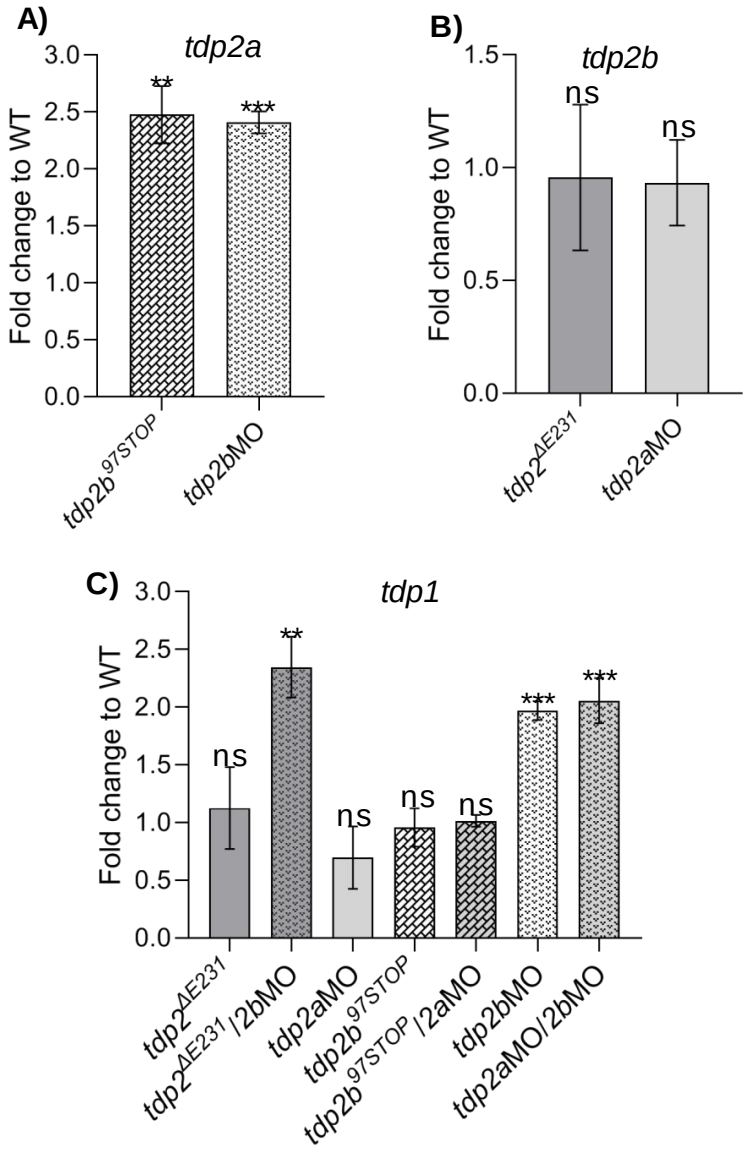

Figure 40. *Tdp2a, tdp2b,* and *tdp1* expression patterns in embryos of *tdp2a* and *tdp2b* mutant lines, and after *tdp2a*, *tdp2b*, or *tdp2a* and *tdp2b* gene silencing. A) qPCR analysis of *tdp2a* expression in *tdp2b*^{97STOP}embryos and in *tdp2b* morphant embryos B) qPCR analysis of *tdp2b* expression in *tdp2a*$^{\Delta E231}$ embryos and in *tdp2a* morphant embryos C) *tdp1* qPCR analysis in *tdp2a* and *tdp2b* mutant embryos, as well as in embryos subjected to individual *tdp2a*, *tdp2b*, and combined *tdp2a* and *tdp2b* silencing in WT, *tdp2a*$^{\Delta E231}$, and *tdp2b*^{97STOP} lines. The housekeeping gene atp50 was used as a reference for normalization. Data are presented as mean ± SD fold change to WT from biological triplicates, and statistical significance was determined using an unpaired one-sample Student's t-test (*p<0.05, **p<0.01, ***p<0.001).

4.20. TDP2 deficiency increases expression of TDP1 and SPRTN in RPE1 cells

It is observed that the expression of *TDP2* remains unaffected following *TDP1* or *SPRTN* silencing in RPE1 cells (Figure 26A). However, when cells are exposed to CPT (50 nM, 1h), a TOP1 poison, the expression of *TDP2* increased by 1.8-fold in *TDP1*-silenced cells and 1.3-fold in *SPRTN*-silenced cells (Figure 26A). Furthermore, successful silencing of TDP2, resulting in a 90% decrease in TDP2 mRNA levels in RPE1 cells (Figure 41A), results in a 50% decrease in cell viability (Figure 27A). To understand interplay between these proteins at the mRNA level, the impact of *TDP2* silencing on *TDP1* and *SPRTN* expression was examined. Interestingly, *TDP2* silencing leads to a 1.3-fold increase in *TDP1* expression ($p<0.001$) and a 1.2-fold increase in *SPRTN* expression ($p<0.05$) (Figures 41B and C).

Exposure to etoposide (ETO) (25 µM for 1h), a commonly used TOP2 poison which induces TOP2-DPCs, did not impact *SPRTN* expression in WT RPE1 cells (Figure 41D). However, *SPRTN* expression significantly increased by 1.3-fold ($p < 0.05$) in TDP2-silenced cells treated with ETO (Figure 41D). Furthermore, ETO treatment resulted in a 1.4-fold increase in *TDP2* expression ($p<0.05$) in WT cells and a 1.7-fold increase in *SPRTN*-silenced cells ($p<0.05$) (Figure 41C).

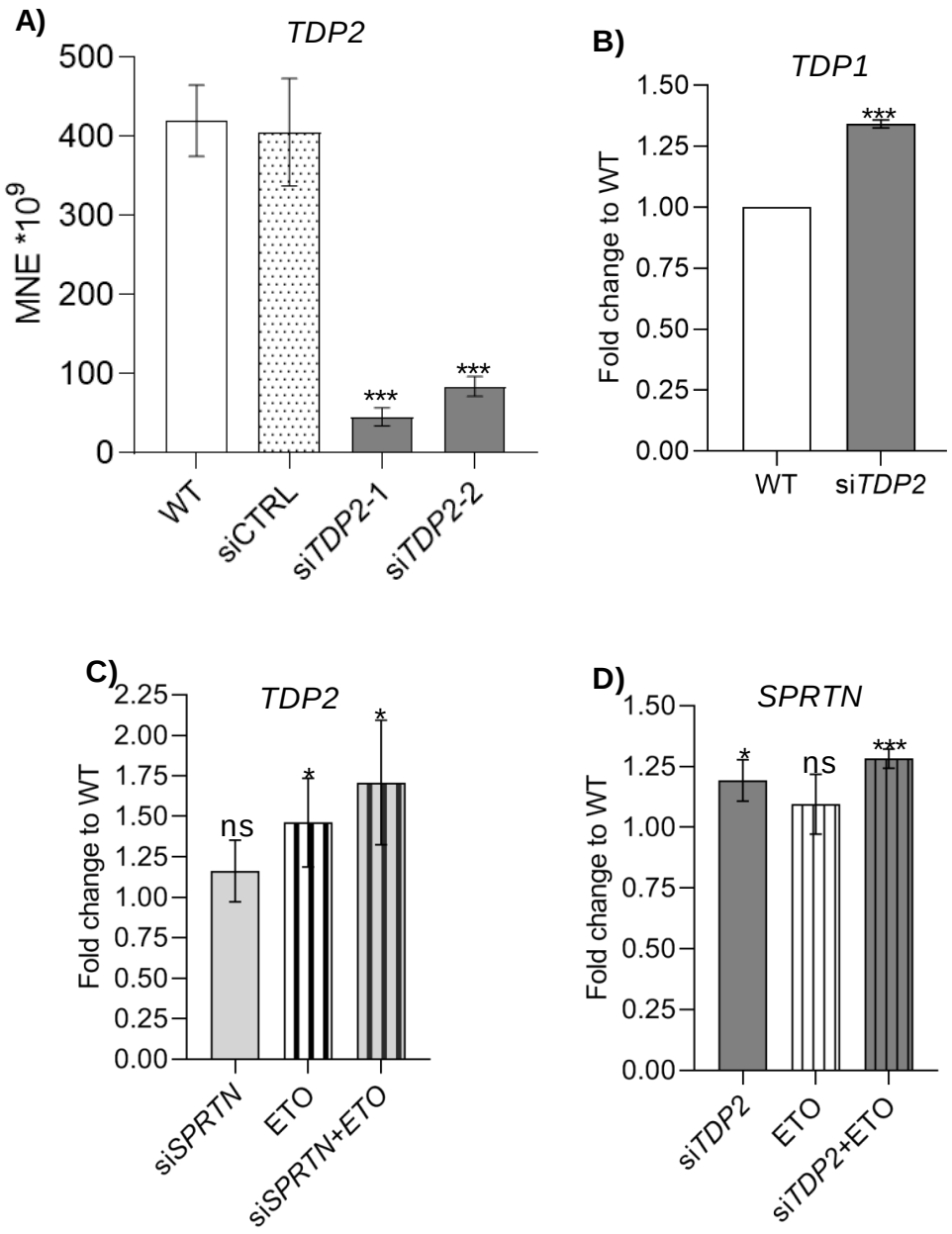

Figure 41. Expression patterns of *TDP1*, *TDP2*, and *SPRTN* following *TDP2* and *SPRTN* Silencing and ETO treatment in RPE1 cells. A) Optimization of *TDP2* silencing in RPE1 cells using two different *TDP2* siRNAs listed in Table 6, followed by qPCR analysis. Data are presented as MNE (mean normalized expression) ± SD (n = 3), normalized to the housekeeping gene ATP synthase peripheral stalk subunit *(atp50)*, and statistical significance was determined using an two-sample unpaired Student's t-test (***p<0.001). B) qPCR expression analysis of *TDP1* after *TDP2* silencing C) qPCR analysis of *TDP2* with or without *SPRTN* silencing in combination with or without ETO treatment (25 µM, 1 h). D) *SPRTN* qPCR analysis in *TDP2*-silenced RPE1 cells and after exposure to ETO (25 µM, 1 h). The housekeeping gene *ATP50* was used as a reference for normalization. Data are presented as

mean ± SD fold change to WT from biological triplicates, and statistical significance was determined using an one-sample unpaired Student's t-test (*p<0.05, **p<0.01, ***p<0.001).

4.21. *Tdp2b* is the main 5' phosphotyrosyl-processing enzyme in zebrafish embryos

To confirm that the enzymatic activity of Tdp2a and Tdp2b is impaired in *tdp2a*$^{\Delta E231}$ and *tdp2b*^{97STOP} as well as after morpholino oligonucleotide mediated gene silencing, the TDP2 activity assay was performed (Zagnoli-Vieira et al., 2018; Zeng et al., 2012). In this assay, a Cy5-labeled oligonucleotide containing a 5' phosphotyrosyl moiety (5'-PY) was incubated with whole embryo lysates (Zaksauskaite et al., 2021) of *tdp2a*$^{\Delta E231}$ and *tdp2b*^{97STOP} mutants and of *tdp2a* and *tdp2b* morphants (Figure 42). In the presence of active Tdp2, the tyrosine residue is removed from the 5' end of the oligomer, resulting in a cleavage product seen as an additional band (p-oligo-Cy5). The lysate of HEK293T cells was used as a positive control. Consistent with previous findings (Zaksauskaite et al., 2021), it is observed that human TDP2 efficiently processed the phosphotyrosyl moiety into a phosphate group, resulting in a lower band on the native gel (p-oligo-Cy5, Figure 3A). Interestingly, also bands were detected that are lower than the band with the phosphate group (oligo-Cy5), suggesting the occurrence of additional repair events in both cell and embryo lysates (Figures 42A and C). When comparing Tdp2 activity in embryos, there were no significant changes observed in the specific band intensity between wild-type (WT) embryos and either the *tdp2a* catalytic mutant or *tdp2a*-silenced embryos (Figures 42A and B). Notably, when *tdp2b* was silenced in *tdp2a* catalytic mutants, a significant reduction of 75% was observed, mirroring the 70% reduction observed when both *tdp2* orthologues were simultaneously silenced (Figures 42A and B). Conversely, *tdp2b*^{97STOP} mutants exhibited a substantial 67% lower Tdp2 activity compared to that measured in WT embryos (Figures 42C and D). Furthermore, the activity was almost completely abolished when *tdp2a* was silenced in *tdp2b*^{97STOP} mutants (93%, Figures 42C and D). Silencing *tdp2b* in WT embryos led to a 78% reduction in activity, similar to the reduction observed after simultaneous silencing of *tdp2a* and *tdp2b* (Figures 42C and D).

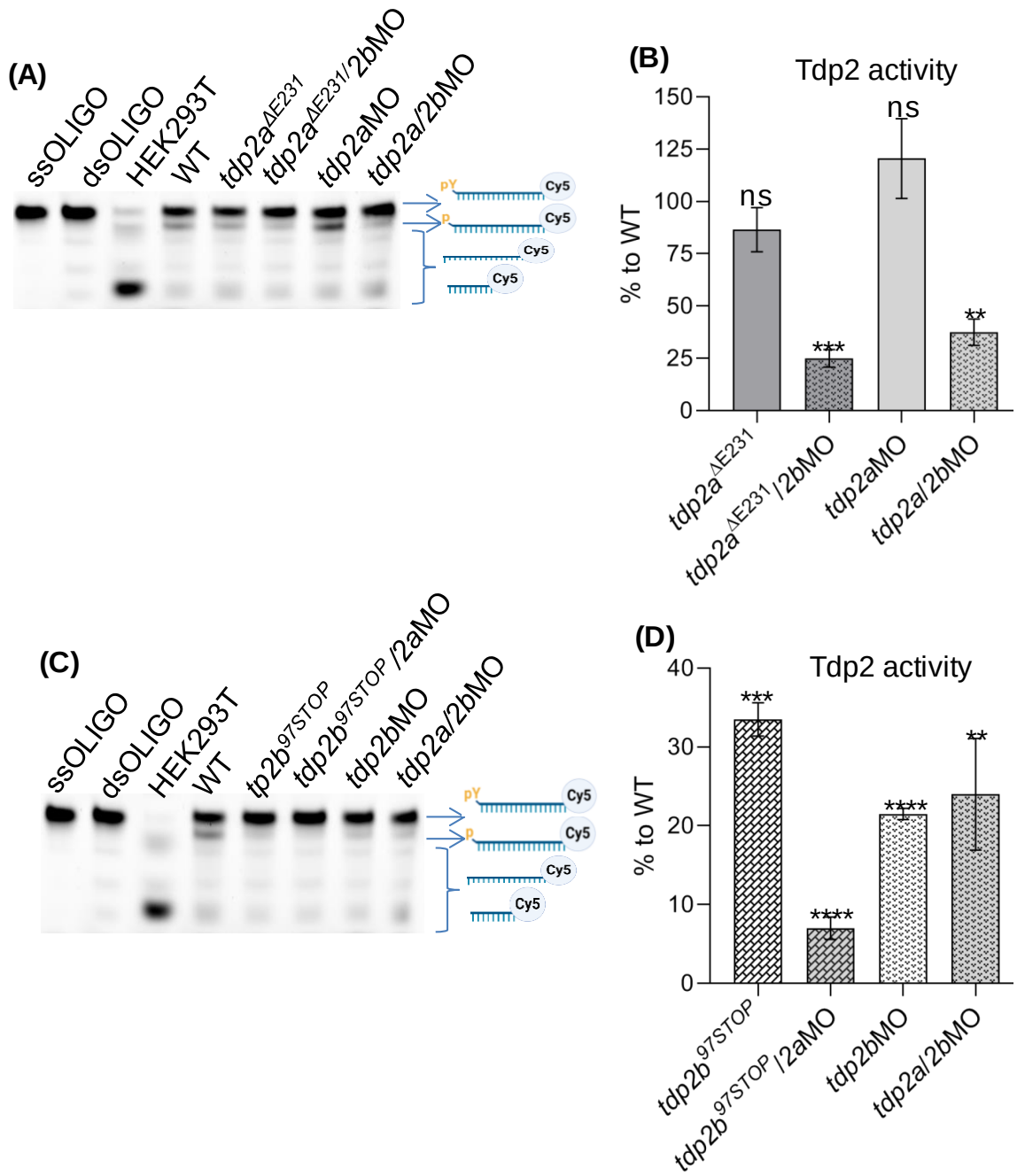

Figure 42. Tdp2 activity in zebrafish embryos in Tdp2 mutant lines and Tdp2 morphants. (A) Tdp2 activity in 2-days old WT and *tdp2a*-deficient zebrafish embryos. Representative denaturing PAGE gels depict the processing of a Tdp2-specific substrate (5'-PY) upon incubation with 10 µg of HEK or embryo lysate, with ssOLIGO and dsOLIGO serving as negative controls. The scheme illustrates the reaction products, indicating TDP2-mediated removal of tyrosine from the 5' end (P), with reduced Tdp2 activity reflected by a lower band intensity of the 5' end product (p). (B) Band intensity quantification of (5'(p), 3'(Cy5)) product from (A) using Image J software. (C) Tdp2 activity in 2-days old WT and

tdp2b-deficient zebrafish embryos (D) Band intensity quantification of (5'(p), 3'(Cy5)) product from (C) using Image J software. The data are presented as mean ± SD fold change compared to WT from biological triplicates, and statistical significance was determined using an unpaired Student's t-test (**p<0.01, ***p<0.001.**** p<0.05).

4.22. Tdp2b deficiency causes significant accumulation of DNA-protein crosslinks

In order to analyse DPC levels in Tdp2-deficient zebrafish embryos, the modified RADAR assay was used. Modified DPC isolation from embryonic tissue and human cells allows better reproducibility and higher sensitivity (see page 98). Total DPCs were isolated from WT, *tdp2* mutant and *tdp2*-silenced embryos at 2 dpf and conclusions were derived from three biological replicates. WT embryos were treated with 5 mM formaldehyde (30 min, 28 ^{o}C) in each experiment. We have previously optimized the conditions for FA exposure so that DPCs are induced with no apparent effects on embryonic phenotypes (Figure 28).

Initially, total DPCs were compared between WT, *tdp2a*$^{\Delta E231}$, and *tdp2b*^{97STOP}mutant embryos. The DPCs were further compared according to size distribution to HMW, MMW and LMW. Surprisingly, no differences in terms of total DPC accumulation as well as accumulation of HMW, MMW nor LMW DPCs were found between the WT and *tdp2* mutants (Figure 43).

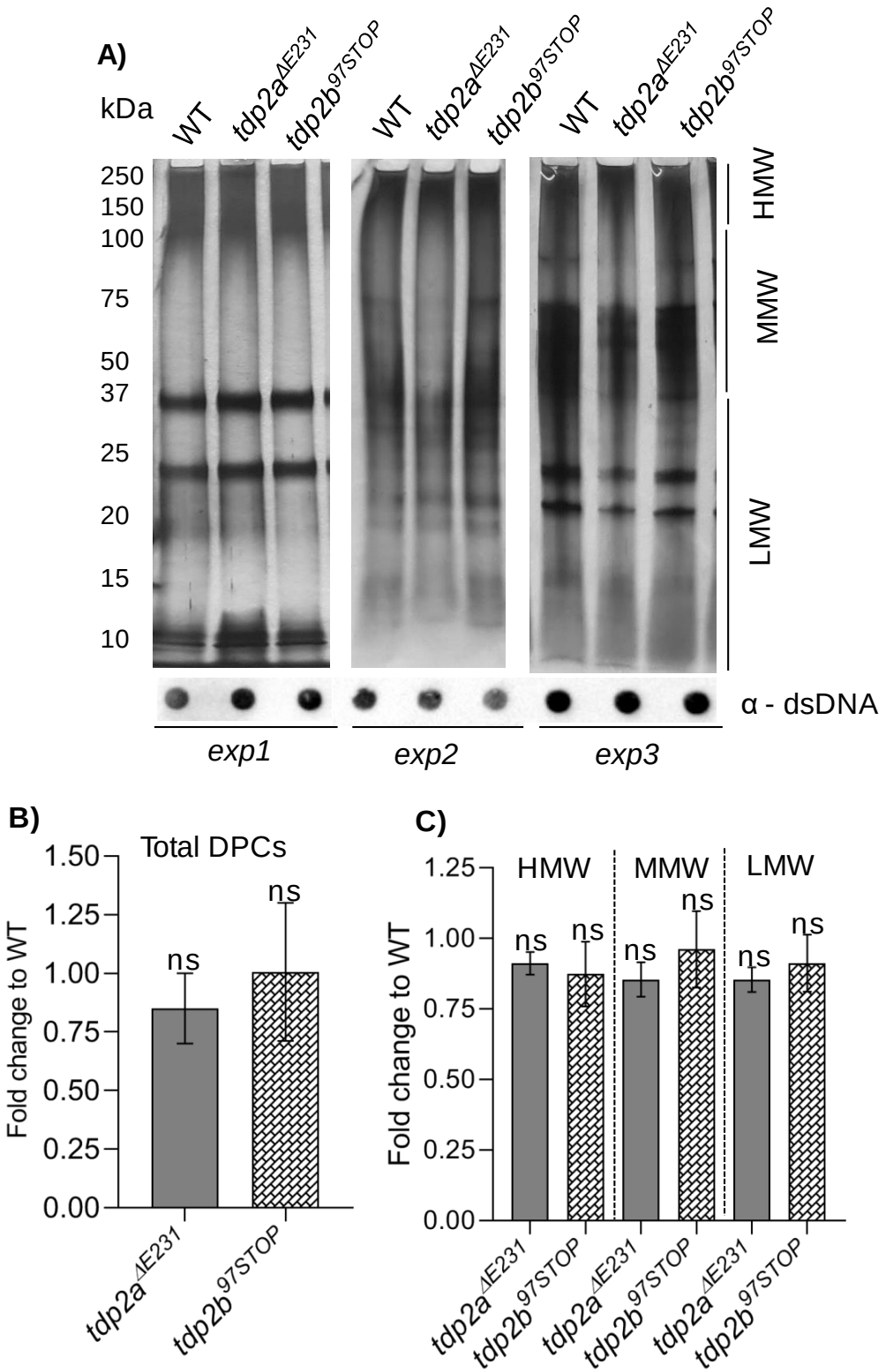

Figure 43. Analysis of DPC levels in 2-dpf stage WT, *tdp2a*$^{\Delta E231}$ and *tdp2b*^{97STOP}zebrafish line A) DPC isolation from 2-day old embryos using the RADAR assay from three different experiment (30 embryos per condition, n = 3). DPCs were resolved on an SDS acrylamide gel and visualized by silver staining. Dot-blots show DNA loading controls for DPC analysis prior to benzonase treatment (equivalent to 250 ng of total DNA loaded per well). B)

Quantification of total DPCs from A). C) Quantification of DPCs from (A) according to their molar weight: High Molecular Weight (HMW) (>150 kDa), Medium Molecular Weight (MMW) (40 kDa to 150 kDa), and Low Molecular Weight (LMW) DPCs (protein size <40 kDa). Data represent mean fold change to WT ± SD (n = 3). Statistical significance was determined using an one-sample unpaired Student's t-test.

Tdp2a silencing had no significant effect on the total DPC levels in zebrafish embryos (Figures 44 and 45), whereas *tdp2b* gene silencing caused a 1.6-fold increase in DPC accumulation compared to WT embryos (Figures 44A and B, 45A and B). Interestingly, simultaneous silencing of both *tdp2a* and *tdp2b* led to a further increase to1.9-fold (Figures 44A and B, 45A and B). DPC accumulation induced by formaldehyde (FA) (5 mM, 30 min) was 2-fold in comparison to WT (Figures 44A and B, 45C). In order to achieve a more detailed analysis of accumulated DPCs, they were quantified based on their sizes as similarly to *tdp1* mutants (Figure 29).

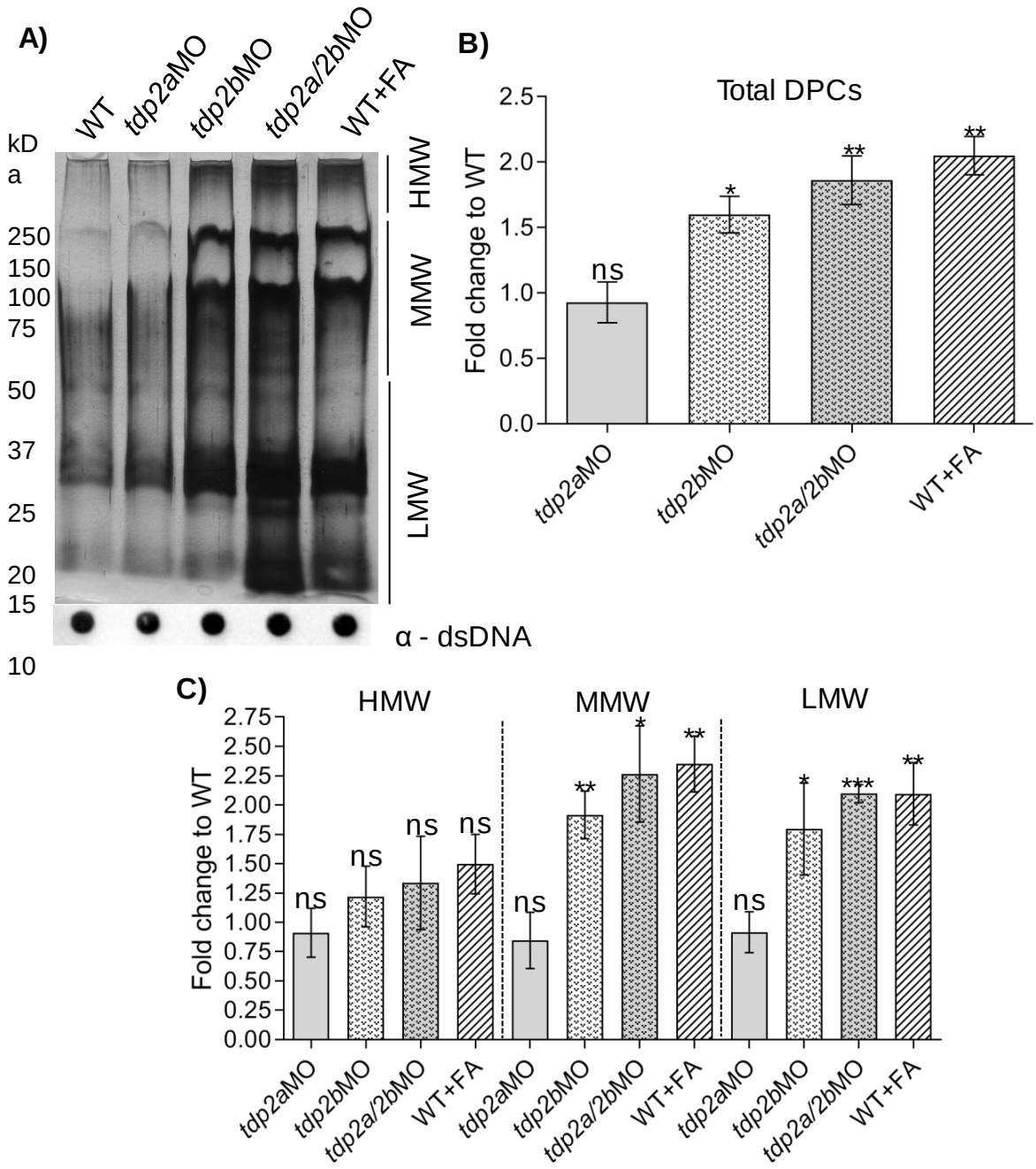

Figure 44. Analysis of DPC levels after silencing of *tdp2a* and *tdp2b* in zebrafish embryos. A) DPCs were isolated from 2-day old embryos using the RADAR assay (30 embryos per condition, n = 3), resolved on an SDS acrylamide gel, and visualized by silver staining. Dot-blots show DNA loading controls for DPC analysis prior to benzonase treatment (equivalent to 250 ng of total DNA loaded per well). WT embryos treated with formaldehyde (5 mM, 30 min) were used as a positive control for DPC induction. B) Quantification of total DPCs from A). C) Quantification of DPCs from A) according to their molar weight: High Molecular Weight (HMW) (>150 kDa), Medium Molecular Weight (MMW) (40 kDa to 150 kDa), and Low Molecular Weight (LMW) DPCs (protein size <40 kDa). Data represent mean

fold change to WT ± SD (n = 3). Statistical significance was determined using an unpaired one-sample Student's t-test (* ($p < 0.05$), ** ($p < 0.01$), *** ($p < 0.001$), and **** ($p < 0.0001$)).

Tdp2a silencing showed no significant effect on DPCs in any size range in comparison to WT embryos (Figures 44A, C and 45A and B). *Tdp2b* silencing caused a 1.9-fold ($p < 0.01$) and 1.8-fold ($p < 0.05$) increase in MMW and LMW DPCs, respectively, compared to WT embryos (Figures 44A, C and 45A and B). Silencing of both *tdp2* orthologues caused significant accumulation of DPCs in the MMW and LMW ranges, with a 2.3-fold ($p < 0.01$) and 2.1-fold ($p < 0.001$) increase, respectively (Figures 44A, C and 45A and B). Simultaneous silencing of *tdp2a* and *tdp2b* had the same impact on MMW and LMW DPCs as the general DPC inducer FA which led to a 2.3-fold ($p < 0.01$) and 2.1-fold ($p< 0.01$) increase, respectively (Figures 44A, C and 45). *Tdp2b* silencing caused slight accumulation of the HMW DPCs with a 1.2-fold change which was not statistically significant (Figures 44A, C and 45A and B). Similar effect on HMW DPCs was observed when both *tdp2a* and *tdp2b* were silenced: 1.3-fold increase (p, ns) and when model inducer FA was used to induce DPCs in WT embryos (1.4-fold increase, ns) (Figures 44A, C and 45).

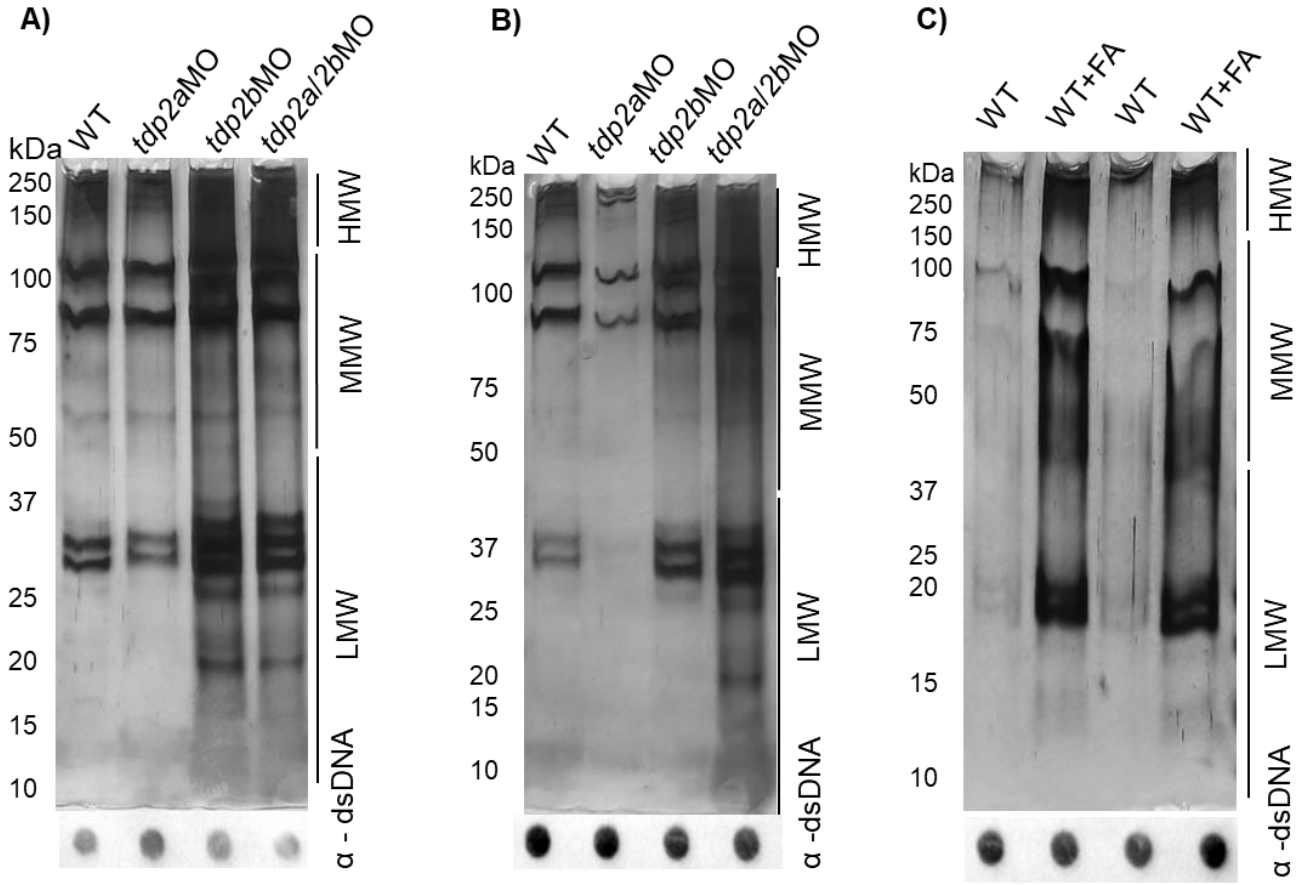

Figure 45. DPC analysis from additional biological replicates used for the quantification of total DPC levels shown in Figure 44. A) Second and third B) experiment showing total DPC analysis after silencing of *tdp2a* and *tdp2b*. DPCs were isolated from 2-day old embryos using the RADAR assay (30 embryos per condition), resolved on an SDS acrylamide gel, and visualized by silver staining. Dot-blots show DNA loading controls for DPC analysis prior to benzonase treatment (equivalent to 250 ng of total DNA loaded per well). C) Second and third biological replicate showing DPC levels in WT embryos after FA treatment (5 mM, 30 min) used as a positive control for DPC induction, with corresponding DNA dot blot, used for the quantification of DPC levels after exposure to FA in WT embryos shown in Figure 44.

4.23. TDP2 silencing in RPE1 cells increases DPC levels

To investigate whether a similar effect observed after *tdp2b* silencing in zebrafish embryos is also observed following *TDP2* silencing in human cells, the analysis of total DPCs and DPC distribution in both WT and *TDP2*-silenced RPE1 cells was performed an. After a 72-hour incubation with *TDP2* siRNA, cells were collected for total DPC analysis, with a separate aliquot designated for quantification of silencing efficiency. After confirming that *TDP2* mRNA levels were reduced by 90% (Figure 41A), DPCs were isolated using the

modified RADAR assay, separated by SDS PAGE and visualised with silver staining. *TDP2* silencing resulted in a 1.3-fold increase in total DPCs compared to WT cells (Figures 46A and B) with the majority of accumulation in the MMW and LMW DPC regions, with a 1.8 - fold increase ($p < 0.01$) and a 1.9 - fold increase ($p < 0.05$), respectively (Figures 46A and C). No significant change was detected in the HMW DPCs (Figures 46A and C).

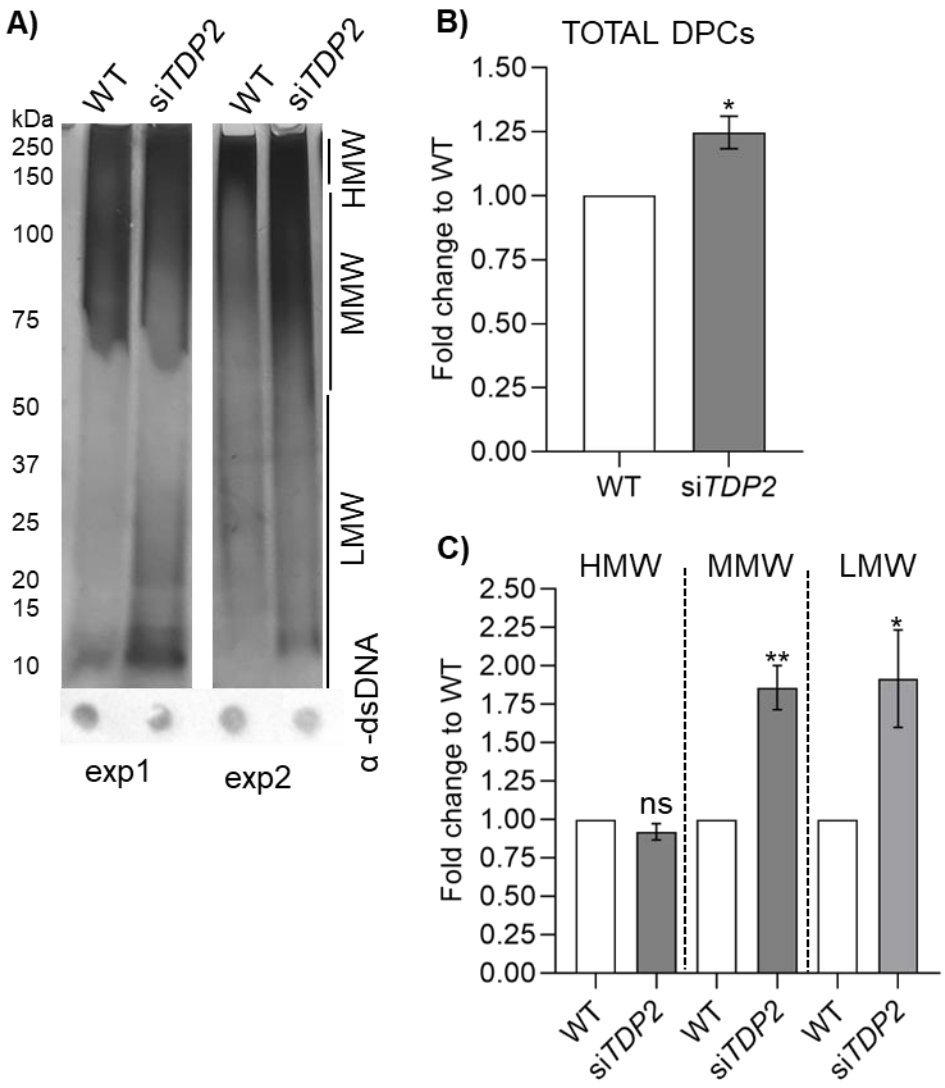

Figure 46. DPC analysis after *TDP2* silencing in RPE1 cells. . A) Silver-stained gels of total DPCs isolated from WT and *TDP2*-silenced RPE1 cells. DPCs were isolated using the RADAR assay, separated on an SDS acrylamide gel, and visualized by silver staining. Two biological duplicates are shown. B) Quantification of total DPCs from A). C) Quantification of DPCs from (A) according to their molar weight: High Molecular Weight (HMW) (>150 kDa), Medium Molecular Weight (MMW) (40 kDa to 150 kDa), and Low Molecular Weight (LMW) DPCs (protein size <40 kDa). Data represent mean fold change to WT ± SD (n = 2).

Statistical significance was determined using an unpaired one-sample Student's t-test (* ($p < 0.05$), ** ($p < 0.01$)).

4.24. *Tdp2b* silencing in embryos causes significant accumulation of Top2-DPCs in zebrafish embryos

First, detection of TOP2-DPCs was optimised using DPCs isolated from WT and ETO-treated HEK293T cells. The cells were treated with 25 µM ETO for 1 h in serum-free media, a concentration known to induce TOP2-DPCs (Vaz et al., 2016). As shown in Figure 47A, TOP2-DPCs were found to accumulate significantly in ETO-treated cells, where the TOP2 monomer is visible along with the modified forms of TOP2-DPCs (upper smear). Subsequently, to confirm the role of TDP2 in TOP2-DPC repair, DPCs isolated from RPE1 cells and *TDP2*-silenced cells were subjected to slot blot analysis. No discernible difference was observed between WT and *TDP2*-silenced cells (Figures 47B and C). However, pronounced accumulation of 1.7 - fold was observed in *TDP2*-silenced cells subjected to ETO treatment (Figures 47B and C). This experiment was carried out once and the result needs to be confirmed in future experiments.

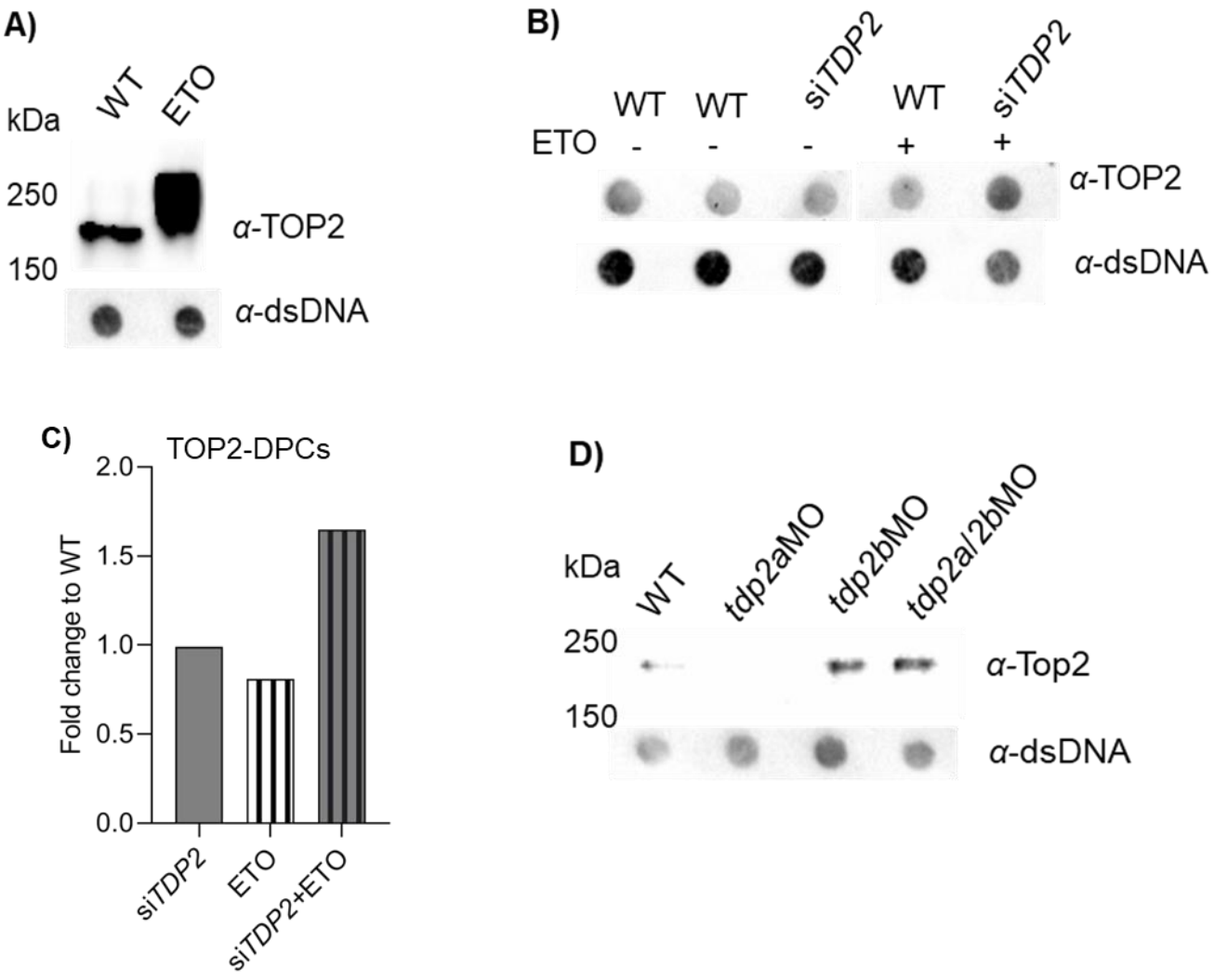

Figure 47. Detection of TOP2-DPCs in HEK293T cells, RPE1 cells and zebrafish embryos after Tdp1 silencing and exposure to ETO. A) Optimization of TOP2-DPCs detection using SDS-PAGE (UREA gels) and western blot TOP2-DPCs were detected using 1 µg of DNA-normalized DPCs from WT and ETO-treated (25 µM, 1 h) HEK 293T cell samples B) slot blot analysis of TOP2-DPCs isolated from RPE1 cells after *TDP2* silencing and exposure to ETO (25 µM, 1 h): 500 ng of DNA-normalized DPCs were used. C) Quantification of (B); D) Western blot analysis of Top2-DPCs isolated from 2-day-old WT and Tdp2-silenced embryos: Detection was performed using 1 µg of DNA normalized DPCs. DNA slots were used as loading controls.

A significant accumulation of TOP2-DPCs was observed in *tdp2b*-silenced embryos as well as in *tdp2a*/*2b*-silenced embryos (Figure 47D). The experiment was performed with one biological replicate and needs further confirmation.

4.25. Tdp2 deficiency leads to DSB accumulation *in vivo*

To determine whether the accumulation of DPCs results in the accumulation of DSBs *in vivo* since previous studies in cell models have demonstrated a significant increase in DSBs upon treatment with etoposide in cells lacking functional TDP2 (Gómez-Herreros et al., 2013; Zagnoli-Vieira et al., 2018), DSB were quantified detecting γH2AX levels. Phosphorylation of histone H2AX at serine 139 (γH2AX) is a well-established early marker of DSBs and its phosphorylation occurs upon recognition of DSBs by the DNA damage-dependent kinases ATM, ATR, and DNA-PK (Paull et al., 2000; Revet et al., 2011). To investigate whether *tdp2* deficiency leads to DSB formation at the organismal level, the γH2AX levels were quantified in WT, *tdp2a*-deficient and *tdp2b*-deficient mutant lines at different developmental stages: 6-hpf, 1-dpf, and 2-dpf. Remarkably, the only detected change was observed in *tdp2a*$^{\Delta E231}$ mutants at 6-hpf, where an upper ubiquitinated form of γH2AX accumulation was observed (Figure 48). This form is a marker of replication stress and indicates the formation of non-apoptotic DSBs (Luczak & Zhitkovich, 2018). It is noteworthy that this signal decreases in the subsequent embryonic stages (Figure 48).

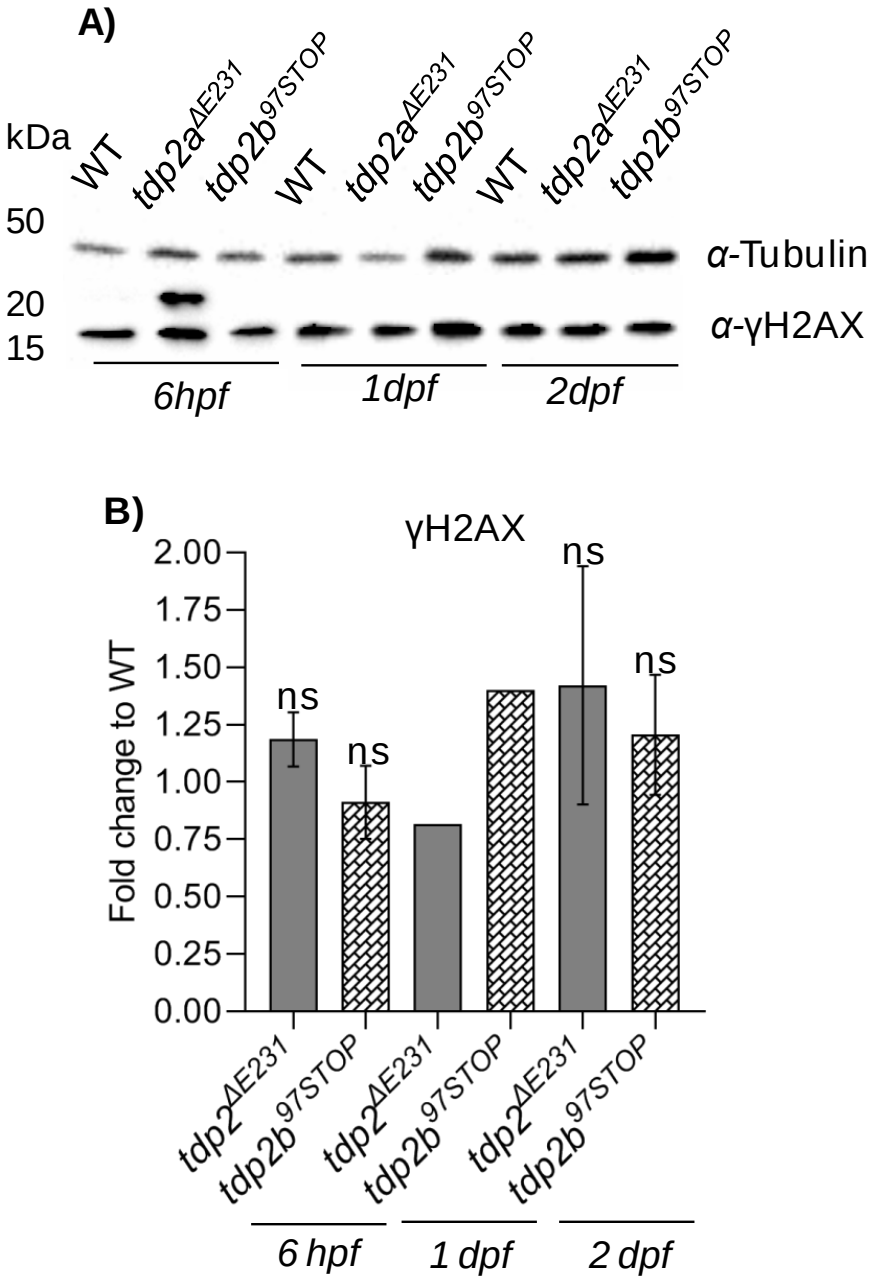

Figure 48. γH2AX levels in WT and *tdp2* mutant zebrafish embryos. A) Western blot analysis of γH2AX levels in zebrafish embryos at different developmental stages (6-hpf, 1-dpf, and 2-dpf) for the WT, *tdp2a*$^{\Delta E231}$, and *tdp2b*^{97STOP} mutants, indicating the extent of DSBs (10 µg of lysate per well). Duplicates were performed for the 6-hpf and 2-dpf stages, while 1-dpf was run as a monoplicate. Tubulin was used as a loading control. B) Quantification of A). Data are presented as mean ± SD fold change compared to WT from biological duplicates. Statistical significance was determined using an unpaired one-sample Student's t-test (ns, $p > 0.05$).

To determine if a similar effect is present after gene silencing, levels of γH2AX leves were measured in *tdp2* silenced embryos. During early development, at 6 hpf, neither *tdp2a* nor *tdp2b* silencing caused an increase in DSBs formation (Figure 49) Similarly, at 1-dpf stage, *tdp2a* silencing exhibited comparable results to the 2-dpf stage, showing no significant increase in DSBs. (Figure 49). However, *tdp2b*-silenced embryos exhibited a 2-fold increase in DSBs at 2 dpf (Figure 49). Remarkably, when both *tdp2* genes were silenced, severe consequences were observed at 1 dpf stage, when DSBs increased by 2-fold (Figure 49). At 2 dpf, DSB accumulation persisted, showing a 2.3-fold increase, similar to DSB induction caused by FA treatment (Figure 49).

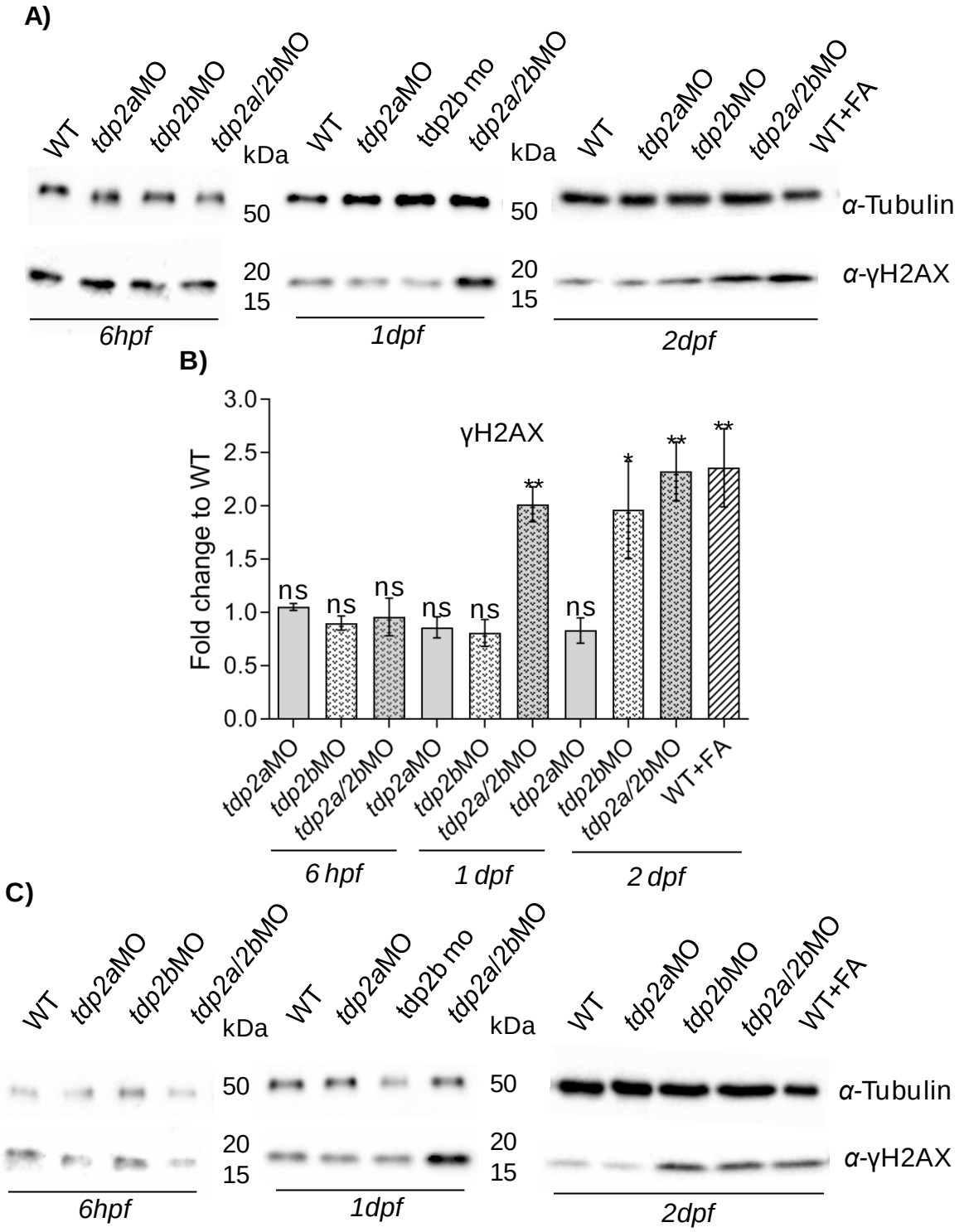

Figure 49. γH2AX levels in WT and *tdp2*-silenced zebrafish embryos. A) Western blot analysis of γH2AX levels in zebrafish embryos at various developmental stages, in WT, *tdp2a*, *tdp2b*, and *tdp2a/tdp2b* silenced embryos, indicating levels of DSBs (10 μg of lysate per well). Tubulin was used as a loading control and FA-mediated DSB induction (5 mM, 30 min) as a positive control. B) Quantification of B); C) Western blot analysis of γH2AX levels

from second biological replicate in zebrafish embryos at different developmental stages (6-hpf, 1-dpf, and 2-dpf) in WT, *tdp2a*, *tdp2b*, and *tdp2a/tdp2b* silenced embryos which was used for the quantification of γH2AX levels shown in C). The data are presented as mean ± SD fold change compared to WT from biological triplicates, and statistical significance was determined using an unpaired one-sample Student's t-test

4.26. Silencing of the SUMO2 E3/E4 ligase *zatt/znf451* causes a phenotype similar to that of *tdp2b*-silenced embryos

ZATT/ZNF451 functions as a SUMO2 E3/E4 ligase in regulating various cellular processes such as transcription, DNA repair and cell-cycle control (Cappadocia et al., 2015). It was also shown *in vitro* that ZATT is involved in TOP2-DPC repair by facilitating TDP2-mediated hydrolysis of phosphotyrosyl bonds (Lee et al., 2018; Schellenberg et al., 2017). To determine its importance at the organismal level, the *zatt/znf451* expression was silenced in zebrafish using a morpholino oligonucleotide which could target both isoforms. Initially, two different morpholino oligonucleotide doses were injected at the one-cell stage, and embryos were collected at 2 dpf for PCR analysis (Figure 50). PCR was performed on cDNA obtained from these embryos, to determine the efficacy of splice blocking (details in Materials and Methods). PCR amplification revealed a silencing efficiency of approximately 35% with the lower morpholino oligonucleotide concentration and approximately 45% with the higher one (Figures 50B and C).

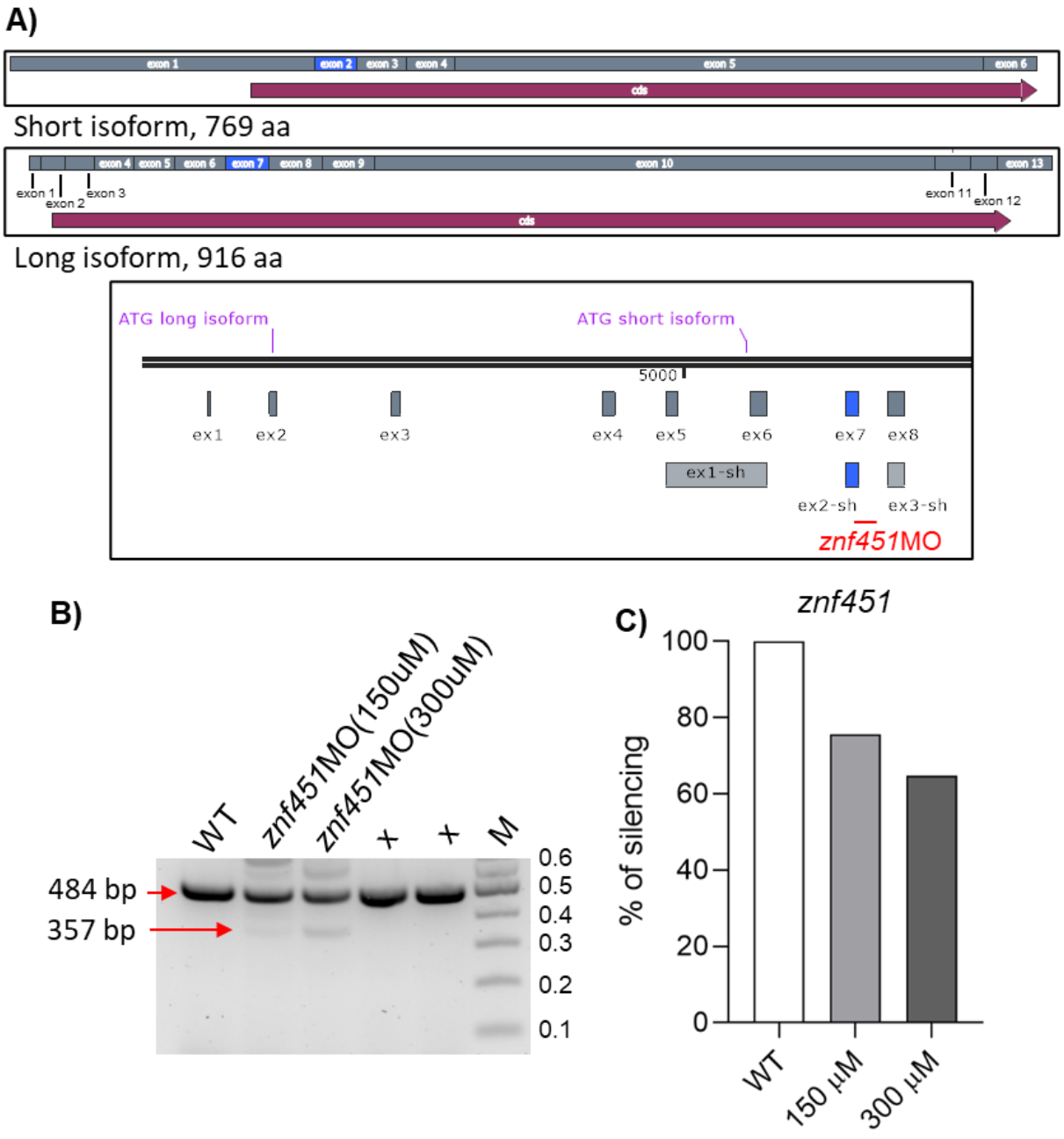

Figure 50. *Zatt*/*znf451* silencing in zebrafish using morpholino oligonucleotides. A) scheme illustrating the targeting of the *znf451* gene using a splice-blocking morpholino oligonucleotide. In zebrafish, *znf451* exists in two isoforms: a longer one with 916 amino acids and a shorter one with 769 amino acids. The morpholino oligonucleotide (red) blocks splicing at the boundary between exon 7 and intron 7 of the long isoform, which also corresponds to the boundary between exon 2 and intron 2 of the short isoform. B) Results of a DNA gel electrophoresis with PCR reactions on cDNA from 2-dpf WT and *znf451* morphant embryos. The primers listed in Table 4 were used for the PCR. The expected WT band is 484

bp long, while a 357 bp band is observed in the *znf551* morpholino oligonucleotide treated samples, which indicates exon skipping (arrows). The numbers next to the marker bands represent sizes in kilobases (kb). C) Quantification of the WT 484 bp band from (B) expressed as a % of the WT band in the WT embryos.

At 2 dpf, changes were noticed in the appearance of the *zatt/znf451* morphants: they had smaller brains and eyes, and their yolk was not used up like in WT embryos (Figure 51). Development of edema around the yolk was also also observed, indicating impaired blood flow (Figure 50). This phenotype was similar to that we had observed in *tdp2b* morphants (Figure 39). The specificity and cause of these effects should be determined in future studies.

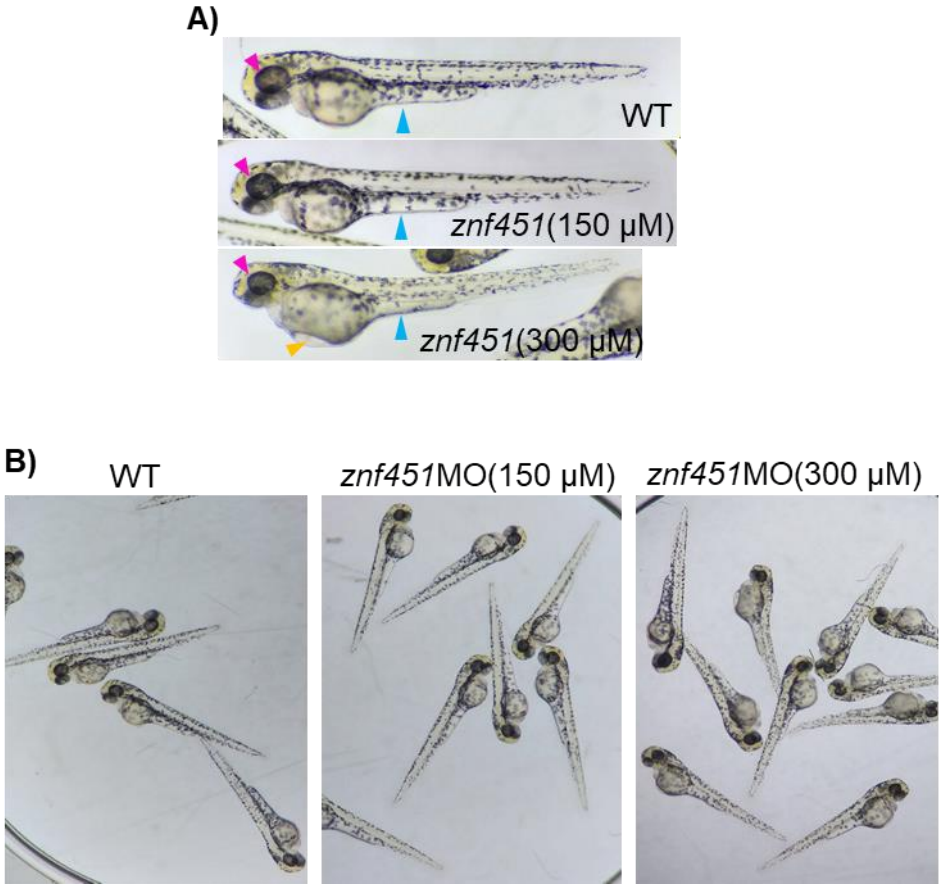

Figure 51. Representative images of live zebrafish embryos after *zatt/znf451* silencing. A) Images of 2-days old WT and *zatt/znf451*-silenced embryos. The magenta arrowhead shows the eyes, the blue arrowhead indicates the yolk, and the yellow arrowhead highlights the edema. B) Overview images of WT and *zatt/znf451*-silence embryos (Cecile Otten, IRB, unpublished results).

4.27. Mre11 is essential for early vertebrate development

The MRE11 protein is an essential enzyme and a part of the MRN complex that is critical for DNA end resection and HR-mediated DSB repair. MRE11 acts as both an exonuclease and an endonuclease, generating short ssDNA overhangs at DSB sites, allowing homology-directed repair (Reginato & Cejka, 2020). Moreover, it can remove protein blocks at DSB sites, allowing for further DNA end processing by other nucleases. Therefore, it was postulated that MRE11 plays a role in repairing DPCs. It was shown *in vitro* that it can remove streptavidin- and TOP2-DPC (Aparicio *et al.*, 2016; Deshpande *et al.*, 2016; Hoa, Shimizu, Zhou, Z. Q. Wang, *et al.*, 2016), and human rhabdomyosarcoma cell lines (RH30) lacking MRE11 activity exhibit accumulation of TOP2 DPCs (Sun et al., 2022). To investigate the role of Mre11 in DPC repair *in vivo*, morpholino oligonucleotide mediated gene silencing was used to block *mre11* expression in zebrafish. A morpholino oligonucleotide targeting the *mre11* ATG site was injected into one-cell stage embryos at two different concentrations (100 µM and 300 µM), and embryo development was monitored over a 5-day period (Figure 51). Interestingly, no immediate changes were observed on the first day. However, after 2-dpf stage, embryos exhibited a curved shape and impaired stretching ability after dechorionation, suggesting muscular issues (Figures 51B and C). Progressive degeneration was observed on the third day, even at a morpholino oligonucleotide concentration of 100 µM (Figures 51B and C). The embryos showed reduced brain and eye size, and the typical absorption of the yolk ball did not occur. By the fifth day, embryos still retained a yolk, and the presence of an edema around the yolk indicated disrupted blood flow. In addition, the embryos lacked a swim bladder, so the future larvae would not be able to swim up and down and feed on their own, eventually leading to larval death (Figures 51B and C). However, this effect remains to be confirmed in the future studies as the efficiency of silencing needs to be determined with a zebrafish specific Mre11 antibody and the specificity of the morpholino oligonucleotide will be confirmed by the injection of a rescue construct, i.e., *mre11* mRNA.

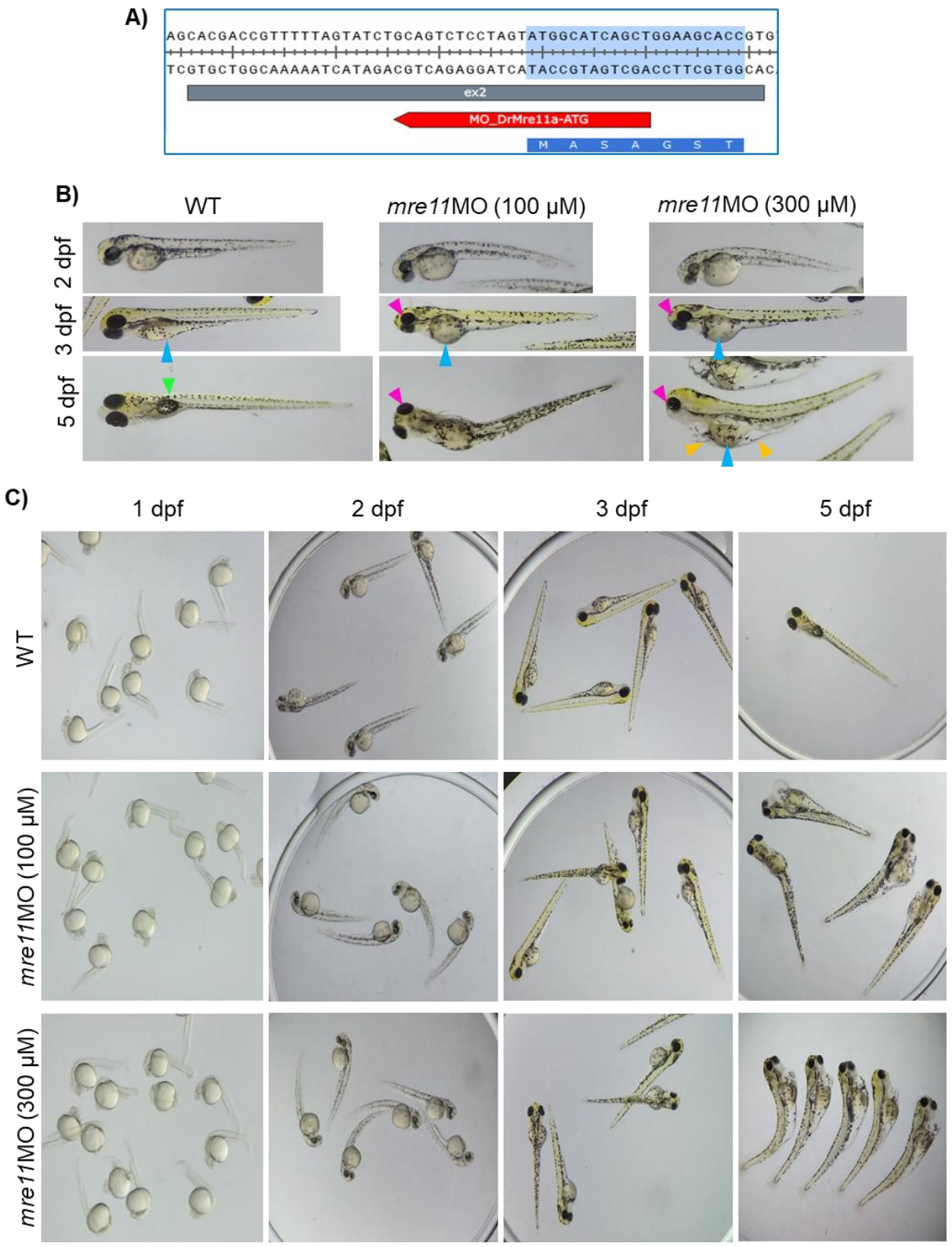

Figure 52. Representative images of live zebrafish embryos after *mre11* silencing. A) Scheme of *mre11* ATG targeting morpholino oligonucleotide where the morpholino oligonucleotide binding site is represented in red; the *mre11* ATG is located in exon 2 of the gene. B) images of 2-, 3-, and 5-day-old embryos, wild-type (WT) and *mre11*-silenced

embryos treated with two concentrations of morpholino oligonucleotide (100 and 300 μM). Magenta arrowheads show the eyes, the blue arrowheads indicate the yolk; the green arrowheads point to the swim bladder, and the yellow arrowheads highlight the edema. C) Overview displaying 1-, 2-, 3-, and 5-day-old WT and *mre11*-silence embryos (Cecile Otten, IRB, unpublished results).

5. DISCUSSION

The study of DNA repair and the DNA-protein crosslink repair (DPCR) pathways in zebrafish complements cell models and offers new perspectives. TDP1 and TDP2 play key roles in DPCR pathways and are essential for the resolution of TOP1- and TOP2-DNA crosslinks (TOP1- and TOP2-DPCs). Investigating Tdp1 and Tdp2 in zebrafish provides new insights, especially since data from vertebrate models are still sparse. Animal models such as zebrafish, play an important role in bridging this gap, as they represent a system comparable to human biology, despite the added challenges of complexity and time consumption compared to cell models.

To study DPC repair *in vivo,* toolbox were established for using the zebrafish animal model in DPC research. The protocol for isolation and detection of DPC from cell culture and embryonic tissues was optimized, Tdp1- and Tdp2- deficient zebrafish strains were generated and detection of specific DPCs including histone H3, TOP1 and TOP2 from human cells and embryonic zebrafish tissues was optimized. Furthermore, morpholino oligonucleotide mediated knockdown was established a for genes important for the DPCR pathway: *tdp2a, tdp2b, sprtn, zatt/znf451* and *mre11,* and characterized the phenotypes after gene silencing. In addition, Tdp1 antibody was developed and validated for derection of the zebrafish and human orthologues. Understanding how DPC repair is orchestrated in organisms is only possible through research on animal models. The tools that were developed will be useful for future studies, including tissue-specific DPC repair, cancer-related studies, potential drug development, and better understanding of human diseases associated with DPCs.

5.1. *In silico* comparative analysis of human and zebrafish TDP1 and TDP2 enzymes: phylogeny, synteny, topology and structure

To ensure that zebrafish is a suitable model for investigating the role of Tdps in DPCR, zebrafish Tdp1 and Tdp2 orthologues were compared with human orthologues in respect to topology, phylogeny, synteny and structure. Degree of conservation analyses of the TDP1 between the different species and found a high degree of evolutionary conservation of one-to-one orthology across all domains of life (Figure 11A and Supplement 1). The very high structural similarity between zebrafish and human orthologues (Figure 12) confirms the importance of TDP1 for DNA repair throughout evolution. Synteny analysis of the *tdp1* gene in zebrafish, human, and mouse revealed partially conserved gene environment (Figure 11B) with the upstream neighbouring gene *kcnk13a* and the downstream neighbouring genes

efcab11 and *foxn3* clustered together (Figure 11B). On the other hand, phylogenetic analysis of *tdp2* genes showed existence of two orthologues in zebrafish, *tdp2a* and *tdp2b*. It is known that the zebrafish genome is characterized by a considerable number of duplicated genes (Howe et al., 2013). This process of duplication and retention of duplicated genes was crucial for the expansion of fish genomes, as a fish-specific whole genome duplication (WGD) event occurred 350 million years ago (Meyer & Van de Peer, 2005). Moreover, this process has played a crucial role in the evolutionary divergence of fish and tetrapods, resulting in a greater diversity of fish genes. Some orthologous genes have evolved to take on specialized functions characterized by specific gene expression patterns, while their original ancestral functions have been taken over by another orthologue, contributing to the diverse genetic profile of the fish genome.(J. Lu et al., 2012). Through a detailed synteny analysis of the *TDP2* genes in humans and Zebrafish showed: the upstream gene cluster associated with human *TDP2* is located adjacent to zebrafish *tdp2b*, while the downstream gene cluster coincides with the *tdp2a* orthologue (Figure 34). Apart from *tdp2* genes, only two other nearby genes (*nrsn1* and *sox4*) remained on chromosomes 16 and 19 (Figure 34), respectively, while the other neighbouring genes (upper and downstream clusters of *TDP2*) were lost after duplication, as was the case for the vast majority (80%) of genes after the WGD event in teleosts (Glasauer & Neuhauss, 2014). This observation provides valuable insights into the ancestral genomic changes in zebrafish and is yet another example of gene duplication event that have shaped their present-day genomic organization. From the two zebrafish *tdp2* orthologues, Tdp2b is evolutionarily closer to human TDP2 (Figures 33 and 35A). Although both zebrafish orthologues have a conserved catalytic domain (Figure 35A), Tdp2b is more similar to human TDP2 when comparing the N-terminal region (Figure 35A).

5.2. Comparative analysis of expression patterns between zebrafish and human *TDP1* and *TDP2* genes

A comparison of the expression patterns of *TDP1* and *TDP2* genes in zebrafish and humans (Karlsson *et al.*, 2023, https://www.proteinatlas.org/) in different tissues revealed partially conserved patterns. Remarkably high expression of the *TDP1/Tdp1* gene was observed in both human and zebrafish testes, followed by intestine, ovary, kidney, and brain in humans, while in zebrafish, the ovaries showed notably higher expression comparable to that in testes followed by brain, liver, kidney, and intestine (Figure 16B). Intriguingly, when comparing TDP1 protein levels in humans and zebrafish, humans showed the highest levels in the brain, followed by comparable levels in all other tissues (Uhlén et al., 2015). In contrast,

tdp1 in zebrafish showed the highest expression in gonads, followed by brain (especially in males), kidney and liver in both genders, with the intestine showing the lowest levels in both genders (Figure 17). Similar to *TDP1*, the expression of *TDP2* genes was also compared. In humans, *TDP2* has the highest expression in the intestine, followed by the kidney and testis. This is followed by the liver, brain, and ovaries (Karlsson et al., 2023). This pattern resembles the expression of zebrafish orthologue *tdp2a* except in the testes where *tdp2a* is dominant, in contrast to the dominant expression of *TDP2* in human intestine (Figure 36B). On the other hand, the *tdp2b* orthologue also follows a similar tissue expression pattern, except for comparatively lower expression of *tdp2b* in the intestine and comparatively higher in the ovaries (Figure 36C). However, it is worth noting that human RNA expression data and protein level data in the Protein Atlas is heavily biased toward the analysis of older individuals (Uhlén et al., 2015), whereas the zebrafish analysis was performed on 1.5-year-old adults, which corresponds to a middle-aged human. Therefore, future studies on human samples are needed to improve the comparative analysis.

The very high expression of the *tdp1* and *tdp2* genes in the zebrafish gonads (Figures 16B, 36B and C) suggests a crucial and protective role in maintaining genome integrity during the process of gametogenesis. Curiously, *tdp2a* appears to play a greater role in the testes, while *tdp2b* is predominantly expressed in the ovaries, which has already been established by microarray analyses in female zebrafish tissue (Small et al., 2009) (Figures 36B and C). It is not surprising that duplicated genes undergo evolutionary changes that result in gender-specific expression, as this ensures their appropriate function in gametogenesis and reproduction (Gnad & Parsch, 2006; Rice, 1984; Whitehead & Crawford, 2006). Remarkably high expression of both *tdp1* and *tdp2* is observed in brain tissue suggesting a protective role in maintaining the integrity of the neuronal genome (Figures 16B, 36B and C). Neurons do not proliferate, and their DNA repair mechanisms differ to some extent from those of cycling cells. Since they are not able to form sister chromatids, error-free HR repair is not present in non-cycling cells. As a result, these cells rely heavily on NHEJ or MMEJ to repair DSBs (McKinnon, 2013), which are more likely to lead to mutations due to their inherent mechanisms (Bétermier et al., 2014; Seol et al., 2018). TDP1 is known to have an important function in the mammalian brain, where mutations in the *TDP1* gene lead to SCAN1 syndrome in humans, characterized by age-progressive cerebellar ataxia, distal sensorimotor axonal neuropathy (Hirano et al., 2007), and mice lacking Tdp1 show age-progressive reductions in cerebrum and cerebellum size (Katyal et al., 2007). Combined with the demonstrated function of TDP2 in neural tissue (Gómez-Herreros et al., 2013, 2014, 2017), it

is not surprising that *tdp2a* and *tdp2b* show high expression in the zebrafish brain (Figures 36B and C). Individuals with a mutation in the *TDP2* gene develop SCAR23 syndrome which is characterized by progressive ataxia, dysarthria, and intellectual disability (Errichiello et al., 2020; Zagnoli-Vieira et al., 2018). It was previously suggested that SCAR23 phenotype is caused by the role of TDP2 in NHEJ repair of DSBs following TOP2 DNA cleavage. Considering that neurons are highly dependent on NHEJ and that TDP2 was shown to promote error-free NHEJ pathway ''via the cleaning'' of 5' DNA TOP2 and potentially TOP2-like overhangs, leaving a 4 bases long sticky ends that are suitable for rejoining (Gómez-Herreros et al., 2013). This is in contrast to the error-prone NHEJ repair of DSBs, which generates blunt DNA ends during the repair process. These blunt ends, when rejoined, often lead to insertions or deletions at the break site. Furthermore, the high expression of *tdp2a* in intestinal tissue also suggests a protective role of TDP2 (Figure 36B). Considering that mice lacking TDP2 exhibit intestinal damage and significant weight loss following etoposide treatment (Gómez-Herreros et al., 2013). These results suggest a protective role of TDP2 in preventing TOP2-DPC accumulation and highlight its importance for DPCR. In the absence of TDP2, a severe phenotype is observed in TDP2 knockout mice after ETO treatment. This is likely due to the initial accumulation of TOP2-DPCs that develop into DSBs. These DSBs are then rapidly repaired by error-prone NHEJ, leading to genomic instability, especially in non-replicating and rapidly dividing cells. In summary, the expression data presented provide substantial evidence that zebrafish is an excellent model for studying mechanisms involving TDP1 and TDP2.

In addition to examining tissue expression levels, the expression changes of *tdp1* and *tdp2* during early embryonic development werw also investigated. Starting from 6-hpf, when embryonic transcription begins and maternal transcripts are degraded (Laue et al., 2019; Mathavan et al., 2005) until the 5-dpf stage, the expression of the *tdp* genes and *sprtn* was measured. All three genes showed high expression levels (Figures 16A and 36A), which is not surprising given the rapid cell division and transcription during this period, which in turn require accurate and rapid DNA repair processes necessary for development (Keller, 2013). A detailed comparison of *sprtn* and *tdp1* expression during 5-day embryonic development shows a similar expression pattern between the two genes at later stages. However, the expression of *sprtn* is notably increased at 6 hpf with 33-fold higher mRNA levels than *tdp1* (Figure 16A). This observation suggests a higher demand for SPRTN proteolysis in the initial stages of embryonic development. Analysis of *tdp2* orthologues *tdp2a* and *tdp2b* during zebrafish development revealed that *tdp2b* is dominantly and consistently highly expressed

from early development (6 hpf) to 5 days of age, suggesting that *tdp2b* is a more important orthologue during embryonic development (Figure 36A).

5.3. Optimization of *in vivo* methods to study the interaction of TDP1 and SPRTN

Sincie it is established that zebrafish is a good model for studying the role of TDP1 and TDP2 in DPCR, TOP1-DPC repair was investigated *in vivo*. The focus was on understanding the interplay between TDP1 and SPRTN, which is thought to play an important role in TOP1-DPC removal (Fielden et al., 2020; Stingele et al., 2014; Vaz et al., 2016). Aim was to investigated this interplay of these two proteins at the endogenous level and when DPCs were induced with the TOP1 inhibitor CPT and with a general DPC inducer, FA. In addition, comparative analysis of DPCR in cell culture with human RPE1 cells was also preformed.

To monitor the interaction between these two proteins and their effects on cellular DPCs, the isolation, detection and quantification of DPCs was optimized. Modification of the RADAR assay, an established technique for DPC isolation (Kiianitsa & Maizels, 2013), where lyophilization step was introduced as an alternative to TCA protein precipitation and subsequent pellet washing. This modification greatly improved the reproducibility of total and specific DPC detection (Figures 18, 19, 28 and 30), thus significantly increasing the throughput and accuracy of results (Figures 43, 44 and 45). In addition, new animal model was successfully created, a Tdp1-deficient zebrafish strain. Embryos lacking *tdp1* develop normally, and phenotypic changes were not detectd in fish aged up to one year (Figure 14). This is consistent with the results of the other recently characterized zebrafish model (Zaksauskaite et al., 2021) and previously characterized mouse model (Hirano et al., 2007; Katyal et al., 2007). However, it remains to be seen whether older zebrafish will exhibit similar phenotypes as observed in mice lacking TDP1 or humans with TDP1 mutations (Hawkins et al., 2009; Hirano et al., 2007; Katyal et al., 2007). Next, gene silencings for *TDP1* and *SPRTN* in RPE1 cells and morpholino oligonucleotide based *sprtn* silencing in zebrafish embryos were optimized. Successful silencing of the *sprtn* gene in zebrafish was achieved by microinjection of a combination of morpholino oligonucleotides, one targeting the UTR and blocking the ATG site, and the second targeting the ex2-in2 boundary resulting in splice blocking (Figure 22). The splice-blocking morpholino oligonucleotide led to an 80% reduction in *sprtn* mRNA levels (Figure 22C), but evidence of silencing at the protein level is still lacking. Despite this significant reduction, the zebrafish embryos developed normally and without any discernable phenotypic effects (Figure 22D). This was somewhat surprising considering that SPRTN is an essential gene and is thought to be the major DPC protease that

initiates repair of various DPCs during S-phase (Maskey et al., 2017; Ruggiano et al., 2021; Vaz et al., 2016). Patients with impaired SPRTN activity develop RJALS syndrome, which is characterised by genome instability, progeria, and early-onset hepatocellular carcinoma (Lessel et al., 2014; Vaz et al., 2016; Weickert et al., 2023). Interestingly, in a previous work from 2014, Lessel et al. had successfully used an ATG-targeting morpholino oligonucleotide to silence *sprtn* in zebrafish, resulting in an early lethality phenotype, even at low doses. As described in that paper, it was found that zebrafish injected with this morpholino oligonucleotide exhibited an early lethality phenotype (data not shown), but injection of splice-blocking, UTR-targeting, and even combination of these two did not result in any observable phenotypic changes. The efficacy of the splice-blocking morpholino oligonucleotide was confirmed by qPCR analysis (Figure 22B) and the analysis of DNA-protein crosslinks revealed elevated levels of total DPCs (Figure 28) and specific TOP1- and H3-DPCs (Figures 18 and 20), when the combination of *sprtn* UTR and splice morpholino oligonucleotide was used. Therefore, it is hypothesized that the ATG morpholino oligonucleotide used in a previous study by Lessel et al. (2014) is efficient, but not specific, and that the observed lethality phenotype is due to off-target effects. Therefore, all experiments were preformed with the combination of UTR and splice-blocking MO, as this silencing approach resulted in DPC accumulation (Figure 28) and the efficiency of splice-blocking morpholino oligonucleotide silencing was confirmed by splice-specific PCR (Figure 22).

5.4. SPRTN and TDP1 are crucial for the resolution of TOP1-DPCs *in vivo* and in cell models and they function independently in the repair of endogenous TOP1-DPCs

With respect to the canonical TDP1 substrate, TOP1, it is found that TDP1 is crucial for the removal of TOP1-DPCs, both at the organism level and in RPE1 cells (Figures 18 and 19). Consistent with previous findings in human HEK293 cells (Fielden et al., 2020), silencing *TDP1* in RPE1 cells resulted in increased TOP1-DPC levels (Figure 19). In contrast, knock-out of *TDP1* in RPE1 cells did not lead to TOP1-DPC increase (Meroni et al., 2022), suggesting adaptive mechanisms in permanent knock-out as opposed to temporary gene silencing. Given the importance of TOP1 inhibition in cancer therapy (Fengzhi Li, 2017; Martino et al., 2017), the role of TDP1 in TOP1-DPC repair has been extensively studied *in vitro* and in cell culture (Gao et al., 2014; Heidrun & James, 2011; Pouliot et al., 1999; Yang et al., 1996), but data on vertebrate models are sparse (Hirano et al., 2007; Katyal et al., 2007;

Zaksauskaite et al., 2021). Using the zebrafish model, we show that the lack of Tdp1 leads to a significant 4.2-fold increase in endogenous Top1-DPCs (Figure 18), demonstrating that TDP1 is crucial repair factor for the resolution of TOP1-DPCs. In a previous study by Zaksauskaite *et al.* (2021), no difference in Top1-DPC levels was found between wild-type and Tdp1-deficient zebrafish embryos. The discrepancy is likely due to the different approaches to DPC isolation, as the RADAR assay used in this study is more specific and sensitive than the CsCl fractionation method used in the previous study (Kiianitsa & Maizels, 2013, 2014, 2020). It is also shown that SPRTN is critical for TOP1-DPC repair at the organism level (Figures 18C, D and E), supporting previous studies in cell culture that showed an increase in TOP1-DPC levels after SPRTN silencing (Maskey et al., 2017; Stingele et al., 2014; Vaz et al., 2016) and that SPRTN proteolyzes TOP1 *in vitro* (Vaz et al., 2016). Moreover, simultaneous silencing of TDP1 and SPRTN in RPE1 cells and, silencing of *sprtn* in *tdp1* mutant fish show non-epistatic relationship between these two proteins in the repair of endogenous TOP1-DPCs (Figures 18 and 19). Since it is known that TDP1 cannot process TOP1-DPCs alone (Heidrun & James, 2011), it is hypothesized that another protease is involved in the upstream proteolysis of endogenous TOP1-DPCs (Figure 53). Possible candidates include DDI1, DDI2, FAM111A, and the proteasome (Dirac-Svejstrup et al., 2020; Kojima et al., 2020; Larsen et al., 2019; Serbyn et al., 2020). On the other hand, the peptide remnant left on the 3' DNA strand after SPRTN proteolysis could potentially be removed by the APEX1/2 nuclease pathway (H. Zhang et al., 2022). This is supported by the observation that *tdp1* mutant fish showed increased expression of the *apex1* gene (Zaksauskaite et al., 2021).

5.5. SPRTN and TDP1 act in separate pathways in resolving total DPCs, but they work epistatically in resolving histone H3-DPCs

It is known that SPRTN and TDP1 play different roles in DPC repair. SPRTN initiates the repair of many crosslinked proteins (Fielden et al., 2018), while TDP1 has previously been specifically associated with the repair of TOP1-DPCs (Kawale & Povirk, 2018). The function of TDP1 in the repair of DPCs other than TOP1-DPCs has not previously been studied *in vivo*. Surprisingly, it is observed that loss of Tdp1 in zebrafish embryos and RPE1 cells leads to a significant increase in cellular DPCs that is not solely due to the increase in TOP1-DPCs (Figures 28 and 30), suggesting that TDP1 has multiple DPC substrates. Regarding the role of SPRTN protease in DPCR, also SPRTN is a crucial protease for the resolution of multiple cellular DPCs *in vivo* and, in particular for the removal of low and medium molecular weight

DPCs (Figures 28, 29 and 30). Analysis of DPCs in SPRTN-deficient embryos provides the first evidence of how DPC levels are affected in an organism. Compared with embryos, the effect of SPRTN deficiency was somewhat weaker in RPE1 cells. In the line with non-epistatic relationship between these two proteins in the repair of endogenous TOP1-DPCs the same effect is observed for total cellular DPCs (Figures 18, 19, 28 and 30).

A more detailed analysis of DPC distribution in *tdp1* mutant embryos and TDP1-deficient RPE1 cells shows an increase in low molecular weight DPCs (Figures 28, 29 and 30) which is most likely due to the increase in histone-DPCs, considering that endogenous H3-DPCs accumulate strongly in Tdp1-deficient embryos and human cells (Figures 20 and 21). It is very important to understand how histone-DPCs are repaired, as they are very abundant under physiological conditions. More than 10,000 abasic sites are generated daily (Lindahl, 1993), and about 10% of these lead to the formation of DPCs, most of which are histone-DPCs (Kiianitsa & Maizels, 2020). This suggests that hundreds, possibly even thousands of histones are crosslinked at abasic sites in each individual cell every day (Ren et al., 2019). The function of TDP1 in the repair of cellular DPCs and histone-DPCs has not been previously investigated. This results support recent observations by Wei *et al.* (2022), who showed that TDP1 can remove histone H2B and H4 from AP sites *in vitro*, and provide the first evidence for a novel, TDP1-dependent repair pathway for histone-DPC resolution *in vivo*. This finding should be considered in the development of TDP1 inhibitors for cancer therapy (Sun, Saha, Wang, et al., 2020).

This results also show that SPRTN plays an important role in the resolution of H3-DPCs *in vivo*, as knockdown of *sprtn* in zebrafish resulted in a 5.7-fold increase in H3-DPC levels (Figures 20 and 21), supporting *in vitro* data characterising H3 as a substrate of SPRTN (Vaz et al., 2016). Therefore, this study finally demonstrates the crucial role of SPRTN in resolving DPCs at the organism level and highlights SPRTN as a promising chemotherapeutic target. Unlike endogenous TOP1-DPC repair, SPRTN and TDP1 work together in the resolution of endogenous H3-DPCs in zebrafish and human cells (Figures 20 and 21), suggesting that SPRTN is the main protease acting upstream of TDP1-mediated peptide removal in the resolution of histone-DPCs at AP sites (Figures 53). These results are the first to show that SPRTN proteolysis is required for histone-DPC resolution *in vivo*. It is worth noting that TDP1 can remove H2B and H4 crosslinks *in vitro* without the requirement of upstream proteolysis (Wei et al., 2022). The known discrepancies between *in vitro* and *in vivo* data further emphasizes the urgent need for the experimental data from the animal models.

5.6. SPRTN and TDP1 act epistatically in the resolution of DPCs induced by CPT and FA

In contrast to physiological conditions, after exposure to CPT, when TOP1-DPCs are induced, we show that SPRTN and TDP1 act epistatically in the resolution of total DPCs and TOP1-DPCs in RPE1 cells (Figures 19 and 31). These results are consistent with data from cell survival assays showing that simultaneous depletion of TDP1 and SPRTN in yeast (Stingele *et al.*, 2014; Lopez-Mosqueda *et al.*, 2016) and HeLa cells (Vaz et al., 2016) reduce cell growth upon CPT treatment to a similar extent as depletion of either component alone when exposed to CPT, suggesting that SPRTN and TDP1 function in the same pathway for repair of CPT-induced TOP1-DPCs. It is important to note that DPCR factors may behave differently under physiological conditions and under stress, when DPC load exceeds certain thresholds. In summary, these results suggest that repair of CPT-induced TOP1-DPCs depends on the SPRTN-TDP1 axis, in contrast to repair of endogenous TOP1-DPCs, where TDP1 and SPRTN function in separate pathways (Figure 53). It is observed that CPT also induces H3-DPCs in human cells and in zebrafish embryos (Figures 20 and 21), showing for the first time that CPT is not specific for TOP1-DPC induction, as previously thought (Ramawat & Mérillon, 2013). This effect is likely indirect, considering that CPT has been characterized as an agent that directly and specifically crosslinks TOP1 (Martino et al., 2017). It is conceivable that the increased requirement for TOP1-DPC repair following CPT exposure results in reduced recruitment of TDP1 to H3-DPC lesions that occur endogenously at high frequency (Kiianitsa & Maizels, 2020), ultimately leading to an increase in H3-DPCs. However, this remains to be investigated in future studies.

Formaldehyde is a potent crosslinker of various cellular proteins ranging in size from 10 kDa to over 200 kDa (Stingele *et al.*, 2014; Lopez-Mosqueda *et al.*, 2016; Ruggiano *et al.*, 2021). These results show that the interplay of SPRTN and TDP1 in DPCR is altered when cells and embryos are exposed to high acute doses of FA, compared to physiological conditions where only endogenous DPCs are present. SPRTN and TDP1 act together (in epistasis) in the repair of FA-induced total cellular DPCs (Figures 28 and 32) and in the repair of FA-induced H3- and TOP1-DPCs (Figures 18, 19, 20 and 21). Considering that large amounts of DPCs accumulate under these conditions, it is hypothesized that SPRTN is fully activated and performs upstream proteolysis of many crosslinked proteins given its pleiotropic nature (Vaz et al., 2016), and that TDP1 is crucial for the resolution of H3- and TOP1-DPCs as well as other crosslinked protein residues at 3' DNA ends.

5.7. Interplay between TDP1, TDP2, and SPRTN at the level of mRNA expression

The interplay between TDP1 and SPRTN was evident at the level of mRNA and protein expression. Silencing of *SPRTN* leads to increased mRNA expression of *TDP1* in human cells (Figure 24C) and increased expression of *tdp1* at the mRNA and protein levels in zebrafish embryos (Figures 24A and 25). Both proteins are critical for human cell functioning, as RPE1 cells in which *TDP1* and *SPRTN* silenced have 68% reduced viability (Figure 27). It is suggested that phenotype is the result of impaired DPCR due to the reduction in TDP1 and SPRTN protein levels (Figures 19, 21 and 30). It is known that *SPRTN*-silenced human cells exit S phase with abnormal replication intermediates (Mórocz et al., 2017) and *TDP1*-silenced cells show an increase in ssDNA and dsDNA breaks (Fielden et al., 2020). On the other hand, TDP2 is thought to compensate for the loss of function of TDP1 *in vitro* and in cell models (Ledesma et al., 2009; Shimizu et al., 2023; Zeng et al., 2012). Consistent with this, expression analysis of both *tdp2* orthologues showed a significant increase in *tdp2* expression when *tdp1* was absent in embryos, suggesting that TDP2 may compensate for the loss of TDP1 *in vivo* (Figures 26B and C). Furthermore, TDP2 expression increased when TDP1-silenced RPE1 cells were challenged with CPT, and simultaneous silencing of TDP1 and TDP2 resulted in an additional 80% reduction in cell viability (Figures 26A and 27).

In summary, this results show that TDP1 is a key factor for the repair of histone H3- and TOP1-DPCs, while SPRTN is crucial for the repair of many cellular DPCs including TOP1- and H3-DPCs in human cells and zebrafish (Figure 53). Resolution of H3-DPCs depends on upstream proteolysis by SPRTN and subsequent peptide removal by TDP1 in cells and embryos (Figure 53). In contrast to H3-DPC repair, where SPRTN and TDP1 work together, they function in separate pathways in the repair of endogenous TOP1-DPCs (Figure 53). However, after human cells are exposed to clinically relevant concentrations of camptothecin, SPRTN and TDP1 act epistatically in the resolution of total DPCs, histone H3- and TOP1-DPCs (Figure 53). In depth understanding of this DPCR orchestration at the organism level is important particularly for TOP1-DPC repair, asTOP1-DPC inducers, the camptothecin derivatives irinotecan and topotecan, are used to treat various cancers, including ovarian, colon, small-cell lung, central nervous system tumours, and sarcomas (Martino et al., 2017). Combination therapies with TOP1 and TDP1 inhibitors could significantly improve current clinical protocols, and therefore it is essential to know how TDP1 functions in repairing DPCs at the organism level. Additionally, this findings provide support for future research in developing SPRTN inhibitors. Such inhibitors have the potential to significantly affect tumour

cells and can be used in combination with TDP1 inhibitors and/or drugs that induce TOP1-DPCs.

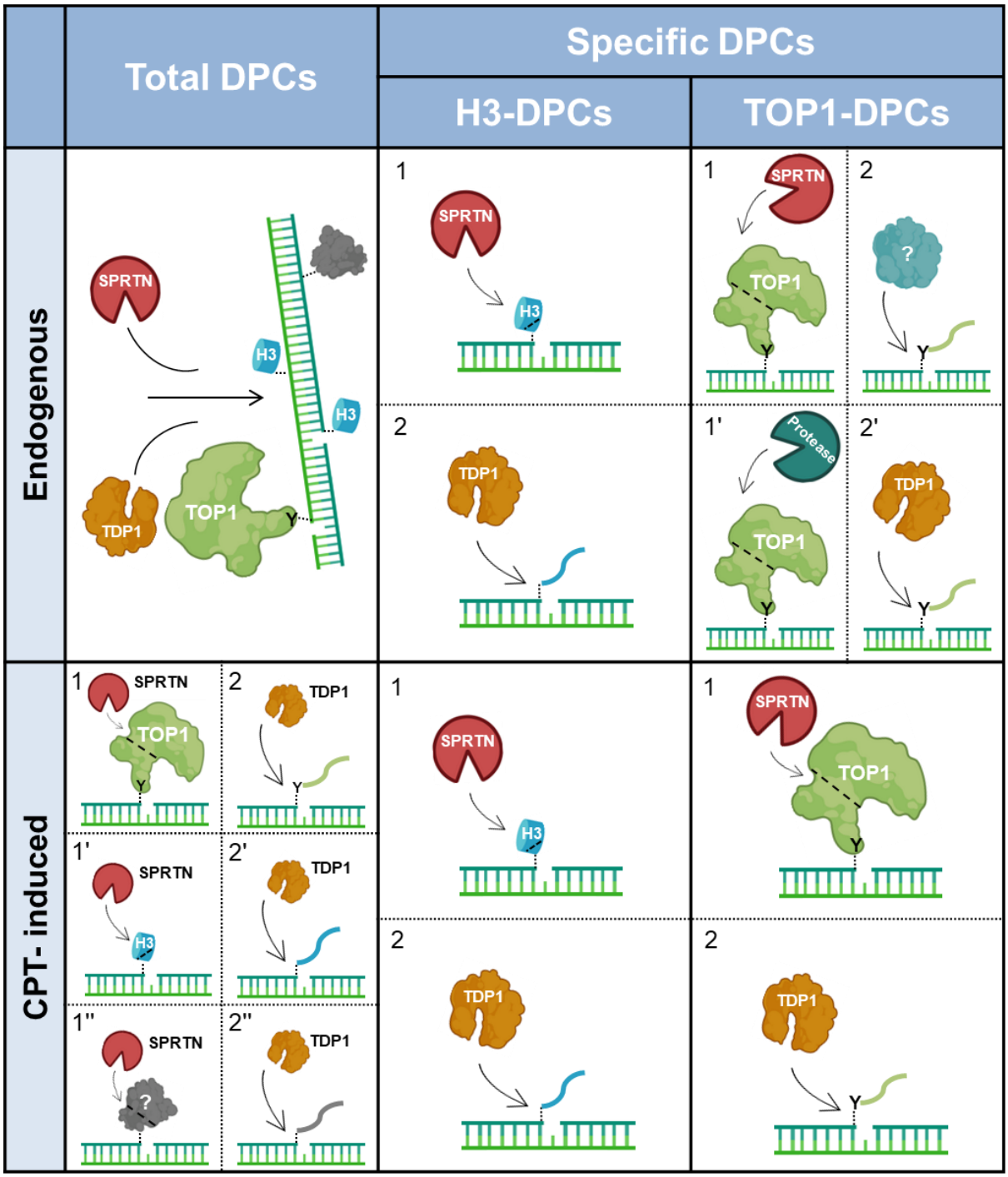

Figure 53. Model of coordinated action of SPRTN and TDP1 in DNA-protein crosslink repair in human cells and zebrafish model. SPRTN is a general DPC protease that cleaves a wide spectrum of crosslinked proteins, whereas TDP1 removes protein residues bound to the 3' end of the ssDNA break. Under physiological conditions, these two proteins function

independently to resolve total DPCs, including specific TOP1-DPCs. Importantly, resolution of endogenous histone-DPCs originating at abasic (AP) sites depends on SPRTN-mediated proteolysis followed by TDP1 phosphodiesterase activity, by which the crosslinked peptide residue is removed from the DNA backbone. In response to the DNA-damaging agent camptothecin, an epistatic relationship between SPRTN and TDP1 is required for the successful removal of histones and TOP1-DPCs as well as other DPCs at the 3' ends of ssDNA breaks. The model was created with BioRender.com

5.8. Optimization of *in vivo* models to study TDP2-associated TOP2-DPC repair

To investigate TOP2-DPC repair *in vivo*, similar approach was used as for TOP1-DPCs. In this case, zebrafish strains that lacks Tdp2 were created, as Tdp2 it plays a key role in the downstream resolution of Top2-DPC remnants. Two strains were successfully generated: one carrying a catalytically impaired *tdp2a* variant and the other lacking zebrafish *tdp2b*. To completely abolish Tdp2 activity, morpholino oligonucleotide mediated *tdp2* gene silencing was optimized. In this way, effective silencing of both *tdp2a* and *tdp2b* gene was established in zebrafish embryos. In addition to *tdp2* silencing, the silencing of the *zatt*/*znf451* and *mre11* genes in zebrafish was also optimized, both of which are presumably important for Top2-DPC resolution. In addition, the successfully Top2-DPC detection was optimized in zebrafish embryos and human cells.

To create zebrafish strains with Tdp2 deficiency, CRISPR/Cas9 system was used the to specifically modify *tdp2a* and *tdp2b*. This resulted in two new strains: one with a catalytic mutation in *tdp2a* (ΔE231) and another strain with an induced frameshift mutation in *tdp2b*, leading to a premature stop at position 97 aa (Figure 35). *Tdp2a* mutant is the first animal model with catalytically impaired Tdp2 known to date, while both strains are the first Tdp2 fish models.Tdp2 knockout mouse has been generated in 2013 (Gómez-Herreros et al., 2013). Embryos and young adults deficient in *tdp2a* and *tdp2b* did not reveal any discernible phenotypic changes (Figure 35), probably because *tdp2a* mutants possess active *tdp2b*, and vice versa. Both orthologues possess the TDP2 active site (Figure 35A) and exhibit relatively high expression levels during embryonic development and in adults across tissues (Figure 36). It is noteworhy, only the zebrafish strain deficient in both orthologues can be compared to the Tdp2 mouse model and patients with TDP2 mutations which will be the subject in future studies. In Tdp2 mouse model, no phenotypic alterations were observed upon TDP2 loss, both at the cellular and *in vivo* levels (Gómez-Herreros et al., 2013). However, pronounced effects were evident following etoposide treatment in adults (Gómez-Herreros et al., 2013). In

contrast, the rare recessive autosomal human syndrome SCAR23, associated with a mutation in TDP2, that abolishes its activity, leads to progressive intellectual disability, cerebellar ataxia, and seizures at an early age (6-years old) (Errichiello et al., 2020; Zagnoli-Vieira et al., 2018). It remains to be seen if zebrafish model will recapitulate mouse and/or human phenotypes.

Using morpholino oligonucleotide mediated gene silencing, successful knockdown of both *tdp2* genes in zebrafish embryos was achieved. Using splice-blocking morpholino oligonucleotides for *tdp2a* and *tdp2b*, *tdp2a* gene eas silenced with a remarkable silencing efficiency of 100% and *tdp2b* with 50% (Figure 38). Notably, *tdp2b* morphants displayed a visible degeneration phenotype (Figure 39), whereas *tdp2a* mutants did not (Figure 37). This discrepancy suggests the Tdp2b probably compensate for complete loss of Tdp2a function. It is noteworthy that the previous study by Esguerra et al. (2007) also targeted *tdp2b* using morpholino oligonucleotides. In their study, zebrafish with silenced Tdp2b displayed pericardial edemas and abnormalities in blood circulation in the trunk and tail regions. They proposed that Tdp2b acts as a modulator of Nodal signalling during left-right axis establishment. However, after *in silico* analysis of the morpholino oligonucleotide sequences used in that study, design flaws were identified based on information from the morpholino oligonucleotide manufacturer, Genetools. Specifically, morpholino oligonucleotide 1 (Esguerra et al., 2007) was designed to bind to exon1 and exon2 which cannot block splicing rather than targeting the exon-intron boundary which could block splicing, while morpholino oligonucleotide 2 (Esguerra et al., 2007) was positioned more than 80 bp downstream of the start codon which is too far for efficient ATG silencing (Moulton, 2007). These design flaws make it highly improbable that these morpholino probes could effectively silence *tdp2b* and indeed, the efficiency of morpholino oligonucleotide silencing was not confirmed. Nevertheless, *tdp2b* morphants were analysed for the heart laterality defects, as described in Esguerra et al. (2007), and no defects were found (Figure 39). In conclusion, it is important to note that silencing Tdp2b in fish does not necessarily lead to a severe phenotype and that the observed developmental delay in *tdp2b*MO-injected embryos should be confirmed with the rescue experiment, in which *tdp2b* mRNA is co-injected with the morpholino oligonucleotide. Ongoing experiments will reveal whether the splice-blocking morpholino oligonucleotide specifically silences *tdp2b* and has no off-target effects.

5.9. Tdp2b is the primary enzyme responsible for removing Top2-DPC residues

To investigate the effects of Tdp2 deficiency on Top2-DPC removal in zebrafish, TDP2 activity assay which measures the ability of Tdp2 to remove the tyrosine moiety from the 5' end of DNA, which mimics TOP2-DNA covalent bond (Ledesma et al., 2009; Zeng et al., 2011) was performed. It is observed that only the combination where *tdp2a* orthologue is silenced in *tdp2b* mutants resulted in an almost complete absence of Tdp2 activity (Figures 42C and D). Notably, *tdp2a* mutants and *tdp2a* morphants exhibited no reduction in Tdp2 activity (Figures 42A and B). Also, while *tdp2b* mutants and *tdp2b* morphants did show a decrease in Tdp2 activity, the activity was still present (Figures 42C and D). These results strongly suggest that Tdp2b functions as the primary enzyme for processing the 5' end of DNA in zebrafish embryos. Moreover, it implies that both Tdp2, Tdp2a and Tdp2b, contribute to the resolution of 5' DNA ends.

To validate the activity data, isolated DNA-protein crosslinks (DPCs) from *tdp2*-silenced embryos were subjected to western blot analysis, to specifically detect Top2-DPCs. Surprisingly, tremendous accumulation of Top2-DPCs was observed in zebrafish embryos with silenced *tdp2b*, as well as in cases where both *tdp2* orthologues were simultaneously silenced (Figure 47D). This is the first evidence demonstrating that TDP2 deficiency results in the accumulation of TOP2-DPCs *in vivo*. Intriguingly, silencing of *tdp2a* did not induce Top2-DPCs (Figure 47D). For comparative analysis, TOP2-DPC levels were measured in RPE1 cells. Notably, *TDP2*-silenced RPE1 cells did not show increase in TOP2-DPCs until exposed to ETO (Figure 47B). This result is consistent with findings from TDP2-silenced K562 human cells, where silenced cells showed no significant TOP2 chromatin trapping, until exposed to ETO. Additionally, K562 TDP2-silenced cells exposed to ETO showed distinct accumulation compared to untreated WT cells, but no differences were observed when compared to WT ETO-treated cells (Lee et al., 2018). It is worth noting that the method used in this study, the TARDIS assay (trapped in agarose DNA immunostaining assay), has low sensitivity, is not designed to specifically detect tightly bound TOP2-DPCs, and relies heavily on antibody epitopes (Cowell et al., 2010), which could be an obstacle if the epitope is located near protein-DNA binding sites and becomes inaccessible when DNA-protein complexes are embedded in agarose gel. Additionally, the detection of TOP2-DPCs in *tdp2b*-silenced morphants and *TDP2*-silenced RPE1 cells was conducted with a single set of measurements. Therefore, it is crucial to validate these results with additional replicates, particularly given the absence of TOP2-DPC induction following ETO treatment in RPE1 cells (Figure 47B),

while at the same time the same ETO concentration caused significant DPC accumulation in HEK-293T cells (Figure 47A), similar to published results (Vaz et al., 2016).

5.10. Silencing of TDP2 results in a significant accumulation of total DPCs both *in vivo* and in cell models

The most surprising result of *tdp2* silencing was the significant increase in total DPC levels. While it is expected that the major DPC-processing enzymes induce total DPCs when impaired in cell models and *in vivo* (Figures 28 and 30) (Anticevic et al., 2023; Vaz et al., 2016), or when exposed to DPC inducers such as formaldehyde (Figures 28 and 32) (Anticevic et al., 2023; Ruggiano et al., 2021), this increase is unexpected, as TDP2 is considered to be involved only in the removal of TOP2-DPCs (Gómez-Herreros et al., 2017; Ledesma et al., 2009; Lee et al., 2018; Schellenberg et al., 2017). Previous studies have not examined the effects of TDP2 deficiency on total DPC levels. These results reveal a novel role for TDP2 in DPC repair *in vivo*. Silencing of *Tdp2b* caused a 1.6-fold increase in DPC levels with crosslinked proteins ranging in size from 10 to 250 kDa (Figures 44 and 45), while combined silencing of *tdp2a* and *tdp2b* resulted in 1.9-fold increase (Figures 44 and 45). The observed increase is comparable to the DPC induction by the model inducer, formaldehyde (2-fold) (Figures 44 and 45). Interestingly, protein crosslinks ranging in size from 10 to 150 kDa (low and medium molecular weight) were most affected, with an almost 2-fold increase when only *tdp2b* was silenced, and a 2.3-fold increase when both orthologues were silenced, again very similar to the effect of formaldehyde induction (Figure 44). Consistent with this, silencing of TDP2 also induced the total DPC levels in RPE1 cells with a 1.3-fold increase and again with large effects on LMW and MMW DPC size with a 1.8-fold increase respectively (Figure 46). Even more surprisingly, the same effect was not observed in *tdp2* mutants. Neither the catalytic *tdp2a* mutant nor the *tdp2b* mutant (premature stop) showed a significant increase of DPC levels (Figure 43). Again, this suggests the presence of compensatory mechanisms when we induce a complete loss of function of Tdp2a or Tdp2b. Our results are the first to investigate the effects of *tdp2* silencing on cellular DPCs beyond TOP2-DPCs, and the first one to show these effects *in vivo*, in an animal model. These results suggest that Tdp2 is not only important for the resolution of TOP2-DPCs, but may also play a role in the resolution of other DPCs. Another possibility is that the observed effects are also indirect, and are not only due to impaired TOP2-DPC repair, but also to other impaired cellular processes in which Tdp2 is involved. In human cells, TDP2 has been implicated in NF-κB signalling (Pype et al., 2000; Rodrigues-Lima et al., 2001), ETS1-mediated

transcriptional regulation (Pei et al., 2003), and apoptotic regulation (Zucchelli et al., 2009), all of which could be affected by TDP2 silencing.

5.11. Impaired Tdp2 activity leads to DSB accumulation

DPCs that are not repaired in a timely manner eventually cause DSBs (Shoulkamy et al., 2012; Sun,et al., 2020). It is known that TDP2 deficiency in combination with exposure to etoposide, a TOP2-DPC inducer, leads to DSB accumulation in cell culture (Kont et al., 2016) and in mice (Gómez-Herreros et al., 2013). *Tdp2* knockout mice showed increased mortality and lymphoid tissue toxicity when treated with etoposide and mouse embryonic fibroblasts (MEFs) from these animals also showed increased DSBs and chromosome breaks after treatment with etoposide (Gómez-Herreros et al., 2013). Therefore, DSB formation was measured in *tdp2*- deficient zebrafish embryos. First, DSB formation was measured in *tdp2* mutants, and the only notable change was the appearance of an upper monoubiquitinated form of γH2AX at the 6 hpf stage in the catalytic *tdp2a* mutant (Figure 48). This monoubiquitinated form of γH2AX typically occurs after treatment with DSB-inducing chemicals such as CPT and ETO. It serves as an initial signal for the repair of non-apoptotic DSBs, which are usually rapidly resolved. This signal is absent in DSBs that stem from apoptotic events triggered by heat shock or induced by Tumour necrosis (TNF)-related apoptosis-inducing ligand (TRAIL) (Luczak & Zhitkovich, 2018). It appears that *tdp2a* plays a crucial role in maintaining the zebrafish genome in early stages of embryonic development, as evidenced by its highest expression at the 6 hpf (Figure 36A). The absence of Tdp2a leads to an accumulation of non-apoptotic DSBs, that are rapidly resolved (Figure 48), possibly by the activity of Tdp2b. Strikingly, the knockdown of *tdp2a* does not cause the same outcome. *Tdp2a* and *tdp2b* silencing in zebrafish embryos did not increase DSB formation at 6 hpf and at 1 dpf (Figure 49). However, at 2 dpf, *tdp2b*-silenced embryos showed a 2-fold increase in DSBs, while simultaneous silencing of both *tdp2a* and *tdp2b* led to a severe 2-fold increase at the 1 dpf and a 2.3-fold increase at 2 dpf (Figure 49). The observed increase in DSB is striking, considering that a similar 2-fold increase was observed in embryos after exposure to FA (Figure 49), a known DSB inducer. In the absence of TDP2, DSBs with 5' overhangs originating from unresolved TOP2-DPCs progress to blunt-ended DNA ends. These blunt ends are rapidly repaired through NHEJ, potentially introducing mutations. Alternatively, if the cells are in the S phase of the cell cycle, a more accurate HR pathway may come into play for repair. (Gómez-Herreros et al., 2013; Kawale & Povirk, 2018). The rapid cell turnover during embryonic development increases the challenge of DSB repair (J. Liu et al., 2012;

Vierstraete et al., 2017). In the absence of TDP2, this leads to a build-up of unrepaired DSBs (Gómez-Herreros et al., 2013, 2017). In summary, TDP2 deficiency in zebrafish embryos results in the accumulation of unrepaired DNA-protein crosslinks, leading to an increase in double-strand breaks which highlights the crucial role of TDP2 in maintaining genomic stability during embryonic development.

The results presented underscore the crucial role of TDP2 in the functioning of cells and organisms and show that TDP2 plays a crucial role during vertebrate development. Silencing of *tdp2b*, the dominant *tdp2* orthologue in zebrafish embryos, leads to a marked accumulation of TOP2-DPCs and total DPCs in both embryos and cells. This accumulation also results in the formation of DSBs in embryos, which collectively contribute to the observed delayed developmental phenotype in *tdp2b*-silenced embryos and reduced cell viability after *TDP2* silencing in RPE1 cells (Figure 27). The lack of a phenotype in *tdp2b* mutants, together with the absence of DPC accumulation and apoptotic DSBs, points to the presence of compensatory mechanisms. Analysis of the expression data suggests that the absence of Tdp2b in zebrafish embryos may be compensated by Tdp2a, based on the increased expression of the *tdp2a* orthologue in *tdp2b* mutants and in *tdp2b* morpholino oligonucleotide silenced embryos (Figure 40A). Notably, silencing of *tdp2b* increases *tdp1* expression which is not observed in *tdp2b* mutants (Figure 40C). This increased expression of *tdp1* upon *tdp2b* silencing in embryos is also observed in RPE1 cells where the *TDP1* expression is increased after *TDP2* silencing (Figure 41B). Interestingly, *SPRTN* expression in RPE1 cells also increases after *TDP2* silencing, and expression is even further increased by treatment with etoposide (ETO) (Figure 41D). Notably *TDP2* expression is also increased in RPE1 cells after *SPRTN* silencing (Figure 41C), supporting recently published data showing that that SPRTN and TDP2 cooperate in resolving TOP3A-DPCs (Saha et al., 2023).

5.12. *Zatt/znf451* knockdown in zebrafish causes severe phenotypes, likely due to the disruption of multiple pathways

The successfully *in vivo* silencing of *zatt/znf451* using the morpholino oligonucleotide approach in zebrafish embryos was also optimized. In the context of TOP2-DPC repair, the N-terminal SIM domain of ZATT is crucial for its SUMO E3 ligase activity (J.-M. Park et al., 2023), which facilitates the SUMOylation of TOP2-DPC and its subsequent removal by TDP2 (Schellenberg et al., 2017). Silencing of *zatt/znf451* in zebrafish leads to a severe phenotype (Figure 51), which is even more pronounced then that observed in *tdp2b*-silenced embryos (Figure 39). It is likely that the described phenotype is the collective result of

impairments in several pathways involving *zatt/znf451*: 1) TOP2-DPC repair, as recent studies shows reduction in cell growth of *ZATT* knockout HEK293T cells after ETO treatment, (J.-M. Park et al., 2023) 2) ZNF451-mediated SUMO2 modification of SATB2 (Special AT-rich sequence-binding protein 2) which contributes to the differentiation potential of embryonic stem cells (Antonio Urrutia et al., 2021), and 3) the negative regulation of TGF-β (Transforming growth factor beta) signalling by ZNF451 who supresses growth-inhibitory responses induced by TGF-β (Feng et al., 2014). Since ZNF451 is involved in different pathways, embryonic cell differentiation, growth hormone regulation and TOP2-DPC repair, it is not surprising that knockout mice develop severe and rapidly progressive breast cancer (Y. Zhang et al., 2023). In summary, the effective silencing of *zatt*/*znf451* in zebrafish embryos results in a severe phenotype, likely stemming from disruptions in various pathways, including inefficient TOP2-DPC repair. However, the specificity of the morpholino oligonucleotide still needs to be confirmed through ongoing rescue experiments and biochemical analysis of DPCs is underway.

5.13. Knockdown of *mre11* in zebrafish causes a lethal phenotype

Zebrafish *mre11* gene was silenced using ATG blocking morpholino oligonucleotide (Figure 52). After morpholino oligonucleotide injecting lethal and progressive phenotype occurred already after two days which was expected due to the integral role of Mre11 as a part of MRN complex which maintains genomic stability by bridging DNA ends and initiating DNA damage signalling through the activation of the ATM kinase (Hartsuiker et al., 2009; Reginato & Cejka, 2020).

MRE11 has DNA nuclease activities that are highly conserved across evolution and plays an essential role in DNA end resection at DSB sites (Stracker et al., 2004). Consistent with our results, deficiency in MRE11 nuclease activity results in severe phenotypes, including early embryonic lethality and pronounced genomic instability in mice (Buis et al., 2008). Considering that we successfully optimized *mre11* silencing *in vivo*, it is now possible to determine the role of MRE11 in TOP2-DPC repair. However, it will be challenging to separate the two roles of this enzyme, i.e. in DPCR vs in DSB repair. Considering the high demand for cellular division during early embryonic development, it is likely that the DSBs that occur in this time window primarily undergo HR repair due to the presence of sister chromatids (J. Liu et al., 2012) and that MRE11 has an essential role in this process. In its absence, HR repair is impaired, and DSBs are instead repaired via the rapid, error-prone NHEJ repair, leading to the accumulation of mutations throughout embryonic progression and

eventual genomic instability, culminating in lethality. Additionally, the elevated requirements for replication and transcription during this developmental phase result in increased torsional stress on DNA and a heightened demand for TOP2 activity (Dovey et al., 2009). Again, in the absence of MRE11-mediated nucleolytic resolution of TOP2-DPCs, DSB accumulation occurs, further contributing to the observed lethal phenotype. Analysis of DPC and DSB repair during the vertebrate development will reveal the contribution of Mre11 to the DNA repair within both pathways, DPCR and HR.

In summary, comprehensive analysis of the role of TDP1 and SPRTN in the resolution of DPCs in zebrafish and human cells was performed. These results reveal the interplay of these repair factors in the resolution of cellular DPCs, H3- and TOP1-DPCs and introduce a novel TDP1-mediated repair pathway for histone-DPCs revealing the epistatic relationship between upstream SPRTN proteolysis and downstream TDP1-mediated processing of 3' DNA ends (Figure 53). Furthermore, it is shown that SPRTN and TDP1 do not act epistatically in the resolution of endogenous TOP1-DPCs and total DPCs, while they do act together in the repair of histone-DPCs in human cells and zebrafish embryos. In contrast, after DPCs are induced by CPT or FA, SPRTN and TDP1 act within the same pathway in the repair of total DPCs, TOP1- and H3-DPCs. This study also demonstrates that Tdp2b is the dominant orthologue responsible for the resolution of Top2-DPC remnants in zebrafish. Impaired Tdp2b activity and the resulting unsuccessful Top2-DPC resolution led to a severe *in vivo* phenotype due to substantial DPC accumulation, eventually leading to the accumulation of DSBs. These findings provide new insights into the complex DPC repair pathways and their implications for human disease and cancer treatments. Further research in this area will improve our understanding of DPC repair factors and their potential therapeutic applications. It is important to point out that mechanistic, *in vitro* studies are essential for understanding DPC repair processes, but that research in animal models is essential for understanding and contextualising the interplay of the different repair factors at the organism level, which is a prerequisite for translating the acquired knowledge into the understanding and treatment of human diseases.

6. CONCLUSION

This study provides a comprehensive investigation of DNA-protein crosslink (DPC) repair mechanisms in zebrafish (*Danio rerio*) and highlights the role of TDP1 and TDP2 proteins in the resolution of TOP1- and TOP2-DPCs. The research emphasizes the important role of zebrafish as a model for the study of TOP1- and TOP2-DPC repair, the consequences of disrupted repair, and repair-related disorders. The remarkable evolutionary conservation of TDP1 across species has been demonstrated, while structural parallels between human and zebrafish TDP1 proteins underline their functional similarities. The study reveals the crucial role of TDP1 in the resolution of TOP1-DPCs *in vivo*, and shows for the first time that TDP1 repairs histone-DPCs in human cells and zebrafish At the same time, the study investigates TDP2 in zebrafish and reveals the presence of two orthologues, *tdp2a* and *tdp2b*, both of which exhibit Tdp2 activity. Notably, *tdp2b* emerges as the dominant orthologue, critical for the resolution of TOP2-DPCs. Its importance for DPC repair is evident, as its knockdown results in severe phenotypic changes due to extensive DPC accumulation and subsequent DSB formation. The main conclusions from this study are:

- We have improved the reproducibility and accuracy of the RADAR assay for DPC isolation by introducing a freeze-drying step and optimising the assay for human cells and zebrafish embryos, thus hopefully improving all future DPC studies.
- We have created three new zebrafish strains using the CRISPR-Cas9 system: Tdp1-deficient strain (premature STOP), Tdp2b deficient strain (premature STOP), and a Tdp2a catalytically impaired strain, which provide an alternative to mouse models and are a valuable tool for studying TDP-related repair mechanisms and diseases, as well as for developing new treatments for related diseases and for improving cancer treatments.
- TDP1 exhibits remarkable conservation across multiple domains of life and shows one-to-one orthology and structural similarity between human and zebrafish TDP1, highlighting their functional equivalence.
- TDP2 shows significant conservation across different domains of life and has two orthologues in zebrafish: *tdp2a* and *tdp2b*, which arose from the teleost-specific whole genome duplication event.
- During zebrafish embryonic development, the DPC repair factors *tdp1*, *tdp2a*, *tdp2b* and *sprtn* are highly expressed at the mRNA level, indicating their importance for DNA repair during early vertebrate development.

- *Tdp1*, *tdp2a* and *tdp2b* are expressed in adult zebrafish tissues including testis, ovary, brain, liver, intestine and kidney, suggesting their important role in maintaining genomic integrity in adult vertebrates across multiple tissues.
- Tdp1 is a key enzyme in the resolution of TOP1-DPCs, both *in vivo* and in cell models.
- Beyond its recognized role in the TOP1-DPC repair, Tdp1 is important for the resolution of H3-DPCs *in vivo* and in cell models, and potentially for other 3' end-trapped DPCs.
- SPRTN protease is responsible for the repair of a broad spectrum of DPCs, including TOP1- and H3-DPCs, both *in vivo* and in cell models.
- TDP1 and SPRTN act in different DPCR pathways for the resolution of endogenous DPCs, including TOP1- DPCs. However, they act epistatically to resolve endogenous H3-DPCs, both *in vivo* and in cell models.
- Following DPC induction by CPT and FA, TDP1 and SPRTN act epistatically in the repair of total, TOP1-, and H3-DPCs, both *in vivo* and in cell models.
- The non-epistatic relationship between TDP1 and SPRTN was also observed at the cellular level, as simultaneous silencing resulted in a significant reduction in cell growth, in contrast to the effects of individual gene silencing.
- When comparing two systems used to study DPCR: human RPE1 cells and zebrafish embryos, we observed similar patterns of DPC dynamics, both after gene disruption and after exposure to CPT and FA.
- The novel role of TDP1 in the repair of cellular DPCs and histone-DPCs should be considered for its implications for the development of cancer therapies.
- In zebrafish, Tdp2b is the dominant orthologue for resolution of TOP2-DPCs. Silencing of *Tdp2b* in zebrafish leads to accumulation of Top2-DPCs, total DPCs, apoptotic DSBs, and phenotypic changes. A similar result is observed in human RPE1 cells, where silencing of *TDP2* leads to accumulation of DPCs and reduced cell growth.
- The absence of phenotypic changes in Tdp2b mutants suggests the existence of compensatory mechanisms, probably involving Tdp2a, TDP1, and/or SPRTN. This is supported by the increased expression of *tdp2a* and *tdp1* following silencing of *tdp2b* in zebrafish and the increased expression of *SPRTN* after *TDP2* silencing in RPE1 cells.

- Tdp2a mutants show a considerable accumulation of non-apoptotic DSBs in the early stages of embryonic development, indicating the importance of Tdp2a in early vertebrate development.
- Silencing of *zatt/znf451* in zebrafish results in a more severe phenotype than *tdp2b* silencing, indicating its important role in DPCR and other cellular processes during the vertebrate development.
- Silencing of *mre11* in zebrafish embryos results in a severe and lethal phenotype, which was expected due to its established role in homologous recombination-mediated repair of DSBs and its role in DPCR.

7. ABBREVIATIONS

3'-PY - 3' phosphotyrosyl moiety

5'-PY - 5' phosphotyrosyl moiety

5azadC - 5-aza-2'-deoxycytidine

AB site - abasic site

ACRC/GCNA - Acidic repeat containing/germ cell nuclear acidic peptidase

APEX1/2 - Apurinic/apyrimidinic end deoxyribonuclease 1/2

ATM - Ataxia telangiectasia mutated

ATR - Ataxia telangiectasia and Rad3 related

BER - Base Excision Repair

BRCA1/2 - BReast CAncer gene 1, 2

CAT - catalytic

CAS9 - CRISPR-associated protein 9

CHK1/2 - Checkpoint kinase 1, 2

CFD - cutting frequency determination

CPD - cyclobutane pyrimidine dimers

CRISPR - Clustered Regularly Interspaced Short Palindromic Repeats

DDR - DNA Damage Response

DD1/2 - DNA damage inducible homolog 1/2

DPC - DNA-protein crosslinks

DPCR - DNA-protein crosslinks repair

DS DNA - double-strand DNA

DSB - double-strand DNA breaks

dsDNA - double-strand DNA

dpf - days post-fertilization

ETO - etoposide

FAM111A/B - Family with sequence similarity 111 member A/B

FA - formaldehyde

H2B - Histone H2B

H3 - Histone H3

H3-DPC - Histone H3 DNA-protein crosslinks

H4 - Histone H4

HEK - Human embryonic kidney cells

HR - Homologous Recombination

HRM - High-Resolution Melting

MEF - mouse embryonic fibroblasts

MMR - Mismatch repair

MRN - MRE11–RAD50–NBS1 complex

MRE11 - Meiotic recombination 11 homolog

NER - Nucleotide Excision Repair

NF-κB - Nuclear factor-kappa beta

NHEJ - Non-homologous end-joining

PARP1 - Poly (ADP-ribose) polymerase 1

PARP1-DPC - Poly (ADP-ribose) polymerase 1 DNA-protein crosslinks

PCNA - Proliferating cell nuclear antigen

PDVF - polyvinylidene difluoride

Polβ - DNA polymerase β

qPCR - quantitative polymerase chain reaction

RADAR - Rapid approach to DNA adduct recovery

ROS - reactive oxygen species

RNS - reactive nitrogen species

RPE-1 - Human Retinal pigment epithelium-1

SCAN1 - Spino Cerebellar Ataxia with axonal neuropathy

SCAR23 - Spinocerebellar ataxia type 23

SDS-PAGE - Sodium dodecyl-sulfate polyacrylamide gel electrophoresis

SDB - single-strand DNA break

SPRTN - SprT-Like N-Terminal Domain

ssDNA - single-strand DNA

TCA - 2-trichloroacetic acid

TEX264 - Testis expressed 264

Thyb - hybridization temperature

TOP1 - Topoisomerase 1

TOP1ccs - Topoisomerase 1 cleavage complexes

TOP1-DPC - Topoisomerase 1 DNA-protein crosslinks

TOP2 - Topoisomerase 2

TOP2ccs - Topoisomerase 2 cleavage complexes

TOP2-DPC - Topoisomerase 2 DNA-protein crosslinks

TDP1 - Tyrosyl DNA phosphodiesterase 1

TDP2 - Tyrosyl DNA phosphodiesterase 2

TEX264 - Testis expressed 264

Thyb - hybridization temperature

TOP1 - Topoisomerase 1

TOP1ccs - Topoisomerase 1 cleavage complexes

TOP1-DPC - Topoisomerase 1 DNA-protein crosslinks

TOP2 - Topoisomerase 2

TOP2ccs - Topoisomerase 2 cleavage complexes

TOP2-DPC - Topoisomerase 2 DNA-protein crosslinks

TRAF - TNF receptor-associated factors

TTRAP - TNF receptor-associated protein

WT - wild type

XPC-HR23B - Xeroderma pigmentosum group C protein complex

ZATT/ZNF451 - Zinc finger protein Associated with TDP2 and TOP2/ Zinc finger protein 451

8. REFERENCES

Abràmoff, M. D., Magalhães, P. J., & Ram, S. J. (2004). Image processing with imageJ. *Biophotonics International*, *11*(7), 36–41. https://doi.org/10.1201/9781420005615.ax4

Abugable, A. A., Morris, J. L. M., Palminha, N. M., Zaksauskaite, R., Ray, S., & El-Khamisy, S. F. (2019). DNA repair and neurological disease: From molecular understanding to the development of diagnostics and model organisms. *DNA Repair*, *81*, 102669. https://doi.org/10.1016/j.dnarep.2019.102669

Albor, A., Kaku, S., & Kulesz-Martin, M. (1998). Wild-type and mutant forms of p53 activate human topoisomerase I: a possible mechanism for gain of function in mutants. *Cancer Research*, *58*(10), 2091–2094.

Aleström, P., D'Angelo, L., Midtlyng, P. J., Schorderet, D. F., Schulte-Merker, S., Sohm, F., & Warner, S. (2020). Zebrafish: Housing and husbandry recommendations. *Laboratory Animals*, *54*(3), 213–224. https://doi.org/10.1177/0023677219869037

Altschul, S. F., Gish, W., Miller, W., Myers, E. W., & Lipman, D. J. (1990). Basic local alignment search tool. *Journal of Molecular Biology*, *215*(3), 403–410. https://doi.org/10.1016/S0022-2836(05)80360-2

Anisimova, M., & Gascuel, O. (2006). Approximate likelihood-ratio test for branches: A fast, accurate, and powerful alternative. *Systematic Biology*, *55*(4), 539–552. https://doi.org/10.1080/10635150600755453

Anticevic, I., Otten, C., Vinkovic, L., Jukic, L., & Popovic, M. (2023). Tyrosyl-DNA phosphodiesterase 1 (TDP1) and SPRTN protease repair histone 3 and topoisomerase 1 DNA-protein crosslinks in vivo. *Open Biology*, *1*, 2023.03.01.530659.

Antonio Urrutia, G., Ramachandran, H., Cauchy, P., Boo, K., Ramamoorthy, S., Boller, S., Dogan, E., Clapes, T., Trompouki, E., Torres-Padilla, M.-E., Palvimo, J. J., Pichler, A., & Grosschedl, R. (2021). ZFP451-mediated SUMOylation of SATB2 drives embryonic stem cell differentiation. *Genes & Development*, *35*(15–16), 1142–1160. https://doi.org/10.1101/gad.345843.120

Antony, S., Marchand, C., Stephen, A. G., Thibaut, L., Agama, K. K., Fisher, R. J., & Pommier, Y. (2007). Novel high-throughput electrochemiluminescent assay for identification of human tyrosyl-DNA phosphodiesterase (Tdp1) inhibitors and characterization of furamidine (NSC 305831) as an inhibitor of Tdp1. *Nucleic Acids Research*, *35*(13), 4474–4484. https://doi.org/10.1093/nar/gkm463

Aparicio, T., Baer, R., Gottesman, M., & Gautier, J. (2016). MRN, CtIP, and BRCA1 mediate

repair of topoisomerase II-DNA adducts. *Journal of Cell Biology*, *212*(4), 399–408. https://doi.org/10.1083/jcb.201504005

Ashworth, A. (2008). A synthetic lethal therapeutic approach: poly(ADP) ribose polymerase inhibitors for the treatment of cancers deficient in DNA double-strand break repair. *Journal of Clinical Oncology : Official Journal of the American Society of Clinical Oncology*, *26*(22), 3785–3790. https://doi.org/10.1200/JCO.2008.16.0812

Barker, S., Murray, D., Zheng, J., Li, L., & Weinfeld, M. (2005). A method for the isolation of covalent DNA-protein crosslinks suitable for proteomics analysis. *Analytical Biochemistry*, *344*(2), 204–215. https://doi.org/10.1016/j.ab.2005.06.039

Benson, D. A., Cavanaugh, M., Clark, K., Karsch-Mizrachi, I., Lipman, D. J., Ostell, J., & Sayers, E. W. (2013). GenBank. *Nucleic Acids Research*, *41*(D1), 36–42. https://doi.org/10.1093/nar/gks1195

Bétermier, M., Bertrand, P., & Lopez, B. S. (2014). Is non-homologous end-joining really an inherently error-prone process? *PLoS Genetics*, *10*(1), e1004086. https://doi.org/10.1371/journal.pgen.1004086

Bhargava, V., Goldstein, C. D., Russell, L., Xu, L., Ahmed, M., Li, W., Casey, A., Servage, K., Kollipara, R., Picciarelli, Z., Kittler, R., Yatsenko, A., Carmell, M., Orth, K., Amatruda, J. F., Yanowitz, J. L., & Buszczak, M. (2020). GCNA Preserves Genome Integrity and Fertility Across Species. *Developmental Cell*, *52*(1), 38-52.e10. https://doi.org/10.1016/j.devcel.2019.11.007

Bharti, A. K., Olson, M. O., Kufe, D. W., & Rubin, E. H. (1996). Identification of a nucleolin binding site in human topoisomerase I. *The Journal of Biological Chemistry*, *271*(4), 1993–1997. https://doi.org/10.1074/jbc.271.4.1993

Borgermann, N., Ackermann, L., Schwertman, P., Hendriks, I. A., Thijssen, K., Liu, J. C., Lans, H., Nielsen, M. L., & Mailand, N. (2019). SUMO ylation promotes protective responses to DNA -protein crosslinks . *The EMBO Journal*, *38*(8), 1–17. https://doi.org/10.15252/embj.2019101496

Bradford, M. M. (1976). A rapid and sensitive method for the quantitation of microgram quantities of protein utilizing the principle of protein-dye binding. *Analytical Biochemistry*, *72*, 248–254. https://doi.org/10.1006/abio.1976.9999

Bradford, Y. M., Toro, S., Ramachandran, S., Ruzicka, L., Howe, D. G., Eagle, A., Kalita, P., Martin, R., Taylor Moxon, S. A., Schaper, K., & Westerfield, M. (2017). Zebrafish Models of Human Disease: Gaining Insight into Human Disease at ZFIN. *ILAR Journal*, *58*(1), 4–16. https://doi.org/10.1093/ilar/ilw040

Buis, J., Wu, Y., Deng, Y., Leddon, J., Westfield, G., Eckersdorff, M., Sekiguchi, J. M., Chang, S., & Ferguson, D. O. (2008). Mre11 nuclease activity has essential roles in DNA repair and genomic stability distinct from ATM activation. *Cell*, *135*(1), 85–96. https://doi.org/10.1016/j.cell.2008.08.015

Cannan, W. J., & Pederson, D. S. (2016). Mechanisms and Consequences of Double-Strand DNA Break Formation in Chromatin. *Journal of Cellular Physiology*, *231*(1), 3–14. https://doi.org/10.1002/jcp.25048

Cappadocia, L., Pichler, A., & Lima, C. D. (2015). Structural basis for catalytic activation by the human ZNF451 SUMO E3 ligase. *Nature Structural & Molecular Biology*, *22*(12), 968–975. https://doi.org/10.1038/nsmb.3116

Casaubon, J. T., Kashyap, S., & Regan, J.-P. (2023). *BRCA1 and BRCA2 Mutations.*

Champoux, J. J. (2001). DNA Topoisomerases: Structure, Function, and Mechanism. *Annual Review of Biochemistry*, *70*(1), 369–413. https://doi.org/10.1146/annurev.biochem.70.1.369

Chang, H. H. Y., Pannunzio, N. R., Adachi, N., & Lieber, M. R. (2017). Non-homologous DNA end joining and alternative pathways to double-strand break repair. *Nature Reviews Molecular Cell Biology*, *18*(8), 495–506. https://doi.org/10.1038/nrm.2017.48

Chesner, L. N., & Campbell, C. (2018). A quantitative PCR-based assay reveals that nucleotide excision repair plays a predominant role in the removal of DNA-protein crosslinks from plasmids transfected into mammalian cells. *DNA Repair*, *62*(October 2017), 18–27. https://doi.org/10.1016/j.dnarep.2018.01.004

Christina Supina Pavic. (2023). *THE ROLE OF ACRC PROTEASE AND NUCLEOTIDE EXCISION REPAIR PATHWAY IN THE REPAIR OF DNA-PROTEIN CROSSLINKS (DPCs)*.chromeextension://efaidnbmnnnibpcajpcglclefindmkaj/https://mobi.unios.hr/wp-content/uploads/doktorat-objava/christine-supina-pavic.pdf

Ciccia, A., & Elledge, S. J. (2010). The DNA damage response: making it safe to play with knives. *Molecular Cell*, *40*(2), 179–204. https://doi.org/10.1016/j.molcel.2010.09.019

Cowell, I. G., Tilby, M. J., & Austin, C. A. (2010). An overview of the visualisation and quantitation of low and high MW DNA adducts using the trapped in agarose DNA immunostaining (TARDIS) assay. *Mutagenesis*, *26*(2), 253–260. https://doi.org/10.1093/mutage/geq094

Cui, X., McAllister, R., Boregowda, R., Sohn, J. A., Cortes Ledesma, F., Caldecott, K. W., Seeger, C., & Hu, J. (2015). Does Tyrosyl DNA Phosphodiesterase-2 Play a Role in Hepatitis B Virus Genome Repair? *PloS One*, *10*(6), e0128401. https://doi.org/10.1371/journal.pone.0128401

Czubaty, A., Girstun, A., Kowalska-Loth, B., Trzcińska, A. M., Purta, E., Winczura, A., Grajkowski, W., & Staroń, K. (2005). Proteomic analysis of complexes formed by human topoisomerase I. *Biochimica et Biophysica Acta (BBA) - Proteins and Proteomics*, *1749*(1), 133–141. https://doi.org/https://doi.org/10.1016/j.bbapap.2005.03.007

d'Amora, M., & Giordani, S. (2018). The Utility of Zebrafish as a Model for Screening Developmental Neurotoxicity. *Frontiers in Neuroscience*, *12*, 976. https://doi.org/10.3389/fnins.2018.00976

Dalvie, E. D., & Osheroff, N. (2021). DNA Recognition/Processing | DNA Topoisomerases: Type II☆. In J. Jez (Ed.), *Encyclopedia of Biological Chemistry III (Third Edition)* (Third Edit, pp. 479–486). Elsevier. https://doi.org/https://doi.org/10.1016/B978-0-12-809633-8.21378-2

Dang, M., Fogley, R., & Zon, L. I. (2016). Identifying Novel Cancer Therapies Using Chemical Genetics and Zebrafish. *Advances in Experimental Medicine and Biology*, *916*, 103–124. https://doi.org/10.1007/978-3-319-30654-4_5

Das, B. B., Dexheimer, T. S., Maddali, K., & Pommier, Y. (2010). Role of tyrosyl-DNA phosphodiesterase (TDP1) in mitochondria. *Proceedings of the National Academy of Sciences of the United States of America*, *107*(46), 19790–19795. https://doi.org/10.1073/pnas.1009814107

Dasari, S., & Tchounwou, P. B. (2014). Cisplatin in cancer therapy: molecular mechanisms of action. *European Journal of Pharmacology*, *740*, 364–378. https://doi.org/10.1016/j.ejphar.2014.07.025

Davies, D. R., Interthal, H., Champoux, J. J., & Hol, W. G. J. (2002). The crystal structure of human tyrosyl-DNA phosphodiesterase, Tdp1. *Structure*, *10*(2), 237–248. https://doi.org/10.1016/S0969-2126(02)00707-4

Dawes, M. L., Soeller, C., & Scholpp, S. (2020). Studying molecular interactions in the intact organism: fluorescence correlation spectroscopy in the living zebrafish embryo. *Histochemistry and Cell Biology*, *154*(5), 507–519. https://doi.org/10.1007/s00418-020-01930-5

Delgado, J. L., Hsieh, C.-M., Chan, N.-L., & Hiasa, H. (2018). Topoisomerases as anticancer targets. *The Biochemical Journal*, *475*(2), 373–398. https://doi.org/10.1042/BCJ20160583

DeMott, M. S., Beyret, E., Wong, D., Bales, B. C., Hwang, J.-T., Greenberg, M. M., & Demple, B. (2002). Covalent trapping of human DNA polymerase beta by the oxidative DNA lesion 2-deoxyribonolactone. *The Journal of Biological Chemistry*, *277*(10), 7637–7640.

https://doi.org/10.1074/jbc.C100577200
Deng, C., Brown, J. A., You, D., & Brown, J. M. (2005). Multiple endonucleases function to repair covalent topoisomerase I complexes in Saccharomyces cerevisiae. *Genetics*, *170*(2), 591–600. https://doi.org/10.1534/genetics.104.028795
Deshpande, R. A., Lee, J.-H., Arora, S., & Paull, T. T. (2016). Nbs1 Converts the Human Mre11/Rad50 Nuclease Complex into an Endo/Exonuclease Machine Specific for Protein-DNA Adducts. *Molecular Cell*, *64*(3), 593–606. https://doi.org/10.1016/j.molcel.2016.10.010
Dirac-Svejstrup, A. B., Walker, J., Faull, P., Encheva, V., Akimov, V., Puglia, M., Perkins, D., Kümper, S., Hunjan, S. S., Blagoev, B., Snijders, A. P., Powell, D. J., & Svejstrup, J. Q. (2020). DDI2 Is a Ubiquitin-Directed Endoprotease Responsible for Cleavage of Transcription Factor NRF1. *Molecular Cell*, *79*(2), 332-341.e7. https://doi.org/10.1016/j.molcel.2020.05.035
DNA Damage. (2005). In *DNA Repair and Mutagenesis* (pp. 9–69). John Wiley & Sons, Ltd. https://doi.org/https://doi.org/10.1128/9781555816704.ch2
Doench, J. G., Fusi, N., Sullender, M., Hegde, M., Vaimberg, E. W., Donovan, K. F., Smith, I., Tothova, Z., Wilen, C., Orchard, R., Virgin, H. W., Listgarten, J., & Root, D. E. (2016). Optimized sgRNA design to maximize activity and minimize off-target effects of CRISPR-Cas9. *Nature Biotechnology*, *34*(2), 184–191. https://doi.org/10.1038/nbt.3437
Dokshin, G. A., Davis, G. M., Sawle, A. D., Eldridge, M. D., Nicholls, P. K., Gourley, T. E., Romer, K. A., Molesworth, L. W., Tatnell, H. R., Ozturk, A. R., de Rooij, D. G., Hannon, G. J., Page, D. C., Mello, C. C., & Carmell, M. A. (2020). GCNA Interacts with Spartan and Topoisomerase II to Regulate Genome Stability. *Developmental Cell*, *52*(1), 53-68.e6. https://doi.org/10.1016/j.devcel.2019.11.006
Dovey, M., Patton, E. E., Bowman, T., North, T., Goessling, W., Zhou, Y., & Zon, L. I. (2009). Topoisomerase II alpha is required for embryonic development and liver regeneration in zebrafish. *Molecular and Cellular Biology*, *29*(13), 3746–3753. https://doi.org/10.1128/MCB.01684-08
Duxin, J. P., Dewar, J. M., Yardimci, H., & Walter, J. C. (2014). Repair of a DNA-protein crosslink by replication-coupled proteolysis. *Cell*, *159*(2), 346–357. https://doi.org/10.1016/j.cell.2014.09.024
Dwight, Z., Palais, R., & Wittwer, C. T. (2011). uMELT: prediction of high-resolution melting curves and dynamic melting profiles of PCR products in a rich web application. *Bioinformatics (Oxford, England)*, *27*(7), 1019–1020. https://doi.org/10.1093/bioinformatics/btr065

El-Khamisy, S. F., Saifi, G. M., Weinfeld, M., Johansson, F., Helleday, T., Lupski, J. R., & Caldecott, K. W. (2005). Defective DNA single-strand break repair in spinocerebellar ataxia with axonal neuropathy-1. *Nature*, *434*(7029), 108–113. https://doi.org/10.1038/nature03314

Errichiello, E., Zagnoli-Vieira, G., Rizzi, R., Garavelli, L., Caldecott, K. W., & Zuffardi, O. (2020). Characterization of a novel loss-of-function variant in TDP2 in two adult patients with spinocerebellar ataxia autosomal recessive 23 (SCAR23). *Journal of Human Genetics*, *65*(12), 1135–1141. https://doi.org/10.1038/s10038-020-0800-4

Esguerra, C. V., Nelles, L., Vermeire, L., Ibrahimi, A., Crawford, A. D., Derua, R., Janssens, E., Waelkens, E., Carmeliet, P., Collen, D., & Huylebroeck, D. (2007). Ttrap is an essential modulator of Smad3-dependent Nodal signaling during zebrafish gastrulation and left-right axis determination. *Development*, *134*(24), 4381–4393. https://doi.org/10.1242/dev.000026

Feng, Y., Wu, H., Xu, Y., Zhang, Z., Liu, T., Lin, X., & Feng, X.-H. (2014). Zinc finger protein 451 is a novel Smad corepressor in transforming growth factor-β signaling. *The Journal of Biological Chemistry*, *289*(4), 2072–2083. https://doi.org/10.1074/jbc.M113.526905

Fengzhi Li, T. J. Q. L. X. L. (2017). Camptothecin analogues and their molecular targets. *Am J Cancer Res*, *7*(12), 2350–2394. https://www.ncbi.nlm.nih.gov/pmc/articles/PMC5752681/

Fielden, J., Ruggiano, A., Popović, M., & Ramadan, K. (2018). DNA protein crosslink proteolysis repair: From yeast to premature ageing and cancer in humans. *DNA Repair*, *71*(August), 198–204. https://doi.org/10.1016/j.dnarep.2018.08.025

Fielden, J., Wiseman, K., Torrecilla, I., Li, S., Hume, S., Chiang, S. C., Ruggiano, A., Narayan Singh, A., Freire, R., Hassanieh, S., Domingo, E., Vendrell, I., Fischer, R., Kessler, B. M., Maughan, T. S., El-Khamisy, S. F., & Ramadan, K. (2020). TEX264 coordinates p97- and SPRTN-mediated resolution of topoisomerase 1-DNA adducts. *Nature Communications*, *11*(1), 1–16. https://doi.org/10.1038/s41467-020-15000-w

Fiorani, P., Amatruda, J. F., Silvestri, A., Butler, R. H., Bjornsti, M. A., & Benedetti, P. (1999). Domain interactions affecting human DNA topoisomerase I catalysis and camptothecin sensitivity. *Molecular Pharmacology*, *56*(6), 1105–1115. https://doi.org/10.1124/mol.56.6.1105

Flett, F. J., Ruksenaite, E., Armstrong, L. A., Bharati, S., Carloni, R., Morris, E. R., Mackay, C. L., Interthal, H., & Richardson, J. M. (2018). Structural basis for DNA 3′-end processing by human tyrosyl-DNA phosphodiesterase 1. *Nature Communications*, *9*(1). https://doi.org/10.1038/s41467-017-02530-z

Fumagalli, M., Rossiello, F., Mondello, C., & d'Adda di Fagagna, F. (2014). Stable cellular

senescence is associated with persistent DDR activation. *PloS One*, *9*(10), e110969. https://doi.org/10.1371/journal.pone.0110969

Gao, R., Das, B. B., Chatterjee, R., Abaan, O. D., Agama, K., Matuo, R., Vinson, C., Meltzer, P. S., & Pommier, Y. (2014). Epigenetic and genetic inactivation of tyrosyl-DNA-phosphodiesterase 1 (TDP1) in human lung cancer cells from the NCI-60 panel. *DNA Repair*, *13*(1), 1–9. https://doi.org/10.1016/j.dnarep.2013.09.001

Gao, R., Huang, S. N., Marchand, C., & Pommier, Y. (2012). Biochemical characterization of human tyrosyl-DNA phosphodiesterase 2 (TDP2/TTRAP): a Mg(2+)/Mn(2+)-dependent phosphodiesterase specific for the repair of topoisomerase cleavage complexes. *The Journal of Biological Chemistry*, *287*(36), 30842–30852. https://doi.org/10.1074/jbc.M112.393983

Geisler, R., Borel, N., Ferg, M., Maier, J. V., & Strähle, U. (2016). Maintenance of Zebrafish Lines at the European Zebrafish Resource Center. *Zebrafish*, *13 Suppl 1*(Suppl 1), S19-23. https://doi.org/10.1089/zeb.2015.1205

Ghetti, S., Burigotto, M., Mattivi, A., Magnani, G., Casini, A., Bianchi, A., Cereseto, A., & Fava, L. L. (2021). CRISPR/Cas9 ribonucleoprotein-mediated knockin generation in hTERT-RPE1 cells. *STAR Protocols*, *2*(2), 100407. https://doi.org/10.1016/j.xpro.2021.100407

Glasauer, S. M. K., & Neuhauss, S. C. F. (2014). Whole-genome duplication in teleost fishes and its evolutionary consequences. *Molecular Genetics and Genomics : MGG*, *289*(6), 1045–1060. https://doi.org/10.1007/s00438-014-0889-2

Glisic, B., Mihaljevic, I., Popovic, M., Zaja, R., Loncar, J., Fent, K., Kovacevic, R., & Smital, T. (2015). Characterization of glutathione-S-transferases in zebrafish (Danio rerio). *Aquatic Toxicology*, *158*, 50–62. https://doi.org/10.1016/j.aquatox.2014.10.013

Glumac, M., Polović, M., Batel, A., Gelemanović, A., Maček, B., Velić, A., & Marinović-Terzić, I. (2023). SPRTN-dependent DPC degradation precedes repair of damaged DNA: a proof of concept revealed by the STAR assay. *Nucleic Acids Research*, *51*(6), e35. https://doi.org/10.1093/nar/gkad022

Gnad, F., & Parsch, J. (2006). Sebida: a database for the functional and evolutionary analysis of genes with sex-biased expression. *Bioinformatics*, *22*(20), 2577–2579. https://doi.org/10.1093/bioinformatics/btl422

Goellner, E. M., Svilar, D., Almeida, K. H., & Sobol, R. W. (2012). Targeting DNA polymerase ß for therapeutic intervention. *Current Molecular Pharmacology*, *5*(1), 68–87.

Gómez-Herreros, F., Romero-Granados, R., Zeng, Z., Álvarez-Quilón, A., Quintero, C., Ju, L., Umans, L., Vermeire, L., Huylebroeck, D., Caldecott, K. W., & Cortés-Ledesma, F. (2013). TDP2-Dependent Non-Homologous End-Joining Protects against Topoisomerase II-

Induced DNA Breaks and Genome Instability in Cells and In Vivo. *PLoS Genetics*, *9*(3). https://doi.org/10.1371/journal.pgen.1003226

Gómez-Herreros, F., Schuurs-Hoeijmakers, J. H. M., McCormack, M., Greally, M. T., Rulten, S., Romero-Granados, R., Counihan, T. J., Chaila, E., Conroy, J., Ennis, S., Delanty, N., Cortés-Ledesma, F., de Brouwer, A. P. M., Cavalleri, G. L., El-Khamisy, S. F., de Vries, B. B. A., & Caldecott, K. W. (2014). TDP2 protects transcription from abortive topoisomerase activity and is required for normal neural function. *Nature Genetics*, *46*(5), 516–521. https://doi.org/10.1038/ng.2929

Gómez-Herreros, F., Zagnoli-Vieira, G., Ntai, I., Martínez-Macías, M. I., Anderson, R. M., Herrero-Ruíz, A., & Caldecott, K. W. (2017). TDP2 suppresses chromosomal translocations induced by DNA topoisomerase II during gene transcription. *Nature Communications*, *8*(1), 233. https://doi.org/10.1038/s41467-017-00307-y

Gottlin, E. B., Rudolph, A. E., Zhao, Y., Matthews, H. R., & Dixon, J. E. (1998). Catalytic mechanism of the phospholipase D superfamily proceeds via a covalent phosphohistidine intermediate. *Proceedings of the National Academy of Sciences of the United States of America*, *95*(16), 9202–9207. https://doi.org/10.1073/pnas.95.16.9202

Gouy, M., Guindon, S., & Gascuel, O. (2010). Sea view version 4: A multiplatform graphical user interface for sequence alignment and phylogenetic tree building. *Molecular Biology and Evolution*, *27*(2), 221–224. https://doi.org/10.1093/molbev/msp259

Graille, M., Cladière, L., Durand, D., Lecointe, F., Gadelle, D., Quevillon-Cheruel, S., Vachette, P., Forterre, P., & van Tilbeurgh, H. (2008). Crystal structure of an intact type II DNA topoisomerase: insights into DNA transfer mechanisms. *Structure (London, England : 1993)*, *16*(3), 360–370. https://doi.org/10.1016/j.str.2007.12.020

Guan, L., & Greenberg, M. M. (2010). Irreversible inhibition of DNA polymerase beta by an oxidized abasic lesion. *Journal of the American Chemical Society*, *132*(14), 5004–5005. https://doi.org/10.1021/ja101372c

Guindon, S., & Gascuel, O. (2003). A Simple, Fast, and Accurate Algorithm to Estimate Large Phylogenies by Maximum Likelihood. *Systematic Biology*, *52*(5), 696–704. https://doi.org/10.1080/10635150390235520

Halder, S., Torrecilla, I., Burkhalter, M. D., Popović, M., Fielden, J., Vaz, B., Oehler, J., Pilger, D., Lessel, D., Wiseman, K., Singh, A. N., Vendrell, I., Fischer, R., Philipp, M., & Ramadan, K. (2019). SPRTN protease and checkpoint kinase 1 cross-activation loop safeguards DNA replication. *Nature Communications*, *10*(1). https://doi.org/10.1038/s41467-019-11095-y

Hall, T. A. (1999). BioEdit: a user friendly biological seque. In *Nucleid Acids Symposium Series* (Issue 41, pp. 95–98).

Hartsuiker, E., Neale, M. J., & Carr, A. M. (2009). Distinct Requirements for the Rad32Mre11 Nuclease and Ctp1CtIP in the Removal of Covalently Bound Topoisomerase I and II from DNA. *Molecular Cell*, *33*(1), 117–123. https://doi.org/10.1016/j.molcel.2008.11.021

Hawkins, A. J., Subler, M. A., Akopiants, K., Wiley, J. L., Taylor, S. M., Rice, A. C., Windle, J. J., Valerie, K., & Povirk, L. F. (2009). In vitro complementation of Tdp1 deficiency indicates a stabilized enzyme-DNA adduct from tyrosyl but not glycolate lesions as a consequence of the SCAN1 mutation. *DNA Repair*, *8*(5), 654–663. https://doi.org/10.1016/j.dnarep.2008.12.012

Heidrun, I., & James, J. (2011). effects of DNA and protein size on substrate cleavage by human tyrosyl-DNA phosphodiesterase 1 (TDP1). *Biochemical Journal*, *436*(3), 559–566. https://doi.org/10.1042/BJ20101841.Effects

Hesselson, D., Anderson, R. M., Beinat, M., & Stainier, D. Y. R. (2009). Distinct populations of quiescent and proliferative pancreatic beta-cells identified by HOTcre mediated labeling. *Proceedings of the National Academy of Sciences of the United States of America*, *106*(35), 14896–14901. https://doi.org/10.1073/pnas.0906348106

Hirano, R., Interthal, H., Huang, C., Nakamura, T., Deguchi, K., Choi, K., Bhattacharjee, M. B., Arimura, K., Umehara, F., Izumo, S., Northrop, J. L., Salih, M. A. M., Inoue, K., Armstrong, D. L., Champoux, J. J., Takashima, H., & Boerkoel, C. F. (2007). Spinocerebellar ataxia with axonal neuropathy: Consequence of a Tdp1 recessive neomorphic mutation? *EMBO Journal*, *26*(22), 4732–4743. https://doi.org/10.1038/sj.emboj.7601885

Hoa, N. N., Shimizu, T., Zhou, Z. W., Wang, Z.-Q., Deshpande, R. A., Paull, T. T., Akter, S., Tsuda, M., Furuta, R., Tsutsui, K., Takeda, S., & Sasanuma, H. (2016). Mre11 Is Essential for the Removal of Lethal Topoisomerase 2 Covalent Cleavage Complexes. *Molecular Cell*, *64*(3), 580–592. https://doi.org/10.1016/j.molcel.2016.10.011

Hoffmann, S., Pentakota, S., Mund, A., Haahr, P., Coscia, F., Gallo, M., Mann, M., Taylor, N. M., & Mailand, N. (2020). FAM111 protease activity undermines cellular fitness and is amplified by gain-of-function mutations in human disease. *EMBO Reports*, *21*(10), e50662. https://doi.org/10.15252/embr.202050662

Hornyak, P., Askwith, T., Walker, S., Komulainen, E., Paradowski, M., Pennicott, L. E., Bartlett, E. J., Brissett, N. C., Raoof, A., Watson, M., Jordan, A. M., Ogilvie, D. J., Ward, S. E., Atack, J. R., Pearl, L. H., Caldecott, K. W., & Oliver, A. W. (2016). Mode of action of

DNA-competitive small molecule inhibitors of tyrosyl DNA phosphodiesterase 2. *The Biochemical Journal*, *473*(13), 1869–1879. https://doi.org/10.1042/BCJ20160180
Hoshijima, K., Jurynec, M. J., & Grunwald, D. J. (2016). Precise Editing of the Zebrafish Genome Made Simple and Efficient. *Developmental Cell*, *36*(6), 654–667. https://doi.org/10.1016/j.devcel.2016.02.015
Hossain, M. A., Lin, Y., & Yan, S. (2018). Single-Strand Break End Resection in Genome Integrity: Mechanism and Regulation by APE2. *International Journal of Molecular Sciences*, *19*(8). https://doi.org/10.3390/ijms19082389
Howe, K., Clark, M. D., Torroja, C. F., Torrance, J., Berthelot, C., Muffato, M., Collins, J. E., Humphray, S., McLaren, K., Matthews, L., McLaren, S., Sealy, I., Caccamo, M., Churcher, C., Scott, C., Barrett, J. C., Koch, R., Rauch, G.-J., White, S., … Stemple, D. L. (2013). The zebrafish reference genome sequence and its relationship to the human genome. *Nature*, *496*(7446), 498–503. https://doi.org/10.1038/nature12111
Hu, Q., Klages-Mundt, N., Wang, R., Lynn, E., Kuma Saha, L., Zhang, H., Srivastava, M., Shen, X., Tian, Y., Kim, H., Ye, Y., Paull, T., Takeda, S., Chen, J., & Li, L. (2020). The ARK Assay Is a Sensitive and Versatile Method for the Global Detection of DNA-Protein Crosslinks. *Cell Reports*, *30*(4), 1235-1245.e4. https://doi.org/10.1016/j.celrep.2019.12.067
Huang, S.-Y. N., & Pommier, Y. (2019). Mammalian Tyrosyl-DNA Phosphodiesterases in the Context of Mitochondrial DNA Repair. *International Journal of Molecular Sciences*, *20*(12). https://doi.org/10.3390/ijms20123015
Hwang, W. Y., Fu, Y., Reyon, D., Maeder, M. L., Tsai, S. Q., Sander, J. D., Peterson, R. T., Yeh, J.-R. J., & Joung, J. K. (2013). Efficient genome editing in zebrafish using a CRISPR-Cas system. *Nature Biotechnology*, *31*(3), 227–229. https://doi.org/10.1038/nbt.2501
Ide, H., Nakano, T., Salem, A. M. H., & Shoulkamy, M. I. (2018). DNA-protein cross-links: Formidable challenges to maintaining genome integrity. *DNA Repair*, *71*, 190–197. https://doi.org/10.1016/j.dnarep.2018.08.024
Interthal, H., & Champoux, J. J. (2011). Effects of DNA and protein size on substrate cleavage by human tyrosyl-DNA phosphodiesterase 1. *The Biochemical Journal*, *436*(3), 559–566. https://doi.org/10.1042/BJ20101841
Interthal, H., Chen, H. J., & Champoux, J. J. (2005). Human Tdp1 cleaves a broad spectrum of substrates, including phosphoamide linkages. *Journal of Biological Chemistry*, *280*(43), 36518–36528. https://doi.org/10.1074/jbc.M508898200
Interthal, H., Chen, H. J., Kehl-Fie, T. E., Zotzmann, J., Leppard, J. B., & Champoux, J. J. (2005). SCAN1 mutant Tdp1 accumulates the enzyme–DNA intermediate and causes

camptothecin hypersensitivity. *The EMBO Journal*, *24*(12), 2224–2233. https://doi.org/https://doi.org/10.1038/sj.emboj.7600694

Jackson, S. P., & Bartek, J. (2009). The DNA-damage response in human biology and disease. *Nature*, *461*(7267), 1071–1078. https://doi.org/10.1038/nature08467

Jatllon, O., Aury, J. M., Brunet, F., Petit, J. L., Stange-Thomann, N., Maucell, E., Bouneau, L., Fischer, C., Ozouf-Costaz, C., Bernot, A., Nicaud, S., Jaffe, D., Fisher, S., Lutfalla, G., Dossat, C., Segurens, B., Dasilva, C., Salanoubat, M., Levy, M., … Roest Crollius, H. (2004). Genome duplication in the teleost fish Tetraodon nigroviridis reveals the early vertebrate proto-karyotype. *Nature*, *431*(7011), 946–957. https://doi.org/10.1038/nature03025

Jeppesen, D. K., Bohr, V. A., & Stevnsner, T. (2011). DNA repair deficiency in neurodegeneration. *Progress in Neurobiology*, *94*(2), 166–200. https://doi.org/10.1016/j.pneurobio.2011.04.013

Jiang, M., Xiao, Y., E, W., Ma, L., Wang, J., Chen, H., Gao, C., Liao, Y., Guo, Q., Peng, J., Han, X., & Guo, G. (2021). Characterization of the Zebrafish Cell Landscape at Single-Cell Resolution. *Frontiers in Cell and Developmental Biology*, *9*, 743421. https://doi.org/10.3389/fcell.2021.743421

Kankanala, J., Marchand, C., Abdelmalak, M., Aihara, H., Pommier, Y., & Wang, Z. (2016). Isoquinoline-1,3-diones as Selective Inhibitors of Tyrosyl DNA Phosphodiesterase II (TDP2). *Journal of Medicinal Chemistry*, *59*(6), 2734–2746. https://doi.org/10.1021/acs.jmedchem.5b01973

Karlsson, M., Zhang, C., Méar, L., Zhong, W., Digre, A., Katona, B., Sjöstedt, E., Butler, L., Odeberg, J., Dusart, P., Edfors, F., Oksvold, P., von Feilitzen, K., Zwahlen, M., Arif, M., Altay, O., Li, X., Ozcan, M., Mardinoglu, A., … Lindskog, C. (2023). A single–cell type transcriptomics map of human tissues. *Science Advances*, *7*(31), eabh2169. https://doi.org/10.1126/sciadv.abh2169

Kastan, M. B., & Bartek, J. (2004). Cell-cycle checkpoints and cancer. *Nature*, *432*(7015), 316–323. https://doi.org/10.1038/nature03097

Katerji, M., & Duerksen-Hughes, P. J. (2021). DNA damage in cancer development: special implications in viral oncogenesis. *American Journal of Cancer Research*, *11*(8), 3956–3979.

Katoh, K., Misawa, K., Kuma, K. I., & Miyata, T. (2002). MAFFT: A novel method for rapid multiple sequence alignment based on fast Fourier transform. *Nucleic Acids Research*, *30*(14), 3059–3066. https://doi.org/10.1093/nar/gkf436

Katyal, S., El-Khamisy, S. F., Russell, H. R., Li, Y., Ju, L., Caldecott, K. W., & McKinnon, P. J. (2007). TDP1 facilitates chromosomal single-strand break repair in neurons and is

neuroprotective in vivo. *EMBO Journal*, *26*(22), 4720–4731. https://doi.org/10.1038/sj.emboj.7601869

Kawale, A. S., & Povirk, L. F. (2018). Tyrosyl-DNA phosphodiesterases: Rescuing the genome from the risks of relaxation. *Nucleic Acids Research*, *46*(2), 520–537. https://doi.org/10.1093/nar/gkx1219

Keeney, S., Giroux, C. N., & Kleckner, N. (1997). Meiosis-Specific DNA Double-Strand Breaks Are Catalyzed by Spo11, a Member of a Widely Conserved Protein Family. *Cell*, *88*(3), 375–384. https://doi.org/https://doi.org/10.1016/S0092-8674(00)81876-0

Keller, P. J. (2013). In vivo imaging of zebrafish embryogenesis. *Methods*, *62*(3), 268–278. https://doi.org/10.1016/j.ymeth.2013.03.015

Kelley, L. A., Mezulis, S., Yates, C. M., Wass, M. N., & Sternberg, M. J. (2015). The Phyre2 web portal for protein modeling, prediction and analysis. *Nature Protocols*, *10*(6), 845–858. https://doi.org/10.1038/nprot.2015-053

Kent, M. L., Harper, C., & Wolf, J. C. (2012). Documented and potential research impacts of subclinical diseases in zebrafish. *ILAR Journal*, *53*(2), 126–134. https://doi.org/10.1093/ilar.53.2.126

Khan, F. R., & Alhewairini, S. S. (2018). Zebrafish (Danio rerio) as a Model Organism. In L. Streba, D. I. Gheonea, & M. Schenker (Eds.), *Current Trends in Cancer Management*. IntechOpen. https://doi.org/10.5772/intechopen.81517

Kiianitsa, K., & Maizels, N. (2013). A rapid and sensitive assay for DNA-protein covalent complexes in living cells. *Nucleic Acids Research*, *41*(9), 1–7. https://doi.org/10.1093/nar/gkt171

Kiianitsa, K., & Maizels, N. (2014). Ultrasensitive isolation, identification and quantification of DNA-protein adducts by ELISA-based RADAR assay. *Nucleic Acids Research*, *42*(13), 1–12. https://doi.org/10.1093/nar/gku490

Kiianitsa, K., & Maizels, N. (2020). The “adductome”: A limited repertoire of adducted proteins in human cells. *DNA Repair*, *89*(December 2019), 102825. https://doi.org/10.1016/j.dnarep.2020.102825

Klages-Mundt, N. L., & Li, L. (2017). Formation and repair of DNA-protein crosslink damage. *Science China. Life Sciences*, *60*(10), 1065–1076. https://doi.org/10.1007/s11427-017-9183-4

Kojima, Y., Machida, Y., Palani, S., Caulfield, T. R., Radisky, E. S., Kaufmann, S. H., & Machida, Y. J. (2020). FAM111A protects replication forks from protein obstacles via its trypsin-like domain. *Nature Communications*, *11*(1). https://doi.org/10.1038/s41467-020-

15170-7
Königer, C., Wingert, I., Marsmann, M., Rösler, C., Beck, J., & Nassal, M. (2014). Involvement of the host DNA-repair enzyme TDP2 in formation of the covalently closed circular DNA persistence reservoir of hepatitis B viruses. *Proceedings of the National Academy of Sciences of the United States of America*, *111*(40), E4244-53. https://doi.org/10.1073/pnas.1409986111
Kont, Y. S., Dutta, A., Mallisetty, A., Mathew, J., Minas, T., Kraus, C., Dhopeshwarkar, P., Kallakury, B., Mitra, S., Üren, A., & Adhikari, S. (2016). Depletion of tyrosyl DNA phosphodiesterase 2 activity enhances etoposide-mediated double-strand break formation and cell killing. *DNA Repair*, *43*, 38–47. https://doi.org/10.1016/j.dnarep.2016.04.009
Kroeger, K. M., Hashimoto, M., Kow, Y. W., & Greenberg, M. M. (2003). Cross-linking of 2-deoxyribonolactone and its beta-elimination product by base excision repair enzymes. *Biochemistry*, *42*(8), 2449–2455. https://doi.org/10.1021/bi027168c
Krokan, H. E., & Bjørås, M. (2013). Base excision repair. *Cold Spring Harbor Perspectives in Biology*, *5*(4), a012583. https://doi.org/10.1101/cshperspect.a012583
Kühbacher, U., & Duxin, J. P. (2020). How to fix DNA-protein crosslinks. *DNA Repair*, *94*, 102924. https://doi.org/10.1016/j.dnarep.2020.102924
Laev, S. S., Salakhutdinov, N. F., & Lavrik, O. I. (2016). Tyrosyl-DNA phosphodiesterase inhibitors: Progress and potential. *Bioorganic and Medicinal Chemistry*, *24*(21), 5017–5027. https://doi.org/10.1016/j.bmc.2016.09.045
Lai, Y., Yu, R., Hartwell, H. J., Moeller, B. C., Bodnar, W. M., & Swenberg, J. A. (2016). Measurement of Endogenous versus Exogenous Formaldehyde-Induced DNA-Protein Crosslinks in Animal Tissues by Stable Isotope Labeling and Ultrasensitive Mass Spectrometry. *Cancer Research*, *76*(9), 2652–2661. https://doi.org/10.1158/0008-5472.CAN-15-2527
Langereis, M. A., Feng, Q., Nelissen, F. H. T., Virgen-Slane, R., van der Heden van Noort, G. J., Maciejewski, S., Filippov, D. V, Semler, B. L., van Delft, F. L., & van Kuppeveld, F. J. M. (2014). Modification of picornavirus genomic RNA using “click” chemistry shows that unlinking of the VPg peptide is dispensable for translation and replication of the incoming viral RNA. *Nucleic Acids Research*, *42*(4), 2473–2482. https://doi.org/10.1093/nar/gkt1162
Larsen, N. B., Gao, A. O., Sparks, J. L., Gallina, I., Wu, R. A., Mann, M., Räschle, M., Walter, J. C., & Duxin, J. P. (2019). Replication-Coupled DNA-Protein Crosslink Repair by SPRTN and the Proteasome in Xenopus Egg Extracts. *Molecular Cell*, *73*(3), 574-588.e7. https://doi.org/10.1016/j.molcel.2018.11.024

Laue, K., Rajshekar, S., Courtney, A. J., Lewis, Z. A., & Goll, M. G. (2019). The maternal to zygotic transition regulates genome-wide heterochromatin establishment in the zebrafish embryo. *Nature Communications*, *10*(1). https://doi.org/10.1038/s41467-019-09582-3

Lay, M. J., & Wittwer, C. T. (1997). Real-time fluorescence genotyping of factor V Leiden during rapid-cycle PCR. *Clinical Chemistry*, *43*(12), 2262–2267.

Ledesma, F. C., El Khamisy, S. F., Zuma, M. C., Osborn, K., & Caldecott, K. W. (2009). A human 5′-tyrosyl DNA phosphodiesterase that repairs topoisomerase-mediated DNA damage. *Nature*, *461*(7264), 674–678. https://doi.org/10.1038/nature08444

Lee, K. C., Swan, R. L., Sondka, Z., Padget, K., Cowell, I. G., & Austin, C. A. (2018). Effect of TDP2 on the Level of TOP2-DNA Complexes and SUMOylated TOP2-DNA Complexes. *International Journal of Molecular Sciences*, *19*(7). https://doi.org/10.3390/ijms19072056

Lessel, D., Vaz, B., Halder, S., Lockhart, P. J., Marinovic-Terzic, I., Lopez-Mosqueda, J., Philipp, M., Sim, J. C. H., Smith, K. R., Oehler, J., Cabrera, E., Freire, R., Pope, K., Nahid, A., Norris, F., Leventer, R. J., Delatycki, M. B., Barbi, G., Von Ameln, S., … Kubisch, C. (2014). Mutations in SPRTN cause early onset hepatocellular carcinoma, genomic instability and progeroid features. *Nature Genetics*, *46*(11), 1239–1244. https://doi.org/10.1038/ng.3103

Li, C., Fan, S., Owonikoko, T. K., Khuri, F. R., Sun, S.-Y., & Li, R. (2011). Oncogenic role of EAPII in lung cancer development and its activation of the MAPK-ERK pathway. *Oncogene*, *30*(35), 3802–3812. https://doi.org/10.1038/onc.2011.94

Li, F., Raczynska, J. E., Chen, Z., & Yu, H. (2019). Structural Insight into DNA-Dependent Activation of Human Metalloprotease Spartan. *Cell Reports*, *26*(12), 3336-3346.e4. https://doi.org/10.1016/j.celrep.2019.02.082

Li, G.-M. (2008). Mechanisms and functions of DNA mismatch repair. *Cell Research*, *18*(1), 85–98. https://doi.org/10.1038/cr.2007.115

Li, X., & Heyer, W.-D. (2008). Homologous recombination in DNA repair and DNA damage tolerance. *Cell Research*, *18*(1), 99–113. https://doi.org/10.1038/cr.2008.1

Lin, C. P., Ban, Y., Lyu, Y. L., Desai, S. D., & Liu, L. F. (2008). A ubiquitin-proteasome pathway for the repair of topoisomerase I-DNA covalent complexes. *Journal of Biological Chemistry*, *283*(30), 21074–21083. https://doi.org/10.1074/jbc.M803493200

Lin, C. Y., Chiang, C. Y., & Tsai, H. J. (2016). Zebrafish and Medaka: New model organisms for modern biomedical research. *Journal of Biomedical Science*, *23*(1), 1–11. https://doi.org/10.1186/s12929-016-0236-5

Lin, X., Kapoor, A., Gu, Y., Chow, M. J., Peng, J., Zhao, K., & Tang, D. (2020). Contributions of DNA Damage to Alzheimer's Disease. *International Journal of Molecular*

Sciences, *21*(5). https://doi.org/10.3390/ijms21051666
Lindahl, T. (1993). Instability and decay of the primary structure of DNA. *Nature*, *362*(6422), 709–715. https://doi.org/10.1038/362709a0
Lindahl, T., Modrich, P., & Sancar, A. (2016). The 2015 Nobel Prize in Chemistry The Discovery of Essential Mechanisms that Repair DNA Damage. *Journal of the Association of Genetic Technologists*, *42*(1), 37–41.
Liu, C., Zhou, S., Begum, S., Sidransky, D., Westra, W. H., Brock, M., & Califano, J. A. (2007). Increased expression and activity of repair genes TDP1 and XPF in non-small cell lung cancer. *Lung Cancer (Amsterdam, Netherlands)*, *55*(3), 303–311. https://doi.org/10.1016/j.lungcan.2006.10.019
Liu, J., Gong, L., Chang, C., Liu, C., Peng, J., & Chen, J. (2012). Development of Novel Visual-Plus Quantitative Analysis Systems for Studying DNA Double-Strand Break Repairs in Zebrafish. *Journal of Genetics and Genomics*, *39*(9), 489–502. https://doi.org/https://doi.org/10.1016/j.jgg.2012.07.009
Liu, P., Luk, K., Shin, M., Idrizi, F., Kwok, S., Roscoe, B., Mintzer, E., Suresh, S., Morrison, K., Frazão, J. B., Bolukbasi, M. F., Ponnienselvan, K., Luban, J., Zhu, L. J., Lawson, N. D., & Wolfe, S. A. (2019). Enhanced Cas12a editing in mammalian cells and zebrafish. *Nucleic Acids Research*, *47*(8), 4169–4180. https://doi.org/10.1093/nar/gkz184
Liu, Y. (2023). Zebrafish as a Model Organism for Studying Pathologic Mechanisms of Neurodegenerative Diseases and other Neural Disorders. *Cellular and Molecular Neurobiology*, *43*(6), 2603–2620. https://doi.org/10.1007/s10571-023-01340-w
Lončar, J., Popović, M., Krznar, P., Zaja, R., & Smital, T. (2016). The first characterization of multidrug and toxin extrusion (MATE/SLC47) proteins in zebrafish (Danio rerio). *Scientific Reports*, *6*(June), 1–15. https://doi.org/10.1038/srep28937
Lončar, J., Popović, M., Zaja, R., & Smital, T. (2010). Gene expression analysis of the ABC efflux transporters in rainbow trout (Oncorhynchus mykiss). *Comparative Biochemistry and Physiology - C Toxicology and Pharmacology*, *151*(2), 209–215. https://doi.org/10.1016/j.cbpc.2009.10.009
Lopez-Mosqueda, J., Maddi, K., Prgomet, S., Kalayil, S., Marinovic-Terzic, I., Terzic, J., & Dikic, I. (2016). SPRTN is a mammalian DNA-binding metalloprotease that resolves DNA-protein crosslinks. *ELife*, *5*(NOVEMBER2016), 1–19. https://doi.org/10.7554/eLife.21491
Lord, C. J., & Ashworth, A. (2017). PARP inhibitors: Synthetic lethality in the clinic. *Science (New York, N.Y.)*, *355*(6330), 1152–1158. https://doi.org/10.1126/science.aam7344
Louis, A., Muffato, M., & Crollius, H. R. (2013). Genomicus: Five genome browsers for

comparative genomics in eukaryota. *Nucleic Acids Research*, *41*(D1), 700–705. https://doi.org/10.1093/nar/gks1156

Lu, J., Peatman, E., Tang, H., Lewis, J., & Liu, Z. (2012). Profiling of gene duplication patterns of sequenced teleost genomes: evidence for rapid lineage-specific genome expansion mediated by recent tandem duplications. *BMC Genomics*, *13*(1), 246. https://doi.org/10.1186/1471-2164-13-246

Lu, T., Pan, Y., Kao, S.-Y., Li, C., Kohane, I., Chan, J., & Yankner, B. A. (2004). Gene regulation and DNA damage in the ageing human brain. *Nature*, *429*(6994), 883–891. https://doi.org/10.1038/nature02661

Luczak, M. W., & Zhitkovich, A. (2018). Monoubiquitinated γ-H2AX: Abundant product and specific biomarker for non-apoptotic DNA double-strand breaks. *Toxicology and Applied Pharmacology*, *355*, 238–246. https://doi.org/10.1016/j.taap.2018.07.007

Martin, C. S., Butler, L., & Bronstein, I. (1995). Quantitation of PCR products with chemiluminescence. *BioTechniques*, *18*(5), 908–913.

Martino, E., Della Volpe, S., Terribile, E., Benetti, E., Sakaj, M., Centamore, A., Sala, A., & Collina, S. (2017). The long story of camptothecin: From traditional medicine to drugs. *Bioorganic and Medicinal Chemistry Letters*, *27*(4), 701–707. https://doi.org/10.1016/j.bmcl.2016.12.085

Maskey, R. S., Flatten, K. S., Sieben, C. J., Peterson, K. L., Baker, D. J., Nam, H. J., Kim, M. S., Smyrk, T. C., Kojima, Y., Machida, Y., Santiago, A., Van Deursen, J. M., Kaufmann, S. H., & Machida, Y. J. (2017). Spartan deficiency causes accumulation of Topoisomerase 1 cleavage complexes and tumorigenesis. *Nucleic Acids Research*, *45*(8), 4564–4576. https://doi.org/10.1093/nar/gkx107

Maskey, R. S., Kim, M. S., Baker, D. J., Childs, B., Malureanu, L. A., Jeganathan, K. B., Machida, Y., Van Deursen, J. M., & Machida, Y. J. (2014). Spartan deficiency causes genomic instability and progeroid phenotypes. *Nature Communications*, *5*, 1–12. https://doi.org/10.1038/ncomms6744

Mathavan, S., Lee, S. G. P., Mak, A., Miller, L. D., Murthy, K. R. K., Govindarajan, K. R., Tong, Y., Wu, Y. L., Lam, S. H., Yang, H., Ruan, Y., Korzh, V., Gong, Z., Liu, E. T., & Lufkin, T. (2005). Transcriptome analysis of zebrafish embryogenesis using microarrays. *PLoS Genetics*, *1*(2), 0260–0276. https://doi.org/10.1371/journal.pgen.0010029

McKinnon, P. J. (2013). Maintaining genome stability in the nervous system. *Nature Neuroscience*, *16*(11), 1523–1529. https://doi.org/10.1038/nn.3537

Meroni, A., Grosser, J., Agashe, S., Ramakrishnan, N., Jackson, J., Verma, P., Baranello, L.,

& Vindigni, A. (2022). NEDDylated Cullin 3 mediates the adaptive response to topoisomerase 1 inhibitors. *Science Advances*, *8*(49), 1–20. https://doi.org/10.1126/sciadv.abq0648

Meyer, A., & Van de Peer, Y. (2005). From 2R to 3R: evidence for a fish-specific genome duplication (FSGD). *BioEssays : News and Reviews in Molecular, Cellular and Developmental Biology*, *27*(9), 937–945. https://doi.org/10.1002/bies.20293

Modzelewski, A. J., Chen, S., Willis, B. J., Lloyd, K. C. K., Wood, J. A., & He, L. (2018). Efficient mouse genome engineering by CRISPR-EZ technology. *Nature Protocols*, *13*(6), 1253–1274. https://doi.org/10.1038/nprot.2018.012

Moreno-Mateos, M. A., Vejnar, C. E., Beaudoin, J. D., Fernandez, J. P., Mis, E. K., Khokha, M. K., & Giraldez, A. J. (2015). CRISPRscan: Designing highly efficient sgRNAs for CRISPR-Cas9 targeting in vivo. *Nature Methods*, *12*(10), 982–988. https://doi.org/10.1038/nmeth.3543

Mórocz, M., Zsigmond, E., Tóth, R., Zs Enyedi, M., Pintér, L., & Haracska, L. (2017). DNA-dependent protease activity of human Spartan facilitates replication of DNA-protein crosslink-containing DNA. *Nucleic Acids Research*, *45*(6), 3172–3188. https://doi.org/10.1093/nar/gkw1315

Moulton, J. D. (2007). Using morpholinos to control gene expression. *Current Protocols in Nucleic Acid Chemistry*, *Chapter 4*(1), Unit 4.30. https://doi.org/10.1002/0471142700.nc0430s27

Murai, J., Huang, S. N., Das, B. B., Renaud, A., Zhang, Y., Doroshow, J. H., Ji, J., Takeda, S., & Pommier, Y. (2012). Trapping of PARP1 and PARP2 by Clinical PARP Inhibitors. *Cancer Research*, *72*(21), 5588–5599. https://doi.org/10.1158/0008-5472.CAN-12-2753

Nakamura, J., & Nakamura, M. (2020). DNA-protein crosslink formation by endogenous aldehydes and AP sites. *DNA Repair*, *88*, 102806. https://doi.org/https://doi.org/10.1016/j.dnarep.2020.102806

Narumanchi, S., Wang, H., Perttunen, S., Tikkanen, I., Lakkisto, P., & Paavola, J. (2021). Zebrafish Heart Failure Models. *Frontiers in Cell and Developmental Biology*, *9*, 662583. https://doi.org/10.3389/fcell.2021.662583

Nasevicius, A., & Ekker, S. C. (2000). Effective targeted gene “knockdown” in zebrafish [In Process Citation]. *Nat Genet*, *26*(2), 216–220. https://doi.org/https://doi.org/10.1038/79951

Nastasi, C., Mannarino, L., & D’Incalci, M. (2020). DNA Damage Response and Immune Defense. *International Journal of Molecular Sciences*, *21*(20). https://doi.org/10.3390/ijms21207504

Nikfarjam, S., & Singh, K. K. (2023). DNA damage response signaling: A common link between cancer and cardiovascular diseases. *Cancer Medicine*, *12*(4), 4380–4404. https://doi.org/10.1002/cam4.5274

Nishimasu, H., Ran, F. A., Hsu, P. D., Konermann, S., Shehata, S. I., Dohmae, N., Ishitani, R., Zhang, F., & Nureki, O. (2014). Crystal structure of Cas9 in complex with guide RNA and target DNA. *Cell*, *156*(5), 935–949. https://doi.org/10.1016/j.cell.2014.02.001

Nitiss, J. L. (2009). Targeting DNA topoisomerase II in cancer chemotherapy. *Nature Reviews Cancer*, *9*(5), 338–350. https://doi.org/10.1038/nrc2607

Noda, T., Takahashi, A., Kondo, N., Mori, E., Okamoto, N., Nakagawa, Y., Ohnishi, K., Zdzienicka, M. Z., Thompson, L. H., Helleday, T., Asada, H., & Ohnishi, T. (2011). Repair pathways independent of the Fanconi anemia nuclear core complex play a predominant role in mitigating formaldehyde-induced DNA damage. *Biochemical and Biophysical Research Communications*, *404*(1), 206–210. https://doi.org/https://doi.org/10.1016/j.bbrc.2010.11.094

Nowicka, U., Zhang, D., Walker, O., Krutauz, D., Castañeda, C. A., Chaturvedi, A., Chen, T. Y., Reis, N., Glickman, M. H., & Fushman, D. (2015). DNA-damage-inducible 1 protein (Ddi1) contains an uncharacteristic ubiquitin-like domain that binds ubiquitin. *Structure (London, England : 1993)*, *23*(3), 542–557. https://doi.org/10.1016/j.str.2015.01.010

Otten, C., Supina-Pavic, C., Kutnjak, M., Anticevic, I., Medved, V., & Popovic, M. (2023). ACRC/GCNA is an essential protease for the repair of DNA-protein crosslinks during vertebrate development. *BioRxiv*, 2023.03.07.531502. https://doi.org/10.1101/2023.03.07.531502

Paiano, J., Wu, W., Yamada, S., Sciascia, N., Callen, E., Paola Cotrim, A., Deshpande, R. A., Maman, Y., Day, A., Paull, T. T., & Nussenzweig, A. (2020). ATM and PRDM9 regulate SPO11-bound recombination intermediates during meiosis. *Nature Communications*, *11*(1), 857. https://doi.org/10.1038/s41467-020-14654-w

Park, J.-M., Zhang, H., Nie, L., Wang, C., Huang, M., Feng, X., Tang, M., Chen, Z., Xiong, Y., Lee, N., Li, S., Yin, L., Hart, T., & Chen, J. (2023). Genome-Wide CRISPR Screens Reveal ZATT as a Synthetic Lethal Target of TOP2-Poison Etoposide That Can Act in a TDP2-Independent Pathway. *International Journal of Molecular Sciences*, *24*(7). https://doi.org/10.3390/ijms24076545

Park, J., Throop, A. L., & LaBaer, J. (2015). Site-specific recombinational cloning using gateway and in-fusion cloning schemes. *Current Protocols in Molecular Biology*, *110*, 3.20.1-3.20.23. https://doi.org/10.1002/0471142727.mb0320s110

Paull, T. T., Rogakou, E. P., Yamazaki, V., Kirchgessner, C. U., Gellert, M., & Bonner, W.

M. (2000). A critical role for histone H2AX in recruitment of repair factors to nuclear foci after DNA damage. *Current Biology*, *10*(15), 886–895. https://doi.org/10.1016/S0960-9822(00)00610-2

Pearl, L. H., Schierz, A. C., Ward, S. E., Al-Lazikani, B., & Pearl, F. M. G. (2015). Therapeutic opportunities within the DNA damage response. *Nature Reviews. Cancer*, *15*(3), 166–180. https://doi.org/10.1038/nrc3891

Pećina-Šlaus, N., Kafka, A., Salamon, I., & Bukovac, A. (2020). Mismatch Repair Pathway, Genome Stability and Cancer. *Frontiers in Molecular Biosciences*, *7*, 122. https://doi.org/10.3389/fmolb.2020.00122

Pei, H., Yordy, J. S., Leng, Q., Zhao, Q., Watson, D. K., & Li, R. (2003). EAPII interacts with ETS1 and modulates its transcriptional function. *Oncogene*, *22*(18), 2699–2709. https://doi.org/10.1038/sj.onc.1206374

Penn, O., Privman, E., Ashkenazy, H., Landan, G., Graur, D., & Pupko, T. (2010). GUIDANCE: A web server for assessing alignment confidence scores. *Nucleic Acids Research*, *38*(SUPPL. 2), 23–28. https://doi.org/10.1093/nar/gkq443

Permana, P. A., & Snapka, R. M. (1994). Aldehyde-induced protein—DNA crosslinks disrupt specific stages of SV4I) DNA replication. *Carcinogenesis*, *15*(5), 1031–1036. https://doi.org/10.1093/carcin/15.5.1031

Pommier, Y. (2006). Topoisomerase I inhibitors: camptothecins and beyond. *Nature Reviews Cancer*, *6*(10), 789–802. https://doi.org/10.1038/nrc1977

Pommier, Y., Barcelo, J. M., Rao, V. A., Sordet, O., Jobson, A. G., Thibaut, L., Miao, Z. H., Seiler, J. A., Zhang, H., Marchand, C., Agama, K., Nitiss, J. L., & Redon, C. (2006). Repair of Topoisomerase I-Mediated DNA Damage. *Progress in Nucleic Acid Research and Molecular Biology*, *81*(06), 179–229. https://doi.org/10.1016/S0079-6603(06)81005-6

Pommier, Y., Huang, S. yin N., Gao, R., Das, B. B., Murai, J., & Marchand, C. (2014). Tyrosyl-DNA-phosphodiesterases (TDP1 and TDP2). *DNA Repair*, *19*, 114–129. https://doi.org/10.1016/j.dnarep.2014.03.020

Pommier, Y., Nussenzweig, A., Takeda, S., & Austin, C. (2022). Human topoisomerases and their roles in genome stability and organization. *Nature Reviews Molecular Cell Biology*, *23*(6), 407–427. https://doi.org/10.1038/s41580-022-00452-3

Popovic, M., Zaja, R., Fent, K., & Smital, T. (2013). Molecular characterization of zebrafish Oatp1d1 (Slco1d1), a novel organic anion-transporting polypeptide. *Journal of Biological Chemistry*, *288*(47), 33894–33911. https://doi.org/10.1074/jbc.M113.518506

Popovic, M., Zaja, R., Loncar, J., & Smital, T. (2010). A novel ABC transporter: The first

insight into zebrafish (Danio rerio) ABCH1. *Marine Environmental Research*, *69*(SUPPL. 1), S11–S13. https://doi.org/10.1016/j.marenvres.2009.10.016

Popovic, M., Zaja, R., & Smital, T. (2010). Organic anion transporting polypeptides (OATP) in zebrafish (Danio rerio): Phylogenetic analysis and tissue distribution. *Comparative Biochemistry and Physiology - A Molecular and Integrative Physiology*, *155*(3), 327–335. https://doi.org/10.1016/j.cbpa.2009.11.011

Pouliot, J. J., Yao, K. C., Robertson, C. A., & Nash, H. A. (1999). Yeast gene for a Tyr-DNA phosphodiesterase that repairs topoisomerase I complexes. *Science (New York, N.Y.)*, *286*(5439), 552–555. https://doi.org/10.1126/science.286.5439.552

Povirk, L. F. (2012). Processing of damaged DNA ends for double-strand break repair in mammalian cells. *ISRN Molecular Biology*, *2012*. https://doi.org/10.5402/2012/345805

Prasad, R., Horton, J. K., Chastain, P. D. 2nd, Gassman, N. R., Freudenthal, B. D., Hou, E. W., & Wilson, S. H. (2014). Suicidal cross-linking of PARP-1 to AP site intermediates in cells undergoing base excision repair. *Nucleic Acids Research*, *42*(10), 6337–6351. https://doi.org/10.1093/nar/gku288

Pype, S., Declercq, W., Ibrahimi, A., Michiels, C., Van Rietschoten, J. G., Dewulf, N., de Boer, M., Vandenabeele, P., Huylebroeck, D., & Remacle, J. E. (2000). TTRAP, a novel protein that associates with CD40, tumor necrosis factor (TNF) receptor-75 and TNF receptor-associated factors (TRAFs), and that inhibits nuclear factor-kappa B activation. *The Journal of Biological Chemistry*, *275*(24), 18586–18593. https://doi.org/10.1074/jbc.M000531200

Quiñones, J. L., & Demple, B. (2016). When DNA repair goes wrong: BER-generated DNA-protein crosslinks to oxidative lesions. *DNA Repair*, *44*, 103–109. https://doi.org/10.1016/j.dnarep.2016.05.014

Quiñones, J. L., Thapar, U., Yu, K., Fang, Q., Sobol, R. W., & Demple, B. (2015). Enzyme mechanism-based, oxidative DNA-protein cross-links formed with DNA polymerase β in vivo. *Proceedings of the National Academy of Sciences of the United States of America*, *112*(28), 8602–8607. https://doi.org/10.1073/pnas.1501101112

Ramawat, K. G., & Mérillon, J.-M. (2013). Natural Products: Phytochemistry, Botany and Metabolism of Alkaloids, Phenolics and Terpenes. *Natural Products*.

Rao, T., Gao, R., Takada, S., Al Abo, M., Chen, X., Walters, K. J., Pommier, Y., & Aihara, H. (2016). Novel TDP2-ubiquitin interactions and their importance for the repair of topoisomerase II-mediated DNA damage. *Nucleic Acids Research*, *44*(21), 10201–10215. https://doi.org/10.1093/nar/gkw719

Rastogi, R. P., Richa, Kumar, A., Tyagi, M. B., & Sinha, R. P. (2010). Molecular mechanisms of ultraviolet radiation-induced DNA damage and repair. *Journal of Nucleic Acids*, *2010*, 592980. https://doi.org/10.4061/2010/592980

Ravi, V., & Venkatesh, B. (2008). Rapidly evolving fish genomes and teleost diversity. *Current Opinion in Genetics and Development*, *18*(6), 544–550. https://doi.org/10.1016/j.gde.2008.11.001

Ray Chaudhuri, A., Hashimoto, Y., Herrador, R., Neelsen, K. J., Fachinetti, D., Bermejo, R., Cocito, A., Costanzo, V., & Lopes, M. (2012). Topoisomerase i poisoning results in PARP-mediated replication fork reversal. *Nature Structural and Molecular Biology*, *19*(4), 417–423. https://doi.org/10.1038/nsmb.2258

Ray Chaudhuri, A., & Nussenzweig, A. (2017). The multifaceted roles of PARP1 in DNA repair and chromatin remodelling. *Nature Reviews Molecular Cell Biology*, *18*(10), 610–621. https://doi.org/10.1038/nrm.2017.53

Raymond, A. C., Rideout, M. C., Staker, B., Hjerrild, K., & Burgin, A. B. (2004). Analysis of human tyrosyl-DNA phosphodiesterase I catalytic residues. *Journal of Molecular Biology*, *338*(5), 895–906. https://doi.org/10.1016/j.jmb.2004.03.013

Redinbo, M. R., Stewart, L., Kuhn, P., Champoux, J. J., & Hol, W. G. (1998). Crystal structures of human topoisomerase I in covalent and noncovalent complexes with DNA. *Science (New York, N.Y.)*, *279*(5356), 1504–1513. https://doi.org/10.1126/science.279.5356.1504

Reginato, G., & Cejka, P. (2020). The MRE11 complex: A versatile toolkit for the repair of broken DNA. *DNA Repair*, *91–92*, 102869. https://doi.org/https://doi.org/10.1016/j.dnarep.2020.102869

Reinking, H. K., Hofmann, K., & Stingele, J. (2020). Function and evolution of the DNA-protein crosslink proteases Wss1 and SPRTN. *DNA Repair*, *88*, 102822. https://doi.org/10.1016/j.dnarep.2020.102822

Ren, M., Bai, J., Xi, Z., & Zhou, C. (2019). DNA damage in nucleosomes. *Science China Chemistry*. https://doi.org/10.1007/s11426-018-9421-5

Revet, I., Feeney, L., Bruguera, S., Wilson, W., Dong, T. K., Oh, D. H., Dankort, D., & Cleaver, J. E. (2011). Functional relevance of the histone γH2Ax in the response to DNA damaging agents. *Proceedings of the National Academy of Sciences*, *108*(21), 8663–8667. https://doi.org/10.1073/pnas.1105866108

Ribas, L., Liew, W. C., Díaz, N., Sreenivasan, R., Orbán, L., & Piferrer, F. (2017). Heat-induced masculinization in domesticated zebrafish is family-specific and yields a set of

different gonadal transcriptomes. *Proceedings of the National Academy of Sciences of the United States of America*, *114*(6), E941–E950. https://doi.org/10.1073/pnas.1609411114

Rice, W. R. (1984). SEX CHROMOSOMES AND THE EVOLUTION OF SEXUAL DIMORPHISM. *Evolution; International Journal of Organic Evolution*, *38*(4), 735–742. https://doi.org/10.1111/j.1558-5646.1984.tb00346.x

Rodrigues-Lima, F., Josephs, M., Katan, M., & Cassinat, B. (2001). Sequence analysis identifies TTRAP, a protein that associates with CD40 and TNF receptor-associated factors, as a member of a superfamily of divalent cation-dependent phosphodiesterases. *Biochemical and Biophysical Research Communications*, *285*(5), 1274–1279. https://doi.org/10.1006/bbrc.2001.5328

Ruggiano, A., & Ramadan, K. (2021). DNA–protein crosslink proteases in genome stability. *Communications Biology*, *4*(1), 1–11. https://doi.org/10.1038/s42003-020-01539-3

Ruggiano, A., Vaz, B., Kilgas, S., Popović, M., Rodriguez-Berriguete, G., Singh, A. N., Higgins, G. S., Kiltie, A. E., & Ramadan, K. (2021). The protease SPRTN and SUMOylation coordinate DNA-protein crosslink repair to prevent genome instability. *Cell Reports*, *37*(10). https://doi.org/10.1016/j.celrep.2021.110080

Saha, L. K., Saha, S., Yang, X., Huang, S.-Y. N., Sun, Y., Jo, U., & Pommier, Y. (2023). Replication-associated formation and repair of human topoisomerase IIIα cleavage complexes. *Nature Communications*, *14*(1), 1925. https://doi.org/10.1038/s41467-023-37498-6

Sakai, C., Ijaz, S., & Hoffman, E. J. (2018). Zebrafish Models of Neurodevelopmental Disorders: Past, Present, and Future. *Frontiers in Molecular Neuroscience*, *11*, 294. https://doi.org/10.3389/fnmol.2018.00294

Schärer, O. D. (2013). Nucleotide excision repair in eukaryotes. *Cold Spring Harbor Perspectives in Biology*, *5*(10), a012609. https://doi.org/10.1101/cshperspect.a012609

Schellenberg, M. J., Appel, C. D., Adhikari, S., Robertson, P. D., Ramsden, D. A., & Williams, R. S. (2012). Mechanism of repair of 5′-topoisomerase II-DNA adducts by mammalian tyrosyl-DNA phosphodiesterase 2. *Nature Structural and Molecular Biology*, *19*(12), 1363–1371. https://doi.org/10.1038/nsmb.2418

Schellenberg, M. J., Lieberman, J. A., Herrero-Ruiz, A., Butler, L. R., Williams, J. G., Muñoz-Cabello, A. M., Mueller, G. A., London, R. E., Cortés-Ledesma, F., & Williams, R. S. (2017). ZATT (ZNF451)–mediated resolution of topoisomerase 2 DNA-protein cross-links. *Science*, *357*(6358), 1412–1416. https://doi.org/10.1126/science.aam6468

Schumacher, B., Pothof, J., Vijg, J., & Hoeijmakers, J. H. J. (2021). The central role of DNA

damage in the ageing process. *Nature*, *592*(7856), 695–703. https://doi.org/10.1038/s41586-021-03307-7

Sciascia, N., Wu, W., Zong, D., Sun, Y., Wong, N., John, S., Wangsa, D., Ried, T., Bunting, S. F., Pommier, Y., & Nussenzweig, A. (2020). Suppressing proteasome mediated processing of topoisomerase II DNA-protein complexes preserves genome integrity. *ELife*, *9*, 1–27. https://doi.org/10.7554/eLife.53447

Seol, J.-H., Shim, E. Y., & Lee, S. E. (2018). Microhomology-mediated end joining: Good, bad and ugly. *Mutation Research*, *809*, 81–87. https://doi.org/10.1016/j.mrfmmm.2017.07.002

Serbyn, N., Noireterre, A., Bagdiul, I., Plank, M., Michel, A. H., Loewith, R., Kornmann, B., & Stutz, F. (2020). The Aspartic Protease Ddi1 Contributes to DNA-Protein Crosslink Repair in Yeast. *Molecular Cell*, *77*(5), 1066-1079.e9. https://doi.org/10.1016/j.molcel.2019.12.007

Shi, K., Kurahashi, K., Gao, R., Tsutakawa, S. E., Tainer, J. A., Pommier, Y., & Aihara, H. (2012). Structural basis for recognition of 5′-phosphotyrosine adducts by Tdp2. *Nature Structural and Molecular Biology*, *19*(12), 1372–1377. https://doi.org/10.1038/nsmb.2423

Shimizu, N., Hamada, Y., Morozumi, R., Yamamoto, J., Iwai, S., Sugiyama, K., Ide, H., & Tsuda, M. (2023). Repair of topoisomerase 1-induced DNA damage by tyrosyl-DNA phosphodiesterase 2 (TDP2) is dependent on its magnesium binding. *Journal of Biological Chemistry*, 104988. https://doi.org/https://doi.org/10.1016/j.jbc.2023.104988

Shoulkamy, M. I., Nakano, T., Ohshima, M., Hirayama, R., Uzawa, A., Furusawa, Y., & Ide, H. (2012). Detection of DNA-protein crosslinks (DPCs) by novel direct fluorescence labeling methods: distinct stabilities of aldehyde and radiation-induced DPCs. *Nucleic Acids Research*, *40*(18), e143. https://doi.org/10.1093/nar/gks601

Simon, P. (2003). Q-Gene: processing quantitative real-time RT-PCR data. *Bioinformatics (Oxford, England)*, *19*(11), 1439–1440. https://doi.org/10.1093/bioinformatics/btg157

Słomka, M., Sobalska-Kwapis, M., Wachulec, M., Bartosz, G., & Strapagiel, D. (2017). High Resolution Melting (HRM) for High-Throughput Genotyping—Limitations and Caveats in Practical Case Studies. *International Journal of Molecular Sciences*, *18*(11). https://doi.org/10.3390/ijms18112316

Small, C. M., Carney, G. E., Mo, Q., Vannucci, M., & Jones, A. G. (2009). A microarray analysis of sex- and gonad-biased gene expression in the zebrafish: evidence for masculinization of the transcriptome. *BMC Genomics*, *10*, 579. https://doi.org/10.1186/1471-2164-10-579

Snow, C. J., Peterson, M. T., Khalil, A., & Henry, C. A. (2008). Muscle development is

disrupted in zebrafish embryos deficient for fibronectin. *Developmental Dynamics : An Official Publication of the American Association of Anatomists*, *237*(9), 2542–2553. https://doi.org/10.1002/dvdy.21670

Soll, J. M., Sobol, R. W., & Mosammaparast, N. (2017). Regulation of DNA Alkylation Damage Repair: Lessons and Therapeutic Opportunities. *Trends in Biochemical Sciences*, *42*(3), 206–218. https://doi.org/10.1016/j.tibs.2016.10.001

Stingele, J., Bellelli, R., Alte, F., Hewitt, G., Sarek, G., Maslen, S. L., Tsutakawa, S. E., Borg, A., Kjær, S., Tainer, J. A., Skehel, J. M., Groll, M., & Boulton, S. J. (2016). Mechanism and Regulation of DNA-Protein Crosslink Repair by the DNA-Dependent Metalloprotease SPRTN. *Molecular Cell*, *64*(4), 688–703. https://doi.org/10.1016/j.molcel.2016.09.031

Stingele, J., Habermann, B., & Jentsch, S. (2015). DNA-protein crosslink repair: Proteases as DNA repair enzymes. *Trends in Biochemical Sciences*, *40*(2), 67–71. https://doi.org/10.1016/j.tibs.2014.10.012

Stingele, J., & Jentsch, S. (2015). DNA-protein crosslink repair. *Nature Reviews Molecular Cell Biology*, *16*(8), 455–460. https://doi.org/10.1038/nrm4015

Stingele, J., Schwarz, M. S., Bloemeke, N., Wolf, P. G., & Jentsch, S. (2014). A DNA-dependent protease involved in DNA-protein crosslink repair. *Cell*, *158*(2), 327–338. https://doi.org/10.1016/j.cell.2014.04.053

Stracker, T. H., Theunissen, J.-W. F., Morales, M., & Petrini, J. H. J. (2004). The Mre11 complex and the metabolism of chromosome breaks: the importance of communicating and holding things together. *DNA Repair*, *3*(8–9), 845–854. https://doi.org/10.1016/j.dnarep.2004.03.014

Streich, F. C. J., & Lima, C. D. (2014). Structural and functional insights to ubiquitin-like protein conjugation. *Annual Review of Biophysics*, *43*, 357–379. https://doi.org/10.1146/annurev-biophys-051013-022958

Su, T., Liu, F., Gu, P., Jin, H., Chang, Y., Wang, Q., Liang, Q., & Qi, Q. (2016). A CRISPR-Cas9 Assisted Non-Homologous End-Joining Strategy for One-step Engineering of Bacterial Genome. *Scientific Reports*, *6*, 37895. https://doi.org/10.1038/srep37895

Sun, Y., Saha, L. K., Saha, S., Jo, U., & Pommier, Y. (2020). Debulking of topoisomerase DNA-protein crosslinks (TOP-DPC) by the proteasome, non-proteasomal and non-proteolytic pathways. *DNA Repair*, *94*, 102926. https://doi.org/10.1016/j.dnarep.2020.102926

Sun, Y., Saha, S., Wang, W., Saha, L. K., Huang, S. Y. N., & Pommier, Y. (2020). Excision repair of topoisomerase DNA-protein crosslinks (TOP-DPC). *DNA Repair*, *89*(January), 102837. https://doi.org/10.1016/j.dnarep.2020.102837

Sun, Y., Soans, E., Mishina, M., Petricci, E., Pommier, Y., Nitiss, K. C., & Nitiss, J. L. (2022). Requirements for MRN endonuclease processing of topoisomerase II-mediated DNA damage in mammalian cells. *Frontiers in Molecular Biosciences*, *9*(September), 1–16. https://doi.org/10.3389/fmolb.2022.1007064

Svoboda, M., Konvalinka, J., Trempe, J.-F., & Grantz Saskova, K. (2019). The yeast proteases Ddi1 and Wss1 are both involved in the DNA replication stress response. *DNA Repair*, *80*, 45–51. https://doi.org/10.1016/j.dnarep.2019.06.008

Takahashi, D. T., Da Cunha, V., Krupovic, M., Mayer, C., Forterre, P., & Gadelle, D. (2020). Expanding the type IIB DNA topoisomerase family: identification of new topoisomerase and topoisomerase-like proteins in mobile genetic elements. *NAR Genomics and Bioinformatics*, *2*(1), lqz021. https://doi.org/10.1093/nargab/lqz021

Takahashi, D. T., Gadelle, D., Agama, K., Kiselev, E., Zhang, H., Yab, E., Petrella, S., Forterre, P., Pommier, Y., & Mayer, C. (2022). Topoisomerase I (TOP1) dynamics: conformational transition from open to closed states. *Nature Communications*, *13*(1), 59. https://doi.org/10.1038/s41467-021-27686-7

Takashima, H., Boerkoel, C. F., John, J., Saifi, G. M., Salih, M. A. M., Armstrong, D., Mao, Y., Quiocho, F. A., Roa, B. B., Nakagawa, M., Stockton, D. W., & Lupski, J. R. (2002). Mutation of TDP1, encoding a topoisomerase I-dependent DNA damage repair enzyme, in spinocerebellar ataxia with axonal neuropathy. *Nature Genetics*, *32*(2), 267–272. https://doi.org/10.1038/ng987

Tofano, D., Wiechers, I. R., & Cook-Deegan, R. (2006). Edwin Southern, DNA blotting, and microarray technology: A case study of the shifting role of patents in academic molecular biology. In *Genomics, society, and policy* (Vol. 2, Issue 2). https://doi.org/10.1186/1746-5354-2-2-50

Tom, R., Bisson, L., & Durocher, Y. (2008). Transfection of adherent HEK293-EBNA1 cells in a six-well plate with branched PEI for production of recombinant proteins. *Cold Spring Harbor Protocols*, *3*(3). https://doi.org/10.1101/pdb.prot4978

Tretyakova, N. Y., Groehler, A. 4th, & Ji, S. (2015). DNA-Protein Cross-Links: Formation, Structural Identities, and Biological Outcomes. *Accounts of Chemical Research*, *48*(6), 1631–1644. https://doi.org/10.1021/acs.accounts.5b00056

Tsai, W.-H., & Chang, W.-T. (2014). Construction of simple and efficient siRNA validation systems for screening and identification of effective RNAi-targeted sequences from mammalian genes. *Methods in Molecular Biology (Clifton, N.J.)*, *1101*, 321–338. https://doi.org/10.1007/978-1-62703-721-1_15

Tuzmen, S., Kiefer, J., & Mousses, S. (2007). Validation of short interfering RNA knockdowns by quantitative real-time PCR. *Methods in Molecular Biology (Clifton, N.J.)*, *353*, 177–203. https://doi.org/10.1385/1-59745-229-7:177

Uhlén, M., Fagerberg, L., Hallström, B. M., Lindskog, C., Oksvold, P., Mardinoglu, A., Sivertsson, Å., Kampf, C., Sjöstedt, E., Asplund, A., Olsson, I. M., Edlund, K., Lundberg, E., Navani, S., Szigyarto, C. A. K., Odeberg, J., Djureinovic, D., Takanen, J. O., Hober, S., … Pontén, F. (2015). Tissue-based map of the human proteome. *Science*, *347*(6220). https://doi.org/10.1126/science.1260419

Uyhazi, K. E., & Bennett, J. (2021). A CRISPR view of the 2020 Nobel Prize in Chemistry. *The Journal of Clinical Investigation*, *131*(1). https://doi.org/10.1172/JCI145214

van Waardenburg, R. C. A. M. (2016). Tyrosyl-DNA Phosphodiesterase I a critical survival factor for neuronal development and homeostasis. *Journal of Neurology & Neuromedicine*, *1*(5), 25–29. https://doi.org/10.29245/2572.942x/2016/5.1048

Vann, K. R., Oviatt, A. A., & Osheroff, N. (2021). Topoisomerase II Poisons: Converting Essential Enzymes into Molecular Scissors. *Biochemistry*, *60*(21), 1630–1641. https://doi.org/10.1021/acs.biochem.1c00240

Varshney, G. K., Sood, R., & Burgess, S. M. (2015). Understanding and Editing the Zebrafish Genome. *Advances in Genetics*, *92*, 1–52. https://doi.org/10.1016/bs.adgen.2015.09.002

Vaz, B., Popovic, M., Newman, J. A., Fielden, J., Aitkenhead, H., Halder, S., Singh, A. N., Vendrell, I., Fischer, R., Torrecilla, I., Drobnitzky, N., Freire, R., Amor, D. J., Lockhart, P. J., Kessler, B. M., McKenna, G. W., Gileadi, O., & Ramadan, K. (2016). Metalloprotease SPRTN/DVC1 Orchestrates Replication-Coupled DNA-Protein Crosslink Repair. *Molecular Cell*, *64*(4), 704–719. https://doi.org/10.1016/j.molcel.2016.09.032

Vaz, B., Popovic, M., & Ramadan, K. (2017). DNA–Protein Crosslink Proteolysis Repair. *Trends in Biochemical Sciences*, *42*(6), 483–495. https://doi.org/10.1016/j.tibs.2017.03.005

Veldman, M. B., & Lin, S. (2008). Zebrafish as a Developmental Model Organism for Pediatric Research. *Pediatric Research*, *64*(5), 470–476. https://doi.org/10.1203/PDR.0b013e318186e609

Verdine, G. L., & Norman, D. P. G. (2003). Covalent trapping of protein-DNA complexes. *Annual Review of Biochemistry*, *72*, 337–366. https://doi.org/10.1146/annurev.biochem.72.121801.161447

Vierstraete, J., Willaert, A., Vermassen, P., Coucke, P. J., Vral, A., & Claes, K. B. M. (2017). Accurate quantification of homologous recombination in zebrafish: brca2 deficiency as a paradigm. *Scientific Reports*, *7*(1), 16518. https://doi.org/10.1038/s41598-017-16725-3

von Kobbe, C. (2019). Targeting senescent cells: approaches, opportunities, challenges. *Aging*, *11*(24), 12844–12861. https://doi.org/10.18632/aging.102557

Wang, H., & Xu, X. (2017). Microhomology-mediated end joining: new players join the team. *Cell & Bioscience*, *7*(1), 6. https://doi.org/10.1186/s13578-017-0136-8

Wang, P., Elsayed, M. S. A., Plescia, C. B., Ravji, A., Redon, C. E., Kiselev, E., Marchand, C., Zeleznik, O., Agama, K., Pommier, Y., & Cushman, M. (2017). Synthesis and Biological Evaluation of the First Triple Inhibitors of Human Topoisomerase 1, Tyrosyl-DNA Phosphodiesterase 1 (Tdp1), and Tyrosyl-DNA Phosphodiesterase 2 (Tdp2). *Journal of Medicinal Chemistry*, *60*(8), 3275–3288. https://doi.org/10.1021/acs.jmedchem.6b01565

Wang, P., Henning, S. M., & Heber, D. (2010). Limitations of MTT and MTS-based assays for measurement of antiproliferative activity of green tea polyphenols. *PLoS ONE*, *5*(4). https://doi.org/10.1371/journal.pone.0010202

Wang, Y., Xu, M., & Jiang, T. (2016). Crystal structure of human PCNA in complex with the PIP box of DVC1. *Biochemical and Biophysical Research Communications*, *474*(2), 264–270. https://doi.org/10.1016/j.bbrc.2016.04.053

Wei, X., Peng, Y., Bryan, C., & Yang, K. (2021). Mechanisms of DNA−protein cross-link formation and repair. *Biochimica et Biophysica Acta (BBA) - Proteins and Proteomics*, *1869*(8), 140669. https://doi.org/https://doi.org/10.1016/j.bbapap.2021.140669

Wei, X., Wang, Z., Hinson, C., & Yang, K. (2022). Human TDP1, APE1 and TREX1 repair 3′-DNA–peptide/protein cross-links arising from abasic sites in vitro. *Nucleic Acids Research*, *50*(7), 3638–3657. https://doi.org/10.1093/nar/gkac185

Weickert, P., Li, H.-Y., Götz, M. J., Dürauer, S., Yaneva, D., Zhao, S., Cordes, J., Acampora, A. C., Forne, I., Imhof, A., & Stingele, J. (2023). SPRTN patient variants cause global-genome DNA-protein crosslink repair defects. *Nature Communications*, *14*(1), 352. https://doi.org/10.1038/s41467-023-35988-1

Werdich, A. A., Brzezinski, A., Jeyaraj, D., Khaled Sabeh, M., Ficker, E., Wan, X., McDermott, B. M. J., Macrae, C. A., & Rosenbaum, D. S. (2012). The zebrafish as a novel animal model to study the molecular mechanisms of mechano-electrical feedback in the heart. *Progress in Biophysics and Molecular Biology*, *110*(2–3), 154–165. https://doi.org/10.1016/j.pbiomolbio.2012.07.006

White, R. M., Sessa, A., Burke, C., Bowman, T., LeBlanc, J., Ceol, C., Bourque, C., Dovey, M., Goessling, W., Burns, C. E., & Zon, L. I. (2008). Transparent Adult Zebrafish as a Tool for In Vivo Transplantation Analysis. *Cell Stem Cell*, *2*(2), 183–189. https://doi.org/https://doi.org/10.1016/j.stem.2007.11.002

Whitehead, A., & Crawford, D. L. (2006). Variation within and among species in gene expression: raw material for evolution. *Molecular Ecology*, *15*(5), 1197–1211. https://doi.org/10.1111/j.1365-294X.2006.02868.x

Xue, B., Dunbrack, R. L., Williams, R. W., Dunker, A. K., & Uversky, V. N. (2010). PONDR-FIT: A meta-predictor of intrinsically disordered amino acids. *Biochimica et Biophysica Acta - Proteins and Proteomics*, *1804*(4), 996–1010. https://doi.org/10.1016/j.bbapap.2010.01.011

Xue, C., & Greene, E. C. (2021). DNA Repair Pathway Choices in CRISPR-Cas9-Mediated Genome Editing. *Trends in Genetics*, *37*(7), 639–656. https://doi.org/https://doi.org/10.1016/j.tig.2021.02.008

Yang, S. W., Burgin, A. B., Huizenga, B. N., Robertson, C. A., Yao, K. C., & Nash, H. A. (1996). A eukaryotic enzyme that can disjoin dead-end covalent complexes between DNA and type I topoisomerases. *Proceedings of the National Academy of Sciences of the United States of America*, *93*(21), 11534–11539. https://doi.org/10.1073/pnas.93.21.11534

Yudkina, A. V, Dvornikova, A. P., & Zharkov, D. O. (2018). Variable termination sites of DNA polymerases encountering a DNA–protein cross-link. *PLOS ONE*, *13*(6), 1–17. https://doi.org/10.1371/journal.pone.0198480

Zagnoli-Vieira, G., Bruni, F., Thompson, K., He, L., Walker, S., Brouwer, A. P. M. D., Taylor, R., Niyazov, D., & Caldecott, K. W. (2018). Confirming TDP2 mutation in spinocerebellar ataxia autosomal recessive 23 (SCAR23). *Neurology: Genetics*, *4*(4). https://doi.org/10.1212/NXG.0000000000000262

Zaksauskaite, R., Thomas, R. C., Van Eeden, F., & El-Khamisy, S. F. (2021). Tdp1 protects from topoisomerase 1-mediated chromosomal breaks in adult zebrafish but is dispensable during larval development. *Science Advances*, *7*(5), 1–16. https://doi.org/10.1126/SCIADV.ABC4165

Zeng, Z., Cortés-Ledesma, F., El Khamisy, S. F., & Caldecott, K. W. (2011). TDP2/TTRAP is the major 5′-tyrosyl DNA phosphodiesterase activity in vertebrate cells and is critical for cellular resistance to topoisomerase II-induced DNA damage. *Journal of Biological Chemistry*, *286*(1), 403–409. https://doi.org/10.1074/jbc.M110.181016

Zeng, Z., Sharma, A., Ju, L., Murai, J., Umans, L., Vermeire, L., Pommier, Y., Takeda, S., Huylebroeck, D., Caldecott, K. W., & El-Khamisy, S. F. (2012). TDP2 promotes repair of topoisomerase I-mediated DNA damage in the absence of TDP1. *Nucleic Acids Research*, *40*(17), 8371–8380. https://doi.org/10.1093/nar/gks622

Zhang, H., & Pommier, Y. (2008). Mitochondrial topoisomerase I sites in the regulatory D-

loop region of mitochondrial DNA. *Biochemistry*, *47*(43), 11196–11203. https://doi.org/10.1021/bi800774b

Zhang, H., Xiong, Y., & Chen, J. (2020). DNA–protein cross-link repair: what do we know now? *Cell & Bioscience*, *10*(1), 3. https://doi.org/10.1186/s13578-019-0366-z

Zhang, H., Xiong, Y., Su, D., Wang, C., Srivastava, M., Tang, M., Feng, X., Huang, M., Chen, Z., & Chen, J. (2022). TDP1-independent pathways in the process and repair of TOP1-induced DNA damage. *Nature Communications*, *13*(1). https://doi.org/10.1038/s41467-022-31801-7

Zhang, J., Wang, J., Li, W., Huang, L., Tian, L., Xue, J., Chen, J., & Jia, W. (2009). Cellular protein TTRAP interacts with HIV-1 integrase to facilitate viral integration. *Biochemical and Biophysical Research Communications*, *387*(2), 256–260. https://doi.org/10.1016/j.bbrc.2009.06.153

Zhang, M., Kothari, P., Mullins, M., & Lampson, M. A. (2014). Regulation of zygotic genome activation and DNA damage checkpoint acquisition at the mid-blastula transition. *Cell Cycle (Georgetown, Tex.)*, *13*(24), 3828–3838. https://doi.org/10.4161/15384101.2014.967066

Zhang, W., Gou, P., Dupret, J. M., Chomienne, C., & Rodrigues-Lima, F. (2021). Etoposide, an anticancer drug involved in therapy-related secondary leukemia: Enzymes at play. *Translational Oncology*, *14*(10), 101169. https://doi.org/10.1016/j.tranon.2021.101169

Zhang, Y., Wang, W., Min, J., Liu, S., Wang, Q., Wang, Y., Xiao, Y., Li, X., Zhou, Z., & Liu, S. (2023). ZNF451 favors triple-negative breast cancer progression by enhancing SLUG-mediated CCL5 transcriptional expression. *Cell Reports*, *42*(6), 112654. https://doi.org/https://doi.org/10.1016/j.celrep.2023.112654

Zhitkovich, A., & costa, M. (1992). A simple, sensitive assay to detect DNA–protein cromlinks in intact cells and in vivo. *Carcinogenesis*, *13*(8), 1485–1489. https://doi.org/10.1093/carcin/13.8.1485

Zhu, L., Mon, H., Xu, J., Lee, J. M., & Kusakabe, T. (2015). CRISPR/Cas9-mediated knockout of factors in non-homologous end joining pathway enhances gene targeting in silkworm cells. *Scientific Reports*, *5*(1), 18103. https://doi.org/10.1038/srep18103

Zucchelli, S., Vilotti, S., Calligaris, R., Lavina, Z. S., Biagioli, M., Foti, R., De Maso, L., Pinto, M., Gorza, M., Speretta, E., Casseler, C., Tell, G., Del Sal, G., & Gustincich, S. (2009). Aggresome-forming TTRAP mediates pro-apoptotic properties of Parkinson's disease-associated DJ-1 missense mutations. *Cell Death & Differentiation*, *16*(3), 428–438. https://doi.org/10.1038/cdd.2008.169

9. AUTHOR BIOGRAPHY

Ivan Antičević was born on January 28, 1995, in Split, Croatia. After completing high school, he pursued a Master's degree in Biology and Chemistry at the University of Zagreb, Faculty of Science, Department of Biology, from which he graduated in 2019. Following his graduation, Ivan became employed at the Institute Ruđer Bošković, Division for Marine and Environmental Research, in the Laboratory for Molecular Ecotoxicology within the DNA Damage Group. He enrolled in a PhD program at the University of Zagreb, Faculty of Science, Department of Biology. During his Ph.D. program, Ivan participated in two EMBO workshops: in 2019, 'The DNA-Damage Response in Cell Physiology and Disease,' for which he received the Best Poster Award, and in 2020, 'Chromatin Dynamics and Nuclear Organization in Genome Maintenance.' He also attended three conferences: YSF and FEBS 2021 45th Congress, FEBS 2022 46th Congress, where he received full attendance grants, and the International Congress of the HDBMB Society ('From Science to Knowledge'), for which he was awarded a fellowship to attend. Ivan attended two PhD student symposiums at the Faculty of Science, during one of which he gave an oral presentation. Over the course of his Ph.D. program, Ivan published two scientific papers: one stemming from his prior work and another publication based on his Ph.D. research. He was also a mentor to two master's students and as a supervisor to three student internships. Ivan is a member of several organizations, including the Croatian Society of Biochemistry and Molecular Biology (HDBMB), the Croatian Association for Cancer Research (HDIR), and the Croatian Biophysical Society.

Publications:

Anticevic, I., Otten, C., Vinkovic, L., Jukic, L., & Popovic, M. (2023). Tyrosyl-DNA phosphodiesterase 1 (TDP1) and SPRTN protease repair histone 3 and topoisomerase 1 DNA-protein crosslinks in vivo. *Open Biology*, *1*, 2023.03.01.530659.

Kekez, M., Zanki, V., Antičević, I., Rokov-Plavec, J., & Maršavelski, A. (2021). Importance of protein intrinsic conformational dynamics and transient nature of non-covalent interactions in ligand binding affinity. *International Journal of Biological Macromolecules*, *192*, 692–700. https://doi.org/10.1016/j.ijbiomac.2021.10.045

10. SUPPLEMENT

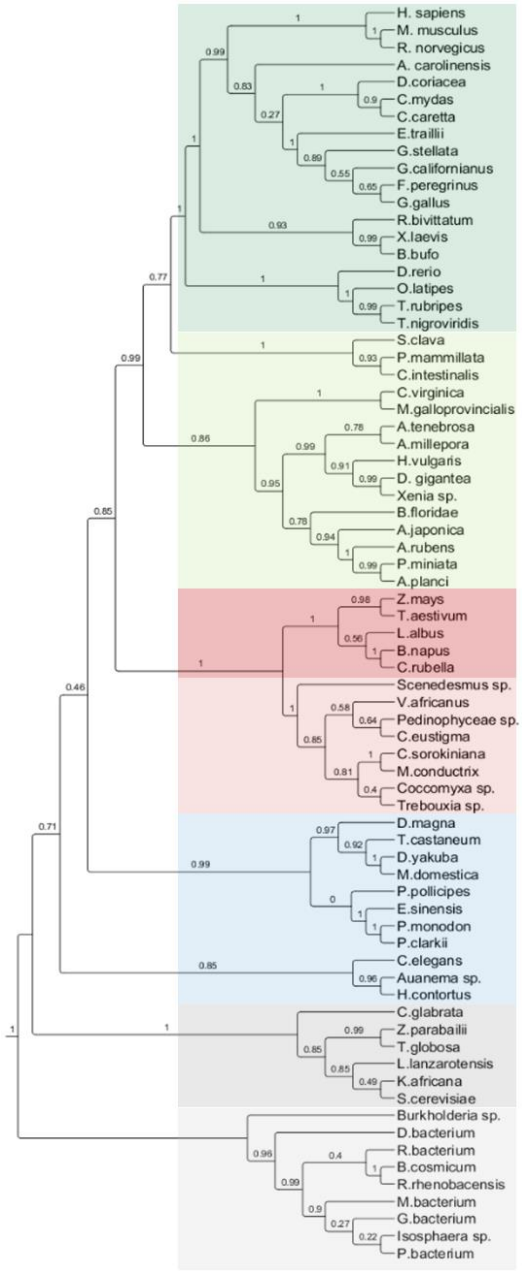

Supplement 1. Extended phylogenetic analysis of TDP1 proteins.

Extended phylogenetic tree of TDP1 proteins from bacteria to humans was performed using the Maximum Likelihood method with branch support Alrt values (Approximate likelihood-ratio test) which are shown at tree nodes on a scale of 0 - 1, where 1 is maximum node confidence.

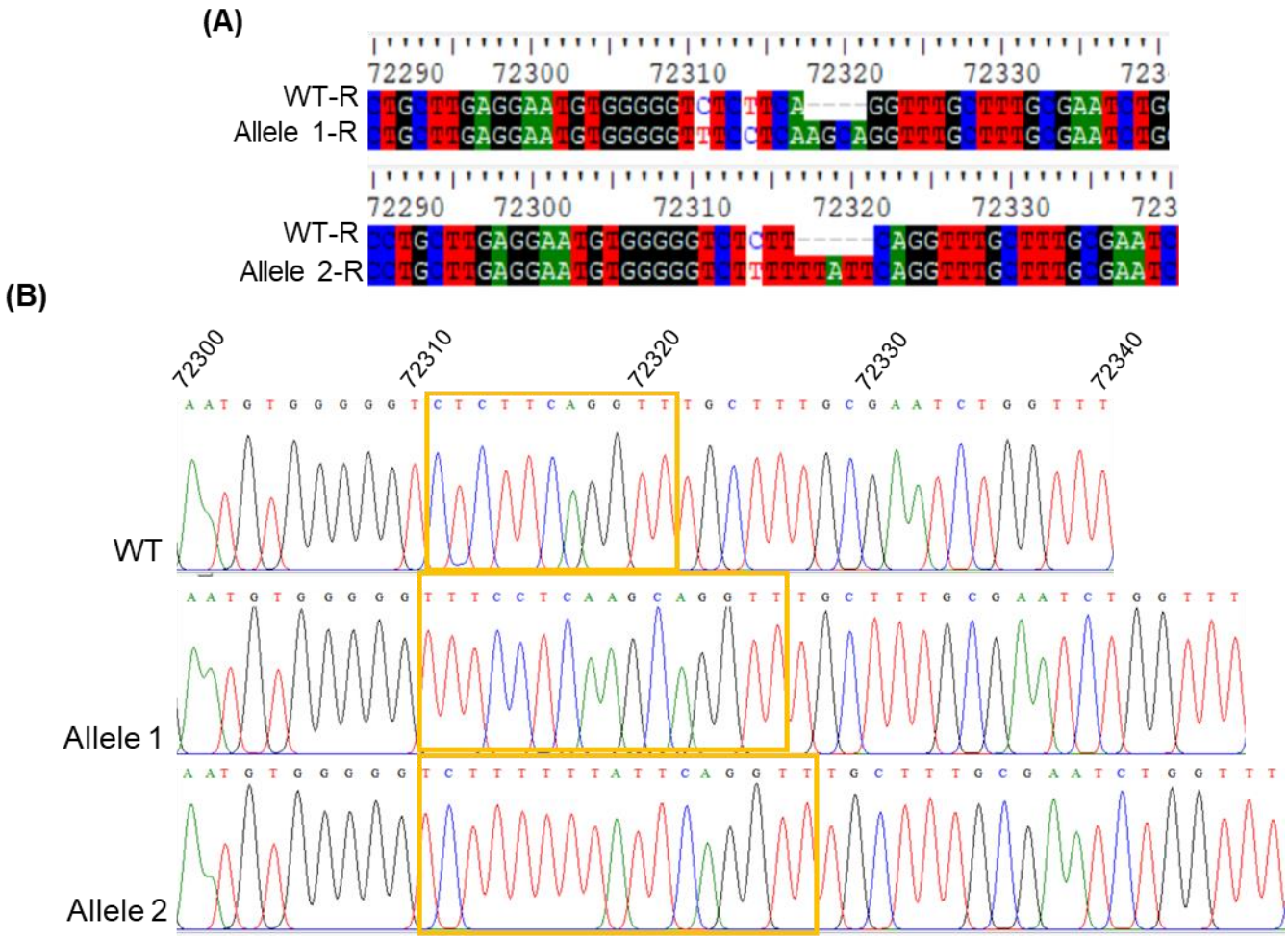

Supplement 2. Sequences from the target region in wild-type (WT) and tdp1 mutant zebrafish

A) Alignment of sequences in reverse complement. B) Histograms depicting allele-specific sequencing for WT and *tdp1* mutants. Part with the changes is highlighted in orange. The numbers above the histograms indicate the genomic position.

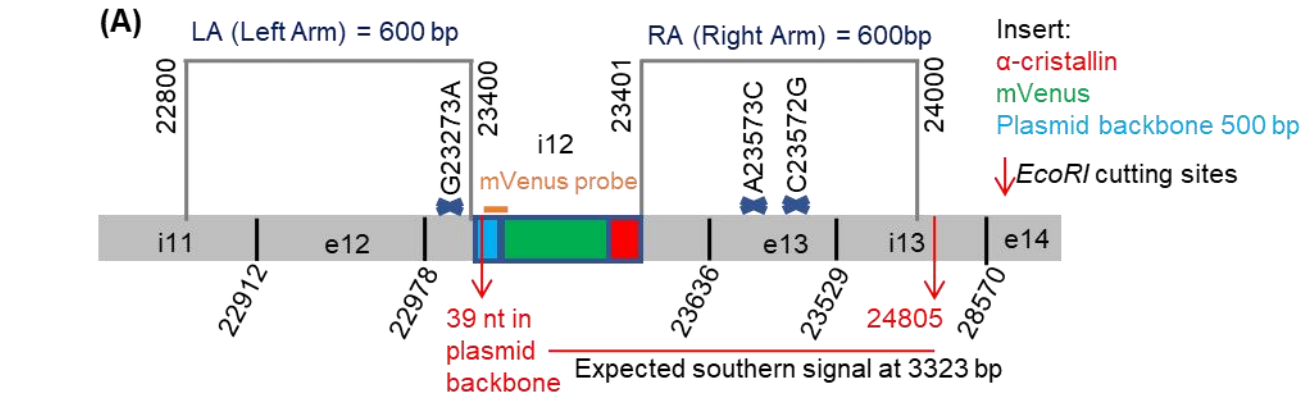

(B)

```
R.T.          657 ttcttaaaaaacctcccacacctccccctgaacctgaaacataaaatgaatgcaattgttgttgttaacttgtttattgcagcttataat
pKHR5_plasmid 793 ttcttaaaaaacctcccacacctccccctgaacctgaaacataaaatgaatgcaattgttgttgttaacttgtttattgcagcttataat
mVenus_probe    1 ----------------------ctccccctgaacctgaaacataaaatgaatgcaattgttgttgttaacttgtttattgcagcttataat

R.T.          747 ggttacaaataaagcaatagcatcacaaatttcacaaataaagcatttttttcactgcattctagttgtggtttgtccaaactcatcaat
pKHR5_plasmid 883 ggttacaaataaagcaatagcatcacaaatttcacaaataaagcatttttttcactgcattctagttgtggtttgtccaaactcatcaat
mVenus_probe   70 ggttacaaataaagcaatagcatcacaaatttcacaaataaagcatttttttcactgcattctagttgtggtttgtccaaactcatcaat

R.T.          837 gtatcttatcatgtctggatcatcatcgatggtacccaccgcggtggcggcgatctctccccagcatgcctgctattgtcttcccaatcc
pKHR5_plasmid 973 gtatcttatcatgtctggatcatcatcgatggtacccaccgcggtggcggcgatctctccccagcatgcctgctattgtcttcccaatcc
mVenus_probe  160 gtatcttatcatgtctggatcatcatcgatggtacccaccgcggtggcggcgatctctccccagcatgcctgctattgtcttcccaatcc

R.T.          927 tccccttgctgtcctgccccaccccaccccccagaatagaatgacacctactcagacaatgcgatgcaatttcctcattttattaggaa
pKHR5_plasmid 1063 tccccttgctgtcctgccccaccccaccccccagaatagaatgacacctactcagacaatgcgatgcaatttcctcattttattaggaa
mVenus_probe   250 tccccttgctgtcctgccccaccccaccccccagaatagaatgacacctactcagacaatgcgatgcaatttcctcattttattaggaa

R.T.         1017 aggacagtgggagtggcaccttccagggtcaaggaaggcacgggggagggggcaaacaacagatggctggcaactagaaggcacagtcgag
pKHR5_plasmid 1153 aggacagtgggagtggcaccttccagggtcaaggaaggcacgggggagggggcaaacaacagatggctggcaactagaaggcacagtcgag
mVenus_probe   340 aggacagtgggagtggcaccttccagggtcaaggaaggcacgggggagggggcaaacaacagatggctggcaactagaaggcacagtcgag

R.T.         1107 gctgatcagcgggccgctttacttgtacagctcgtccatgccgagagtgatcccggcggcggtcacgaactccagcaggaccatgtgatc
pKHR5_plasmid 1243 gctgatcagcgggccgctttacttgtacagctcgtccatgccgagagtgatcccggcggcggtcacgaactccagcaggaccatgtgatc
mVenus_probe   430 gct----------------------------------------------------------------------------------------
```

Supplement 3. Schematic of mVenus probe. A) An orange mark denotes the location where the mVenus probe will hybridize in *tdp1* lens-positive embryos. B) Sequence alignment showing the mVenus probe sequence aligned with the sequences of the Repair template and pKHR plasmid

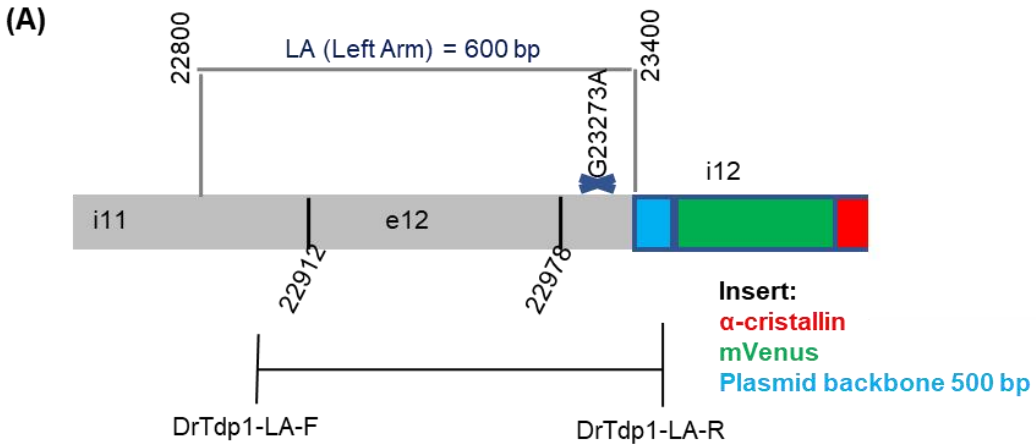

(B)

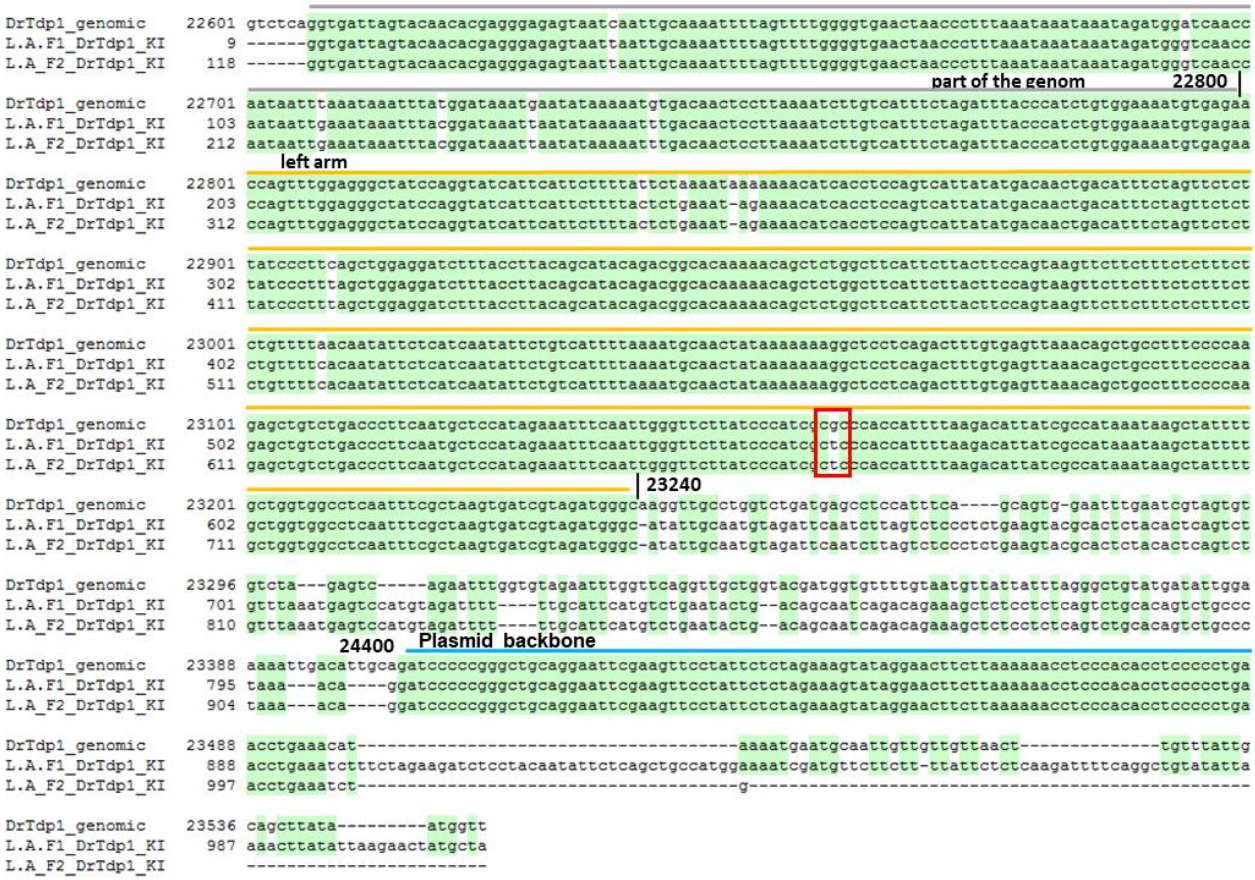

Supplement 4. Genomic location sequencing of the Left Arm A) Schematic illustration of the sequencing strategy for the left arm genomic location. Sheme shows that the DrTdp–L.A F primer resides outside the left arm in the genomic region, while the DrTdp1–L.A R primer is located in the plasmid backbone of the insert. B) Sequencing result for the genomic location of the left arm. The sequenced portion of the genome is represented by a grey bar, with an orange section indicating the left arm (L.A.) and a blue section representing the plasmid backbone. A red square highlights the PAM mutation site.

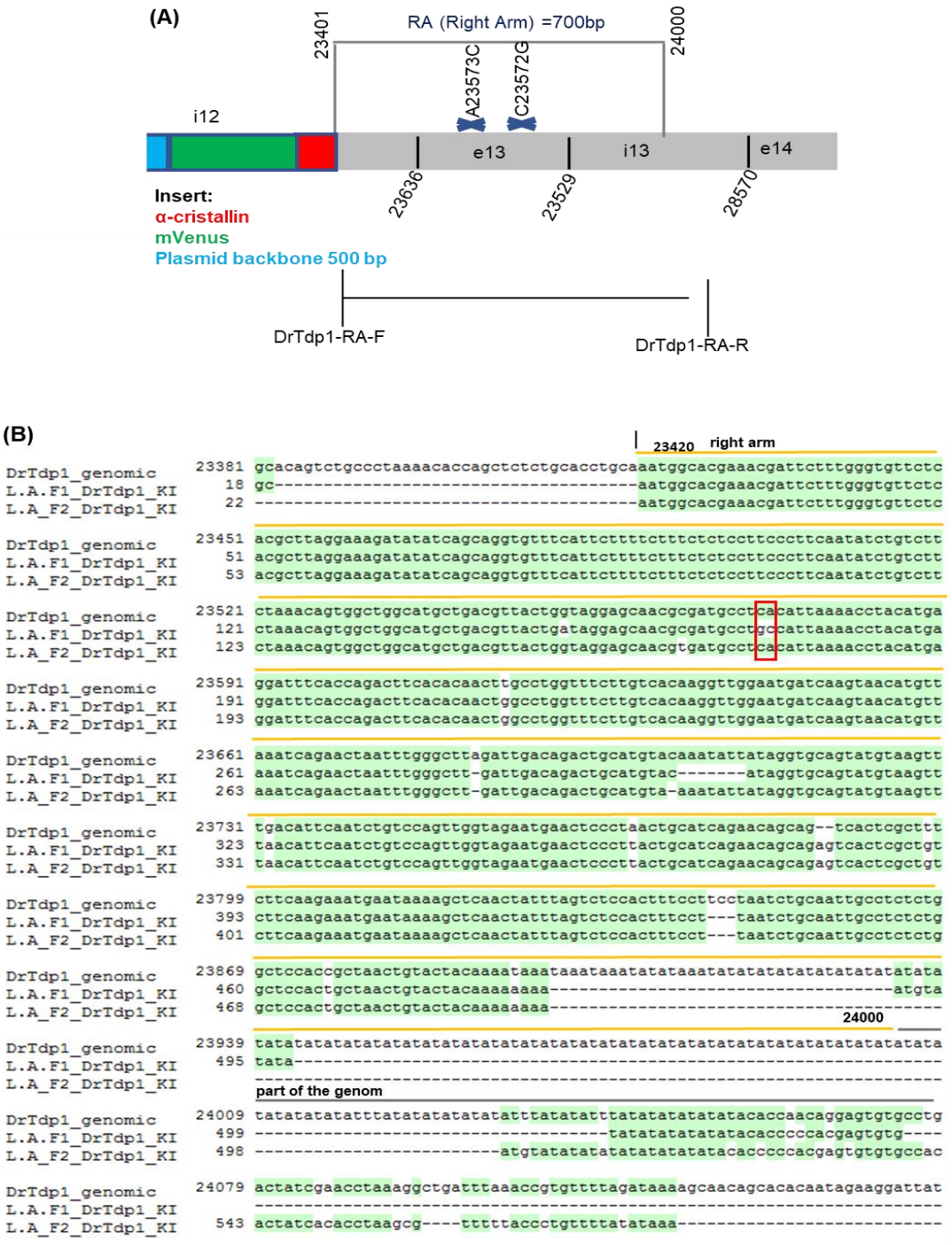

Supplement 5. Genomic location sequencing of the Right arm. A) Schematic illustration of the sequencing approach for the genomic location of the right arm. The schema demonstrates that the DrTdp1-RA-geno-F primer is positioned at the start of the right arm, whereas the DrTdp1–L.A R primer is located outside the right arm in the genomic region. B) Sequencing results for the genomic location of the right arm. An orange section indicates the right arm, while a grey section represents the genomic region. A red square highlights the catalytic mutation site.

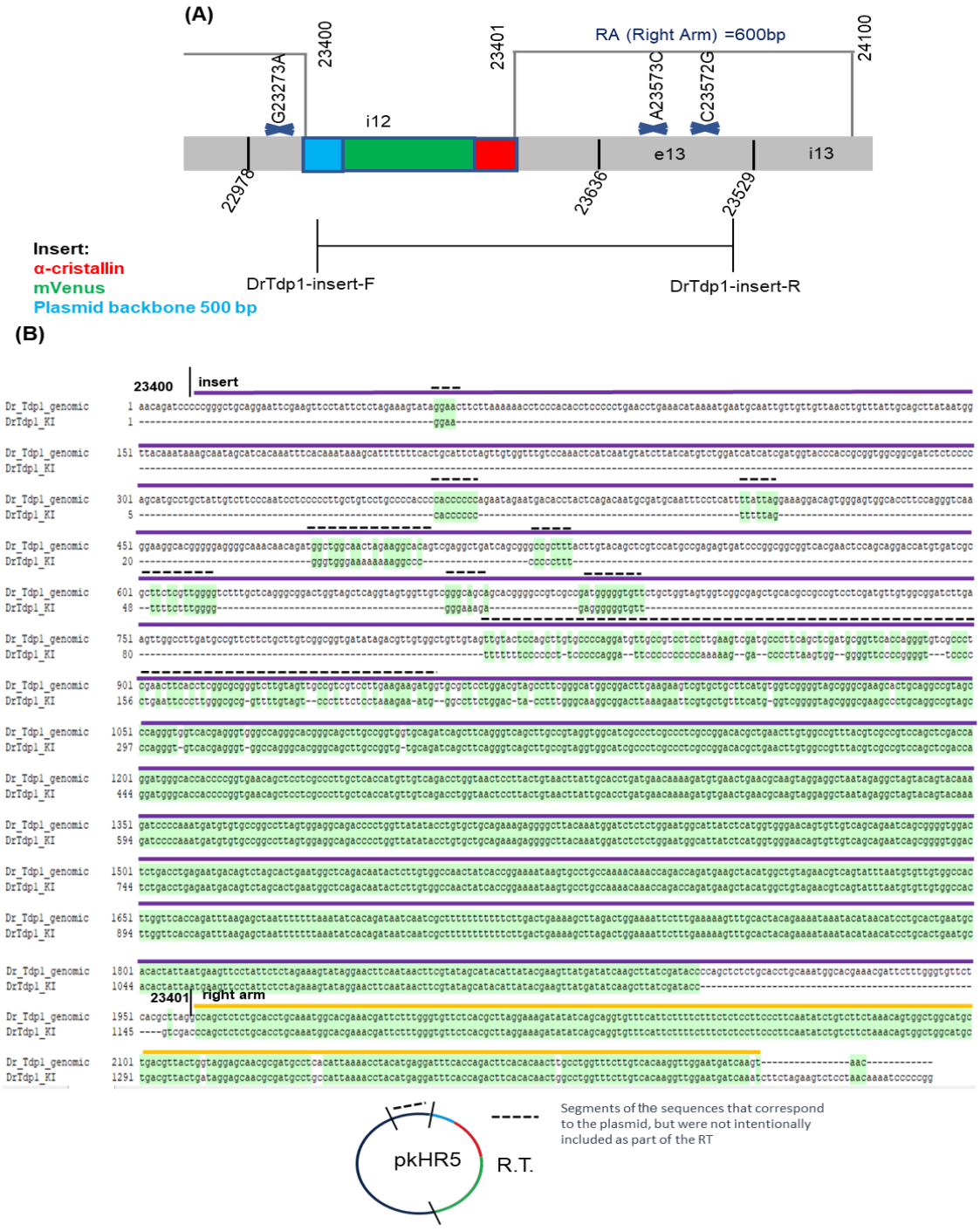

Supplement 6. Genomic location sequencing of the insert and portion of right arm: A) Schematic illustration shows the sequencing strategy for the genomic location of the insert and a portion of the right arm. The diagram illustrates that the DrTdp1-insert-F primer is situated at the beginning of the insert, while the DrTdp1-insert-R primer is positioned in the middle of the right arm. B) Sequencing results for the genomic location of the insert. A purple section designates the insert sequence, while an orange section represents the right arm. Interrupted lines represent plasmid sequences that are not part of the repair template (depicted in the pKHR plasmid scheme). A red square highlights the catalytic mutation site.

Abbreviation	Accession no.	Species	Group
H.sapiens	NP_057698.2	Homo sapiens	mammals
R.norvegicus	NP_001030119.1	Rattus norvegicus	mammals
M.musculus	NP_062424.1	Mus musculus	mammals
S.scrofa	NP_001230615.1	Sus scrofa	mammals
G.gallus	NP_001383838.1	Gallus gallus	birds
N.meleagris	XP_021243246.1	Numida meleagris	birds
T.alba	XP_042653803.1	Tyto alba	birds
C.mydas	XP_043395969.1	Chelonia mydas	reptiles
D.coriacea	XP_043364228.1	Dermochelys coriacea	reptiles
X.tropicalis	NP_001016944.1	Xenopus tropicalis	amphibians
B.bufo	XP_040288823.1	Bufo bufo	amphibians
R.bivittatum	XP_029446631.1	Rhinatrema bivittatum	amphibians
T.rubripes	XP_003969421.2	Takifugu rubripes	fish
A.anguilla	XP_035285258.1	Anguilla anguilla	fish
A.alosa	XP_048116466.1	Alosa alosa	fish
P.hypophthalmus	XP_026769283.3	Pangasianodon hypophthalmus	fish
O.mykiss	XP_036801243.1	Oncorhynchus mykiss	fish
D.rerio-Tdp2a	XP_005158360.1	Danio rerio	fish-cyprinids
D.rerio-Tdp2b	NP_001073171.1	Danio rerio	fish-cyprinids
C.carpio-Tdp2a	XP_042597347.1	Cyprinus carpio	fish-cyprinids
C.carpio-Tdp2b	XP_018979408.2	Cyprinus carpio	fish-cyprinids
L.rohita	XP_050986413.1	Labeo rohita	fish-cyprinids
P.tetrazona	XP_043115990.1	Puntigrus tetrazona	fish-cyprinids
S.clava-1	XP_039249622.1	Styela clava	tunicates
S.clava-2	XP_039249603.1	Styela clava	tunicates
A.rubens	XP_033640609.1	Asterias rubens	echinoderms
A.japonica-1	XP_033125731.1	Anneissia japonica	echinoderms
A.japonica-2	XP_033125743.1	Anneissia japonica	echinoderms
S.purpuratus	XP_030830225.1	Strongylocentrotus purpuratus	echinoderms
D.gigantea-1	XP_028404357.1x1	Dendronephthya gigantea	cnidarians
D.gigantea-2	XP_028404302.1	Dendronephthya gigantea	cnidarians
A.tenebrosa	XP_031559050.1	Actinia tenebrosa	cnidarians
N.vectensis	XP_048590272.1	Nematostella vectensis	cnidarians
F.occidentalis	XP_026275622.2	Frankliniella occidentalis	insects
S.gregaria	XP_049857278.1	Schistocerca gregaria	insects
T.palmi	XP_034253788.1	Thrips palmi	insects
C.secundus	XP_023714828.1	Cryptotermes secundus	insects
H.americanus	XP_042210742.1	Homarus americanus	crustaceans
L.salmonis	XP_040576899.1	Lepeophtheirus salmonis	crustaceans
D.magna	XP_032779054.1x1	Daphnia magna	crustaceans
P.vulgata	XP_050401716.1	Patella vulgata	molluscs
M.californianus	XP_052086001.1	Mytilus californianus	molluscs
S.pharaonis	CAE1267020.1	Sepia pharaonis	molluscs
D.polymorpha	XP_052249405.1	Dreissena polymorpha	molluscs
Caenorhabditis sp.	36 PRJEB53466CAI2294593.1	Caenorhabditis sp	nematodes
T.canis	KHN83998.1	Toxocara canis	nematodes
A.bicaudatus	KAI6182797.1	Aphelenchoides bicaudatus	nematodes
T.spiralis	XP_003368460.1	Trichinella spiralis	nematodes
S.natans	CAE7551941.1	Symbiodinium natans	algae
Amoebophrya sp.	A25CAD7957563.1	Amoebophrya sp.	algae
A.thaliana	NP_563894.2	Arabidopsis thaliana	plants
E.salsugineum	XP_024007814.1	Eutrema salsugineum	plants
T.pratense	XP_045818405.1	Trifolium pratense	plants
C.sativa	XP_010458587.1	Camelina sativa	plants
P.euphratica	XP_011046946.1	Populus euphratica	plants
C.karsti	XP_038749009.1	Colletotrichum karsti	fungi
F.coicis	KAF5987320.1	Fusarium coicis	fungi
G.convolvens	KAI0264424.1	Gloeopeniophorella convolvens	fungi
L.hengduanensis	KAH9039705.1	Lactarius hengduanensis	fungi
Mycobacterium sp.	Root265KRD19330.1	Mycobacterium sp.	bacteria
C.bacterium	SZAS-1MBS1964549.1	Chloroflexi bacterium	bacteria
Polyangium sp.	WP_271916946.1	Polyangium sp.	bacteria
Arthrobacter sp.	SLBN-53TQK27412.1	Arthrobacter sp.	bacteria

Supplement 7. Accession numbers and full species names of protein sequences used for phylogenetic analysis. Sequences were retrieved from the National Center for Biotechnology Information (NCBI) database using blast algorithm, with the human TDP2 protein as the query sequence.

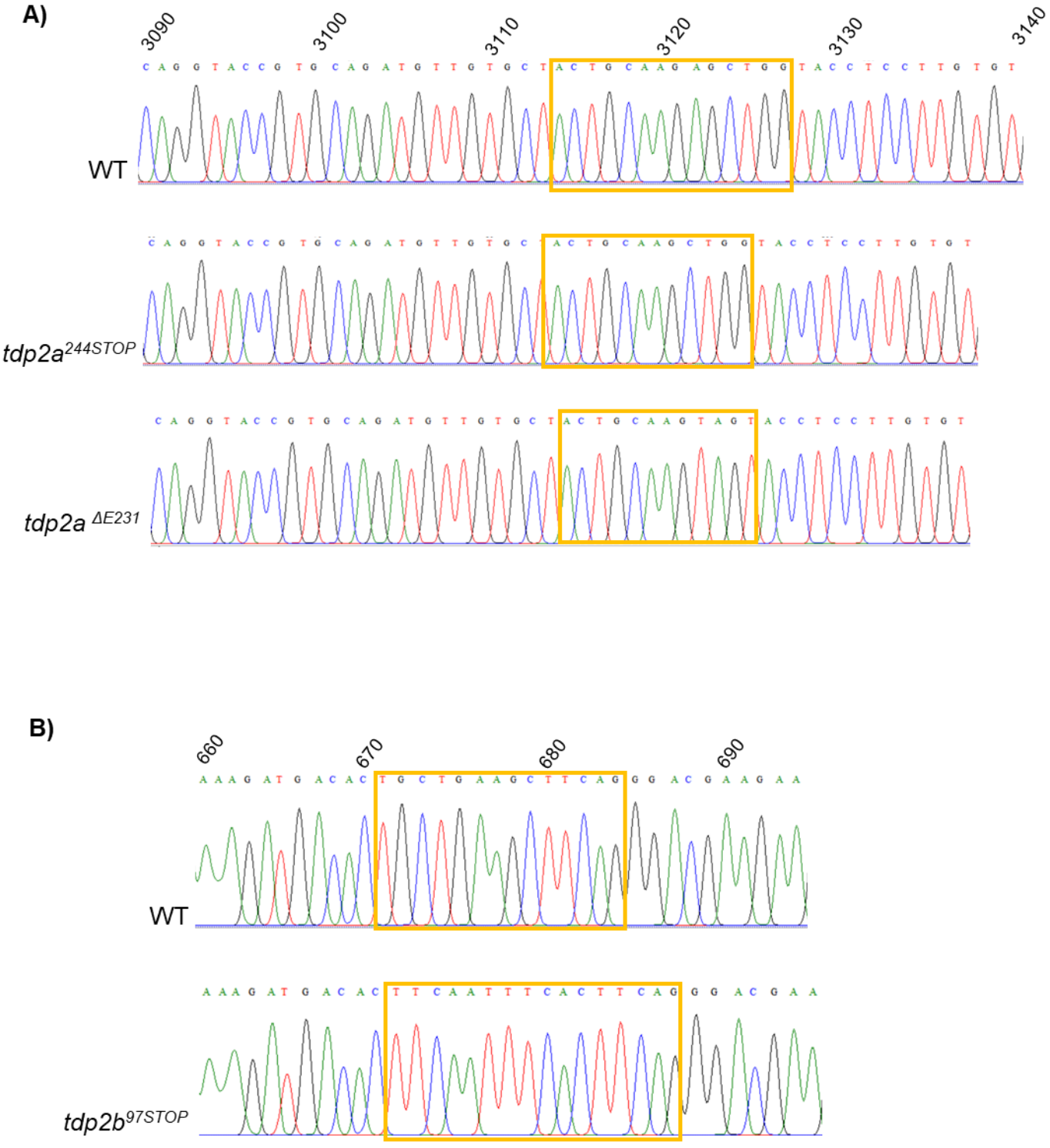

Supplement 8. Sequence results from the target region in both wild-type (WT) zebrafish and *tdp2a* and *tdp2b* mutant fish lines. A) Sequencing histogram of *tdp2a* mutant fish lines related to Figure 35. B) Histogram sequences of *tdp2b*- mutant fish lines related to Figure 35. The numbers above the histograms indicate the genomic position.